CHARACTERISATION OF HYPOXIA-INDUCIBLE FACTOR-MEDIATED GENOPROTECTION IN CLEAR-CELL RENAL CELL CARCINOMA

PhD Thesis Submission

S. ElBadry

September 2023

CHARACTERISATION OF HYPOXIA-INDUCIBLE FACTOR-MEDIATED GENOPROTECTION IN CLEAR-CELL RENAL CELL CARCINOMA

PhD Thesis Submission

Sameh Kamel Abdelhakim Mohamed ElBadry

University of Sheffield

School of Biosciences

Faculty of Science

Sheffield, United Kingdom

September 2023

Acknowledgements

First and foremost, I would like to thank my supervisors Dr Fredericus van Eeden and Professor Sherif El-Khamisy for their never-ending belief that I could do this project, even when I sometimes didn't believe it myself, and their constant support and willingness to help me succeed. I would not have been able to finish this project without the moral support and guidance of my advisor Dr Kyra Campbell, who was available when I struggled and always lent me her ear. I do not think it would have been possible to complete this journey without the support of the van Eeden and El-Khamisy labs, who I have grown extremely close to and consider them my second family. In particular, I would like to thank Dr Arwa Abugable, Dr Chunyan Liao, Dr Ruth Thomas, and Eleanor Markham for welcoming me into the lab and for answering my seemingly never-ending questions. I would also have not been able to even begin this project without the pioneering efforts of Dr Rosemary Kim and Dr Davide Marchi, who I learnt so much from.

The year of 2023 was not what I expected it to be. Most of this thesis was written in the immediate aftermath of the passing of my father, who was also a Sheffield alumnus and one of my biggest motivators. I would not be here if it wasn't for his efforts. I wish he was here to celebrate and share this moment with me. My family have been incredibly supportive throughout this journey - and I could not imagine doing any of this without them. My mother has never failed to stand by my side even when it seemed like I was making the wrong choices. She believed in my potential and never allowed anyone to think otherwise. My two brothers, Ahmed and Omar, along with my sister, Ranya, kept me grounded and calm during stressful days and helped me remember what was important. It has been a hard year for us all, but I know we will get through it together and come out stronger.

Finally, my partner, Jordan, has been there every single step of this journey – from being the first person to find out I had an interview for a PhD, all the way to meticulously proofreading my thesis, she has been an ever-present rock in my life. I could think of no one better to come home to every single night after a failed experiment.

Table of contents

List of figures

List of tables

List of abbreviations

53BP1	p53-binding protein 1
AP	Apurinic/apyrimidinic site
Alt-EJ	Alternative end-joining
APE1	APEX nuclease
APLF	PNKP-like factor
APS	Ammonium persulphate
APTX	Aprataxin
ART	ADP-ribosyltransferase
ATM	Ataxia-telangiectasia mutated
ATP	Adenosine triphosphate
ATR	Ataxia-telangiectasia and Rad3-related
BAF180	BRG1-associated factor 180
BER	Base excision repair
bHLH	Basic helix-loop-helix
BLM	Bloom helicase
BRCA1	Breast cancer type 1 susceptibility protein
BRCA2	Breast cancer type 2 susceptibility protein
BSA	Bovine serum albumin
ccRCC	Clear-cell renal cell carcinoma
cDNA	Complementary DNA
ChIP-Seq	Chromatin immunoprecipitation sequencing
Chk1	Checkpoint kinase 1
Chk2	Checkpoint kinase 2
CKD	Chronic kidney disease
COX	Cytochrome c oxidase
CPT	Camptothecin
CRISPR	Clustered regularly interspaced short palindromic repeats
Ct	Quantification cycle

CTAD	C-terminal transactivation domain
CtIP	C-terminal-binding protein interacting protein
Ctrl	Control
Cul2	Cullin-2
ddH_2O	Double distilled water
DDR	DNA damage response
DMEM	Dulbecco's Modified Eagle Medium
DMOG	Dimethyloxalylglycine
DMSO	Dimethyl sulfoxide
DNA	Deoxyribonucleic acid
DNA2	DNA replication helicase/nuclease 2
DNA-PK	DNA-dependent protein kinase
DNA-PKc	DNA-dependent protein kinase C
dpf	Days post-fertilisation
DSB	Double-strand break
DTT	Dithiothreitol
EDTA	Ethylenediaminetetraacetic acid
ELB	Elongin B
ELC	Elongin C
EPO	Erythropoietin
ERCC1	Excision repair cross-complementation group 1
ETC	Electron transport chain
EXO1	Exonuclease 1
FA	Fanconi anaemia
FDA	U.S. Food and Drug Administration
FEN1	Flap structure-specific endonuclease 1
FIH	Factor-inhibiting HIF
GFP	Green fluorescent protein
GG-NER	Global genome nucleotide excision repair
gRNA	Guide RNA
H2AX	H2A histone family member X

HIF	Hypoxia-inducible factor
HIF1α	Hypoxia-inducible factor 1 α
HIF1β	Hypoxia-inducible factor 1 β
HIF2α	Hypoxia-inducible factor 2 α
HIF2β	Hypoxia-inducible factor 2 β
HIF3α	Hypoxia-inducible factor 3 α
hpf	Hours post-fertilisation
HR	Homologous recombination
HRE	Hypoxia-responsive element
ICI	Immune checkpoint inhibitor
ICL	Interstrand cross-link
IFNα	Interferon α
IL2	Interleukin 2
IR	Ionising radiation
JNJ	JNJ-42041935
LDHA	Lactate dehydrogenase A
LIG1	DNA ligase 1
LIG2	DNA ligase 2
LIG3	DNA ligase 3
LIG4	DNA ligase 4
LOH	Loss of heterozygosity
MDC1	Mediator of DNA damage checkpoint 1
MMR	Mismatch repair
MQ	Milli-Q®
MRN	MRE11-RAD50-NBS1
mRNA	Messenger RNA
mTOR	Mammalian target of rapamycin
NER	Nucleotide excision repair
NF-κB	Nuclear factor-κB
NHEJ	Non-homologous end-joining
NLS	Nuclear translocation sequence

NSCLC	Non-small cell lung carcinoma
NTAD	N-terminal transactivation domain
NuMA	Nuclear mitotic apparatus
ODD	Oxygen-dependent degradation
p300/CBP	p300/CREB binding protein
PALB2	Partner and localiser of BRCA2
PAR	Poly (ADP-ribose)
PARP	Poly (ADP-ribose) polymerase
PARP1	Poly (ADP-ribose) polymerase 1
PARP2	Poly (ADP-ribose) polymerase 2
PARP3	Poly (ADP-ribose) polymerase 3
PAS	Per-ARNT-SIM
PBAF	Polybromo BRG1-associated factor
PBS	Phosphate-buffered saline
pChk1	Phosphorylated Chk1
PCNA	Proliferating cell nuclear antigen
PDH	Pyruvate dehydrogenase
PDK1	Pyruvate dehydrogenase kinase 1
PHD	Prolyl hydroxylase
PHI	Prolyl hydroxylase inhibitor
PIKK	Phosphatidylinositol 3 kinase-like kinase
PLD	Phospholipase D
PNKP	Polynucleotide kinase-phosphatase
pNuMA	Phosphorylated NuMA
POL β	DNA polymerase β
POL γ	DNA polymerase γ
POL δ	DNA polymerase δ
POL ε	DNA polymerase ε
POL θ	DNA polymerase θ
POL ι	DNA polymerase ι
POL κ	DNA polymerase κ

POL λ	DNA polymerase λ
POL μ	DNA polymerase μ
POL ν	DNA polymerase ν
pXRCC1	Phosphorylated XRCC1
Rbx1	RING-box protein 1
RCC	Renal cell carcinoma
RIPA	Radioimmunoprecipitation assay
RNA	Ribonucleic acid
RNF168	RING finger protein 168
RNF8	RING finger protein 8
ROS	Reactive oxygen species
ROX	Roxadustat
RPA	Replication protein A
RT-qPCR	Quantitative reverse transcription polymerase chain reaction
SBRT	Stereotactic body radiation therapy
SDS	Sodium dodecyl sulphate
siRNA	Small interfering RNA
SOCS1	Suppressor of cytokine signalling 1
SSB	Single-strand break
SSBR	Single-strand break repair
ssDNA	Single-stranded DNA
TBE	Tris-borate-EDTA
TBS	Tris-buffered saline
TBST	Tris-buffered saline with 0.1% Tween® 20 detergent
TC-NER	Transcription-coupled nucleotide excision repair
TDP1	Tyrosyl-DNA phosphodiesterase 1
TDP2	Tyrosyl-DNA phosphodiesterase 2
TKI	Tyrosine kinase inhibitor
TLS	Translesion synthesis
TME	Tumour microenvironment
TOP1	Topoisomerase 1

TOP2	Topoisomerase 2
TOP1-CC	TOP1-cleavage complex
UV	Ultraviolet
VEGF	Vascular endothelial growth factor
VEGFR	VEGF receptor
VHL	von Hippel-Lindau
Vll	Vhl-like
WRN	Werner syndrome protein
WT	Wild type
XLF	XRCC4-like factor
XRCC1	X-ray repair cross complementing 1
XRCC4	X-ray repair cross complementing 4
γH2AX	γ H2A histone family member X

Abstract

Clear-cell renal cell carcinoma (ccRCC) is the most common form of renal cell carcinoma (RCC) and is often characterised by von Hippel-Lindau gene (*VHL)* inactivation, causing constitutive upregulation of downstream hypoxia-inducible factor (HIF) targets. Despite recent advances in understanding the molecular mechanisms surrounding ccRCC tumour progression, ccRCC patients are often resistant to both radiotherapy and chemotherapy. Cell lines isolated from ccRCC patients provide an ideal opportunity to analyse the reasons behind radioresistance and chemoresistance.

The *VHL*-mutant cell line, RCC4-VHL -/-, is expected to be more resistant to ionising radiation (IR) and chemotherapeutic agents, compared to the complementary *VHL*-wild type cell line, RCC4-VHL WT. Although I did not find any measurable impact on sensitivity to IR, RCC4-VHL -/- showed greater resistance to chemotherapeutic agents. I discovered that RCC4-VHL -/- had greater expression of several DNA repair components, notably tyrosyl-DNA phosphodiesterase 1 (TDP1) and phosphorylated nuclear mitotic apparatus protein (pNuMA). In addition, TDP1 was found to be a direct or indirect target of HIF2α, suggesting that the HIF pathway is responsible for enhancing resistance to chemotherapeutic agents. Surprisingly, I did not find any measurable impact on chemosensitivity following siRNA or CRISPR-Cas9 mediated downregulation of HIF2α, suggesting HIF2α-independent mechanisms are involved in the DNA damage response.

I also investigated the contribution of Hif in zebrafish to genoprotection, confirming previous literature identifying pharmacological Hif activation as sufficient to protect zebrafish embryos from genotoxic stress. However, I identified downregulation of Tdp1 in *vhl*-mutant zebrafish embryos, suggesting Tdp1-independent mechanisms are involved. Due to the presence of the tumour microenvironment in zebrafish, future experiments need to incorporate both cell lines and zebrafish when analysing HIF-mediated genoprotection due to the unique advantages associated with both models.

Chapter 1 Introduction

1.1. Oxygen homeostasis

Oxygen is a crucial element that most living organisms require to survive. Ambient air is composed of 21% oxygen (150 mm Hg). However, physiological normoxia in human embryonic and adult cells can fall between 2-9% oxygen (14.4-64.8 mm Hg). Some regions of the human body have abnormally low oxygen concentrations which can fall as low as 1%. Low oxygen in bone marrow contributes to the growth and differentiation of stem cell niches (Simon and Keith, 2008), whilst kidney medulla has a high discrepancy between blood supply and oxygen tension due to the parallel arrangement of renal arteries and veins, allowing oxygen to diffuse from arterial system to venous system before diffusion into capillaries, causing variable oxygen supply in the kidney (Eckardt et al., 2005).

Decreased oxygen levels, known as hypoxia, are usually defined as a reduction in oxygen levels compared to normal for each cell type (Bhutta et al., 2022). Intermittent periods of hypoxia have been shown to be important for controlling embryonic cardiovascular development, vascularisation, and forming the nervous system (Iyer et al., 1998; Ryan et al., 1998; Webb et al., 2009). Hypoxia can trigger distinct transcriptional responses that help cells overcome challenges associated with low oxygen. A well-known early discovered example is the body's response to acute hypoxia at high altitudes, such as those found on mountains, which causes an increased production of red blood cells to improve oxygenation (Viault, 1890). Therefore, hypoxia is important both in proper organism development, as well as a stressor that cells need to respond to.

Oxygen homeostasis is crucial to ensure normal development, promote cell survival, and prevent disease. Cells will respond to hypoxia by upregulating transcription factors to maintain sufficient oxygenation and shift aerobic adenosine triphosphate (ATP) generation to anaerobic ATP generation (Cummins and Taylor, 2005). One of the main pathways involved in moderating the cellular response to hypoxia is orchestrated by the hypoxia-inducible factors (HIFs). The upregulation of HIFs causes the increased transcriptional activation of genes that promote angiogenesis, thus improving oxygen delivery to tissues

(Majmundar et al., 2010). Hypoxic cells are a common feature of many tumours, with chronic hypoxia stimulating adaptation mechanisms allowing tumours to form new and disorganised blood vessel networks with insufficient oxygen supply, allowing for the selection of cells able to withstand changing oxygen levels in the microenvironment (Gupta and Massagué, 2006).

1.2. Hypoxia-inducible factor pathway

1.2.1. HIF isoforms

The HIF family of transcriptional activators was identified by establishing the presence of an oxygen-responsive transcriptional enhancer in erythropoietin gene (*EPO*), which is transcriptionally upregulated under hypoxia (Goldberg et al., 1988). The oxygen-responsive transcriptional enhancer was also found in numerous other oxygen-responsive genes, altogether stimulating various mechanisms that promote cell survival, such as angiogenesis, cell growth, mitochondrial function, and influencing metabolism. The enhancer was termed the hypoxia-responsive element (HRE) and has a core sequence of 5'-RCGTG-3' (Semenza et al., 1996). Wang and Semenza (1993a) identified the nuclear factor that is bound to HRE and termed it hypoxia-inducible factor 1 (HIF1), which is required for the transcriptional activation of HRE. A direct link between HIF1 and oxygen levels in cells became clear when increasing concentrations of oxygen caused a drop in HIF1 levels, in both mammalian cells and *Drosophila melanogaster* cells (Wang and Semenza, 1993b; Nagao et al., 1996).

HIF is a heterodimeric protein consisting of an alpha protein (HIFα) and a beta protein (HIFβ/ARNT). The alpha and beta proteins contain one N-terminal basic helix-loop-helix (bHLH) domain, which mediates DNA binding, and a Per-ARNT-SIM (PAS, consisting of PAS-A and PAS-B) domain, which mediates dimerisation (Bersten et al., 2013). In alpha isoforms, there is also an oxygen-dependent degradation (ODD) domain that controls protein stability, as well as an N-terminal transactivation domain (NTAD) involved in target gene activation. A nuclear translocation sequence (NLS) aids in transfer of HIFα through the nuclear pore complex. Lastly, in both alpha and beta isoforms, there is a C-terminal transactivation domain (CTAD) contributing to target gene activation. The beta subunit is constitutively

expressed, whilst the alpha subunits respond strongly to oxygen concentration by having an increased expression under hypoxia (Jaakkola et al., 2001). Under stimulatory conditions, HIFα enters the nucleus and forms a complex with HIFβ, which binds to HRE on HIF-responsive genes and can also recruit p300/CREB-binding protein (p300/CBP) transcriptional co-activators (Arany et al., 1996; Webb et al., 2009).

Three genes encoding for HIFα subunits have been subsequently identified in mammalian systems. The alpha chains are HIF1α, HIF2α, and HIF3α. HIF1α is widely expressed, whilst HIF2α is more localised to specific tissues, including kidney, vascular endothelial cells, lung, and liver (Bertout et al., 2009; Rankin et al., 2009; Stransky et al., 2022). Meanwhile, three genes encode for different HIFβ subunits with varying expression profiles. HIF1β is widely expressed in all tissues (Carver et al., 1994), HIF2β is localised to central nervous system and kidney (Drutel et al., 1996), whilst HIF3β is limited to brain and muscle (Shimba et al., 2005). The functions of HIF2β and HIF3β are not fully understood, although HIF2β is a paralogue of HIF1β (Bersten et al., 2013) and has been reported to have a role in the central nervous system's response to hypoxia (Maltepe et al., 2000).

HIF3α is more distantly related to HIF1α/HIF2α and its precise roles and expression are less understood. Unlike HIF1α/HIF2α, HIF3α lacks an NLS, whilst CTAD is replaced by a leucine zipper mediating protein-protein interactions (Ravenna et al., 2016). Some splice variants of HIF3α have been found to be induced under normoxia by HIF1α, whilst HIF1α and HIF2α appear to induce HIF3α during hypoxia (Tanaka et al., 2009; Augstein et al., 2011). HIF3α has also been found to act as a negative transcriptional regulator of HIF1α/HIF2α by preventing their nuclear translocation. Therefore, HIF3α appears to be involved in a negative-feedback loop that can fine-tune hypoxic response (Heikkilä et al., 2011). Several splice variants of HIF3α have been discovered, although the precise functions of splice variant remain not fully understood (Ravenna et al., 2016). The different domains of each HIF subunit of interest are summarised in **Figure 1.1.**

1.2.2. Modulation of HIFs

Many diseases that have rapidly expanding cells with poor vasculature contain hypoxic cores, such as clear-cell renal cell carcinoma (ccRCC, discussed in **Section 1.3**). HIFs are key transcription factors for hypoxia-responsive genes; therefore, HIF modulation is crucial to prevent aberrant cellular growth. One of the key proteins involved in regulating HIF protein stability is the tumour suppressor von Hippel-Lindau (VHL), which has been implicated in VHL disease, whereby patients were identified as having high levels of EPO as well as increased angiogenesis. Indeed, several genes that had previously been identified as being regulated by HIF1α were insensitive to oxygen in cell lines lacking functional VHL, such as *VEGF* and *PDGFB* which are all involved in angiogenesis. Therefore, the overproduction of these genes in such cells appears to lead to increased angiogenesis and cell survival (Iliopoulos et al., 1996). Gene cloning established a biochemical link between VHL and HIF, in which VHL was shown to be responsible for normoxic breakdown of HIF.

Further work has now established a model of VHL-HIF signalling. Under normoxic conditions in the cellular environment, prolyl hydroxylases (PHDs) utilise oxygen as a substrate to hydroxylate HIFα subunits. Alongside oxygen, PHDs also require Fe^{+2}, 2-oxoglutarate, and ascorbate as co-substrates (Webb et al., 2009). Hydroxylated HIFα is recognised by VHL, which acts as the recognition part of an E3 ubiquitin ligase complex, leading to proteasomal degradation via ubiquitination of HIFα. The other components of the E3 ubiquitin ligase complex are elongin B (ELB), elongin C (ELC), cullin-2 (Cul2), and RING-box protein 1 (Rbx1). PHDs are inactivated under hypoxia as they can no longer use oxygen as a substrate. Therefore, HIFα subunits stabilise and translocate to the nucleus where they can form functional heterodimers with HIFβ subunits, leading to downstream binding of HRE in target genes (Haase, 2009). This pathway is summarised in **Figure 1.2**.

There are three PHDs, PHD1-3, of which PHD2 is the main mediator of HIF1α hydroxylation, whilst HIF2α is preferentially regulated by PHD1 and PHD3 (Appelhoffl et al., 2004). Despite low oxygen during hypoxia, PHD3 is transcriptionally upregulated as it is a transcriptional target of HIFα. This has been suggested as an intrinsic feedback mechanism to prevent excessive hypoxic signalling (Appelhoffl et al., 2004). PHD-mediated hydroxylation occurs by hydroxylating two proline residues within the ODD domain of HIFα (Minamishima et al.,

2009). However, HIF3α only contains one hydroxylated proline residue in its ODD. VHL complex can bind to this singular hydroxylation site; however, it does not seem to be highly effective at inducing proteasomal degradation of HIF3α (Maynard et al., 2003; Ravenna et al., 2014). In addition to PHDs, HIFα can also be modulated by the aspariginyl hydroxylase factor-inhibiting HIF (FIH), which hydroxylates HIFα on asparagine residues located in CTAD. This prevents the recruitment of p300/CBP to HIF, reducing HIF transcriptional activation and fine-tuning hypoxic response (Hashimoto and Shibasaki, 2015).

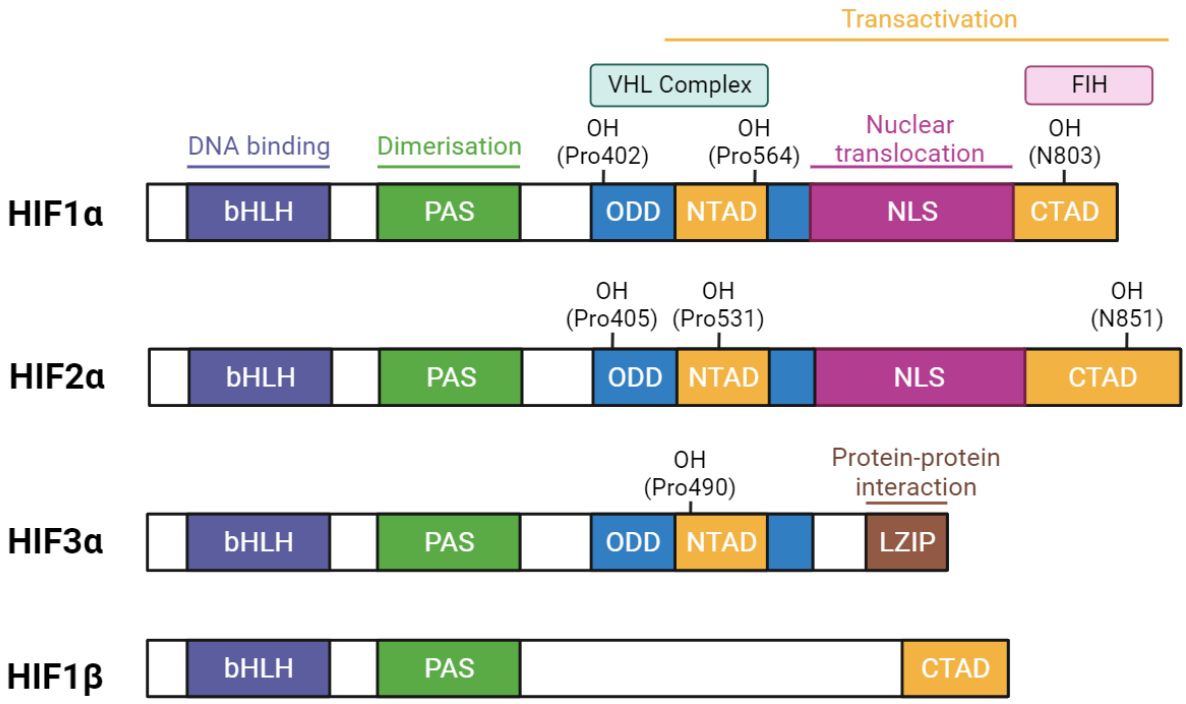

Figure 1.1: HIF isoforms have similar and differing functional domains. The three subunits of HIFα (HIF1α, HIF2α, and HIF3α) all contain a basic helix-loop-helix (bHLH) domain important for DNA binding as well as a Per-ARNT-SIM (PAS) domain for dimerization. HIFα subunits contain an oxygen-dependent degradation (ODD) domain, which is the site of hydroxylation (OH) by prolyl hydroxylase enzymes. In humans, HIF1α is hydroxylated at proline (Pro) residues Pro402 and Pro564. HIF2α is hydroxylated at Pro405 and Pro531. HIF3α is hydroxylated at Pro490. VHL complex binding occurs at hydroxylation sites of HIFα. An N-terminal transactivation domain (NTAD) is located within ODD. NTAD, alongside C-terminal transactivation domain (CTAD), are responsible for target gene activation. HIF1β only contains a CTAD. A leucine zipper (LZIP) replaces CTAD in HIF3α, which mediates protein-protein interactions. HIF1α and HIF2α contain nuclear localisation sequences (NLS) which aid in directing HIF1α/HIF2α towards the nucleus. HIF1α and HIF2α contain a hydroxylation site within CTAD on asparagine (N) residues N803 (HIF1α) and N851 residue (HIF2α). This hydroxylation site allows for the binding of factor-inhibiting HIF (FIH), which modulates hypoxic response by inhibiting HIF transcriptional activation. Figure adapted from Ravenna et al., (2016) and created in Biorender.com.

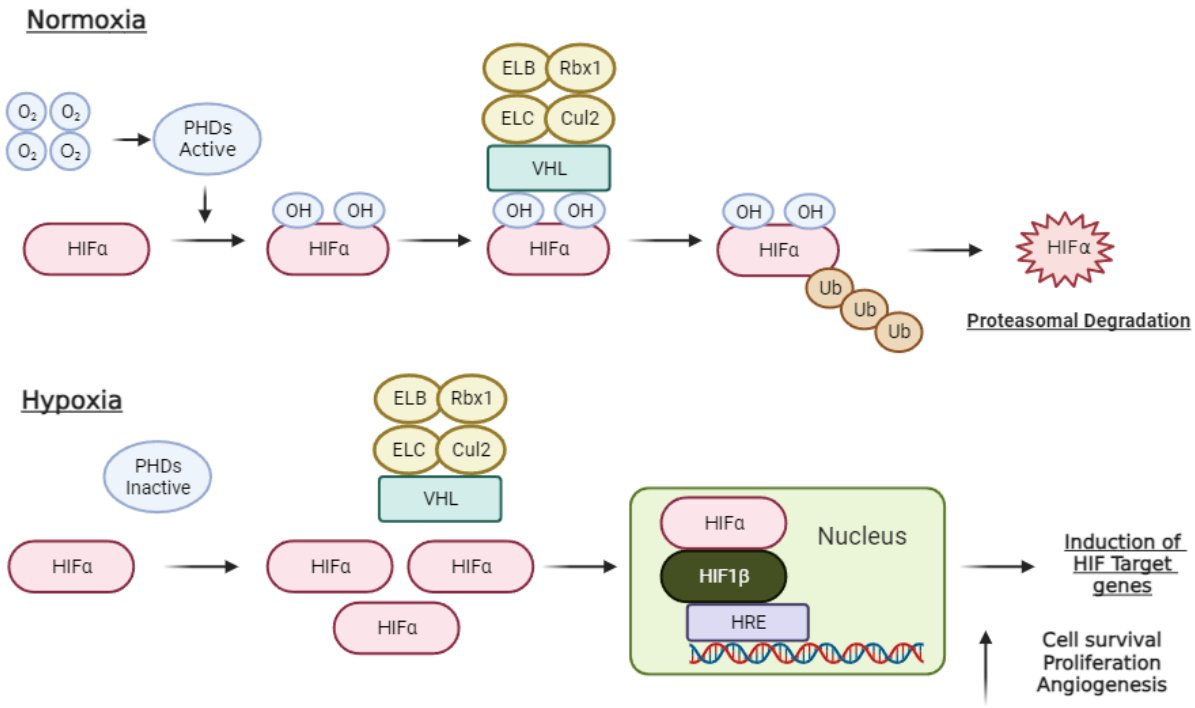

Figure 1.2: VHL/HIF pathway. Under normal oxygen levels in the cellular environment, prolyl hydroxylase enzymes (PHDs) are activated, causing them to utilise oxygen in the atmosphere to form a hydroxylation site (OH) on HIFα. These hydroxylation sites allow binding of the VHL complex to HIFα. The VHL complex consists of the VHL protein, ELB, ELC, Cul-2, and Rbx1. The binding of this complex to HIFα attracts ubiquitin proteins (Ub) to HIFα, causing it to break down via proteasomal degradation. Under low oxygen levels in the cellular environment (hypoxia), PHDs are inactivated. Therefore, the HIFα hydroxylation sites are not created, preventing the VHL complex from binding to HIFα, allowing HIFα to accumulate and translocate downstream to the nucleus, whereby it forms a dimeric complex with HIF1β. This dimeric complex binds to a specific stretch of DNA present in some genes known as the hypoxia response element (HRE), causing the induction of target genes that promote cell survival, proliferation, angiogenesis, and several other pathways. Figure created in Biorender.com.

1.2.3. The response to hypoxic stress by HIFs

HIF1α and HIF2α share many structural similarities and often overlap in expression pattern and function. However, they also play nonredundant roles and both are required for oxygen homeostasis.

1.2.3.1. Metabolism

Oxygen is involved in mitochondrial aerobic respiration to produce ATP, which is involved in providing energy. To maintain homeostasis under hypoxia, metazoans have developed adaptation mechanisms preventing a mismatch between ATP demand and supply (Semenza, 2007). One of the ways to achieve this is reducing the reliance on oxygen by stimulating a shift from aerobic metabolism to anaerobic metabolism, which does not rely on oxygen as the final electron acceptor in the mitochondria, but takes place in the cytoplasm instead where pyruvate is used as the final electron acceptor, producing lactate (Müller et al., 2012). HIF1α activation promotes the expression of glucose transporters and glycolytic enzymes to facilitate anaerobic metabolism. Pyruvate dehydrogenase kinase 1 (PDK1), which is upregulated by HIF1α, inactivates the catalytic subunit of pyruvate dehydrogenase (PDH) to prevent the conversion of pyruvate to acetyl-CoA, which is an important step in aerobic metabolism. PDK1 also diverts carbon away from the mitochondria, preventing carbon use in cellular respiration. Another protein upregulated by HIF1α is lactate dehydrogenase A (LDHA), which converts pyruvate to lactate. The upregulation of both PDK1 and LDHA by HIF1α thus diverts pyruvate away from aerobic metabolism in the mitochondria towards anaerobic metabolism in the cytoplasm (Holness and Sugden, 2003; Heiden et al., 2009). However, this is unsustainable in humans due to low yields of ATP production (Müller et al., 2012).

HIF1α upregulation via hypoxia reduces ATP production in the mitochondria by lowering the activity of the mitochondrial electron transport chain (ETC), which is the site of oxidative phosphorylation in the mitochondria (Wheaton and Chandel, 2011). Hypoxia decreases the activity of cytochrome c oxidase (COX), which is responsible for transferring electrons to oxygen in the mitochondria during respiration. To prevent COX activity becoming too low so that cells are unable to survive, HIF1α upregulation induces the COX4-1 subunit to switch to COX4-2 through increased mRNA/protein synthesis of COX4-2, and degradation of COX4-1

via upregulating the mitochondrial LON protease. The precise functional relevance of this subunit switch is unclear, but it is hypothesised to optimise ETC activity under hypoxic conditions (Fukuda et al., 2007; Douiev et al., 2021).

HIF2α has also been reported to have distinct roles in modulating metabolism during hypoxia. Antioxidant genes, such as *SOD2*, are upregulated by HIF2α to suppress reactive oxygen species (ROS) that accumulate during hypoxia. This was initially demonstrated in murine models (Scortegagna et al., 2003) and then observed in ccRCC cell lines (Bertout et al., 2009). In addition, under hypoxic stress HIF2α reprogrammes lipid metabolism to shuttle lipid-derived carbon away from the mitochondria and promotes lipid storage in droplets (Qiu et al., 2015).

1.2.3.2. Vascular response

HIFs are known to play an important role in regulating angiogenesis genes during both embryonic development and in adults, particularly in a pathological setting (Rey and Semenza, 2010). In response to oxygenated blood not reaching tissue, such as in ischaemia, HIF1α/HIF2α upregulate pro-angiogenic genes that stimulate blood vessel formation, increase vessel permeability, and increase red blood cell formation. These responses restore the delivery of oxygenated blood to ischaemic sites, restoring normal function (Majmundar et al., 2010). In contrast to regular blood vessels, tumour vasculature is notably leaky and disorganised, favouring continued tumour growth beyond the reach of oxygenated blood (de Heer et al., 2020).

1.2.3.3. Inflammation

HIF function has high degree of overlap with nuclear factor-κB (NF-κB) function in inflammatory diseases. Inflammation is an important part of the body's immune defence mechanism, whereby the immune system recognises and removes harmful stimuli, followed by a healing process. Chronic inflammation can result from a failure to eliminate a particular stimulus, or the immune system attacking normal cells of the body (Furman et al., 2020). There is some crosstalk between hypoxia and inflammation in diseases, with several

diseases, such as rheumatoid arthritis and inflammatory bowel disease, expressing combined areas of hypoxia and inflammation (Gaber et al., 2005; Brown and Taylor, 2018). A key signal in inflammatory pathways are proteins of the NF-κB family, consisting of five members that can form any combination of homodimers or heterodimers. In canonical NF-κB signalling, NF-κB translocates to the nucleus where it activates a complex regulatory network. Due to the varied dimer combinations that NF-κB can form, multiple different outcomes can arise from signalling, including apoptosis control, cellular growth, and carcinogenesis (Perkins and Gilmore, 2006; Biddlestone et al., 2015). Several common target genes and stimuli exist between HIF and NF-κB, whilst NF-κB also stabilises HIF1α in hypoxic regions (D'Ignazio et al., 2016). On the other hand, HIF1α appears to repress NF-κB in inflammatory regions, whilst HIF2α activates inflammatory pathways (Ryu et al., 2014; Bandarra et al., 2015). Although the exact relationship between HIFs and NF-κB remains not fully understood, both pathways appear to regulate one another and closely coordinate signalling.

1.2.3.4. Apoptosis

Apoptosis is programmed cell death that eliminates dangerous or unwanted cells. The intrinsic apoptotic pathway can be triggered by chemotherapeutic agents; therefore, the apoptotic response has been studied extensively in cancers with hypoxic regions as these appear to be more chemoresistant (Sendoel and Hengartner, 2023). The role of HIFs in apoptosis is not fully understood, with reports suggesting that HIFs could either promote or inhibit apoptosis.

HIF1α has been implicated in both pro- and anti-apoptotic changes as it has been linked to causing both upregulation and downregulation of various apoptotic factors (Carmeliet et al., 1998; Greijer and van der Wall, 2004; Kim et al., 2004; Sasabe et al., 2005; Liu et al., 2006). In addition, HIF1α has been shown to enlarge mitochondrial morphology by inducing mitofusin-1, which inhibits apoptosis (Chiche et al., 2010). Due to HIF1α's widespread expression in human cells, HIF1α may have cell-type specific responses to hypoxia that causes differential effects on apoptosis, whereby it could be beneficial to protect certain cell types during hypoxia, such as endothelial cells in vasculature, or it could be beneficial to eliminate unwanted cells. HIF2α appears to have a clearer anti-apoptotic role, with HIF2α

linked to negative regulation of pro-apoptotic factors in VHL-deficient cells (Raval et al., 2005).

p53 is a tumour suppressor protein involved in signalling to the intrinsic apoptotic pathway, triggering programmed cell death (Ozaki and Nakagawara, 2011). The status of p53 in hypoxic cells has been under scrutiny in recent years, with contradictory results often found. Although p53 is the most mutated gene in human cancers, it is not commonly mutated in ccRCC (Soussi et al., 2000). However, downstream target genes of p53 appear to be transcriptionally repressed in ccRCC, despite normal activation of p53 through its accumulation, localisation, and phosphorylation. Several mechanisms have been proposed for this response, one of which is HIFs competing for the same co-transcription factors as p53 under hypoxic conditions, such as p300 (Gurova et al., 2004; Diesing et al., 2021).

1.2.3.5. DNA repair

Due to enhanced chemoresistance in several hypoxic cancers, the role of HIFs in DNA repair mechanisms has been studied recently with contrasting results. HIFs and DNA repair are discussed extensively later **(Section 1.5.4)**.

1.3. Clear-cell renal cell carcinoma

1.3.1. Clinical features

Renal cell carcinoma (RCC) is the 6th most diagnosed cancer in men, and the 10th most diagnosed cancer in women. It is the 13th most common cause of cancer death worldwide with more than 170000 RCC-related deaths annually, with a greater incidence in older people, particularly men. Some potential risk factors have been identified, including comorbidities, environmental causes, and lifestyle choices (Capitanio et al., 2019). RCC accounts for 80% of all kidney cancers, of which 70-80% of these are described as 'clear-cell' (Escudier et al., 2019) due to the appearance of the cancer cells under a microscope, which have a transparent phenotype due to the accumulation of glycogen and lipids in cellular cytosol (Ericsson et al., 1966).

VHL disease is an autosomal dominant hereditary cancer, characterised mainly by retinal angiomas, hemangioblastoma in the cerebellum, and renal cysts and neoplasms (Maher and Kaelin, 1997). VHL disease follows Knudson's two hit model (Knudson, 1971), whereby both copies of the *VHL* tumour suppressor gene are inactivated in patients (Maher and Kaelin, 1997). In more than 70% of VHL cases, patients present with ccRCC, which is the most common cause of death in patients (Maher et al., 1990). ccRCC develops in the proximal tubular cells and metastasises to other regions in 25% of cases. The tumours are solid yellow masses characterised by cortical lesions, haemorrhaging, and necrosis in some regions (Mittal and Sureka, 2016). Due to the tumour obstructing the urogenital tract in the abdomen, patients often present with flank pain as an early symptom. This can be combined with blood in urine (haematuria), due to tumour infiltration into the renal medulla, and oedema in the lower extremities (Mohamed et al., 2015; Hsieh et al., 2017). Upon further investigation, patients can present with several paraneoplastic symptoms, including hepatic dysfunction, increased blood cell production (erythropoiesis), increased calcium in blood (hypercalcaemia), and low blood glucose (hypoglycaemia) (Palapattu et al., 2002; Souma et al., 2016).

1.3.2. Molecular characterisation

Almost 100% of hereditary ccRCC cases arise from patients who also have VHL disease (Maher, 1996). These patients have a mutation in *VHL,* causing the VHL protein to become

non-functional. In non-hereditary cases of ccRCC, 80% arise due to biallelic inactivation of *VHL*, either due to mutations or methylation (Brugarolas, 2014). Non-functional VHL in ccRCC patients causes the VHL/E3 ligase complex to be unable to bind to hydroxylated sites on HIFα under normoxia. Therefore, the proteasomal degradation of HIFα is perturbed, causing a constitutively increased expression of HIFα, allowing HIFα to translocate to the nucleus and bind to HIF1β forming the HIF heterodimeric transcription factor, which binds to HRE and activates HIF-target genes (Krieg et al., 2000). There are several other mutations that commonly occur in ccRCC, which can either be in combination with or separate from *VHL* mutations. *VHL* appears to be the driver gene inactivated in a majority of ccRCC patients, followed by inactivation of several other genes. In total, there are approximately 19 significantly mutated genes in ccRCC patients, of which the following eight are the most common: *VHL, PBRM1, SETD2, KDM5C, PTEN, BAP1, MTOR,* and *TP53*. The most common chromosomal alteration, which occurs in 91% of ccRCC cases, is the loss of chromosome 3p, encompassing four of the commonly mutated genes (*VHL*, *PBRM1, BAP1,* and SETD2) (Brugarolas, 2014).

VHL inactivation can occur due to mutations or hypermethylation (Nickerson et al., 2008). Inactivation often occurs in two stages, whereby one allele is inactivated via a mutation, followed by deletion of chromosome 3p. In some cases, a chromosomal deletion is followed by the duplication of chromosome 3 containing mutated *VHL* causing copy-neutral loss of heterozygosity (LOH) (Sato et al., 2013). *VHL* mutations often introduce a premature stop codon, causing aberrant protein translation (Merla et al., 2009; Taylor et al., 2012; Perrotta et al., 2020). Meanwhile, many missense mutations cluster at the interface between VHL and ELC, preventing the formation of the VHL/E3 ligase complex required for HIFα degradation. Interestingly, the gene for ELC, *TCEB1*, is itself mutated in a small percentage of ccRCC cases, exclusively alongside *VHL* mutations (Stebbins et al., 1999; Sato et al., 2013). In a study by Sato et al., (2013), they found the VHL/E3 ligase complex inactivated in 92% of ccRCC patients, of which 66% were mutations, 21% were caused by increased methylation, and 5% were caused by TCEB1 inactivation, highlighting the crucial role of *VHL* inactivation in a majority of ccRCC patients. The impact of *VHL* inactivation in ccRCC patients is summarised in **Figure 1.3.**

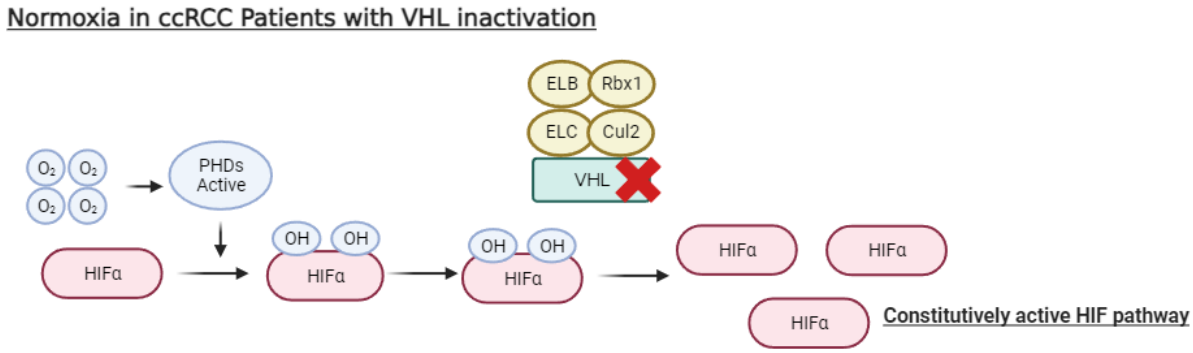

Figure 1.3: *VHL* inactivation in ccRCC patients causes a constitutively upregulated HIF pathway. The VHL complex is unable to bind to hydroxylation sites (OH) on HIFα under normoxia. Therefore, ccRCC patients have a constitutively active HIF pathway as HIFα is not degraded by the proteasome. Figure created in Biorender.com.

1.3.3. Current and emerging treatments

During the early stages of ccRCC before metastasis, treatments can include surgery to remove the affected kidney region (partial nephrectomy) or the whole kidney (radical nephrectomy). In metastatic disease, a nephrectomy is only effective if all metastatic sites are removed. Therefore, nephrectomy has limited effectiveness in advanced ccRCC (Flanigan et al., 2004). After metastasis, treatments often move towards targeted drug therapy. An early strategy to treat ccRCC was to exploit the immune system via cytokines, which modulate the immune system. Cytokines, such as interferon α (IFNα) and interleukin 2 (IL2), endogenously boost the immune system via various mechanisms, slowing tumour development. Therefore, administering these cytokines exogenously has anti-cancer effects (Pyrhönen et al., 1999; Sim and Radvanyi, 2014). However, cytokine therapy has several adverse effects due to the high doses required, so it is no longer considered a first-treatment option (Totsuka et al., 1989; Shah et al., 2021).

At the turn of the 21st century, specific pathways implicated in ccRCC progression were targeted for a more direct response. One of the major phenotypes observed in ccRCC is increased angiogenesis caused by high levels of vascular endothelial growth factor (VEGF), which are targets of HIFs (Mazumder et al., 2023). Targeting either VEGF or its receptor (VEGFR), have successfully been used to reduce tumour invasion via angiogenesis. The most well-established class of drugs are the tyrosine kinase inhibitors (TKIS), such as sorafenib and sunitinib, which inhibit VEGF signalling by modulating VEGFR (Comandone et al., 2021). TKIs are currently used as first-line treatments as they have less side effects compared to cytokines and more patients respond positively to TKIs (Michaelis et al., 2022). The mammalian target of rapamycin (mTOR) pathway is also hyperactivated in ccRCC and is involved in neovascularisation (Pal and Figlin, 2010). Therefore, mTOR inhibitors, such as temsirolimus, have been used as an alternative drug to target angiogenesis (Oudard and Elaidi, 2012). Although adverse effects occur when patients are treated with either VEGF inhibitors or mTOR inhibitors, it is often the drug resistance occurring a few months after the initial treatment that causes major issues (Gacche and Meshram, 2014), as well as heterogeneity in tumour cells that cause varying sensitivity to drugs (Fisher et al., 2013).

Another strategy to treat ccRCC patients is by targeting the innate ability of tumours to escape the immune system. Tumours overexpress certain ligands, such as programmed cell-death ligand 1 (PD-L1), which causes inhibition of the immune system to target tumours for cell death (Kornepati et al., 2022). These are known as immune checkpoint ligands, which can be inhibited using immune checkpoint inhibitors (ICIs), increasing the aggressiveness of the immune response. ICIs are clinically effective in ccRCC patients with *PBRM1* inactivation, which occurs in 40% of ccRCC cases (Gu et al., 2021). *PBRM1* encodes for the tumour suppressor BRG1-associated factor 180 (BAF180), which is a subunit of a polybromo BRG1-associated factor (PBAF) subtype of the SWI/SNF chromatin remodelling complex. Loss of BAF180 causes the formation of unstable PBAF, leading to aberrant recruitment of PBAF to specific loci and abnormal target gene expression (Thompson, 2009; Gao et al., 2017). In addition, the loss of BAF180 has been associated with an upregulation of immuno-stimulatory genes (Miao et al., 2018). ICIs are used in combination with VEGF inhibitors and mTOR inhibitors, combatting drug resistance. Combination therapy shows increased survival in ccRCC patients; however, a complete durable response is rarely seen (Yu et al., 2021a; Ince and Eisen, 2022).

Conventional radiotherapy is often only used in ccRCC patients as a method to control local tumour growth and limit metastasis, as ccRCC is traditionally considered to be a radioresistant tumour (de Meerleer et al., 2014). The mechanisms behind radioresistance are not fully understood, but several explanations have been suggested, including upregulation of DNA damage checkpoint response to repair radiation-induced DNA breaks in tumour-initiating cells (Li et al., 2017a) and upregulation of long non-coding RNAs that modulate apoptosis and DNA repair (Jiang et al., 2020). However, recent trials have suggested that stereotactic body radiation therapy (SBRT), which consists of higher radiation doses in fewer fractions, can be used to treat ccRCC as opposed to conventional radiation doses (Kirste et al., 2022), although these trials have involved small patient numbers, so it is unclear if this applies generally to all ccRCC cases. In addition, SBRT has been shown to synergise with immunotherapy (Liu et al., 2021), which could be beneficial in ccRCC patients who have previously shown toxicity to combinatorial drug treatment strategies (Msaouel et al., 2018). Overall, the literature surrounding radioresistance in ccRCC remains in early stages and more research is required to understand the genetic contributions, as well as

understanding how ccRCC patients with different genetic backgrounds respond to radiotherapy. In addition, it is crucial to understand why SBRT appears to be more effective in ccRCC patients compared to conventional radiotherapy.

There are several new targeted drugs that are currently in clinical trials or have recently been approved for treating patients. The most promising emerging drugs are HIF2α inhibitors, causing downstream target genes to no longer be constitutively upregulated in ccRCC patients (Wallace et al., 2016). HIF2α had been previously considered undruggable (Koehler, 2010), but the development of the HIF2α inhibitor PT2385 has provided clinicians with a new strategy to treat ccRCC by targeting a hydrophobic pocket unique to the HIF2α PASB domain and absent in HIF1α, which allosterically disrupts dimer formation between HIF2α and HIF1β (Wallace et al., 2016; Cowman and Koh, 2022). HIF2α is considered the main promoter of an aggressive phenotype in ccRCC; therefore, its downregulation is also thought to have therapeutic potential (Kondo et al., 2003). Initial results showed that PT2385 was well-tolerated by patients and led to disease stabilisation or remission in 52% and 14% of patients, respectively (Courtney et al., 2018). The second generation HIF2α inhibitor, PT2977 (also known as Belzutifan), is more potent and selective than PT2385 and has recently been approved by the U.S. Food and Drug Administration (FDA) for treating ccRCC patients (Fallah et al., 2022). In a clinical trial, 49% of patients with VHL-associated ccRCC responded positively to Belzutifan, causing a reduction in renal tumour size with low-grade adverse effects, demonstrating the potential of HIF2α inhibition for treating ccRCC (Bensalah et al., 2022).

Current lab trials have focused on utilising bioinformatics and omics technology to find novel targets of ccRCC (Chen et al., 2021b; Zhao et al., 2022). Furthermore, although there are well-known non-*VHL* mutations in ccRCC such as *PBRM1*, *BAP1*, and *SETD2*, there are currently no drugs targeting these proteins.

ccRCC remains a difficult disease to treat due to its resistance to chemotherapy and radiotherapy. Patients can require a combination of several treatments that target different pathways and often find that they develop resistance over time to treatments (Makhov et al., 2018; Rossi et al., 2021). Genetic and epigenetic changes have been implicated in

potentially enhancing radio- and chemoresistance, such as greater efficiency at repairing DNA breaks, downregulation of apoptotic pathways, and histone modifications altering drug transporters (Acharya et al., 2022). Understanding the molecular mechanisms surrounding ccRCC radio- and chemoresistance are crucial to reduce the need of providing dangerously high doses of therapeutic agents and to resensitise patients to safer doses. In addition, this will allow for more targeted therapy that will be dependent on the genetic background of each ccRCC patient.

1.3.4. ccRCC models

1.3.4.1. Cell lines

Primary cells taken directly from patients have a finite lifespan and do not expand rapidly. Therefore, a constant supply of donors would be required to perform large-scale experiments with reliable results (Richter et al., 2021). In contrast, immortalised cell lines are transformed to expand rapidly and have a longer lifespan. Furthermore, they are easier to transfect, allowing for a greater understanding of molecular mechanisms of disease that can be replicated across many laboratories due to the ease of working with cell lines (Gresch and Altrogge, 2012; Chong et al., 2021).

Non-tumour cell lines can be used to study the role of hypoxia in ccRCC as HIFs can be upregulated by using pharmacological mimetics of hypoxia by targeting proteins that contribute to HIFα degradation. PHDs and FIH require oxygen and 2-oxoglutarate as substrates and Fe^{+2} as a co-factor for HIFα degradation, so chemicals targeting these substrates and co-factor have been developed to treat various conditions, such as anaemia, whereby upregulating HIF-target EPO stimulates angiogenesis (Jaakkola et al., 2001; Locatelli et al., 2017). Prolyl hydroxylase inhibitors (PHIs), such as Roxadustat, compete with 2-oxoglutarate, preventing formation of the hydroxylation site on HIFα (Hirota, 2021). Some chemicals prevent the use of Fe^{+2} as a co-factor by PHDs. Cobaltous ions, such as cobalt chloride, can substitute Fe^{+2} (Muñoz-Sánchez and Chánez-Cárdenas, 2019), whilst iron chelators, such as deferoxamine, binds free iron (Cappellini et al., 2009). HIFs can also be upregulated in cell lines by growing them under hypoxic conditions in a low oxygen incubator (Matthiesen et al., 2021). Genes upregulated under low oxygen, or by mimicking hypoxia via pharmacological inhibition of HIFα degradation, do not upregulate the same

genes as *VHL* inactivation, suggesting that VHL has a distinct role besides its activity in HIF modulation (Jiang et al., 2003). Therefore, inducing HIF accumulation in non-mutated cells is insufficient to replicate the molecular mechanisms of ccRCC. Although HIF expression features prominently in hypoxic signalling and PHD/VHL inhibition, manipulating each pathway produces a myriad of effects on other genes that could also influence HIF itself and its downstream targets.

As ccRCC is the most common form of RCC, there are several available cell lines that have been studied. One of the first established ccRCC cell lines was 786-O, which is a *VHL*-mutated line (introduction of a premature stop codon, p.G104Afs*55) that can form clear-cell tumours when injected into nude mice. This cell line is characterised by increased expression of VEGF, which stimulates angiogenesis, and HIF2α. Interestingly, HIF1α expression appears to be absent in 786-O due to truncations in *HIF1α* mRNA (Iliopoulos et al., 1995). The loss of HIF1α is a common event in many ccRCC cell lines, whilst HIF2α appears to be present in all cell lines. In 50% of the most commonly reported RCC cell lines *VHL* is WT, despite *VHL* inactivation occurring in a majority of ccRCC tumours (Shapiro et al., 2022). This has created a discrepancy between the actual molecular mechanisms of ccRCC in patients and the knowledge gained from established ccRCC cell lines.

The RCC4 cell line was derived from a ccRCC primary tumour deficient in VHL originally obtained by Professor C.H.C.M. Buys at the University of Groningen, Netherlands (Maxwell et al., 1999). Similar to 786-O cells, RCC4 cells can form clear-cell tumours when injected into mice (Chittezhath et al., 2014). However, RCC4 cells differ from 786-O cells in that both HIF1α and HIF2α are constitutively upregulated (Maxwell et al., 1999). Therefore, RCC4 cells provide an ideal model to study both the VHL-dependent roles of ccRCC tumourigenesis, as well as the HIF1α/HIF2α-dependent roles.

1.3.4.2. Zebrafish

Danio rerio (zebrafish) have proven to be an effective vertebrate model at studying rare genetic diseases and have been successfully used in a variety of settings (Adamson et al., 2018). Zebrafish embryo development can be tracked easily within the first few hours and

days post-fertilization due to its transparent body (Kimmel et al., 1995; Vacaru et al., 2014). In addition, nearly 80% of human disease genes have an orthologous equivalent in zebrafish, allowing for genetic modification of disease-implicated genes, which has been well-established, especially using CRISPR (Howe et al., 2013).

Teleosts, such as zebrafish, have a partially duplicated genome that caused multiple copies of certain genes to arise (Howe et al., 2013). Two human *VHL* orthologues exist in zebrafish: the *vhl* gene and the more distant vhl-like gene (*vll*). *vhl* was initially thought to play a major role in Hif modulation, whilst *vll* played a minor role (Chen et al., 1995; Van Rooijen et al., 2009). The three human HIFα subunits are duplicated in zebrafish, thereby presenting with a total of six orthologues (Rytkönen et al., 2013). ccRCC research in zebrafish has mostly focused on modulating *Vhl* and *Vll* to recapitulate the phenotypes observed in ccRCC patients with *VHL* inactivation, such as HIF upregulation, as well as less well characterised downstream targets of *VHL*.

The van Eeden lab has successfully created a *vhl* mutant showing strong activation of the Hif pathway, which can be demonstrated *in vivo* by using the *phd3*:EGFP Hif-activity reporter transgene, leading to GFP expression when Hif is activated (Santhakumar et al., 2012). Although this is traditionally used to determine Hif activity, it can also be indirectly used as a reporter for LOH of *vhl* on a cell-by-cell basis in an animal model, as LOH in *vhl* leads to strong activation of Hif. LOH can be enhanced by exposing animals to genotoxic stress. This may be used to identify compounds that could provide a therapeutic impact in humans (Kim et al., 2020).

1.4. Types of DNA damage

1.4.1. Endogenous DNA damage

1.4.1.1. Replication errors

High fidelity DNA replication is crucial for the accurate transmission of genetic information across many generations, whilst low fidelity DNA replication maintains genetic diversity allowing organisms to adapt to changing conditions. DNA replication requires multiple DNA

replication polymerases of varying fidelity to be involved in DNA replication (Kunkel, 2004). It is estimated that errors during DNA replication causing single base pair substitutions, insertions, or deletions accumulate at a frequency of 10^{-6} to 10^{-8} per cell per generation (Loeb et al., 2003; Chatterjee and Walker, 2017). Alterations in the cellular environment, such as deoxyribonucleotide triphosphate or ribonucleotide triphosphate concentrations, can modulate the fidelity of DNA replication polymerases, increasing the frequency of single base pair replication errors or modulating DNA replication speed (Kumar et al., 2011; Forslund et al., 2018). Base insertions and deletions can also occur during DNA replication of repetitive sequences due to strand slippage (Viguera et al., 2001). A failure to repair single base pair changes can cause frameshift mutations, resulting in a different translated protein (Roth, 1974). DNA replication polymerases may also inaccurately incorporate uracil nucleotides in DNA causing impaired replication (Andersen et al., 2005).

1.4.1.2. Topoisomerase-induced DNA breaks

Topoisomerase 1 (TOP1) creates transient DNA breaks to prevent supercoiling during DNA replication, translation, and chromosomal segregation. The binding of TOP1 to DNA creates a transient complex called TOP1-cleavage complex (TOP1-CC), which is reversible. However, TOP1-CC removal can stall, leading to collision with a DNA replication fork, transcription machinery, or a DNA lesion to cause DNA breaks (El-Khamisy and Caldecott, 2006). Further information on topoisomerases and the removal of TOP1-CC can be found in **Section 1.6**.

1.4.1.3. Spontaneous base deamination

Certain nucleotides can spontaneously lose their exocyclic amine, causing conversion to a different nucleotide (Chatterjee and Walker, 2017). Whilst this process can occur randomly, the frequency increases on single-stranded DNA (ssDNA) during DNA replication, transcription, or recombination (Yonekura et al., 2009).

1.4.1.4. Abasic sites

Abasic sites (AP sites, also known as apurinic/apyrimidinic sites) are regions of DNA lacking a purine or pyrimidine base. They are one of the most frequent spontaneous lesions in DNA and can block DNA replication and translation (Boiteux and Guillet, 2004). Approximately

$1x10^4$ AP sites form daily, which is exacerbated by extreme pH and high temperature. The removal of AP sites by AP endonuclease can form single-strand DNA breaks (Lindahl, 1993; Thompson and Cortez, 2020).

1.4.1.5. Oxidative damage

As a by-product of cellular respiration, ROS are produced which serve important functions, such as acting as a cellular messenger and modulating immune system responses (Henle and Linn, 1997; Forman et al., 2010; Martinvalet and Walch, 2022). ROS are tolerated at low levels; however, ROS accumulation can cause oxidative base lesions and 2-deoxyribose modifications (AbdulSalam et al., 2016; Andrés Juan et al., 2021). Cells can trigger various mechanisms to limit ROS accumulation and DNA damage, such as reducing mitochondrial respiration to protect nearby cells or quenching excess ROS by anti-oxidant enzymes, such as superoxide dismutase (Murphy, 2009; Wang et al., 2018). ROS attack DNA bases and DNA backbones, causing DNA strand breaks (Hegde et al., 2012; Sharma et al., 2016). Due to the multiple functions of ROS as well as high ROS levels causing tissue damage, ROS has been implicated in many diseases, including some cancers, inflammatory and neurological diseases, and diabetes (Yang and Lian, 2020).

1.4.1.6. DNA methylation

Methyltransferases utilise methyl donors such as S-adenosylmethionine to spontaneously generate highly mutagenic methylated resides, which can cause nucleotide conversions (Lu, 2000). Methylation via alternative methyl donors are less harmful, but can still cause cytotoxic effects (Chatterjee and Walker, 2017). Unrepaired methylated DNA bases cause genomic instability by modifying coding outcomes of protein translation (Sriraman et al., 2020).

1.4.2. Exogenous DNA damage

1.4.2.1. Ionising radiation

Alpha, beta, gamma, neutrons, and X-rays are the types of ionising radiation (IR) present in our environment that can cause varying amounts of damage directly, or indirectly, to our DNA. IR can disrupt the molecular structure of DNA directly, leading to cell damage or cell

death (Chatterjee and Walker, 2017). IR can also cause indirect DNA damage by attacking surrounding water molecules to produce free radicals, such as hydroxyl and alkoxy, which can cause base lesions similar to that of ROS as well as forming DNA strand breaks (Vignard et al., 2013; Desouky et al., 2015).

1.4.2.2. Ultraviolet radiation

Ultraviolet (UV) radiation is classified into three categories based on wavelength range: UV-A (320-400 nm), UV-B (290-320 nm), and UV-C (190-290 nm) (Chatterjee and Walker, 2017). UV rays emanate from the sun and can be absorbed by DNA with maximal absorption occurring at 260 nm. Therefore, UV-C absorption by DNA is the most harmful, but as the ozone layer filters out a majority of emitted UV-C, most UV absorbed by DNA is UV-A and UV-B. Nevertheless, residual UV-C passing through the ozone layer can still cause considerable DNA damage by covalently linking adjacent pyrimidine dimers, producing lesions such as cyclobutene pyrimidine and pyrimidine (6-4) pyrimidone photoproducts (Hoeijmakers, 2009). These lesions are able to distort the DNA helix, which contributes to mutagenesis via improper DNA replication (Chan et al., 1985). UV-induced DNA damage is the leading cause of skin cancer worldwide, which can often emerge decades after initial UV exposure (Pfeifer, 2020).

1.4.2.3. Chemical agents

There are several chemical agents that can cause DNA damage. Tobacco smoke contains both alkylating agents and aromatic amines that cause DNA lesions (Scherer et al., 2010; Ma et al., 2019). Fossil fuels and automobile exhausts produce polycyclic aromatic hydrocarbons, which are known carcinogens producing reactive intermediaries in the liver that interact with DNA (Schoket, 1999; Siddens et al., 2015). Several strategies to treat a variety of cancers are focused on producing chemotherapeutics that predominantly target cancer cells (due to increased proliferation in cancer cells). These act by damaging DNA or inhibiting DNA repair (Chatterjee and Walker, 2017). Examples of this include crosslinking agents, such as cisplatin and psoralen (Yurkow and Laskin, 1991; Chválová et al., 2007), and TOP1 poisons, such as camptothecin (CPT) (Liu et al., 2000).

1.5. DNA Damage Response

Following DNA damage, the DNA damage response (DDR) is activated to maintain genomic stability. DDR consists of multiple signalling networks that recognise specific DNA lesions and recruit proteins modulating various responses, including DNA repair, chromatin remodelling, apoptosis, and cell cycle regulation. Some lesions are repaired efficiently, allowing DNA to return to a normal state. Other lesions are either repaired inefficiently, causing DNA to behave differently or DNA remains unrepaired, causing the cell to be triggered for apoptosis or senescence, thus eliminating unrepaired DNA. The various pathways are all unique from each other; however, there is overlap between the components used in each one. Two common pathways are the poly (ADP-ribose) polymerase (PARP) pathway and phosphatidylinositol 3 kinase-like kinase (PIKK) pathway.

1.5.1. Signal transduction induced by DNA damage

1.5.1.1. Poly (ADP-ribose) polymerase

ADP-ribosylation is a reversible post-translational modification catalysed by the ADP-ribosyltransferase (ART) protein superfamily, which use NAD^+ as a substrate to transfer single or multiple ADP-ribose (PAR) units onto target proteins and nucleic acids. PARP proteins are an ART member, which recognise DNA breaks via zinc-finger binding motifs (Palazzo et al., 2017). In the DDR, PARP1 and PARP2 are responsible for transferring multiple PAR units (PARylation), creating PAR chains on proteins close to DNA breaks, as well as PARylating themselves. PARylation changes the stability, function, and localisation of nearby proteins as well as allowing PARP to act as a scaffold for DDR components (Liu et al., 2017). Due to PARP's role in coordinating many DDR proteins, PARP inactivation in human cells has been linked to enhanced DNA damaging agent sensitivity (Gibson and Kraus, 2012). An important downstream factor of PARP is the PIKK enzyme Ataxia-telangiectasia mutated (ATM) (Aguilar-Quesada et al., 2007).

1.5.1.2. Phosphatidylinositol 3 kinase-like kinase

PIKK enzymes are a family of protein kinases that activate downstream mediator and effector proteins. The main enzymes are ATM and Ataxia-telangiectasia and Rad3-related

protein (ATR), which phosphorylate Ser/Thr-Glu motifs. ATM/ATR phosphorylation occurs through checkpoint kinase 1/2 (Chk1/Chk2), MAP kinase-activated protein kinase 2 (MK2), and H2A histone family member X (H2AX). ATM/ATR also autophosphorylate to increase their stability on DNA breaks. ATM is recruited to double-strand breaks (DSBs) via the MRE11-RAD50-NBS1 (MRN) complex. ATR is involved in repairing stalled replication forks and single-strand breaks (SSBs), with ATR recruitment dependent on replication protein A (RPA) and ATR interacting protein (ATRIP) (Wagh et al., 2020). Other PIKK enzymes with important DNA repair mechanism roles include DNA-dependent protein kinases (DNA-PKs), mTOR, serine/threonine-protein kinase SMG1, and transformation/transcription domain-associated protein (TRRAP) (Imseng et al., 2018).

1.5.2. Nucleotide base repair

1.5.2.1. DNA damage reversal

Small amounts of DNA damage can be directly reversed in an error-free manner. Photolyases can reverse lesions induced via UV radiation by using blue or near-UV light (Brettel and Byrdin, 2010). Alkylated bases can be corrected by two enzyme classes. The first enzyme class is O^6-alkylguanine-DNA alkyltransferases, which reverse O-alkylated lesions by transferring the alkyl group from oxygen of a DNA base to a cysteine residue located inside the enzyme's catalytic pocket (Pegg, 2011). The second enzyme class able to remove alkylated bases are α-ketoglutarate-dependent dioxygenases, which reverse N-alkylated bases via hydroxylation of alkyl group in an α-ketoglutarate and Fe^{+2}-dependent manner. The oxidised alkyl group is released as a formaldehyde, restoring the original structure of the nucleotide base (Falnes et al., 2007).

1.5.2.2. Base excision repair

Base excision repair (BER) corrects lesions that do not cause DNA helix distortion, such as oxidative deamination and AP site damage. DNA glycosylases, such as 8-oxoguanine glycosylase (Dizdaroglu et al., 2008), recognise and extract damaged bases. The gap created is then repaired by DNA polymerase (POL) β or γ, followed by ligation with DNA ligase I (LIG1) or LIG3 and X-ray repair cross complementing protein 1 (XRCC1) (Krokan and Bjoras, 2013).

1.5.2.3. Nucleotide excision repair

Nucleotide excision repair (NER) removes bulky or multiple base lesions, such as damage from chemotherapeutic agents or UV-induced lesions. There are two distinct NER branches: global genome NER (GG-NER) and transcription-coupled NER (TC-NER).

GG-NER takes place across the whole genome, whilst TC-NER occurs when transcription has stalled. Whilst both branches use the same pathway to cut and excise damaged bases, they are activated and recognised differently. GG-NER is activated by xeroderma pigmentosum, complementation group C (XPC) bound to UV excision repair protein Radiation sensitive 23B (RAD23B) and centrin 2 (CETN2). This complex is also bound to UV-damaged DNA damage-binding protein (UV-DDB) complex when repairing UV-induced lesions (Fousteri and Mullenders, 2008).

TC-NER is activated by RNA polymerase II stalled at a lesion, causing the recruitment of Cockayne syndrome protein A (CSA) and CSB, which assemble other TC-NER components. RNA polymerase II reverse translocates, exposing the lesion (Schärer, 2013).

Both pathways then converge onto the same mechanism by recruitment of transcription initiation factor II H (TFIIH), a complex that switches between transcription initiation and repair. TFIIH causes the unzipping of 30 nucleotides surrounding the lesion, which are then stabilised by xeroderma pigmentosum, complementation group A (XPA) and RPA. xeroderma pigmentosum, complementation group G (XPG) and excision repair cross-complementation group 1 (ERCC1) cleave at 3' and 5' ends, excising the 30 nucleotides surrounding the lesion. Following this, the gap is filled by POL δ, ε, or κ then sealed by LIG1 or LIG2 (Giglia-Mari et al., 2011).

1.5.2.4. Mismatch repair

Mismatch repair (MMR) repairs spontaneous base-base mispairing created during DNA replication. MMR uses the intact DNA strand as a template to repair the damaged strand. The lesion is detected and bound by MutS, which recruits MutL. This mediates downstream MMR effector proteins, such as MutH and UV repair protein D (UvRD). MutH is a type II restriction endonuclease that cleaves GATC sites, creating a DNA nick. This is followed by

excision of erroneous DNA by exonuclease I (EXO1). The gap created is stabilised by RPA, followed by new DNA synthesis and ligation by proteins such as POLδ and LIG1 (Chatterjee and Walker, 2017; Pećina-Šlaus et al., 2020).

1.5.2.5. Interstrand cross-link repair

Interstrand cross-links (ICLs) are lesions in which two bases from complementary strands are covalently linked. These occur due to crosslinking agents, such as cisplatin (Poklar et al., 1996). ICLs in replicating cells are repaired via the Fanconi anaemia (FA) pathway, whilst ICLs in non-replicating cells are repaired through FA-independent pathways, such as NER (Wang and Gautier, 2010; Williams et al., 2013).

1.5.2.6. Translesion synthesis

Translesion synthesis (TLS) polymerases are similar to DNA polymerases but have structural differences allowing them to bypass DNA lesions and synthesise DNA. TLS appears to cooperate with other DNA repair pathways, such as BER and NER (Sale, 2013).

1.5.3. DNA break repair

1.5.3.1. Single-strand break repair

Single-strand break repair (SSBR) can occur through three different pathways depending on the source of damage. In the long-patch pathway, SSBs are recognised by PARP1 which is PARylated, recruiting XRCC1 that acts as a scaffold for APEX nuclease (APE1), polynucleotide kinase-phosphatase (PNKP), aprataxin (APTX), and XRCC1. Flap structure-specific endonuclease 1 (FEN1) removes damaged 5' termini, aided by PARP1 and proliferating cell nuclear antigen (PCNA), forming a ssDNA gap that is filled in by POL β and POL δ/ε. The final step is ligation by LIG1 in association with PCNA and XRCC1.

In the short-patch pathway, damage recognition is by APE1, followed by recruitment of similar factors (Abbots and Wilson III, 2017) as the long-patch pathway. The gap formed is filled by POLβ, then ligated with LIG3, with XRCC1 associating with both POLβ and LIG3 (Brem and Hall, 2005). The third variant is DNA breaks involving topoisomerase 1, which will be discussed extensively in **Section 1.6**.

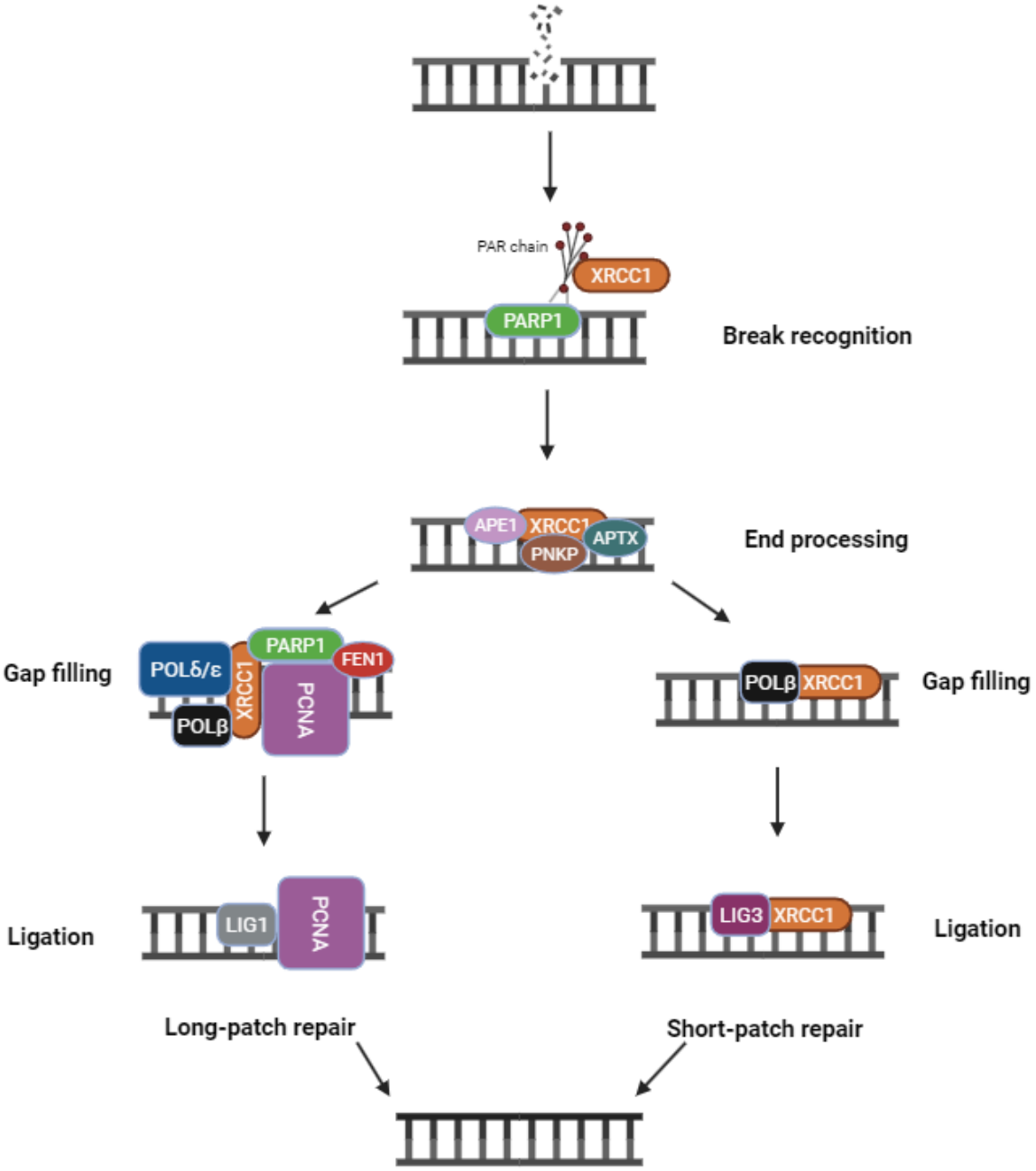

Figure 1.4: **SSBR mechanism**. SSB is recognised by PARP1, leading to the addition of PAR chains (PARylation) on PARP1. XRCC1 attaches to PAR scaffold, followed by recruitment of APE1, PNKP, and APTX for end processing. In the long-patch repair pathway, gap filling occurs via POLβ, POLδ/ε, PCNA, FEN1, and PARP1. DNA is ligated by LIG1 and PCNA. In the short-patch repair pathway, gap filling occurs via POLβ and XRCC1, followed by LIG3 and XRCC1 ligation. Figure adapted (Ray Chaudhuri and Nussenzweig, 2017; Thomas, 2022) and created in Biorender.com.

1.5.3.2. Double-strand break repair

DSBs are considered the most dangerous type of lesion as they can cause deletions of large chromosomal regions. There are an estimated 10 DSBs per day per cell, inducible by many factors, including IR, ROS accumulation, and errors in replication (Chang et al., 2017). The mechanisms involved in deciding the double-strand break repair (DSBR) pathway choice are poorly understood, but is thought to rely on chromatin environment and cell cycle phase (Scully et al., 2019).

1.5.3.2.1. Non-homologous end-joining

Non-homologous end-joining (NHEJ) is considered to be the less accurate form of DSBR due to the higher chance of mutation incorporation following repair, although it appears to be the preferred DSBR pathway outside of G2/S phases (Lieber, 2011). DSB activates tumour suppressor p53-binding protein 1 (53BP1), which recruits NHEJ repair components to the lesion site. Ku is the first protein to bind, forming a Ku:DNA complex, acting as a docking site. As there are two broken DNA ends, a Ku:DNA complex forms on both ends. The NHEJ components that dock to the complex include DNA-PKC, XRCC4, LIG4, XRCC4-like factor (XLF), Werner syndrome protein (WRN), Artemis, APTX and PNKP-like factor (APLF). Ku is pushed inwards by DNA-PKC, which phosphorylates nearby components including itself. DNA ends are processed to remove end blockage, followed by naked strand resection. The gaps left behind are filled by either POL μ (template-dependent) or POL λ (template-independent), followed by ligation with LIG4 (Chatterjee and Walker, 2017).

1.5.3.2.2. Homologous recombination

Homologous recombination (HR) is the more accurate DSBR mechanism; however, it can only take place in G2/S phase as it requires a nearby strand for repair. DSBs are recognised by the MRN complex, followed by ATM, which phosphorylates H2AX (γH2AX). This serves as an anchor for mediator of DNA damage checkpoint 1 (MDC1), which in turn is also phosphorylated by ATM. Phosphorylated MDC1 acts as a scaffold for E3 ligases RING finger protein 8 (RNF8) and RNF168. These two ligases stimulate H2AX ubiquitination, which serves as a docking site for 53BP1 and breast cancer type 1 susceptibility protein (BRCA1), initiating ubiquitination of C-terminal-binding protein interacting protein (CtIP). Other HR

components RPA and RAD51 then make their way to DNA, then DNA ends are resected via nucleolytic degradation in a 5'-to-3' manner, generating 3' overhangs. The initial resection occurs by the endonuclease activity of MRN aided by CtIP, followed by EXO1 or bloom helicase (BLM) with DNA replication helicase/nuclease 2 (DNA2) resection. RPA then coats the 3' overhang, which is displaced by RAD51, forming a nucleoprotein filament that invades a nearby duplex DNA (aided by BRCA2 and partner and localiser of BRCA2 (PALB2)). Template-strand invasion removes RAD51, allowing 3'-OH group to synthesise DNA by POL δ, κ, and ν. The Holliday junction is processed by the BLM-TOP3-RM1-RMI2 complex, GEN1 endonuclease, the MUS81-EME1 complex, and the SLX-SLX14 complex (Chatterjee and Walker, 2017).

1.5.3.2.3. Alternative end-joining

The exact mechanisms behind alternative end-joining (Alt-EJ) remain not fully understood. Alt-EJ shares factors and similar mechanisms to NHEJ and HR. DNA break is recognised by PARP1, followed by recruitment of MRE11 and CtIP. Gap filling occurs by POL θ, then ligation is by LIG1 or LIG3. Similar to HR, Alt-EJ is initiated by end resection, whilst it shares similarities with NHEJ by not requiring a homologous template as a guide for repair. Alt-EJ causes repair that is often error-prone and associated with large deletion, translocation, and chromosomal defects (Sallmyr and Tomkinson, 2018; Ackerson et al., 2021).

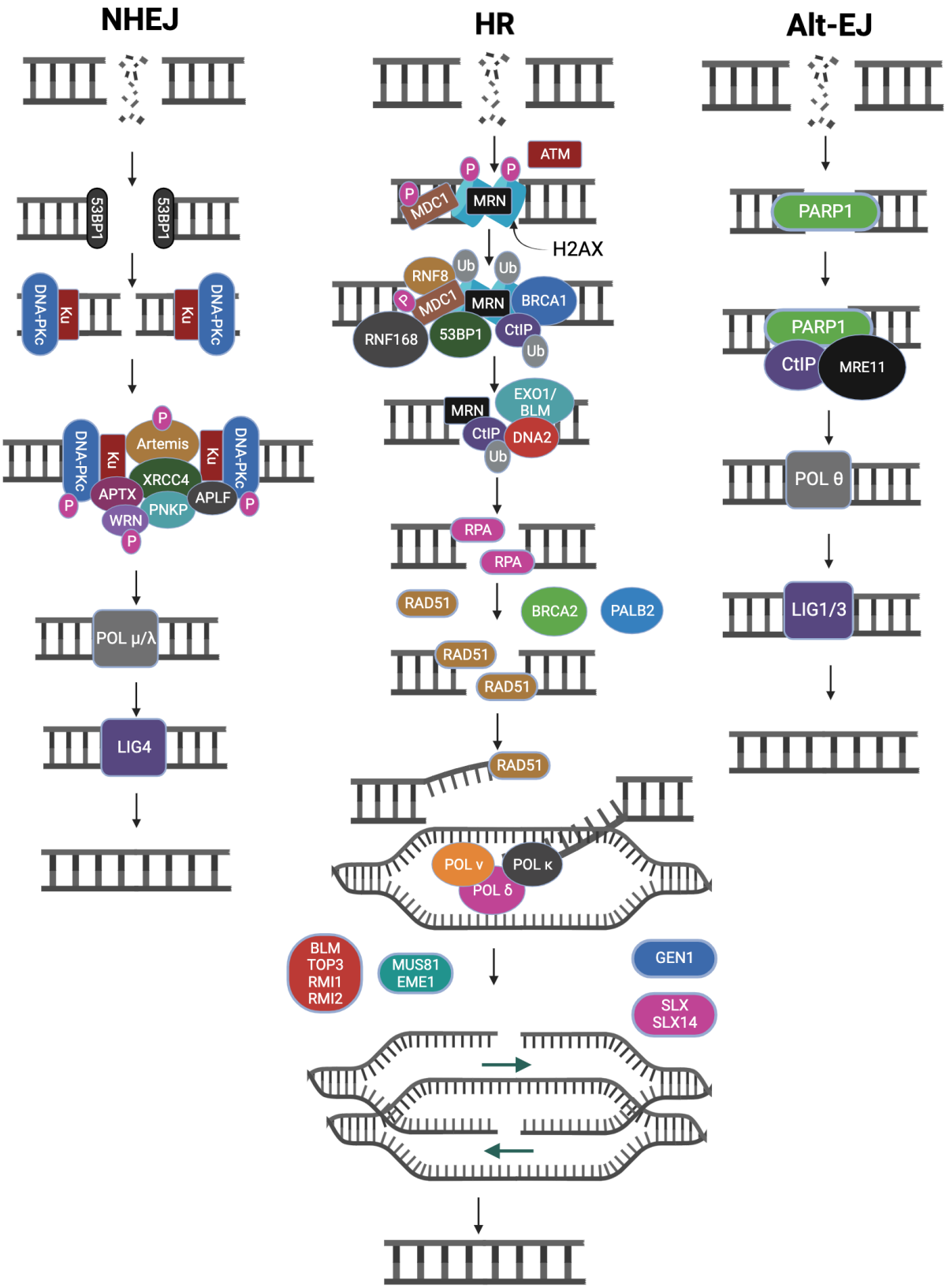
NHEJ
HR
Alt-EJ
53BP1
53BP1
DNA-PKc
Ku
Ku
DNA-PKc
P
Artemis
DNA-PKc
Ku
Ku
DNA-PKc
APTX
XRCC4
APLF
P
P
WRN
PNKP
P
POL μ/λ
LIG4
ATM
P
P
P
MDC1
MRN
H2AX
RNF8
Ub
Ub
P
MDC1
MRN
BRCA1
RNF168
53BP1
CtIP
Ub
MRN
EXO1/
BLM
CtIP
DNA2
Ub
RPA
RPA
RAD51
BRCA2
PALB2
RAD51
RAD51
RAD51
POL ν
POL κ
POL δ
BLM
TOP3
RMI1
RMI2
MUS81
EME1
GEN1
SLX
SLX14
PARP1
PARP1
CtIP
MRE11
POL θ
LIG1/3

Figure 1.5: DSBR mechanism. A) Non-homologous end-joining (NHEJ): 53BP1 recognises DSB, leading to recruitment of DNA-PKc and Ku to lesion site, with a Ku:DNA complex forming on both ends. DNA-PKc pushes Ku inwards and several NHEJ components bind to Ku:DNA complex: Artemis, PNKP, APLF, WRN, APTX, and XRCC4. DNA-PKc phosphorylates (P) nearby components and autophosphorylates itself. Gap filling is performed by POL μ/λ, then ligation by LIG4. **B)** Homologous recombination (HR): DSB is recognised by MRN complex and recruits ATM, which phosphorylates H2AX. This acts as an anchor for MDC1, which is phosphorylated by ATM. Phosphorylated MDC1 acts as a scaffold for RNF8 and RNF168, which stimulates ubiquitination (Ub) of H2AX. This serves as a docking site for 53BP1 and BRCA1, stimulating CtIP ubiquitination. Initial resection occurs via MRN and CtIP, followed by EXO1 (or BLM) followed by DNA2. RPA coats DNA overhang, which is displaced by RAD51 in association, with BRCA2 and PALB2, forming a RAD51 nucleoprotein filament. This filament invades a nearby duplex DNA, forming a D-loop, which primes DNA synthesis on the invading DNA strand, forming a Holliday junction that is processed by the BLM-TOP3-RMI1-RMI2 complex, the MUS81-EME1 complex, GEN1, and the SLX-SLX4 complex. Gap filling is by POL δ, κ, and ν. **C)** Alternative end-joining (Alt-EJ): DSB is recognised by PARP1, which recruits MRE11 and CtIP. Gap filling takes place by POL θ, followed by LIG1/3 mediated ligation. Figure adapted from Thomas et al., (2022) and created in Biorender.com.

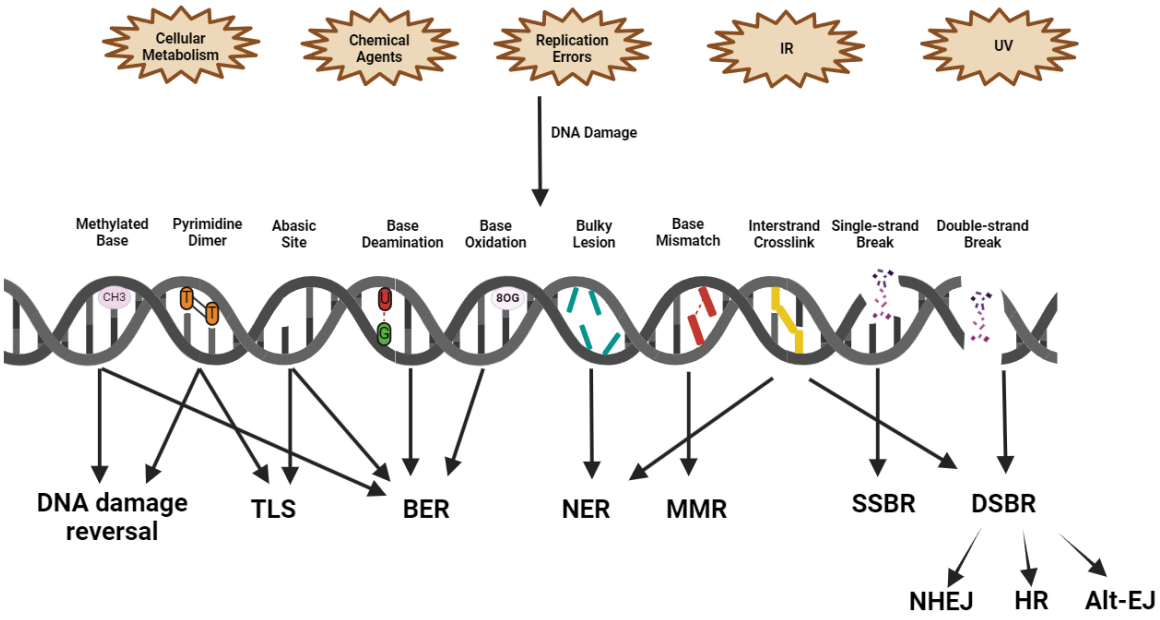

Figure 1.6: Summary of most common sources of DNA damage and their repair pathways. DNA is damaged through both endogenous sources, such as cellular metabolism and replication errors, as well as exogenous sources, such as chemical agents, ionising radiation (IR), and ultraviolet light (UV). These cause a wide variety of DNA damage, which require different repair pathways to resolve. Some types of DNA damage can be repaired through multiple different pathways. CH3 = methyl group, 8OG = 8-oxoguanine. TLS = translesion synthesis, BER = base excision repair, NER = nucleotide excision repair, MMR = mismatch repair, SSBR = single-strand break repair, DSBR = double-strand break repair, NHEJ = non-homologous end-joining, HR = homologous recombination, Alt-EJ = alternative end-joining. Figure created in Biorender.com.

1.5.4. Hypoxia in DDR

Hypoxia has been predicted to play a large role in maintaining genomic stability by influencing DDR; however, the exact contributions are highly complex and not fully understood, with published findings often contradicting each other. This is likely due to the different *in vitro* and *in vivo* models used when studying hypoxia as well as differences in classifying acute, moderate, and severe hypoxia. VHL/HIF pathway has been reported to play a role in DDR, although there are also several DDR mechanisms reliant on hypoxia that are independent of VHL-HIF.

Under acute hypoxia, ATM autophosphorylation (Bencokova et al., 2009) and ATR foci accumulation (Gibson et al., 2005) induces upregulation of downstream target genes that can protect cells from DNA damage triggered by stalled replication forks as well as activation of *BRCA1* (Gibson et al., 2006), *FANCD1*, and *FANCD2* (Scanlon and Glazer, 2014). Although hypoxia-induced activation of ATM/ATR is HIF-independent, there is a degree of crosstalk between DDR and HIF signalling during acute hypoxia. ATM phosphorylation stabilises HIF1α in human colorectal carcinoma cell line HCT116 (Cam et al., 2010), whilst ATR activity is required for HIF1α accumulation in human bone osteosarcoma epithelial cell line U2OS (Fallone et al., 2013). HIF1α is also indirectly stabilised in human hepatocellular carcinoma cell line HepG2 by DNA-PKs via phosphorylation of heat shock factor protein 1 (HSF1) and upregulation of heat shock proteins Hsp70/90 (Kang et al., 2008). This altogether suggests that acute hypoxia initiates DDR, protecting cells from damage.

DNA repair pathways have different responses to chronic hypoxia as well as the severity of hypoxia exposure. MMR gene transcription is reduced in cervical cancer cell line HeLa during severe hypoxia where it is independent of HIF (Mihaylova et al., 2003), as well as moderate hypoxia in human stem cells, although this reduction is HIF-dependent (Rodríguez-Jiménez et al., 2008). HR gene transcription and protein translation is reduced in both severe and moderate hypoxia in human stem cells (Bindra et al., 2005), human non-small cell lung carcinoma (NSCLC) cell line H1299 (Chan et al., 2008), and HeLa cells (Scanlon and Glazer, 2014), with some HIF-contribution in moderate hypoxia in HCT116 cells (To et al., 2006). The effect of hypoxia on NER is unclear, with conflicting results reported. Severe hypoxia in mouse fibroblasts has been shown to cause a downregulation in NER capability (Yuan et al.,

2000); however, NER appears to be more efficient in human breast cancer cell line MCF7 during moderate hypoxia (Madan et al., 2012). NER protein expression has been reported to be unchanged during hypoxia in mouse fibroblasts (Yuan et al., 2000; Mihaylova et al., 2003), although several NER genes contain HRE promoter regions, which HIF1α has been shown to bind to (Rezvani et al., 2009; Liu et al., 2012), suggesting that some NER proteins may be transcriptionally upregulated during hypoxia. Conversely, the NER protein ERCC1 has been reported to be transcriptionally and translationally downregulated during moderate hypoxia in human pharyngeal cancer cell line Detroit 562 (Dudás et al., 2014).

The remaining DNA repair pathways have not been as extensively studied in hypoxia as the previously mentioned ones. The transcriptional status of NHEJ genes is unclear, with some papers suggesting that NHEJ genes are upregulated in both moderate and severe hypoxia (Madan et al., 2012; Ren et al., 2013). A low fidelity DNA polymerase POLι, which is involved in TLS, has been shown to be upregulated under hypoxia-mediated HIF1α binding in many human cancer cell lines (Ito et al., 2006). NHEJ and TLS are both error-prone DNA repair pathways; therefore, their upregulation via hypoxia could promote genomic instability which is common in many cancers (Scanlon and Glazer, 2015). Lastly, chronic hypoxia has been linked to translational repression of BER proteins in H1299 cells (Chan et al., 2014).

1.5.4.1. Zebrafish model to study HIF contribution in DDR

A major issue with utilising cell lines for hypoxia-related mechanisms of DNA repair, especially in cancer, is the absence of surrounding tissues and cells contributing to the microenvironment, as well as culture adaptation of cells (Weissbein et al., 2019). This can be countered via *in vivo* models, such as zebrafish **(Section 1.3.4.2)**. Kim et al., (2020) demonstrated that *vll* $^{-/-}$ embryos are more susceptible to genotoxic stress, suggesting that the DNA repair function of human VHL **(Section 1.5.4.2)** was conserved in *vll*. However, *vhl* $^{-/-}$;*vll* $^{-/-}$ embryos were more resistant to genotoxic stress induced by CPT and X-ray. *vhl* $^{-/-}$;*vll* $^{-/-}$ embryos had greater *phd3:*GFP expression, correlating with expression levels of Hifα, suggesting that Hifα is responsible for the protection, and that the Hif modulatory role of human VHL was conserved in zebrafish Vhl. Pharmacological upregulation of Hifα via Phd inhibitor JNJ-42041935, or by injecting constitutively active forms of Hif1α/Hif2α, protected WT embryos from CPT-induced apoptosis. Therefore, DNA repair defects in *vll* $^{-/-}$ embryos

are countered by Hif activation in *vhl* $^{-/-}$;*vll* $^{-/-}$ embryos. High Hif expression has also been shown to overcome DNA repair defects in zebrafish models with specific DNA repair genes eliminated, such as *brca2* $^{-/-}$ embryos and *atm* deficient embryos. Interestingly, *vhl* $^{-/-}$;*vll* $^{-/-}$ embryos demonstrated greater resistance to genotoxic stress than WT embryos whereby Hifα was exogenously upregulated, suggesting Vhl/Vll are also responsible for Hif-independent mechanisms of DNA repair. Understanding the balance between Hif-modulation via Vhl and DNA repair via Vll might be crucial for a greater understanding of ccRCC cancer initiation.

1.5.4.2. HIF-independent mechanisms of VHL in DDR

The role of VHL in regulating HIF levels has been well established; however, HIF-independent roles of VHL have been identified suggesting that VHL has a role in maintaining genomic stability.

Metcalf et al., (2014) has recently identified a HIF-independent role of VHL in DSBR. In response to DSBs, nuclear redistribution and K63-ubiquitylation of VHL occurs. This ubiquitylation occurs via suppressor of cytokine signalling 1 (SOCS1) protein, which has previously been found to interact with VHL for degradation of Janus-kinase 2 (JAK2), a non-receptor tyrosine kinase promoting cellular proliferation (Russell et al., 2011). SOCS1 has also been associated with ATM in cells undergoing signal transducer and activator of transcription 5 (STAT5)-mediated senescence, linking SOCS1 to DDR (Calabrese et al., 2009). Ubiquitylation is often associated with degradation; however, VHL was not degraded following K63-ubiquitylation (Metcalf et al., 2014). K63-linked chains have previously been identified with regulating signalling pathways, including DNA repair (Aquila and Atanassov, 2020). VHL overexpression in cells caused an increase in γH2AX baseline levels, indicating enhanced recruitment of DSBR components. These effects were all seen in an oxygen-independent manner, confirming that HIF is not involved in these mechanisms, suggesting that genome stability in ccRCC models has a partial HIF-independent contribution. Furthermore, 786-O cells, in which VHL is mutated, were shown to have reduced levels of both γH2AX and phosphorylated Chk1 (pChk1). Upstream of γH2AX, *VHL* inactivation was also shown to cause reduced expression of phosphorylated ATM after DNA damage was induced, as well as an impairment of MRE11 foci. Therefore, this suggests a defect in MRN

complex-dependent DDR and a defect in the recruitment or retention of repair proteins to DSBs (Metcalf et al., 2014). In a neutral comet assay, which only measures DSBs (Roy et al., 2021), 786-O cells resupplied with functional VHL had fewer unrepaired DSBs following IR treatment. This effect was only seen in cells after a long recovery stage, suggesting VHL is contributing to the later stages of HR (Metcalf et al., 2014).

1.6. Tyrosyl-DNA phosphodiesterase 1 and topoisomerase 1

1.6.1. Structure and mechanism of TDP1 and TOP1 protein function

Human tyrosyl-DNA phosphodiesterase 1 (TDP1) is a 68 kDa protein, predominantly located in the nucleus, consisting of two domains: an N-terminal domain important for the recruitment of TDP1 to damaged chromatin, and a catalytic C-terminal domain (Davies et al., 2002). TDP1 translocates to the nucleus via two nuclear localisation sequences: NLS1-H56 to P74 and NLS2-P216 to P223 (Das et al., 2010; Dexheimer et al., 2012). TDP1 also localises to the mitochondria, but the mechanism behind this is not fully understood (Holt, 2009). TDP1 belongs to the phospholipase D (PLD) superfamily, which share a similar role in catalysing a two-step phosphoryl transfer reaction via the formation of covalent phosphoenzyme intermediates (Gottlin et al., 1998; Davies et al., 2002). TDP1 is unique from other PLD members as it contains two catalytic HKN motifs ($H_{263}K_{265}N_{283}$ and $H_{493}K_{495}N_{516}$), unlike other PLD members containing two HKD motifs (Pommier et al., 2014).

DNA is tightly packed in nuclei, but is unwound by helicases during transcription and replication as well as by ATPase translocase motors during chromosomal replication and segregation (Schvartzman et al., 2013; Ma and Wang, 2016; Chand et al., 2020). DNA is unable to rotate freely around itself, so the relaxation of DNA causes overtwisting, also known as supercoiling. This can cause damage to DNA structure, such as DNA deletion (Champoux, 2001) plus blocking transcription and replication machinery (Pommier et al., 2016). Human cells encode for six topoisomerases (TOPs) divided into three groups: Type IA (TOP3α and TOP3β), type IB (TOP1 and TOP1mt), and type IIA (TOP2α and TOP2β) (Pommier et al., 2016). TOP1 is the most well-characterised TOP and is closely linked to TDP1 function, so I will only discuss TOP1.

TOP1 resolves supercoiling by covalently binding to 5’ DNA terminus via a TOP1 tyrosine residue in a transesterification mechanism, cleaving one strand of DNA. This forms an intermediate structure called TOP1-CC. The binding of TOP1 to DNA forms a transient DNA break, which is easily reversible to avoid DNA strand breakage; however, the removal of TOP1-CC can stall. SSBs and DSBs can form if stalled TOP1-CC collides with a replication fork, transcription machinery, or if TOP1-CC is in the vicinity of DNA lesions **(Figure 1.7)** (El-Khamisy and Caldecott, 2006).

TDP1 cleaves the phosphodiester bond at the DNA 3’-end linked to a tyrosyl moiety. This forms an intermediate complex whereby the cleaved substrate is bound to TDP1 forming a phosphoenzyme intermediate, thus removing TOP1 from DNA. TDP1 subsequently hydrolyses the phosphoenzyme intermediate, leading to the release of DNA and its subsequent repair (Kawale and Povirk, 2018).

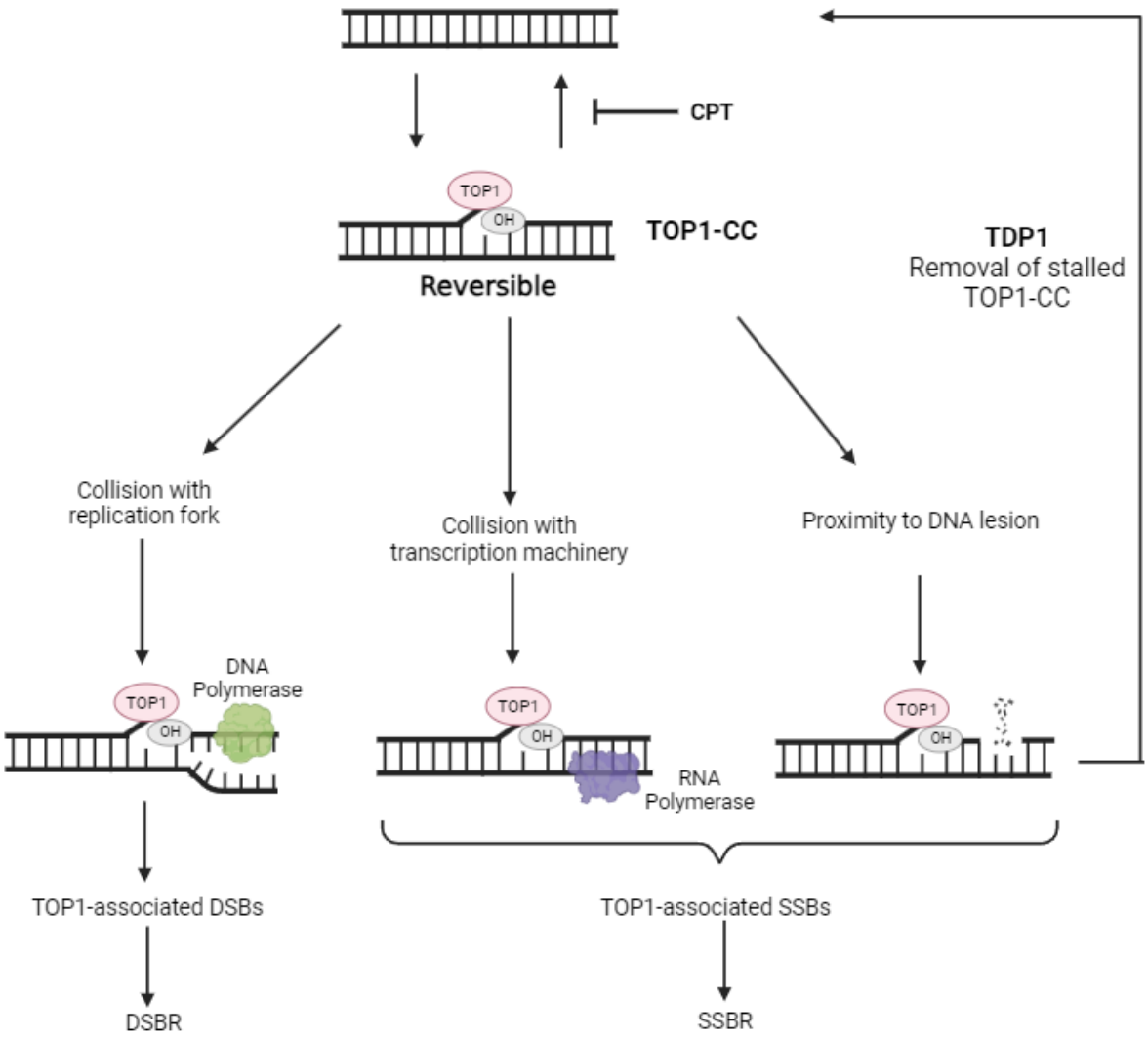

Figure 1.7: TOP1 relieves torsional stress by forming transient DNA breaks. TOP1 prevents DNA supercoiling by forming TOP1-CC. This complex formation is often reversible but can form permanent single-strand breaks (SSBs) or double-strand breaks (DSBs) upon collision with replication fork, transcription machinery, or if the complex is located close to a DNA lesion. In addition, TOP1 poisons, such as CPT, prevent the removal of TOP1 from DNA, increasing the likelihood of permanent DNA breaks forming. TDP1 removes stalled TOP1-CC. Figure adapted from El-Khamisy and Caldecott (2006) and created in Biorender.com.

1.6.2. Clinical relevance of TDP1

High expression of TDP1 in human cells has been associated with a significant reduction in CPT-induced DNA damage. Resistance to CPT is often encountered in NSCLC patients (Chiu et al., 2018), which has been attributed to increased expression and activity of TDP1 (Liu et al., 2007). Similarly, TDP1 overexpression in human cells has been shown to counteract both TOP1 and TOP2 associated DNA damage (Barthelmes et al., 2004; Nivens et al., 2004). In addition, TDP1 overexpression has been associated with enhanced protection against topotecan, a CPT-based TOP poison. This lead to the use of the TDP1/TOP1 ratio as a predictive biomarker for topotecan responses in small cell lung cancer (Meisenberg et al., 2014). Overall, it has been demonstrated in several studies that TDP1 can enhance resistance to TOP1 poisons.

Due to high TDP1 expression correlating with increased resistance to TOP1 poisons, several studies have investigated the impact of TDP1 downregulation in human cells to resensitise previously resistant cancer cells to TOP1 poisons. Cancer cells deficient for TDP1, or depleting TDP1 in CPT-resistant cancer cell lines demonstrated increased sensitivity to CPT (Alagoz et al., 2014). This has also been shown in non-cancerous cell lines, such as HEK293, whereby TDP1 depletion increases sensitivity to CPT treatment (Zhang et al., 2022). Several TDP1 inhibitors are currently under development, although there are no validated models or clinical trials currently under way (Khomenko et al., 2020; Munkuev et al., 2021).

ccRCC is commonly characterised by enhanced resistance to DNA damaging agents, including TOP1 poisons (Fizazi et al., 2003; Feldman et al., 2008). The mechanisms behind this enhanced resistance are not fully understood, so I will be investigating TOP1-relevant repair mechanisms, including TDP1 activity, in a VHL-defective ccRCC cell line.

1.7. Nuclear mitotic apparatus protein

1.7.1. Structure and mechanism of NuMA protein function

Nuclear mitotic apparatus (NuMA) protein is a 238 kDa protein (Yang et al., 1992) consisting of a globular head and tail containing S/TPXX motifs required for DNA binding and found in gene regulatory proteins (Ludérus et al., 1994). The globular heads are separated by a discontinuous 1500 amino acid coiled-coil domain (Yang et al., 1992). NuMA is localised to the nucleus during interphase, but during cell division it rapidly translocates to the mitotic spindle where it is crucial for spindle pole positioning and orientation (Merdes et al., 1996; Lorson et al., 2000; Du and Macara, 2004; Kiyomitsu and Boerner, 2021). PARP3 catalyses PARylation in association with tankyrase 1 and NuMA, which aids in stabilising mitotic spindles and maintaining telomeric integrity (Chang et al., 2005; Boehler et al., 2011).

NuMA appears to be involved in chromatin remodelling, which was initially identified by NuMA impacting chromatin organisation (Lelièvre et al., 1998). Moreover, NuMA was found to functionally interact with the ISWI ATPase chromatin remodeller SNF2h/SMARCA5, which is important for DSBR (Erdel et al., 2010). This interaction occurs at sites of DNA damage, suggesting a role for NuMA in genome maintenance, as evidenced by NuMA depletion in cells causing reduced chromatin decompaction, less focal recruitment of HR repair factors, and increased sensitivity to DNA cross-linking agents (Vidi et al., 2014).

NuMA consists of three isoforms: long, middle, and short. Long and middle isoforms are localised to mitotic spindles during metaphase, whilst the short isoform is distinctly localised to the cytoplasm (Wu et al., 2014). The short isoform has been identified as a potential tumour suppressor as its downregulation has been identified in various cancer cell lines. The overexpression of NuMA's short isoform is sufficient to inhibit cell proliferation and colony formation, whilst whole-genome sequencing identified decreased expression of the proto-oncogene MYB proto-oncogene like 2 (MYBL2) when NuMA's short isoform was overexpressed (Qin et al., 2017).

DSBs are processed by either NHEJ (error-prone) or HR (high fidelity) (Shrivastav et al., 2008). p53-binding protein 1 (53BP1) is a DNA repair protein that prevents excessive resection at DNA ends, thus 53BP1 promotes NHEJ (Callen et al., 2013). NuMA interacts and colocalises with 53BP1, thereby inactivating 53BP1 by limiting its diffusion (Moreno et al., 2019). DNA damage causes ATM to phosphorylate NuMA at serine 395 (S395), which releases NuMA's interaction with 53BP1 (Matsuoka et al., 2007; Moreno et al., 2019). DSBs induce chromatin marks, which are recognised by 53BP1, causing them to accumulate and form 53BP1-repair foci that promote NHEJ. Therefore, 53BP1 mobility is increased in response to DNA damage as NuMA is no longer able to sequester 53BP1. High levels of NuMA predict better patient survival as NHEJ pathway is suppressed, so patients are more sensitive to chemotherapeutics (Moreno et al., 2019).

The El-Khamisy lab have recently characterised NuMA as a novel TDP1-interacting protein. Unrepaired SSBs activate PARP1, causing NuMA-dependent recruitment of SSBR proteins, such as TDP1 and XRCC1, to damaged chromatin, as well as enhancing transcription of SSBR proteins. This function of NuMA is mediated by the interaction of NuMA long isoform's C-terminal globular domain with SSBR machinery (Ray et al., 2022). The multiple functions of NuMA are summarised in **Figure 1.8.**

1.7.2. Clinical relevance of NuMA

Depletion of NuMA causes embryonic lethality in mice due to aberrant spindle pole formation (Silk et al., 2009). Whilst the role of NuMA in DNA repair has been discussed previously, its clinical significance has not been properly established in humans. However, owing to its role in recruiting DNA repair factors to sites of DNA damage, NuMA depletion in human cells is likely to be related to DNA-repair deficiency disorders. In addition, increased expression of NuMA may be related to enhanced chemoresistance due to increased recruitment of DNA repair factors.

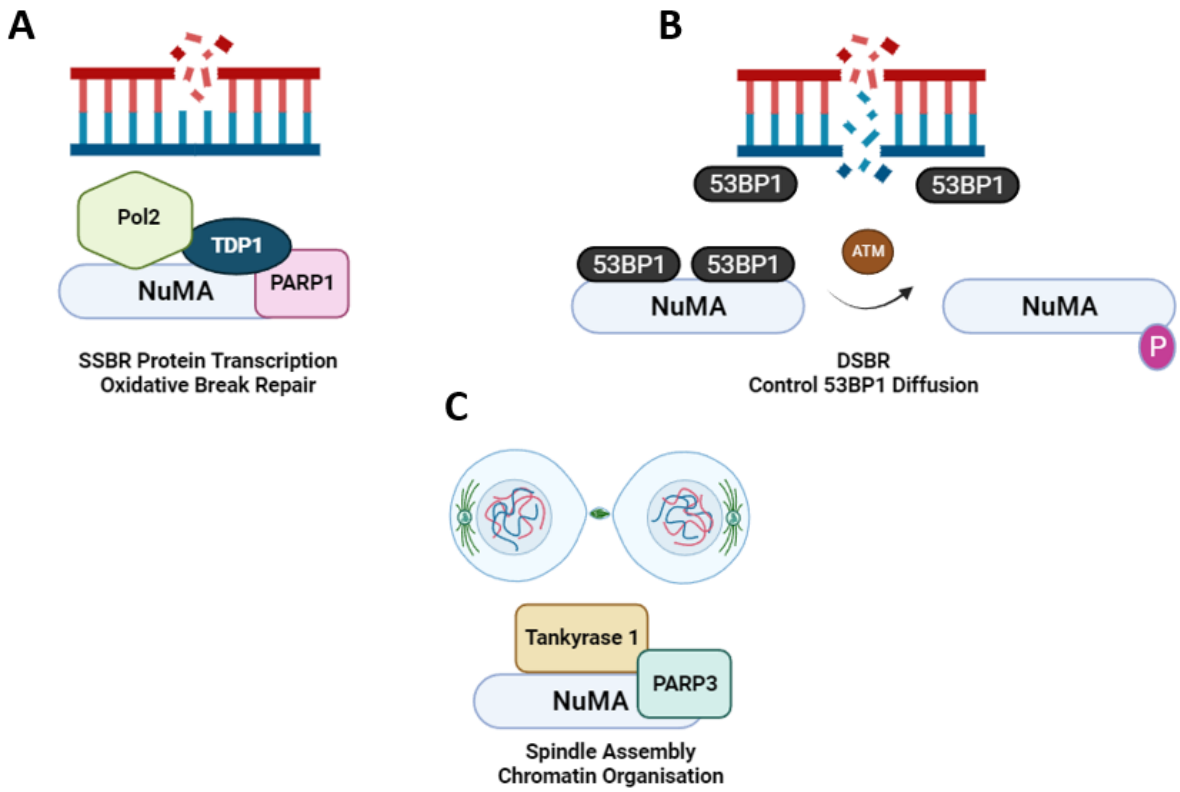

Figure 1.8: NuMA has distinct functions in DNA break repair and chromatin remodelling. A) Oxidative stress activates PARP1, causing NuMA-dependent recruitment of single-strand break repair (SSBR) proteins, such as TDP1, to sites of damaged chromatin, as well as enhancing SSBR-protein transcription by modulating RNA polymerase II (Pol2). **B)** NuMA interacts with 53BP1 limiting its diffusion. DSB activates ATM, which phosphorylates NuMA, releasing 53BP1, which is recruited to DNA lesions for DSBR via NHEJ. **C)** NuMA ensures proper mitotic function and genomic integrity by binding PARP3 and tankyrase 1, causing mitotic spindle stabilisation and maintaining telomeres. Figure adapted from El-Khamisy (2023) and created in Biorender.com.

1.8. Thesis aims

1.8.1. Establish response of ccRCC cell line RCC4 to genotoxic stress

ccRCC remains a difficult cancer to treat due to its resistance to radiotherapy and chemotherapy (Acharya et al., 2022). Genomic instability has been identified as a potential hallmark of cell lines exposed to hypoxia due to transcriptional and translational downregulation of DSBR and SSBR components (Mihaylova et al., 2003; Scanlon and Glazer, 2014). DDR following hypoxic exposure has both HIF-dependent and HIF-independent contributing factors, with HIF appearing to be involved more during moderate hypoxia, whilst DDR changes during severe hypoxia are more likely to be HIF-independent (Mihaylova et al., 2003; To et al., 2006; Rodríguez-Jiménez et al., 2008). Furthermore, exposure time to hypoxia has a markedly different impact on DDR, with acute hypoxia inducing upregulation of DDR genes, whilst chronic hypoxia causes downregulation of DDR genes (Bindra and Glazer, 2005; Gibson et al., 2005; To et al., 2006).

ccRCC patients commonly have mutations in *VHL*, causing a pseudohypoxic effect (Brugarolas, 2014). Whilst this is similar to hypoxic exposure of normal cells, there are unique pathways implicated in ccRCC progression that cannot be recapitulated by hypoxic exposure due to the hypoxia-independent contributions of VHL and other ccRCC mutations. Therefore, understanding the molecular mechanisms behind enhanced radio- and chemoresistance requires utilising a ccRCC cell line, such as RCC4, which has *VHL* inactivated (RCC4-VHL -/-), causing constitutive upregulation of HIF1α and HIF2α, mimicking the phenotypes observed in ccRCC patients (Maxwell et al., 1999).

ccRCC patients are resistant to chemotherapy and radiotherapy, thus I will establish whether these phenotypes are recapitulated in RCC4-VHL -/- by treating the cells with chemotherapeutic agents and IR, then using DNA damage assays to assess their sensitivity. As a comparison, I will also use RCC4 cells with functional VHL resupplied (RCC4-VHL WT) to see if functional VHL causes clear differences in cellular response to DNA damaging agents.

1.8.2. Identify novel DNA repair proteins modulated in RCC4-VHL -/-

Although some proteins implicated in DNA repair have been identified as being modulated under hypoxia, most of these studies did not utilise ccRCC cell lines. Therefore, unanswered questions remain regarding the molecular characteristics of DDR in ccRCC. Once I have established the chemosensitivity and radiosensitivity of RCC4-VHL -/- cells, I will assess the gene and protein expression of novel DNA repair proteins that have not been previously investigated. This will include components of SSBR and DSBR, such as TDP1 and PARP1 (Chowdhuri and Das, 2021), as well as NuMA which has been recently identified as a novel protein in DNA repair (Ray et al., 2022).

Zebrafish are a useful model to study mechanisms of therapy resistance due to the presence of the tumour microenvironment (TME), which cell lines lack. Therefore, zebrafish provide a better understanding into how different cells, proteins, and soluble factors interact with each other, which can impact cellular response to genotoxic agents (Sturtzel et al., 2021; Weiss et al., 2022). Although the zebrafish Vhl/Hif pathway is well-conserved, there remains key differences between the human and zebrafish pathway, such as duplication of Vhl and Hif genes (Rytkönen et al., 2013; Kim et al., 2020). Thus, differences in the molecular characteristics of the DDR may exist between human cells and zebrafish, so it is important to characterise DDR in both ccRCC models. Kim et al., (2020) recently identified that Hif upregulation in zebrafish embryos was sufficient to increase resistance to genotoxic agents. Therefore, I will investigate whether there is a link between HIF expression and any DNA repair proteins of interest in RCC4-VHL -/- cells.

Overall, I hypothesise that increased expression of SSBR and DSBR proteins mediate enhanced resistance to DNA damaging agents in ccRCC.

Chapter 2 Materials and Methods

2.1. Standard solutions

10x Tris-buffered saline (TBS)

24.2 g tris base and 81.8 g NaCl was added to 500 ml ddH_2O, followed by adjusting the pH to 7.9 by the addition of concentrated hydrochloric acid. The solution was made up to a final volume of 1 L using ddH_2O. The solution was stored at room temperature.

1x TBST

900 ml of ddH_2O was added to 100 ml of 10x TBS, followed by 1 ml of Tween® 20 (Sigma-Aldrich, P7949). The solution was stored at room temperature.

10x Running buffer

30.3 g tris base, 187.7 g glycine, and 10 g SDS was added to 1 L of ddH_2O, then the solution was stored at room temperature. Running buffer was diluted to 1x by mixing 100 ml of 10x running buffer and 900 ml ddH_2O.

1x Transfer buffer

200 ml of Trans-Blot® Turbo™ 5x Transfer Buffer (Bio-Rad, 10026938) was mixed with 600ml ddH_2O and 200 ml ethanol to make 1 L of 1x transfer buffer, which was stored at room temperature.

1 M Tris pH 6.8

65.57 g tris base was added to 400 ml ddH_2O, followed by adjusting the pH to 6.8 using concentrated hydrochloric acid. The solution was made up to a final volume of 500 ml using ddH_2O. The solution was stored at room temperature.

1.5 M Tris pH 8.8

90.8 g tris base was added to 400 ml ddH_2O, followed by adjusting the pH to 8.8 using concentrated hydrochloric acid. The solution was made up to a final volume of 500 ml using ddH_2O. The solution was stored at room temperature.

10% Ammonium persulphate (APS)

1 g APS was dissolved in 10 ml ddH_2O, then 1 ml aliquots were stored at -20°C.

10% Sodium dodecyl sulphate (SDS)

100 g SDS was dissolved in 1 L ddH_2O, then the solution was stored at room temperature.

5X Protein loading buffer

The buffer was made as per **Table 2.1** and stored at room temperature.

Component	Stock concentration	Final concentration	Amount required/50ml
SDS	-	10%	5g
Tris HCl pH 6.8	1M	250mM	12.5ml
Glycerol	100%	25%	12.5ml
β-mercaptoethanol	100%	12.5%	6.25ml
Bromophenol blue	-	0.5%	250mg
ddH_2O	-	-	Up to 50ml

Table 2.1: 5x Protein loading buffer. Constituents and concentrations used to make 5x protein loading buffer.

1x Phosphate-buffered saline (PBS)

1 PBS tablet (Fisher Scientific, 11510546) was added to 500 ml ddH_2O. Solution was autoclaved at 121 degrees for 15 mins under 15 psi pressure, then stored at either room temperature or 4°C.

5% Milk

1 g dried skimmed milk (Marvel, 711210) was added to 20 ml TBST and mixed well.

5% Bovine serum albumin (BSA)

1 g BSA (Sigma-Aldrich, A3059) was added to 20 ml TBST and mixed well, followed by filter sterilisation to remove bacterial contaminants.

0.25% (w/v) Trypsin

1 g trypsin 1:250 powder (Gibco, 27250-018) was added to 20 ml PBS, then filter sterilised. This was topped up with 380 ml autoclaved PBS, then stored at 4°C.

4% (w/v) Ethylenediaminetetraacetic acid (EDTA)

27.4 ml 0.5 M filter sterilised EDTA was added to 72.6 ml autoclaved ddH_2O. The solution was stored at 4°C.

Trypsin/EDTA

37.5 ml autoclaved PBS, 30 ml 0.25% (w/v) trypsin, and 7.5 ml 4% (w/v) EDTA were mixed and stored at 4°C.

LB agar

14 g LB agar was dissolved in 400 ml ddH_2O and autoclaved, then stored at room temperature.

LB broth

10 g LB broth powder in 500 ml ddH_2O and autoclaved, followed by storing at room temperature.

Radioimmunoprecipitation assay (RIPA) buffer

RIPA buffer was prepared as shown in **Table 2.2**, then stored at 4°C for up to one year.

Component	Stock concentration	Final concentration	Amount required/50ml (ml)
NaCl	5M	150mM	1.5
NP-40	10%	1%	5
Sodium deoxycholate	10%	0.5%	2.5
SDS	10%	0.1%	0.5
Tris pH8.0	1 M	50mM	2.5
ddH_2O	-	-	38

Table 2.2: RIPA buffer. Constituents and final concentrations used in making RIPA buffer.

10x Tris-borate-EDTA (TBE) buffer

108 g tris base was added to 55 g boric acid and 40 ml 0.5 M EDTA (pH 8.0). The solution was made up to a final volume of 1 L using ddH_2O. The solution was stored at room temperature. 1x TBE buffer was prepared by mixing 100 ml TBE buffer with 900 ml ddH_2O.

2.2. Cell culture

2.2.1. Cell lines

The following utilised cell lines were grown as monolayers:

Cell Line	Source
RCC4 plus VHL (RCC4-VHL WT)	ECACC (UK)
RCC4 plus vector alone (RCC4-VHL -/-)	ECACC (UK)
RCC4-VHL -/- ; HIF2α -/-	This thesis
MRC5	El-Khamisy Lab

Table 2.3: Cell lines. The names and origin of all cell lines used throughout this project.

RCC4 cell lines were verified for VHL and HIFα status via western blotting **(Section 2.5)** and RT-qPCR **(Section 2.6).**

2.2.2. Cell culture solutions

Dulbecco's Modified Eagle Medium (DMEM)

DMEM (Sigma-Aldrich, D6546) was complemented with 10% FBS (Sigma-Aldrich, F7524) and 2 mM L-glutamine (Gibco, 25030081), along with either 0.5 mM G418 (Gibco, 11811031 or 10131027) for RCC4 cells, or 100 U/ml penicillin-streptomycin (Gibco, 15140122) for MRC5 cells. G418 was utilised as a positive selector for the pcDNA3 vector, conferring resistance to neomycin, which has been stably transfected into RCC4 cells. The vector encodes either functional VHL (pcDNA3-VHL) or is empty (pcDNA3). Media was stored at 4°C for no longer than one month and warmed to 37°C before use.

2.2.3. Maintenance of cells

Cells were maintained in T75 flasks and kept in an incubator at 37°C, 5% CO_2. RCC4 cells were passaged once a week, usually 1:10. 3 ml trypsin/EDTA was added to the flask. Cells were discarded once they had reached passage 40. Stock solutions of cells were kept in

liquid nitrogen at low passage numbers in cryotube vials (Thermofisher, 377267) in 90% complete media, 10% dimethyl sulfoxide (DMSO). Vials were thawed briefly at 37°C, then the cells were added to media directly in a T75 flask. The following day, fresh media was added to the flask to remove residual DMSO. Cells were passaged three times after thawing before proceeding with any experimental work.

2.2.4. Cell counting

Cells resuspended in their appropriate growth media were checked for cell density to allow for plating cells accurately. The concentration was established by counting 10 µl of cell suspension under a haemocytometer (Neubauer, AC1000).

2.3. Zebrafish husbandry and maintenance

All adult zebrafish were raised and maintained at the Bateson Centre aquarium facilities at the University of Sheffield under standard conditions (14 hours of light and 10 hours dark cycle, 28 °C).

2.3.1. Zebrafish strains and lines

Two transgenic lines were used throughout this project, originating from the hypoxia reporter line Tg(*phd3*:EGFP)$^{i144/i144}$, whereby GFP is expressed under high expression of the Hif-target gene *phd3* starting from 28 hpf (Santhakumar et al., 2012). These lines were created and validated by Marchi et al., (2020). *vhl*$^{hu2117/+}$;*phd3:*eGFP$^{i144/i144}$ was created by crossing the *vhl*$^{hu2117/+}$ line with Tg(*phd3*:eGFP)$^{i144/i144}$. This fish line was incrossed to generate *vhl*$^{hu2117/+hu2117}$;*phd3:*eGFP$^{i144/i144}$, referred to as *vhl* mutants (*vhl*$^{-/-}$).

The second transgenic line used was *vhl*$^{hu2117/+}$;*vll*$^{i216/i216}$; *phd3*:eGFP$^{i144/+}$. This was created by crossing *vhl*$^{hu2117/+}$;*phd3:*eGFP$^{i144/i144}$ with *vll*$^{i216/i216}$. This fish strain was incrossed to generate *vhl*$^{hu2117/hu2117}$;*vll*$^{i216/i216}$;*phd3*:eGFP$^{i144/+}$, referred to as *vhl;vll* mutants (*vhl*$^{-/-}$;*vll*$^{-/-}$).

The Nacre line, which lacks pigmentation owing to defects in melanophore development (Lister et al., 1999), was used for imaging apoptosis and eye size after drug treatments. The final line used was *tdp1*$^{+/+}$ as a control for functional Tdp1, created by Ruth Thomas.

2.3.2. Embryo collection and maintenance

Trays of marbles were placed in tanks overnight to stimulate zebrafish mating, then embryos were collected the following morning using a fine sieve and aquarium water. Embryos were maintained in 1x E3 medium (5 mM NaCl, 0.17 mM KCl, 0.33 mM $MgCl_2$, 0.33 mM $CaCl_2$, pH 7.2) with 0.0001% methylene blue at 28°C. A maximum of 60 embryos were housed per 10 cm petri dish, in approximately 30 ml 1x E3 medium. Unfertilised or unhealthy embryos were removed daily. Embryos were kept to no longer than 5.2 dpf, and then discarded in accordance with UK Home Office Legislation (License number I01740898). Embryos were anaesthetised, if necessary, by adding 1 ml of 0.4% tricaine (PharmaQ) to a 10 cm petri dish. They were then transferred to fresh 1x E3 medium for recovery.

2.3.3. Drug treatments

Embryos were transferred to 6-well plates for drug treatments. Drugs were made up in 1x E3 medium, then added directly to each well. All drugs used were dissolved in DMSO.

2.3.4. Zebrafish microscopy

Whole embryos and fluorescent images were taken using a Leica M165FC fluorescent stereo microscope, attached to a digital colour camera (DFC310X) and a Leica external fluorescent light source (EL6000). Images were taken with Leica Application Suite v 4.3.0. Live embryos were anaesthetised in tricaine methanesulfonate (MS-222) before imaging and placed on a drop of 2% methylcellulose.

2.4. Whole-cell protein extraction

2.4.1. Lysis buffer-based extraction

2.4.1.1. Mammalian cells

Adherent cells were placed on ice, then washed 1x with ice-cold PBS. An appropriate volume of RIPA buffer supplemented with cOmplete™, EDTA-free protease inhibitor cocktail (Roche, 5056489001) was added, followed by scraping with a cell scraper. Basemuncher endonuclease (Abcam, ab2700949) was added to RIPA buffer at a concentration of 25 U/ml to reduce lysate viscosity when performing western blot. For preservation of phosphorylated proteins, PhosSTOP (phosphatase inhibitor cocktail tablets, Roche,

4906837001) was also added to RIPA buffer. The cells were transferred to a 1.5 ml microcentrifuge tube and kept on ice for 30 mins, while vortexing every 5 mins. The tube was then spun down at 13200 rpm in a 4°C centrifuge for 20 mins to remove cellular debris. The supernatant was transferred to a fresh microcentrifuge tube. Lysates were snap-frozen in liquid nitrogen and then stored at -80°C for long-term storage or used immediately.

2.4.1.2. Zebrafish

20 embryos per condition were transferred to a microcentrifuge tube and de-yolked in 1 ml ice-cold PBS by pipetting the embryos up and down several times. The embryos were washed twice with 1 ml ice-cold PBS to remove the yolk, followed by PBS removal. The embryos were homogenised using a micropestle, then resuspended in 20 µl lysis buffer (50 mM tris pH 8.0, 40 mM NaCl, 2 mM $MgCl_2$, 0.5% Triton™ X-100), supplemented with cOmplete, EDTA-free protease inhibitor cocktail and PhosSTOP. The samples were kept on ice for 30 mins, while vortexing every 5 mins. The lysate was transferred to a new microcentrifuge tube. Lysates were snap-frozen in liquid nitrogen and then stored at -80°C for long-term storage or used immediately.

2.4.2. Bradford assay

Protein concentration in whole-cell extracts was determined using a Bradford assay. 999 µl of Coomassie protein assay reagent (ThermoFisher Scientific, 1856209) and 1 µl of protein lysate was added to a cuvette and vortexed briefly. Lysates were analysed on a Helios Delta spectrophotometer (Unicam) at an optical density of 595 nm. Protein concentrations were calculated by standardising against a 'Lysis buffer only' control.

2.4.3. Protein loading buffer-based extraction

Adherent cells were placed on ice, then washed 1x with ice-cold PBS. An appropriate volume of 1x protein loading buffer supplemented with Basemuncher endonuclease was added, then cells were scraped using a cell scraper or a pipette tip. The cells were transferred to a microcentrifuge tube, briefly vortexed, then left at room temperature for 15 mins. The tubes were then boiled at 95°C for 5 mins, then briefly centrifuged. The extracted protein was stored at -20°C or utilised in a western blot.

2.5. Western blot

2.5.1. SDS-PAGE

Sodium dodecyl sulphate-polyacrylamide gel electrophoresis (SDS-PAGE) was used to visualise protein amounts in protein lysates. The greater the molecular weight of the proteins of interest, the lower the separating gel percentage. The gel was cast in a 1 mm XCell SureLock Mini-Cell cassette (Fisher Scientific, VXNC2010). Handmade 4-20% gradient separating gels were cast when looking at proteins of broader molecular weights. This was achieved by mixing 4% and 20% gels in a stripette, creating a gradient gel, then loading the gel in the cassette.

Constituents	4% Separating Gel (10ml)	8% Separating Gel (10ml)	10% Separating Gel (10ml)	12% Separating Gel (10ml)	15% Separating Gel (10ml)	20% Separating Gel (10ml)	4% Stacking Gel (5ml)
ddH_2O	7.2ml	4.6ml	4.0ml	3.3ml	2.3ml	2.0ml	3.74ml
30% acrylamide	1.35ml	2.7ml	3.3ml	4.0ml	5.0ml	6.6ml	680µl
1.5M Tris pH 8.8	2.5ml	2.5 ml	2.5ml	2.5ml	2.5ml	2.5ml	-
1M Tris pH 6.8	-	-	-	-	-	-	500µl
10% SDS	100µl	100µl	100µl	100µl	100µl	100µl	40µl
10% APS	100µl	100µl	100µl	100µl	100µl	100µl	40µl
TEMED	8µl	6µl	4µl	4µl	4µl	4µl	10µl

Table 2.4: SDS-PAGE gel constituents. Different separating gel percentages were used depending on the molecular weight of the proteins of interest. 4% stacking gel was used for each blot.

2.5.2. Loading samples

5X protein loading buffer was diluted to 1x in 30 µg of quantified protein lysate, to a final volume of 20-50 µl in a 1.5 ml microcentrifuge tube. The tubes were then boiled at 95°C for 5 mins, then briefly centrifuged. The gel was transferred to a BioRad Mini-PROTEAN Tetra electrophoresis cell (BioRad, 16158004). Boiled samples were loaded with a gel loading tip, whilst Precision Plus Protein™ Dual Colour Standard (BioRad, 1610374) was used as a molecular weight ladder. The gel was run for 15 mins at 120 V, then 45 mins at 180 V, or until the loading buffer ran off the bottom of the gel.

2.5.3. Transfer

Gels were transferred onto an 0.2 µm nitrocellulose membrane (Bio-Rad, 1704159) using a Trans-Blot Turbo Transfer System (BioRad, 1704150) with Trans-Blot Turbo nitrocellulose transfer packs (Bio-Rad, 1704158) soaked in 1x Trans-Blot Turbo transfer buffer using the desired setting, depending on the size of the proteins of interest.

2.5.4. Blocking membranes

Transferred membranes were blocked for 1 hour at room temperature with constant shaking in 5% milk or 5% BSA, to prevent non-specific antibody binding. 5% BSA was used when probing phosphorylated proteins as milk contains the phosphoprotein casein, which can interfere with accurate detection of the phosphorylated protein of interest (Gavini and Parameshwaran, 2023).

2.5.5. Probing with antibodies

Blots were probed with appropriate primary antibody **(Table 2.5)**, made up in 5% milk or 5% BSA, overnight at 4°C on an orbital shaker. 5% BSA was used when using probing phosphorylated proteins. Milk/BSA with primary antibody contained 0.02% sodium azide, allowing for the reusing of primary antibody multiple times as sodium azide preserves fouling of antibodies (Winter et al., 2012). Following overnight incubation, blots were washed 3x in TBST, 5 mins for each wash. Blots were probed with the appropriate secondary antibody **(Table 2.5)** (anti-mouse or anti-rabbit) made up in 5% milk solution for 1 hour at room temperature with constant shaking. Blots were washed in TBST as before, followed by the addition of Clarity™ Western ECL Substrate (Biorad, 1705060). Blots were then visualised using a ChemiDoc™ MP Imaging System (BioRad, 1708280) and quantified in Image Lab v 6.1 (BioRad).

Antibody	Host Species	Source/Catalogue number	Dilution
β-tubulin	Rabbit	Abcam/ab179511	1:1000
β-actin	Mouse Mouse	Abcam/ab8226 Proteintech/60008	1:1000 1:5000
VHL	Rabbit	CST/68547	1:1000
HIF1α	Mouse	Invitrogen/MA1-516	1:1000
HIF2α	Rabbit	Invitrogen/PA1-16510	1:1000
TDP1	Rabbit	Abcam/ab4166	1:1000
TDP2/TTRAP	Rabbit	Aviva Systems Biology/ARP33010_P050	1:1000
TOP1	Rabbit	Abcam/ab109374	1:5000
PARP1	Mouse	Santa Cruz/sc-8007	1:1000
pXRCC1 (S485/T488)	Rabbit	Bethyl/IHC-00117	1:1000
ATM	Rabbit	Abcam/ab32420	1:1000
NuMA	Mouse	Santa Cruz/sc-365532	1:1000
pNuMA (S395)	Rabbit	CST/3429	1:500
pChk1 (S345)	Rabbit	CST/2348	1:2000
pH2A.X (S139)	Mouse	Sigma-Aldrich/05-636	1:1000
Mouse IgG (H+L)- HRP Conjugate	Goat	Biorad/1706516	1:4000
Rabbit IgG (H+L)- HRP Conjugate	Goat	Biorad/1706515	1:4000

Table 2.5: Primary and secondary antibodies. Antibodies used throughout western blotting, including the host species, source, and dilution.

2.5.6. Stripping membranes

For reprobing blots, membranes were stripped using Restore™ PLUS western blot stripping buffer (Thermo Scientific, 46430) by incubating blots with buffer at 37°C for 15 mins, then shaking at 80 rpm. Blots were rinsed with TBST then blocked with 5% milk or 5% BSA **(Section 2.5.4)**. Blots were then probed with primary antibodies as described in **Section 2.5.5**.

2.6. RT-qPCR

2.6.1. RNA extraction

2.6.1.1. Mammalian cells

Confluent cells in a 6-well plate were washed 1x with ice-cold PBS, which was then removed. 1 ml of TRIzol™ reagent (Invitrogen, 15596018) was added per well followed by dissociating cells using a cell scraper, then the cells were transferred to a microcentrifuge tube and left at room temperature for 5 mins. Afterwards, 250 µl chloroform was added to each tube, followed by vigorous shaking for 15 secs, then leaving samples at room temperature for 5 mins, followed by centrifugation at 10000 rpm for another 5 mins. The clear, upper aqueous phase was carefully transferred to a new tube, followed by the addition of 550 µl isopropanol and mixing well. Samples were left at room temperature for 5 mins, followed by centrifugation at maximum speed for 20 mins, or 30 mins for low yields. Samples were placed on ice, followed by the removal of the supernatant, then adding 1 ml 75% ethanol. Samples were centrifuged at 9500 rpm for 5 mins, followed by the removal of the supernatant and leaving samples to air dry by leaving tubes open for 2 mins. Samples were centrifuged again to remove excess ethanol. Pellets were resuspended with 30 µl RNase free water. RNA concentration was measured using a nanodrop (ThermoFisher Scientific, ND1000). RNA was stored long-term at -80°C.

2.6.1.2. Zebrafish

10-15 zebrafish embryos in a microcentrifuge tube were homogenised in TRIzol by using a single-use 1 ml syringe (HENKE-JECT, 613-2794) attached to a Microlance™ 3 needle (BD, 304000), then left at room temperature for 5 mins. 100 µl chloroform was added to each tube, followed by vigorous shaking for 15 secs, then leaving the samples at room temperature for 3 mins, followed by centrifugation at 12000 g for 15 mins at 4°C. The clear, upper aqueous phase was transferred to a new tube, followed by the addition of 250 µl isopropanol and mixing well. Samples were left at room temperature for 10 mins, followed by centrifugation at 12000 g for 10 mins at 4°C. The supernatant was removed, then the pellet was washed with 1 ml 75% ethanol, followed by centrifugation at 7500 g for 5 mins at 4°C. The supernatant was removed, followed by a quick spin to remove residual ethanol. The pellets were left to air dry for 2 mins with the tubes open. The pellet was dissolved in

15µl milli-Q® (MQ) water. RNA concentration was measured using a nanodrop. RNA was stored long-term at -80°C.

2.6.2. cDNA synthesis

The ProtoScript® II First Strand cDNA Synthesis Kit (NEB, E6560) was used to reverse-transcribe cDNA from RNA as below:

- Template RNA 500 ng
- $d(T)_{23}$ VN 1 µl
- ProtoScript II Reaction Mix (x2) 5 µl
- ProtoScript II Enzyme Mix (x10) 1 µl
- MQ Water Up to 10 µl

2.6.3. RT-qPCR reaction

cDNA was diluted 1:10, then the reaction was set up as below in a 96-well RT-qPCR plate (BioRad, HSP96061).

- 5x EvaGreen® HOT FIREPol® qPCR Mix (Solis BioDyne, 08-25-00001) 4 µl
- Forward primer (10 µM) 1 µl
- Reverse primer (10 µM) 1 µl
- MQ water 13 µl
- cDNA (1/10 dilution) 1 µl

Reactions were set up as technical repeats of each sample in triplicate, including a non-template negative control. A standard curve was produced via serial dilution (100%, 10%, 1%, and 0.1% cDNA) as templates when testing new primer pairs. All primers were purchased from Integrated DNA technologies (IDT) and can be found in **Table 2.6**.

Gene	Sequence	Forward primer (F) Reverse primer (R)
EGLN3/PHD3	ATTCATAGCAGATGTGGAGCC	F
	TCAGCATCAAAGTACCAGACAG	R
PPIA	GGTCCCAAAGACAGCAGAAA	F
	GTCACCACCCTGACACATAAA	R
TDP1	GCCAGGCAAAGTTGGATATTG	F
	GATGAGGTTGGAGGTGTGTATG	R
BRCA1	GGAATCAGCCTCTTCTCTGATG	F
	TGCAGAGGTTGAAGATGGTATG	R
PNK	AGCGTATGCGGAAGTCAAA	F
	CGTCCCGTCCAGATCAAAG	R
FANCD2	AGGTGCTCACTCGGTTAAAG	F
	GTTTCCAAGAGGAGGGACATAG	R
MRE11	GAGGAGCTTGACTGACCATAAA	F
	TTCCTCTGACTGCATCTTTCTC	R
HIF1a	GTCTGCAACATGGAAGGTATTG	F
	GCAGGTCATAGGTGGTTTCT	R
HIF2a	GACTTACACAGGTGGAGCTAAC	F
	GAGACTCAGGTTCTCACGAATC	R
VEGFA	CCTTGCTGCTCTACCTCCAC	F
	CACACAGGATGGCTTGAAGA	R
XRCC1	CTTCTCAAGGCAGACACTTACC	F
	TGTGTATCTGCTCCTCCTTCT	R
APEX2	AACCAAAGTGACCAGGGATG	F
	GAAGGTGGCTACACCAGAATAG	R
MUS81	CCCAAGGAACAAGAGACACT	F
	CTGCAGTAGAGCTGGGATAAG	R
ERCC4	TGACAAGACAATCCGCCATTA	F
	TGAGAGAGATACTGCAGCAAAG	R

tdp1 (ZF)	GCTCCTCAATTGGCTTCCCT	F
	ATGTTCCAGATCCAAGGCCG	R
rps29 (ZF)	TTTGCTCAAACCGTCACGGA	F
	ACTCGTTTAATCCAGCTTGACG	R

Table 2.6: RT-qPCR primers. List of primers used in RT-qPCR reactions.

The reactions were run in a CFX96 Touch™ Real-Time PCR Detection System (Bio-Rad), under the following thermal cycler conditions:

- 95°C, 10 mins
- 95°C, 15 mins
- 55°C, 15 secs
- 72°C, 30 secs
- Repeat from step 2, 44x

2.6.4. RT-qPCR quantification

CFX Maestro™ Analysis Software (Bio-Rad) was used to calculate quantification cycle (Ct) values, which were then used to calculate fold change by the ΔΔCt method (Livak and Schmittgen, 2001). The difference between Ct values of reference gene and target gene was calculated for both control samples and treated samples (ΔCt). The difference between the average ΔCt for both treatment and control was used as a normaliser to determine the ΔΔCt value. As RT-qPCR is exponential, fold change is calculated as 2^- ΔΔCt.

2.7. Clonogenic analysis

2.7.1. Inducing genotoxic stress

2.7.1.1. Drug treatment

Cells were seeded at 3000-6000 cells/10 cm dish in 10 ml cell culture media and left to adhere overnight. The following day, cells were treated with the desired chemical, which was then washed off with fresh media, or left for the entire duration of the experiment. Cells were left to grow in 37°C, 5% CO_2 until visible, non-overlapping colonies formed (7-10 days).

2.7.1.1.1. Camptothecin

For short-term camptothecin (CPT, Sigma, C9911) treatment, 50-200 nM of CPT was added directly to the media for 1 hour, then replaced by fresh media without CPT. For long-term CPT treatment, 10-18 nM of CPT was added directly to the media, then left for 3 days. The media was then replaced with fresh CPT for another 3 days. DMSO was used as a control.

2.7.1.1.2. Olaparib

5-20 µM Olaparib (Biovision, 1952-5) was added directly to the media, then left for 3 days. The media was then replaced with fresh Olaparib for another 3 days. DMSO was used as a control.

2.7.1.1.3. Cisplatin

1-5 µM cisplatin (Sigma-Aldrich, P4394) was added directly to the media and left for the duration of the experiment. DMSO was used as a control.

2.7.1.2. Ionising radiation

4000 cells were isolated in 10 ml cell culture media in a 15 ml falcon tube then treated using a Cs137 irradiator (Schering, IB 437 C) for either 1, 3, or 5 Gray. The cells were then transferred to a 10 cm dish and left to grow in 37°C, 5% CO_2 until enough colonies formed.

2.7.2. Staining

Cell culture media was poured off, followed by the addition of 80% ethanol for 15 mins. The ethanol was then poured off and left to air dry at room temperature. Once dry, 2% methylene blue was added to each dish for 1 hour. After removing methylene blue, plates were left to air dry at room temperature.

2.7.3. Colony counting

Colonies were counted using the ProtoCOL 3 Colony Counter (Synbiosis, SYNPROC3PLUS). The surviving fraction was calculated as follows: Number of colonies on drug-treated plate/Number of colonies on control plate.

2.8. Cell viability assay

2.8.1. Cell seeding – Day 1

5000 cells/well in a final volume of 100 µl were seeded in a 96-well plate in triplicate repeats for each drug concentration and left overnight to adhere. Cells were not seeded in outer wells to avoid the 'edge' effect, whereby high rates of evaporation occur in outer wells of 96-well plates (Mansoury et al., 2021).

2.8.2. CPT treatment – Day 2

100 µl of cell culture media containing CPT was added to each well at a final concentration of either 10 nM, 50 nM, 250 nM, 500 nM, or 1 µM CPT. Cells treated with 1% DMSO were included as a control. Three wells containing cell culture media without cells was included as a 'media only' control. The plate was left to incubate overnight at 37°C, 5% CO_2.

2.8.3. CellTiter-Blue® assay – Day 3

All the following steps took place in the dark. An aliquot of CellTiter-Blue Cell Viability Assay (Promega, G8081) was taken out of the freezer and left to thaw at room temperature. 20 µl of CellTiter-Blue was added to each well and the plate was shaken gently to disperse the solution, then the plate was incubated at 37°C, 5% CO_2 for 4 hours. The fluorescence of each well was read using a FLUOstar® Omega microplate reader (BMG Labtech) at 490 nm. The 'media only' well readings were used to subtract background fluorescence. The average of the DMSO-treated well readings were used to establish a base level of survival and compared to CPT-treated wells to analyse surviving fraction.

2.9. Alkaline comet assay

2.9.1. Slide preparation – Day 1

The day before treating cells, frosted microscope slides (Leica, 3800280) were labelled with pencil and placed in a clean, dry rack. 0.6% agarose was made in a universal tube by melting 0.06 g agarose in 10 ml PBS, followed by pipetting 150 µl of agarose slowly under each coverslip (2 per slide) avoiding bubbles. The agarose was cooled to 42°C in a water bath before plating. The slides were left overnight in a humidified chamber for the agarose to set.

2.9.2. Cell treatment and harvesting – Day 2

The following day, 1-3 x 10^6 cells were isolated in microcentrifuge tubes and then treated in suspension with either 40 µM CPT or DMSO as a control. The tubes were transferred to a 37°C, 5% CO_2 incubator for 30 mins. Following treatment, cells were spun down briefly in a centrifuge, followed by the removal of drug-containing media. The cells were resuspended in PBS, and then centrifuged for 5 mins at 4°C to remove excess media. The cells were once more resuspended in 0.5-1.0 ml PBS, then 150 µl of the suspended cells were transferred to a 1.5 ml microcentrifuge and kept on ice until ready to plate.

2.9.3. Plating cells

1.2% low melting point agarose was made in a universal tube by melting 0.12 g low melting point agarose in 10 ml PBS, then cooled down to 42°C in a water bath. Coverslips were then carefully removed from slides. With the lights switched off, the suspended 150 µl sample was warmed in the water bath for a few secs, then combined with 150 µl 1.2% low melting point agarose, which was pipetted up and down briefly, then 100 µl of the suspension under a coverslip over the first layer of 0.6% agarose. The slides were left at 4°C in the dark for 30 mins.

2.9.4. Lysing cells

Incomplete alkaline lysis buffer was prepared as described in **Table 2.7** and stored at 4°C.

Component	Stock concentration	Amount /Litre
NaCl	5M	510ml
EDTA	0.5M	204ml
Tris pH10	1M	10.2ml
NaOH	10M	Titrate to pH10
ddH_2O	-	Until 1 litre

Table 2.7: Incomplete alkaline lysis buffer. Components to make incomplete alkaline lysis buffer, which was stored at 4°C long term and combined with DMSO and Triton X-100 to make complete lysis buffer.

Complete lysis buffer (2.5 M NaCl, 100 mM EDTA, 10 mM tris pH 10.0, 1% DMSO, 1% Triton X-100) was prepared less than 20 mins before use by mixing 9.8 ml incomplete alkaline lysis buffer, 0.1 ml DMSO, and 0.1 ml Triton X-100, and then stirring for 10 mins. Once agarose

had set after 30 mins on slides, all steps that followed until specified took place in a 4°C dark room. Coverslips were removed from slides and 1 ml of complete lysis buffer was added to each slide for 1 hour. After lysis, cells were washed 1x with 1 ml chilled ddH_2O.

2.9.5. Electrophoresis

During lysis, complete electrophoresis buffer was prepared as described in **Table 2.8**, followed by stirring for 10 mins.

Component	Stock concentration	Final concentration	Amount/L
EDTA	0.5M	1mM	2ml
NaOH	10M	50mM	5ml
DMSO	100%	1%	10ml
ddH_2O	-	-	Up to 1L

Table 2.8: Complete electrophoresis buffer. Components to make complete electrophoresis buffer, which was prepared during lysis.

The comet assay tank (Thistle Scientific) was filled with 1 L complete electrophoresis buffer, then the slides were carefully lowered and lined up in the same direction. The slides were left to equilibrate in the buffer for 45 mins, then the power pack connected to the tank was switched on at 12 V for 25 mins.

2.9.6. Neutralising comets

Following electrophoresis, slides were washed with 1 ml 0.4 M tris pH 7.0, then left to incubate overnight in the fridge with an additional 1 ml 0.4 M tris pH 7.0.

2.9.7. Scoring comets – Day 3

SYBR green was diluted 1:10000 in PBS, then 1 ml was spread over a slide for 2 mins before scoring in the dark. Using a 10x objective on a Nikon Eclipse TE300, comet tail moments were scored for 200 cell/side (100 cells for each coverslip) captured with Comet Assay IV™ software (Instem). Comet tails refer to the migration of broken DNA from the nucleus, forming a tail-like structure. Comet tail moments measure the distance from the centre of the 'head' of the nucleus towards the centre of the comet tail (Roy et al., 2021) as shown in **Figure 2.1.**

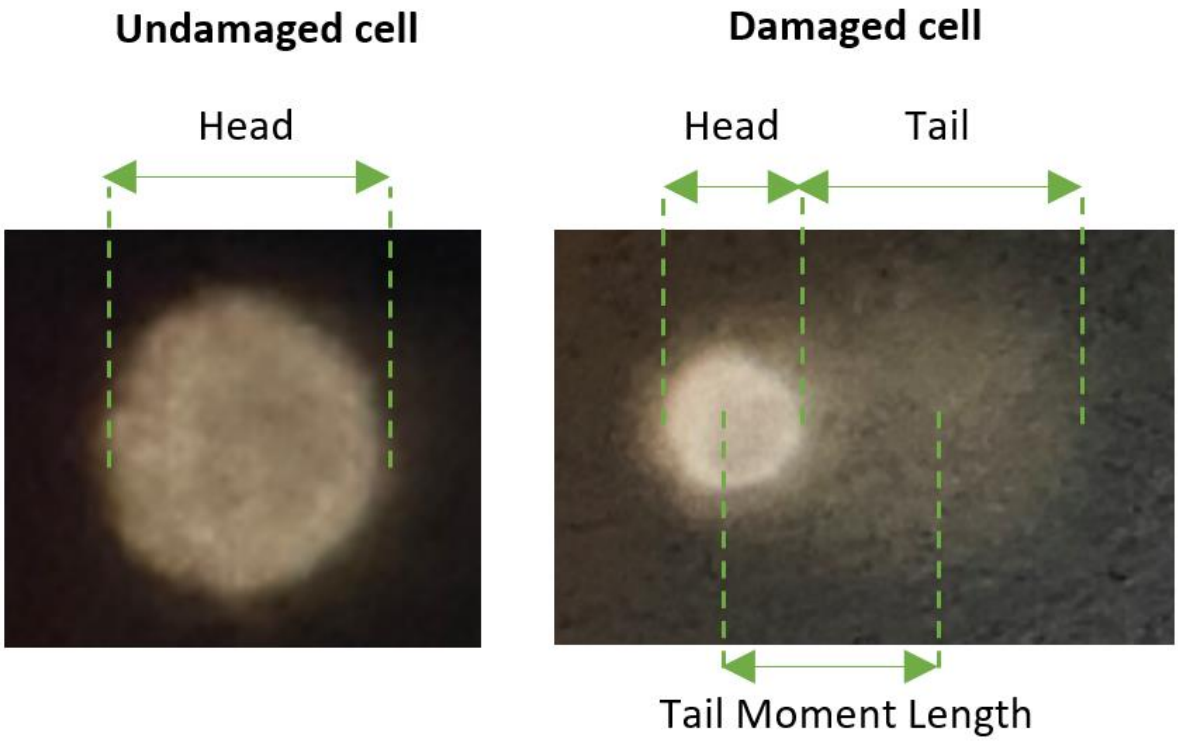

Figure 2.1: Measuring comet tail moment. Damaged DNA migrates from the 'head' of the nucleus towards the cathode producing a comet tail. The extent of DNA damage of a cell embedded in agarose gel is calculated by measuring the length of the comet tail moment, which is the distance between the centre of the 'head' and the centre of the comet tail (Roy et al., 2021). Image taken by my MSc student Ziyan Ma.

2.10. TDP1 activity assay

2.10.1. Preparing samples for assay

TDP1 activity was assessed using the protocol described in Zaksauskaite et al., (2021). Whole-cell protein lysate was prepared as described in **Section 2.4**, ensuring the addition of phosphatase inhibitors. 200-800 ng (mammalian cells) or 20-60 ng (4 dpf zebrafish embryos) of lysate was combined with 1x assay buffer (25 mM HEPES, pH 8.0, 130 mM KCl, 1 mM DTT) and 50 nM Cy5.5-labelled substrate oligomer containing a 3'-phosphotyrosyl group (5'-(Cy5.5)GATCTAAAAGACT(pY)-3') (Midland Certified Reagent Company Texas, USA) and 1mM DTT in a total volume of 10 µl. The reaction was incubated at 37°C for 1 hour and terminated by the addition of 1x loading buffer (44% deionized formamide, 2.25 mM tris-borate, 0.05 mM EDTA, 0.01% xylene cyanol and 1% bromophenol blue) and boiling at 90°C for 10 mins.

2.10.2. Urea gel electrophoresis

A 20% urea gel was cast in a 1 mm XCell SureLock Mini-Cell cassette by mixing components in **Table 2.9**, then left to set for 1 hour at room temperature. The gel was transferred to a BioRad Mini-PROTEAN Tetra electrophoresis cell filled with 1x TBE buffer, then 190 V of current was passed through the gel for 30 mins to remove excess urea. 1x TBE buffer was prewarmed to 60°C before samples were loaded onto the gel and subjected to 150 V electrophoresis for 1.5 hours. The bands were imaged using BioRad ChemiDoc MP Imaging System and quantified in Image Lab v 6.1 (BioRad).

Constituents	Volume
SequaGel concentrate	8ml
SequaGel diluent	1ml
SequaGel buffer	1ml
10% APS	40µl
TEMED	4µl

Table 2.9: Components required to make a 20% urea gel. SequaGel UreaGel 29:1 Denaturing Gel System, National Diagnostics, EC-829.

2.11. mRNA silencing

2.11.1. Cell seeding

Cells were seeded in either 6-well plates or 24-well plates the day before transfection, so that they were 70-80% confluent on the day of transfection. The cells were left to adhere overnight.

2.11.2. siRNA transfection

Media was removed from cells and fresh media was added to each well (1.8 ml in 6-well plate, 450 µl in 24-well plate). Tube A containing Opti-MEM™ (Gibco, 31985070) and siRNA was added to tube B containing Opti-MEM and Lipofectamine™ RNAiMAX (13778075), as per **Table 2.10**, and flicked to mix fully, then left for 5 mins at room temperature. 200 µl (6-well plate) or 50 µl (24-well plate) of the solution was then gently added to each corresponding well. The plates were left for 48 hours at 37°C, 5% CO_2. The final siRNA concentration in each well was 50 nM.

6-well plate	**Opti-MEM (µl)**	**siRNA 20µM stock (µl)**	**Lipofectamine RNAiMAX (µl)**
Tube A	100	5	-
Tube B	100	-	8
24-well plate	**Opti-MEM (µl)**	**siRNA 20µM stock (µl)**	**Lipofectamine RNAiMAX (µl)**
Tube A	25	1.25	-
Tube B	25	-	2

Table 2.10: Volumes and reagents required for siRNA transfection. Opti-MEM, siRNA, and Lipofectamine RNAiMAX were added according to the above volumes and depending on the well size.

Successful knockdown using siRNA was analysed using either western blot **(Section 2.5)** or RT-qPCR **(Section 2.6)**.

All siRNA sequences were purchased from Dharmacon and can be found in **Table 2.11.**

Gene	Sequence	Company (Catalogue no.)
ONTargetplus SMARTPool HIF1α	GAACAAAUACAUGGGAUUA	Dharmacon (J-004018-07)
ONTargetplus SMARTPool HIF1α	AGAAUGAAGUGUACCCUAA	Dharmacon (J-004018-08)
ONTargetplus SMARTPool HIF1α	GAUGGAAGCACUAGACAAA	Dharmacon (J-004018-09)
ONTargetplus SMARTPool HIF1α	CAAGUAGCCUCUUUGACAA	Dharmacon (J-004018-10)
ONTargetplus SMARTPool HIF2α	GGCAGCACCUCACAUUUGA	Dharmacon (J-004814-06)
ONTargetplus SMARTPool HIF2α	GAGCGCAAAUGUACCCAAU	Dharmacon (J-004814-07)
ONTargetplus SMARTPool HIF2α	GACAAGGUCUGCAAAGGGU	Dharmacon (J-004814-08)
ONTargetplus SMARTPool HIF2α	GCAAAGACAUGUCCACAGA	Dharmacon (J-004814-09)
ONTargetplus SMARTPool TDP1	GGAGUUAAGCCAAAGUAUA	Dharmacon (J-016112-05)
ONTargetplus SMARTPool TDP1	UCAGUUACUUGAUGGCUUA	Dharmacon, (J-016112-06)
ONTargetplus SMARTPool TDP1	GACCAUAUCUAGUAGUGAU	Dharmacon (J-016112-07)
ONTargetplus SMARTPool TDP1	CUAGACAGUUUCAAAGUGA	Dharmacon (J-016112-08)
ONTargetplus Non-targeting siRNA #1	UGGUUUACAUGUCGACUAA	Dharmacon (D-001810-01-05)

Table 2.11: siRNA sequences. All siRNAs were diluted to 20 µM using 1x nuclease-free water and used at a final concentration of 50 nM. Sequences purchased from Dharmacon.

2.12. CRISPR Mutagenesis

Mutagenesis was performed as per Ann Ran et al., (2013) with minor adaptations. The plasmids used can be found in **Table 2.12.**

Plasmid	Source
pSpCas9(BB)-2A-Puro	Addgene
pSpCas9(BB)-2A-GFP	Addgene
pSpCas9(BB)-2A-Puro-gHIF1α	This thesis
pSpCas9(BB)-2A-Puro-gHIF2α	This thesis
pSpCas9(BB)-2A-GFP-gHIF1α	This thesis
pSpCas9(BB)-2A-GFP-gHIF2α	This thesis

Table 2.12: DNA constructs. Plasmids utilised in this project.

2.12.1. gRNA design

gRNA target sequences were previously designed and validated (Sanjana et al., 2014). gRNA sequences were selected for both HIF1α and HIF2α. The plasmids used were pSpCas9(BB)-2A-GFP (Addgene plasmid ID:4813), and pSpCas9(BB)-2A-Puro (Addgene plasmid ID:48139), both illustrated in **Figure 2.2**. Appropriate nucleotides were appended at the ends of the top and bottom oligonucleotide strands creating overhangs to allow the guides to clone into the pair of Bpil sites in the plasmid. In addition, an extra guanine nucleotide was appended as the first base at the 5' of the gRNA as U6 RNA polymerase II promoter prefers guanine as the first base of its transcript (Guschin et al., 2010). U6 Forward sequence was purchased to sequence for correct gRNA insertion – all sequences are found in **Table 2.13**, and were purchased from IDT, resuspended to 100 µM using MQ water, and stored at -20 °C.

Name	Sequence
U6 Forward	GAGGGCCTATTTCCCATGATTCC
HIF1α gRNA_1_top	CACCGTACTCATCCATGTGACCATG
HIF1α gRNA_1_bot	AAACCATGGTCACATGGATGAGTAC
HIF2α gRNA_1_top	CACCGCAAGGCCTCCATCATGCGAC
HIF2α gRNA_1_bot	AAACGTCGCATGATGGAGGCCTTGC

Table 2.13: gRNAs and primers: List of gRNA sequences and primers used during CRISPR mutagenesis.

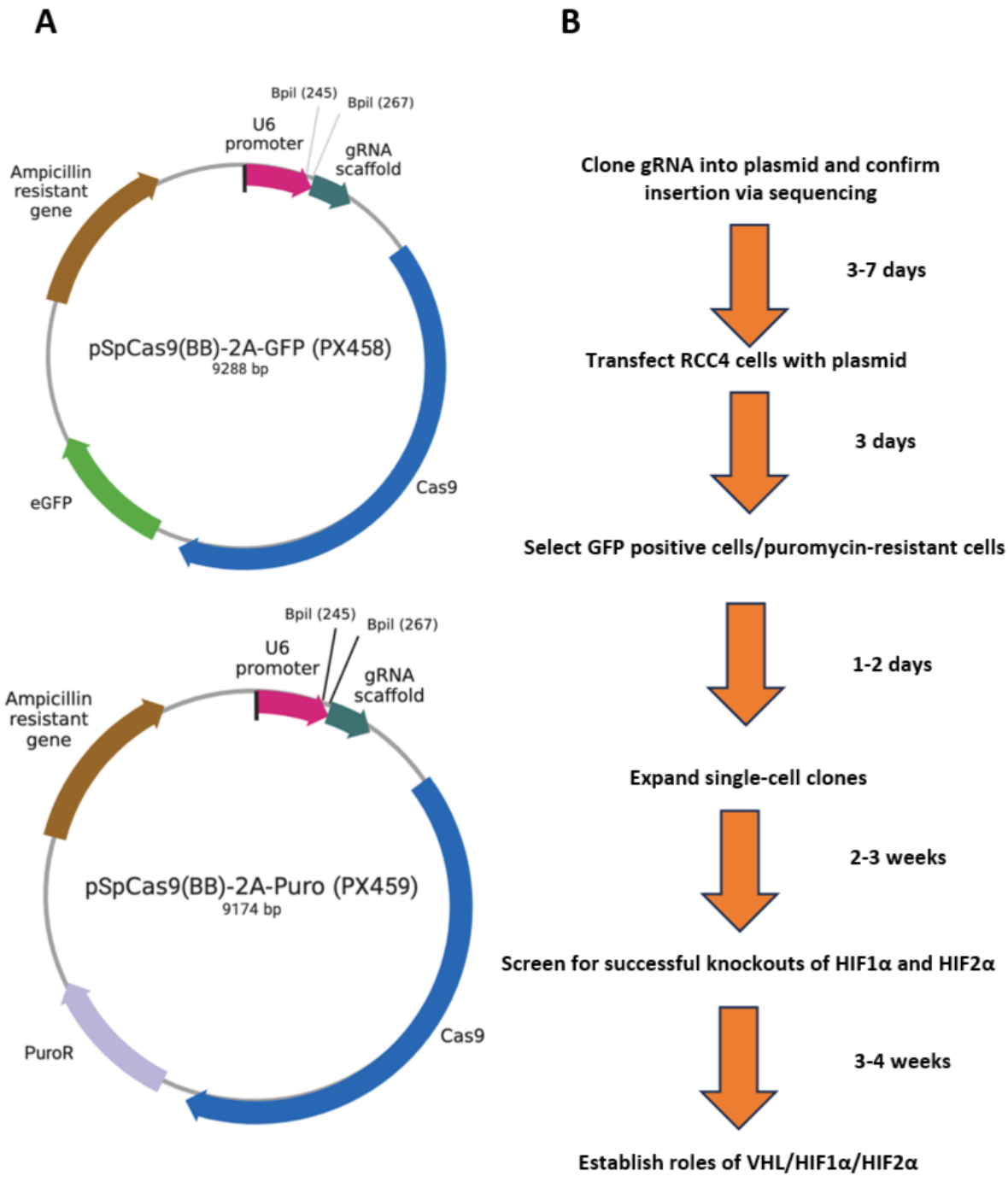

Figure 2.2: Schematic demonstrating the steps involved in CRISPR-Cas9-mediated mutations. A) Map showing the different features located on the pSpCas9(BB)-2A-GFP (PX458) plasmid or pSpCas9(BB)-2A-Puro (PX459) plasmid used to cause CRISPR-Cas9 mediated mutations in HIFα. gRNA was inserted between the U6 promoter and gRNA scaffold. Bpil enzyme was used to cleave DNA, allowing for gRNA insertion into the plasmid. Cas9 is directed towards protospacer adjacent motifs in DNA. eGFP was used to FACS sort transfected cells, or puromycin-resistant gene (PuroR) was used to sort transfected cells with puromycin resistance. Ampicillin resistant gene ensures that only bacteria transfected with the plasmid survive antibiotic treatment. Plasmid taken from Ann Ran et al., (2013). **B)** Schematic showing the steps involved in CRISPR-Cas9-mediated downregulation of HIFα. Figure created using BioRender.com.

2.12.2. gRNA annealing and ligation

The top and bottom strands of each gRNA were phosphorylated and annealed, forming new bonds between each strand. The annealing mix was set up as below:

- gRNA top strand (100 µM) 1 µl
- gRNA bottom strand (100 µM) 1 µl
- T4 ligation buffer (10x) 1 µl
- T4 PNK 1 µl
- MQ water 6 µl

The following thermal cycler settings were used:

- 37°C, 30 mins
- 95°C, 5 mins
- Ramp down to 25°C at 5°C min^{-1}
- 12°C, ∞

The phosphorylated and annealed oligonucleotides were diluted 1:200 by adding 1 µl of oligonucleotide to 199 µl of room temperature MQ water. The ligation reaction for each gRNA was set up as described as below. A 'no-insert, plasmid only' negative control was also set up.

- pSpCas9(BB)-2A-Puro (100 ng/µl) 1 µl
- Diluted oligonucleotide duplex 2 µl
- Tango buffer (10x) 2 µl
- DTT (10 mM) 1 µl
- ATP (10 mM) 1 µl
- FastDigest Bpil 1 µl
- T7 ligase 0.5 µl
- MQ Water 11.5 µl

The following thermal cycler settings were used:

- 37°C, 5 mins
- 21°C, 5 mins
- GOTO step 1, 5x
- 12°C, ∞

The ligation reaction was treated with Plasmid-Safe™ ATP-dependent DNase (Epicentre, E3101K) to digest residual linearised DNA. This reaction was set up as described below:

- Ligation reaction 11 µl
- Plasmid-Safe Buffer (10x) 1.5 µl
- ATP (10 mM) 1.5 µl
- Plasmid-Safe ATP-dependent DNase 1 µl

The following thermal cycler settings were used:

- 37°C, 30 mins
- 70°C, 30 mins
- 12°C, ∞

The reaction could be stored at -20 °C for long-term storage after Plasmid-Safe treatment.

2.12.3. Bacterial transformation

The Plasmid-Safe-treated plasmids were transformed into One Shot™ Stbl3™ Chemically Competent E. coli (ThermoFisher Scientific, C737303) as per manufacturer instructions. 2 µl of the Plasmid-Safe-treated product was added into a vial of thawed Stbl3 cells. The vial was gently mixed, then the mixture incubated on ice for 10 mins. The solution was heat-shocked at 42°C for 30 secs and then returned immediately to ice for 2 mins. Under sterile conditions provided by a Bunsen flame, 100 µl of room temperature SOC medium was added, then the vial was placed in a thermal mixer for 1.5 hours at 300 rpm. 100 µl of the mixture was then plated onto an LB plate containing 100 µg/ml carbenicillin. The plate was incubated overnight at 37°C. Plates were checked for colonies the following day. There were typically no colonies on the negative control and plenty on the transfected plates. Three colonies were picked from each plate and individually inoculated using a sterile pipette tip into a 5 ml

culture of LB medium with 100 µg/ml carbenicillin. The culture was incubated overnight at 37°C, 200 rpm.

2.12.4. Preparing glycerol stocks

Before extracting DNA, glycerol stocks of each colony were prepared under sterile conditions by mixing 750 µl 80% autoclaved glycerol with 250 µl bacterial culture in a cryovial. The vial was briefly vortexed, then stored at -80°C. Glycerol stocks were utilised for future colony streaking if required.

2.12.5. Plasmid DNA extraction

Plasmid DNA was isolated using the QIAprep® spin miniprep kit (Qiagen, 27104). All centrifugation steps took place at 13000 rpm in room temperature unless stated. Bacterial culture was pelleted by centrifugation for 10 mins at 4°C, 4500 rpm. Pelleted bacterial cells were resuspend in 250 µl Buffer P1 and transferred to a 1.5 ml microcentrifuge tube. 250 µl Buffer P2 was added and mixed thoroughly by inverting the tube several times until the solution became clear. 350 µl Buffer N3 was added and mixed by inverting as before, then the tube was centrifuged for 10 mins. 800 µl supernatant was applied to the QIAprep spin column, then centrifuged for 30 secs. The supernatant was discarded, then the tube was washed by adding 0.5 ml Buffer PB, then centrifuged for 30 secs. The tube was further washed with 0.75 ml Buffer PE, then centrifuged. Residual buffer was removed by centrifugation for 1 min. The column was placed in a clean 1.5 ml microcentrifuge tube, then plasmid DNA was eluted by adding 50 µl Buffer EB to the canter of the column, which was left to stand for 1 min, followed by a 1 min centrifugation. Plasmid DNA concentration and purity was analysed by using a nanodrop, then DNA was stored at -20°C for further use.

2.12.6. Plasmid DNA sequencing

75 ng/µl of purified plasmid in 5 µl MQ water was mixed with 5 µM of U6 Fwd primer in 5 µl MQ water. Samples were sent for sequencing via GeneWiz. Sequence traces were analysed using Benchling.com (2022) for the correct insertion of gRNA between the U6 promoter and the gRNA scaffold. Plasmids without gRNA were discarded. Sequence-verified plasmids were kept for downstream applications.

2.12.7. Plasmid transfections in mammalian cells

Cells were seeded onto 24-well plates in complete DMEM 16-24 hrs before transfection in a total volume of 500 µl. Cells were 70-90% confluent on the day of transfection. 500 ng of sequence-verified CRISPR plasmid was transfected into cells in a 1:2 ratio with polyethyleneimine (PEI, Polysciences, 23966-2) as a transfection reagent. Plasmid DNA and PEI were added to Opti-MEM (Gibco, 31985070) in separate microcentrifuge tubes, then the plasmid DNA mixture was added to the PEI mixture and incubated for 5 mins at room temperature, before slowly adding to each well. If two plasmids were transfected, the total amount of plasmid DNA was kept to 500 ng. Transfected cells underwent puromycin selection 24 hours after transfection or GFP sorting 48 hours after transfection.

2.12.8. Puromycin selection

Transfected cells with the puromycin-resistant plasmid were supplemented 24 hours after transfection with 500 µl complete DMEM containing puromycin, to a final concentration of 4 µg/ml. Cells were treated for 48 hours.

2.12.8.1. Serial dilution for puromycin-resistant clones

Transfected cells were washed 1x with PBS, then trypsinised and diluted to a suspension of $2x10^4$ cells/ml in a total volume of 200 µl. Using a multichannel pipette, 100 µl of media was added to all wells in a 96-well plate, except for position A1, where 200 µl of cell suspension was added. 100 µl of cell suspension was transferred from A1 to B1 and mixed gently by pipetting. This 1:2 dilution was repeated down the entire column, discarding 100 µl from H1. An additional 100 µl of medium was added to each well in column 1, then 100 µl of cell suspension was transferred from the wells in the first column to those in the second column. These 1:2 dilutions were repeated across the entire plate, discarding 100 µl from each of the wells in the last column. The final volume of all wells was brought to 200 µl by adding 100 µl medium to each well. The plate was incubated at 37°C, 5% CO_2 until visible colonies were detected. Colonies arising from a single cell were subcultured in 24-well plates, then expanded up to T75 flasks.

2.12.9. GFP sorting

Transfected cells with the eGFP-plasmid were single-cell sorted 48 hours after transfection into 96-well plates using a BD Bioscience FACSJazz™ Cell Sorter as per manufacturer instructions. Colonies arising from a single cell were subcultured in 24-well plates, then expanded up to T75 flasks.

2.13. Immunofluorescence

$1x10^6$ cells were seeded onto coverslips in a 24-well plate and left to adhere overnight. The following day, cells were treated with compounds as required.

2.13.1. Fixation

Cells were placed on ice and washed three times with 500 µl ice-cold PBS, followed by 200µl 4% paraformaldehyde in a fume hood for 20 mins. Cells were washed 3x in PBS, followed by adding 0.2% Triton X-100 while cells were placed on ice. Cells were then washed 3x in PBS, with each wash lasting 5 mins on an orbital shaker, then residual PBS was removed.

2.13.2. Blocking

200 µl 3% BSA, made up in PBS and filter sterilised, was added to each well and incubated at room temperature for 30 mins.

2.13.3. Antibody Staining

200 µl primary antibody mixed in 3% BSA was added to each well and left overnight in a humidified chamber at 4°C. The following day, cells were washed 3x with PBS while on an orbital shaker, followed by adding 200 µl secondary antibody mixed in 3% BSA for an hour at room temperature in the dark. DAPI (Sigma-Aldrich, D9542) was also added at 1:1000 to stain nuclei. After the hour incubation, cells were washed 3x with PBS while on an orbital shaker, followed by submerging the coverslips in ddH_2O. Primary and secondary antibodies used in immunofluorescence can be found in **Table 2.14**.

Antibody	Host Species	Source/Catalogue number	Dilution
γH2AX	Mouse	Sigma-Aldrich/05-636	1:1000
53BP1	Rabbit	Bethyl/A300-273A	1:1000
Anti-Mouse IgG (H+L), Alexa Fluor™ 488	Goat	Invitrogen/A-11001	1:500
Anti-Rabbit IgG (H+L), Alexa Fluor 594	Goat	Invitrogen/A-11012	1:500

Table 2.14: Immunofluorescence antibodies. Antibodies used throughout immunofluorescence, including the source, host species, and dilution.

2.13.4. Imaging

The coverslips were carefully lifted using tweezers, then left to dry for 20 mins on tissue. The coverslips were mounted on Shandon™ SuperFrost® microscope slides (Life Science International, 67761207) using Thermo Scientific Shandon Immu-Mount™ (FIS9990402). The slides were stored at 4°C in the dark for 1-3 days before microscopy. The slides were imaged using a DFC350 FX fluorescent microscope (Leica) connected to a CTR5000 controller (Leica). Images were taken with Leica FW4000. Foci or fluorescent intensity were quantified using FIJI (Image J) software v 2.1 by initially creating a mask to outline visible nuclei stained with DAPI. For γH2AX, the mean fluorescent intensity per cell was quantified, whilst for 53BP1 maxima points were identified and counted within the visible nuclei. Macro scripts for both quantifications can be found in the appendix.

2.14. Statistical Analysis

Quantifications and statistical analysis were performed using GraphPad Prism version 10. $p < 0.05$ was considered to be statistically significant for all statistical tests. Data is presented as Mean ± SEM.

An unpaired Student's t-test was used when comparing the means of two independent groups. A one-way ANOVA was used when comparing the means of more than two independent groups with one variable. A two-way ANOVA was used when comparing the means of more than two independent groups with two variables. ANOVA post-hoc tests were used to control for the family-wise error rate: Tukey correction when comparing all

means against each other, Dunnet correction when comparing every mean to a control mean, and Šidák corrections when comparing selected means. In some results the data was normalised leading to uneven distribution of data; therefore, non-parametric tests were utilised instead: Wilcoxon-signed rank test for two independent samples, or Kruskal-Wallis test for more than two independent samples, followed by Dunn's correction as a post-hoc test (McHugh, 2011; Ranganathan, 2021).

Chapter 3 Chemoresistance and radioresistance in RCC4-VHL -/-

3.1. Introduction

Stable cell lines have been used for decades as a model for disease, allowing researchers to investigate the roles of specific genes and pathways in disease progression. A literature analysis was conducted (Brodaczewska et al., 2016) to establish which cell line was most suitable to model ccRCC and would complement the previous studies performed by Kim et al., (2020) which utilised a zebrafish model with *vhl* knocked out to show constitutive upregulation of Hif1α and Hif2α. I wanted a cell line that also had a mutation in *VHL* causing it to be non-functional, leading to increased expression of HIF1α and HIF2α. I decided to use the RCC4 cell line, which originated from a primary ccRCC tumour as it contained a missense mutation in *VHL* (p.S65W), causing the cells to be in a constant state of pseudohypoxia due to unstable VHL protein structure (Hes et al., 2007). Similar to the zebrafish model, the RCC4 cells also had constitutively high levels of HIF1α and HIF2α, as opposed to other cell lines which possess only one or the other. To obtain a suitable control for RCC4 with functional VHL, I also used the RCC4-VHL WT cell line created by Maxwell et al., (2020) whereby they transfected RCC4 cells with a plasmid containing functional VHL and positively selected for these stably transfected cells; then they validated that VHL had been functionally restored by analysing genes responsive to hypoxia.

It has been well established that ccRCC patients often develop resistance to several types of therapies, such as those targeting receptor tyrosine kinases, VEGF inhibitors, and mTOR inhibitors (Rini, 2010; Gore and Larkin, 2011). RCC4 cells have been used previously to understand the complex mechanisms behind ccRCC tumourigenesis and resistance to therapies (Doan et al., 2019; Arnaiz et al., 2021). Furthermore, Yuen et al., (2007) suggested that high expression of insulin growth factor receptor 1, which is commonly upregulated in ccRCC, can contribute to tumour chemoresistance protecting cells from cytotoxic drugs that induce apoptosis. Lastly, Okamoto et al., (2017) has shown that upregulation of HIF1α can initiate resistance to lidocaine-induced cell death in RCC4 cells.

It is well established that hypoxia is able to enhance resistance to radiotherapy in several cancers (Harrison et al., 2002). There have been few studies utilising ccRCC cell lines to study radioresistance, but previous literature suggests that the ccRCC cell line 786-O, which exclusively expresses HIF2α, becomes more sensitive to radiation once HIF2α expression had been reduced (Bhatt et al., 2008).

Conversely to what would be predicted, it has also been reported that RCC4 cells are more sensitive to DNA damage due to the downregulation of DNA repair genes under hypoxia, such as *BRCA1*, causing the increased formation of DSBs. Furthermore, it has been reported that RCC4 cells had a greater sensitivity to PARP inhibitors compared to their WT counterparts (Scanlon and Glazer, 2015; Scanlon et al., 2018).

Before starting any experiments with RCC4, it was important to confirm that the VHL status of both lines was correct as well as confirming that the levels of HIF1α and HIF2α decrease when VHL function is restored. Following this, I wanted to establish if enhanced chemoresistance and radioresistance would be observed in RCC4-VHL -/- cells compared to RCC4-VHL WT, which would match what has been found in ccRCC patients. Lastly, I wanted to screen various DNA repair proteins to establish if any potential targets responsible for enhanced chemoresistance had not been previously identified.

3.2. Hypothesis

RCC4-VHL -/- cells will have increased expression of HIF1α and HIF2α compared to RCC4-VHL WT cells, causing upregulation of *PHD3.* This gene was chosen as its upregulation had been previously identified in pseudohypoxic zebrafish expressing increased levels of Hif1α/Hif2α (Kim et al., 2020; Marchi, 2020) and has also been shown to be upregulated in RCC4 cell lines expressing constitutively upregulated HIF1α/HIF2α (Harten et al., 2011). Upregulated HIF expression will lead to enhanced chemoresistance, due to the increased expression of various DNA repair genes.

3.3. Aims

1. Identify the presence of VHL in RCC4-VHL WT cells and the absence of VHL in RCC4-VHL -/- cells.
2. Establish that HIF1α and HIF2α expression levels correlate with the absence of VHL.
3. Confirm that *PHD3*, a downstream target gene of HIF1α and HIF2α, is upregulated in RCC4 VHL -/- cells and downregulated in RCC4-VHL WT cells.
4. Establish if RCC4-VHL -/- cells are more sensitive to DNA damaging agents than their WT counterparts.
5. Explore the role of DNA repair proteins that may be involved in enhanced resistance to genotoxic stress.

3.4. Results

3.4.1. Restoration of functional VHL downregulates HIF1α and HIF2α whilst *PHD3* is upregulated when VHL function is perturbed

RCC4-VHL -/- have non-functional VHL, which mimics LOH in VHL expressing cells in cysts and tumours of ccRCC patients who are originally heterozygous for mutations in *VHL*. RCC4-VHL WT has functional VHL stably resupplied to the cells, which acts as the control cell line for my experiments. Before commencing any experiments with the RCC4 cells, it was important to establish that the identity of each cell line was correct. Analysing protein expression via western blot **(Section 2.5)** shows the absence of VHL in RCC4-VHL -/-, whilst RCC4-VHL has a greater VHL expression. The absence of VHL is correlated with upregulation of both HIF1α and HIF2α (**Figure 3.1A)**. Furthermore, when performing RT-qPCR **(Section 2.6)**, the HIF target gene *PHD3* is upregulated in RCC4-VHL -/-, indicating that the upregulation observed in HIF has functional consequences downstream of HIF (**Figure 3.1B)**. Therefore, I can be confident of the identity of both RCC4 cell lines.

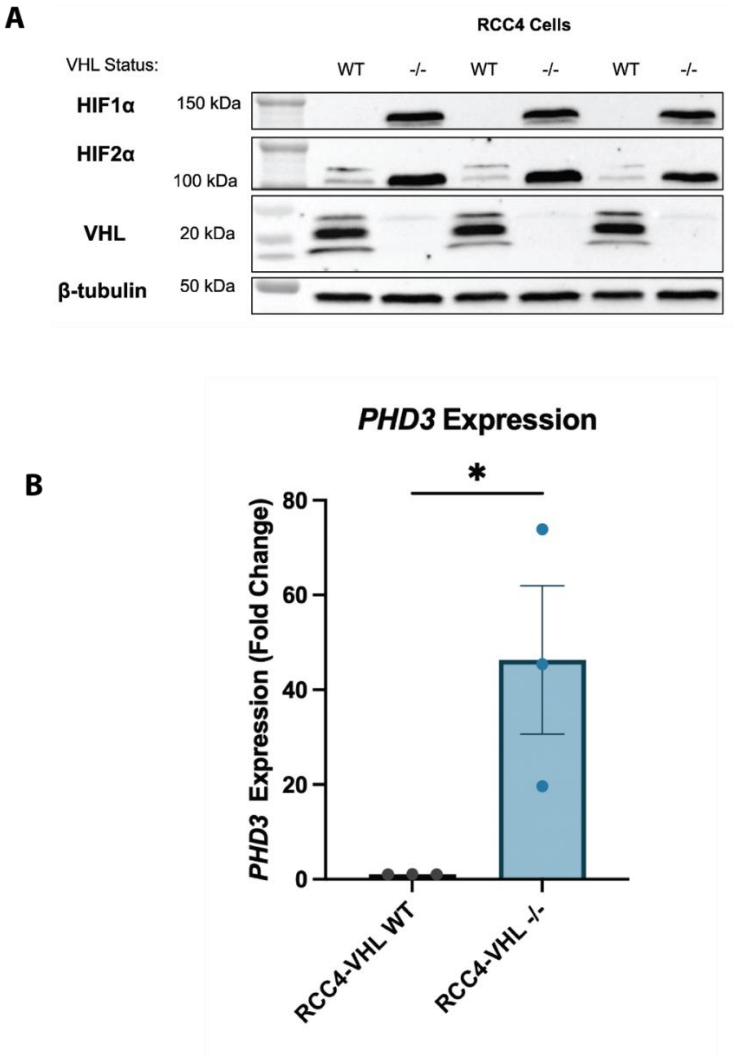

Figure 3.1: RCC4-VHL -/- cells have a constitutively upregulated HIF pathway. A) Lysates from RCC4-VHL WT cells and RCC4-VHL -/- show that restoration of functional VHL downregulates protein levels of HIF1α and HIF2α on a western blot. β-tubulin was used as a loading control. **B)** RT-qPCR on RCC4-VHL WT and RCC4-VHL cells showing mRNA upregulation of HIF target gene*, PHD3*, in RCC4-VHL -/- cells. *PPIA* was used as a housekeeping gene. Unpaired Student's t-test, *p<0.05, Mean ± SEM, n=3.

3.4.2. RCC4-VHL -/- cells have enhanced chemoresistance, but not radioresistance, compared to RCC4-VHL WT cells

Once the identity of the RCC4 cells had been correctly established, I explored whether RCC4-VHL -/- would be more resistant to cytotoxic agents than RCC4-VHL WT. It was important to use different methods and different chemicals that target various pathways to obtain a better understanding of any differences in chemosensitivity between both cell lines.

CPT is a TOP1 poison which prevents the release of TOP1 from DNA, increasing the presence of TOP1-CCs. This causes the increased formation of DSBs and SSBs (Liu et al., 2000). Olaparib is a PARP inhibitor, thereby blocking DNA SSBR. As SSBR is inhibited, DNA is repaired through error-prone pathways leading to cell death (Goulooze et al., 2016). It has been shown that moderate hypoxia enhances resistance to Olaparib through the upregulation of *BRCA1* and *BRCA2* in a HIF-independent manner (Mehibel et al., 2021).

I decided to use several different techniques to measure the effectiveness of CPT and Olaparib to induce DNA damage and loss of cell viability: clonogenic analysis, CellTiter-Blue assay, and alkaline comet assay. Clonogenic formation assays observe the effect of a drug on a cell's ability to form a colony. CellTiter-Blue assay is a viability assay that relies on viable cells converting resazurin into a fluorescent dye, resorufin. Cytotoxic agents will cause cells to become less metabolically active, so there will be a lower fluorescent signal (Riss et al., 2004). The alkaline comet assay measures both SSBs and DSBs by measuring the migration of damaged DNA in drug-treated agarose-fixed cells after electrophoresis. Broken DNA forms a tail-like structure called a 'comet tail' due to the migration of DNA based off size. Larger 'comet tail moments' indicate greater DNA damage (Roy et al., 2021).

Clonogenic analysis was performed as per **Section 2.7.** For both CPT and Olaparib treatments, cells were treated at different doses of CPT/Olaparib or DMSO for 3 days, then the media was replaced with fresh media containing CPT/Olaparib or DMSO for another 3 days, followed by staining and counting colonies. RCC4-VHL -/- cells showed a greater resistance to both CPT and Olaparib treatment at all doses **(Figure 3.2 A-B)**. For both CellTiter-Blue assay and comet assay, only CPT was used as previous work done in the lab had utilised CPT, so more information was available with regards to the treatment times.

CellTiter-Blue assay was performed as per **Section 2.8**. RCC4-VHL -/- cells demonstrated a slightly higher resistance to CPT compared to RCC4-VHL WT as shown by more viable cells at lower concentrations of CPT. At 500 nM and 1 μM CPT, both cell lines exhibited similar tolerance levels to CPT. This suggested that RCC4-VHL -/- cells demonstrate greater chemoresistance that RCC4-VHL WT cells **(Figure 3.2C)**.

Alkaline comet assay **(Section 2.9)** demonstrated that RCC4-VHL -/- cells showed no measurable difference in comet tail moment after treating with CPT, whilst RCC4-VHL WT cells showed clear DNA breaks **(Figure 3.2 D-E)**. Therefore, RCC4-VHL -/- cells showed reduced damage to DNA damaging agents. Taken together with the clonogenic analysis and CellTiter-Blue assay, the increased survival observed in RCC4-VHL -/- cells may be due to the reduced damage caused by CPT, rather than a lack of cellular response to damage.

As tumours from ccRCC patients typically also show enhanced resistance to radiotherapy, it was important to see whether this phenotype could be observed in RCC4 cells. IR induces DNA DSBs by breaking covalent bonds between DNA, thus inducing cell death. In addition, DNA SSBs form as a secondary effect via ROS generation (Borrego-Soto et al., 2015). I treated the cells with increasing doses of IR **(Section 2.7.1.2)**, and then performed clonogenic analysis as previously described. Surprisingly, no significant difference was observed between RCC4-VHL WT and RCC4-VHL -/- **(Figure 3.3)**. This suggested that RCC4 cells may not be a good model to study the effect of radioresistance in ccRCC patients as RCC4-VHL -/- cells do not show enhanced resistance to IR. However, it may have been more accurate to use a different assay to measure DNA damage as clonogenic analysis only measures survival, rather than quantifying DNA damage. Therefore, a different assay that quantifies SSBs and DSBs may be more accurate, such as the comet assay.

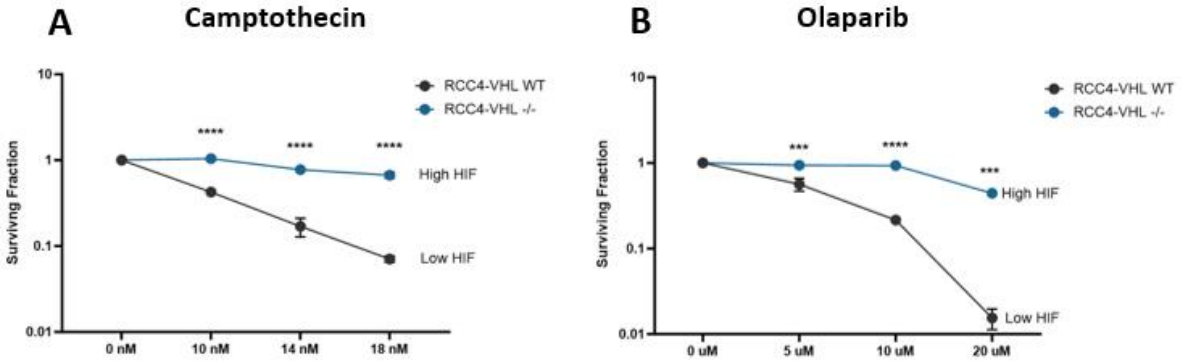
A
Camptothecin
Survivng Fraction
RCC4-VHL WT
RCC4-VHL -/-
High HIF
Low HIF
0 nM
10 nM
14 nM
18 nM
B
Olaparib
Surviving Fraction
0 uM
5 uM
10 uM
20 uM

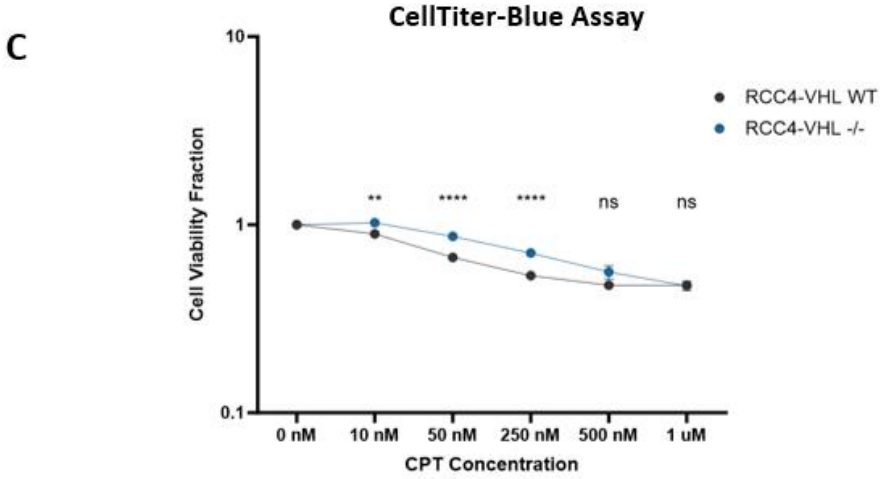
C
CellTiter-Blue Assay
Cell Viability Fraction
RCC4-VHL WT
RCC4-VHL -/-
0 nM
10 nM
50 nM
250 nM
500 nM
1 uM
CPT Concentration

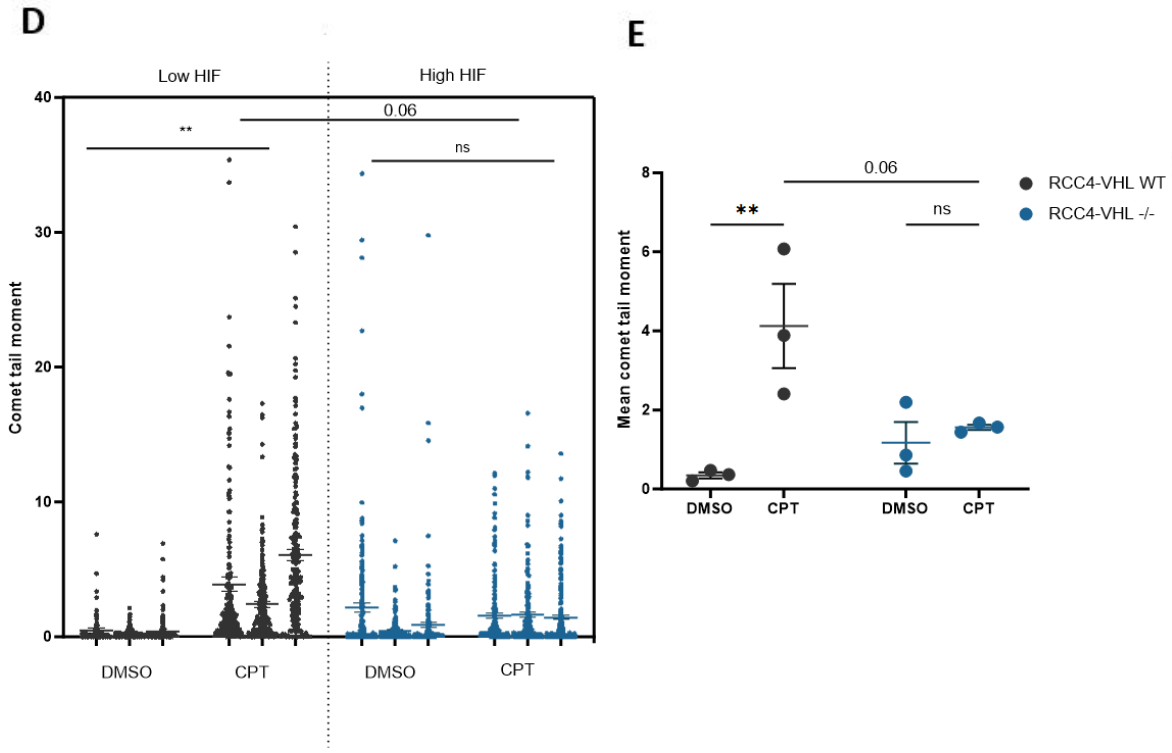
D
Low HIF
High HIF
0.06
Comet tail moment
DMSO
CPT
E
Mean comet tail moment
RCC4-VHL WT
RCC4-VHL -/-

Figure 3.2: RCC4-VHL -/- cells are more chemoresistant than RCC4-VHL WT cells. A-B) Clonogenic analysis comparing CPT or Olaparib resistance between RCC4-VHL WT cells and RCC4-VHL -/- cells. Two-way ANOVA with Šidák correction, ***p<0.001, ****p<0.0001, Mean ± SEM, n=3. **C)** CellTiter-Blue assay comparing cell viability after CPT treatment in RCC4-VHL WT cells and RCC4-VHL -/- cells. Two-way ANOVA with Šidák correction, ns=p>0.05, **p<0.01, ****p<0.0001, Mean ± SEM, n=3. **D-E)** Comet assay comparing CPT (40 µM) resistance between RCC4-VHL WT cells and RCC4-VHL -/- cells. **D)** Raw values for comet tail moments. **E)** Mean come tail moment for all three biological repeats. Two-way ANOVA with Tukey Correction, ns=p>0.05, **p<0.01, Mean ± SEM, n=3.

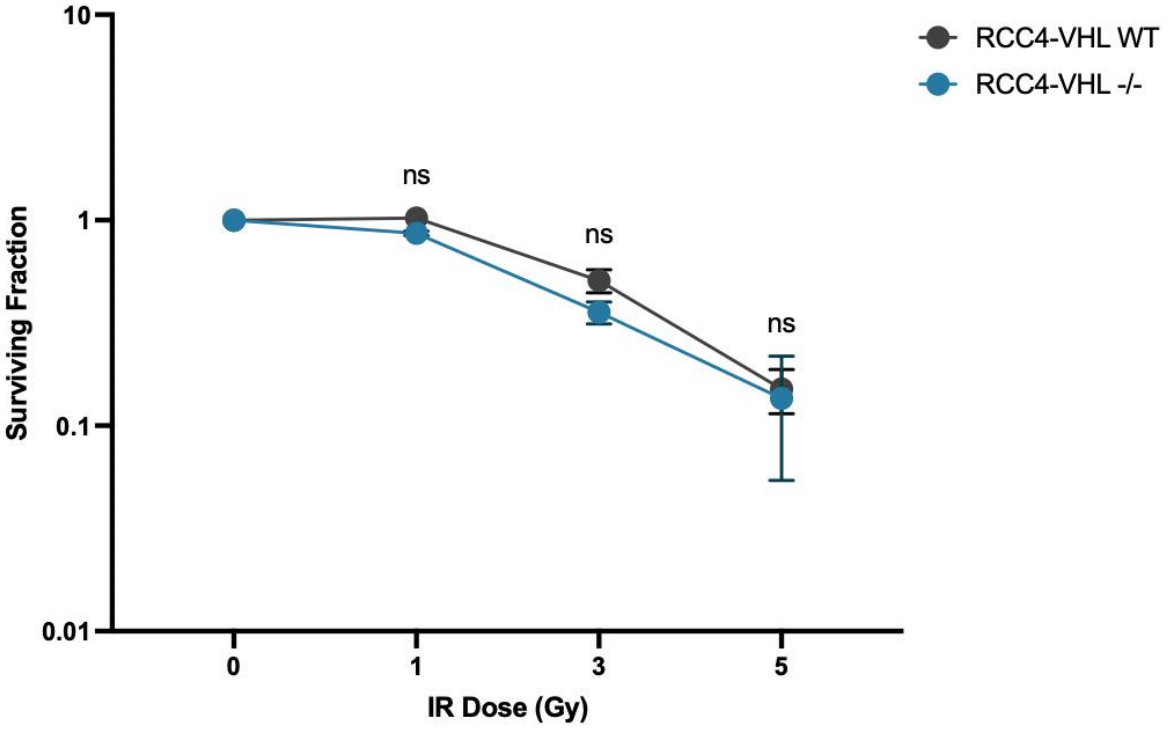

Figure 3.3: RCC4-VHL -/- are not more resistant to IR compared to RCC4-VHL WT cells. Clonogenic analysis comparing IR resistance between RCC4-VHL WT cells and RCC4-VHL -/- cells. Two-way ANOVA with Šidák correction, ns=p>0.05, Mean ± SEM, n=3.

3.4.3. RCC4-VHL -/- cells have an enhanced expression of TDP1, which can be reduced by modulating HIF2α expression

RCC4-VHL -/- clearly showed an enhanced resistance to CPT compared to RCC4-VHL WT **(Figure 3.2)**. Therefore, I decided to explore the molecular mechanisms further to understand how a lack of functional VHL causes this. The first experiment performed was a western blot to probe for various proteins of interest that may be involved in enhancing DNA repair or protecting cells from damage induced by CPT. I settled on probing for NuMA, PARP1, TOP1, TDP1, and pXRCC1 due to their previously reported roles in DNA repair after CPT treatment (Plo et al., 2003; Liu et al., 2007; Jakobsen et al., 2015; Chowdhuri and Das, 2021). RCC4-VHL -/- cells showed a statistically significant upregulation of TDP1 and pXRCC1 compared to RCC4-VHL WT cells **(Figure 3.4)**.

I observed the gene expression of other DNA repair genes via RT-qPCR. *BRCA1* and *FANCD2* are two genes involved in HR to repair DSBs, which were reported to be downregulated in RCC4-VHL -/- cells (Scanlon and Glazer, 2015). MRE11 has been shown to interact with both BRCA1 and FANCD2 (Roques et al., 2009; Kais et al., 2016; Bian et al., 2019), so it would be interesting to see if the expression of these three genes are upregulated or downregulated in my cell lines, and whether my data matched Scanlon and Glazer (2015). Lastly, a functional connection has been identified between polynucleotide kinase (PNK) and XRCC1/TDP1 (Plo et al., 2003). Therefore, the gene expression of *PNK* was also of interest. I found that the gene expression of *BRCA1* was significantly upregulated in RCC4-VHL -/- cells, whilst *MRE11* had mild, but insignificant, upregulation. *PNK* expression did not change between both RCC4 cell lines **(Figure 3.5)**.

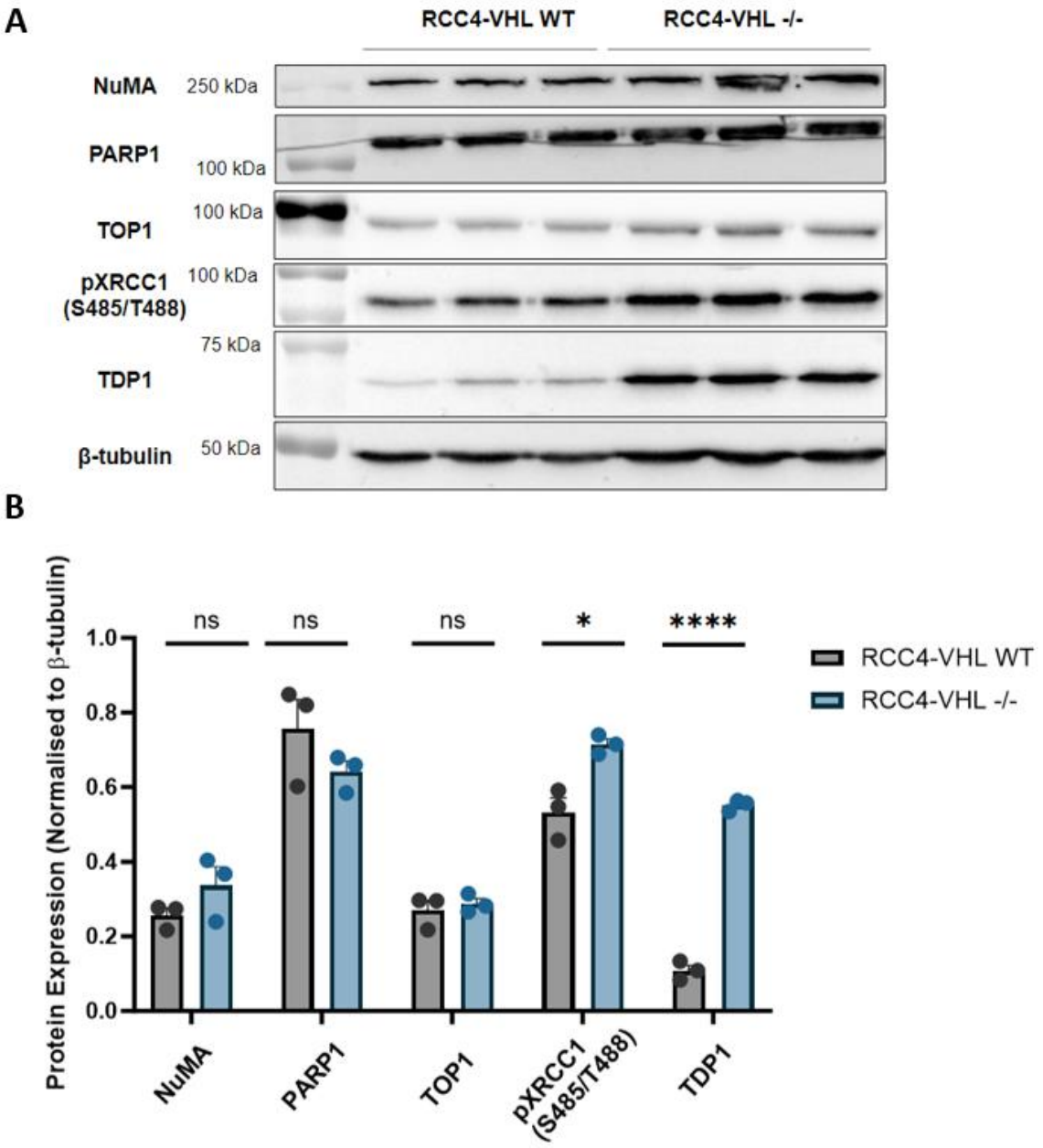

Figure 3.4: Screening various DNA repair proteins in RCC4 cells. A) Lysates from RCC4-VHL WT cells and RCC4-VHL -/- cells were probed for various DNA repair proteins of interest. β-tubulin was used as a loading control. **B)** Quantification of previous western blot, showing statistically significant upregulation of pXRCC1 and TDP1. Multiple unpaired Student's t-test, ns=p>0.05, *p<0.05, ****p<0.0001, Mean ± SEM, n=3.

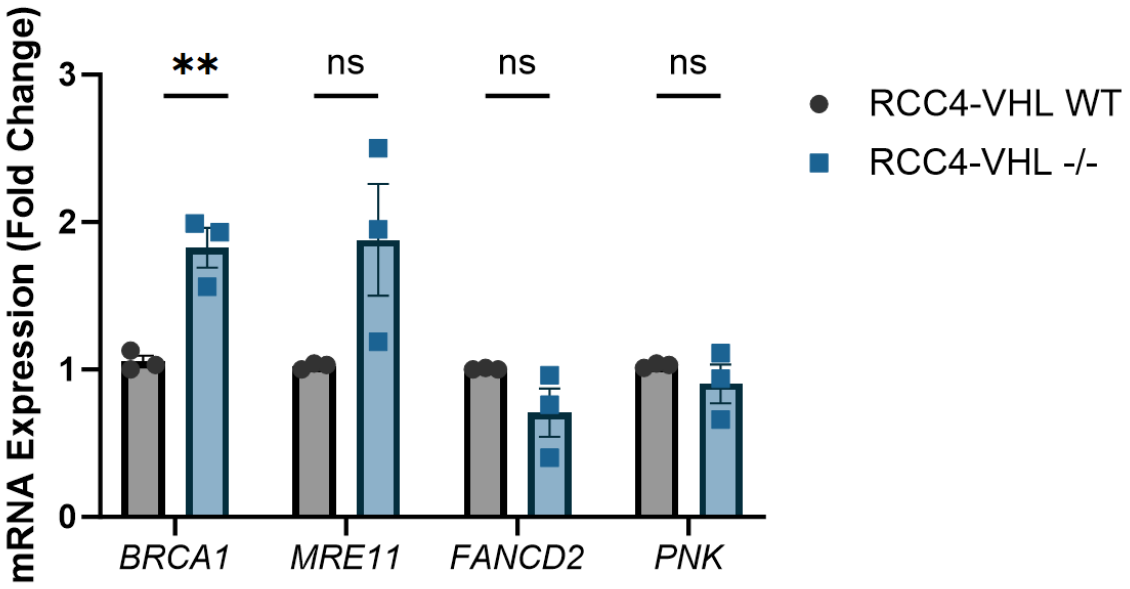

Figure 3.5: *BRCA1* mRNA expression is upregulated in RCC4-VHL -/- cells. RT-qPCR was performed on alternative DNA repair genes of interest which I was unable to probe for on a western blot. *BRCA1* mRNA expression was upregulated in RCC4-VHL -/- cells. *PPIA* was used as a housekeeping gene. Multiple unpaired Students' t-test, **p<0.01, Mean ± SEM, n=3.

The strong upregulation of TDP1 was most interesting to me, as upregulation of TDP1 had been previously identified as one of the causes of enhanced resistance to CPT in NSCLC (Liu et al., 2007). The importance of TDP1 in protecting cells from DNA damage has also been addressed extensively in other papers (Barthelmes et al., 2004; Zaksauskaite et al., 2021). Therefore, most of my experiments tended to focus on the role of TDP1 in protecting cells from cytotoxic agents.

The western blot that I had used **(Figure 3.4A)** to initially identify the upregulation of TDP1 had been stripped and reprobed **(Section 2.5.6)** three times. To make sure that the increase of TDP1 was reproducible, I repeated the western blot once more. TDP1 protein expression showed ~5-fold change increase between RCC4-VHL WT and RCC4-VHL -/- **(Figure 3.6 A-B)**. I wanted to test whether this difference would also be observed at the *TDP1* gene expression level. Therefore, I performed an RT-qPCR between RCC4-VHL WT and RCC4-VHL -/- cells looking at *TDP1* mRNA expression. This showed ~3-fold increase **(Figure 3.6C)**, suggesting that TDP1 is increased at the transcriptional level, and not just the protein level.

To establish whether the increase of TDP1 expression in RCC4-VHL -/- cells was also reflected in an increased TDP1 activity, I used a TDP1 activity assay **(Section 2.10)** comparing the cleavage efficiency of TDP1 on DNA in RCC4-VHL WT and RCC4-VHL -/- cells. Increasing amounts of protein lysate were combined with oligonucleotides containing a Cy5.5 fluorophore at the 5' end, and a phosphotyrosyl group (PY) at the 3' end. TDP1 converts PY to a phosphate (P) group, causing the oligonucleotide to migrate to a lower level on a urea gel. By looking at the fraction of oligonucleotide that has shifted to the lower band, I can calculate TDP1 processing activity **(Figure 3.7A)** (Zaksauskaite et al., 2021). RCC4-VHL -/- cells were more effective at cleaving the oligonucleotide **(Figure 3.7 B-C)**, suggesting that the increase in TDP1 expression translates to an increased capacity for RCC4-VHL -/- to repair damaged DNA through enhanced TDP1 enzymatic activity.

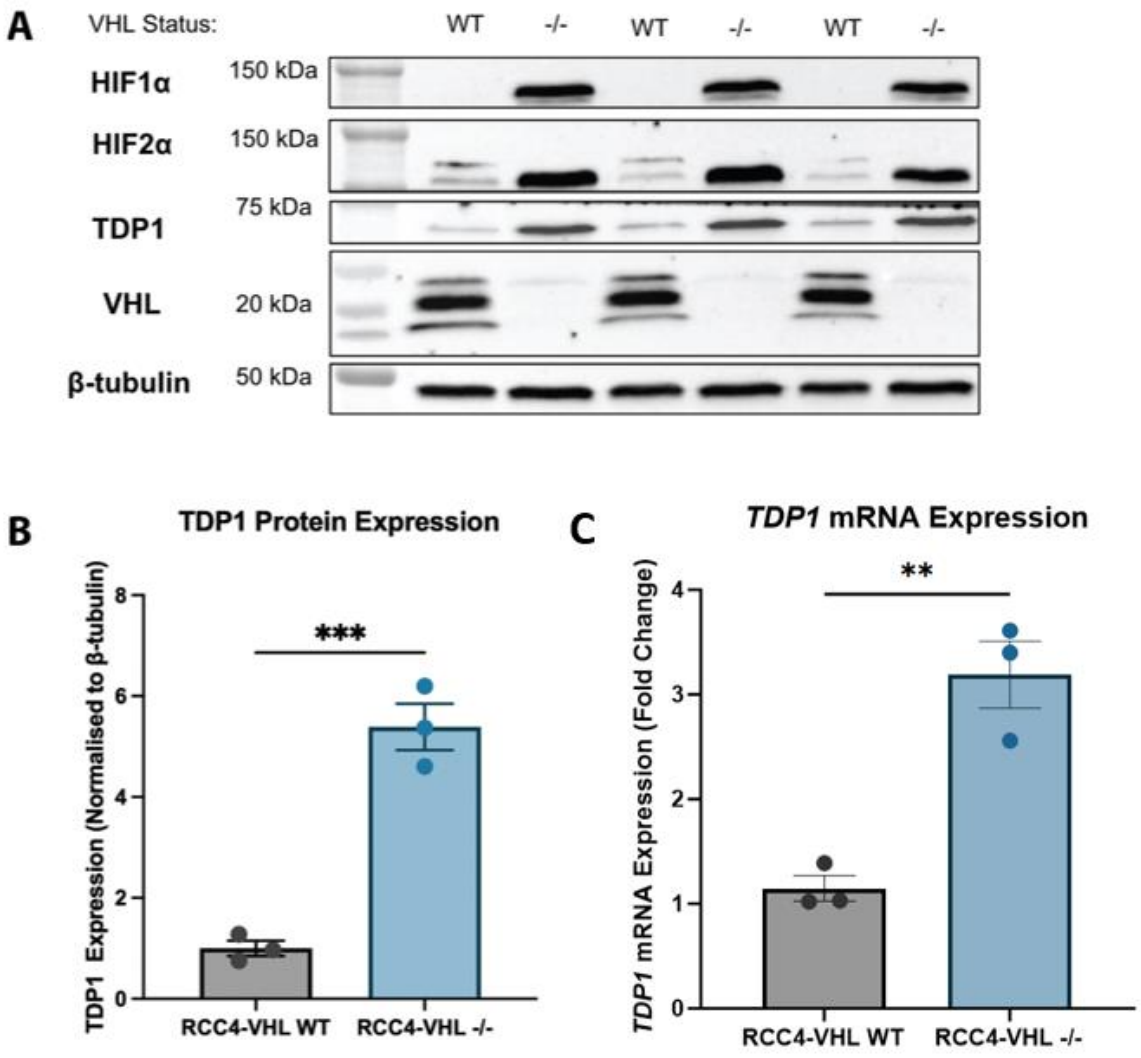

Figure 3.6: TDP1 protein expression, and mRNA expression are upregulated in RCC4-VHL -/- cells. A) Western blot from **Figure 3.1** reprobed for TDP1. β-tubulin was used as a loading control. **B)** Quantification of previous western blot showing upregulated TDP1 protein expression. Unpaired Student's t-test, ***p<0.001, Mean ± SEM, n=3. **C)** RT-qPCR showing upregulated *TDP1* mRNA expression in RCC4-VHL -/- cells. *PPIA* was used as a housekeeping gene. Unpaired Student's t-test, **p<0.01, Mean ± SEM, n=3.

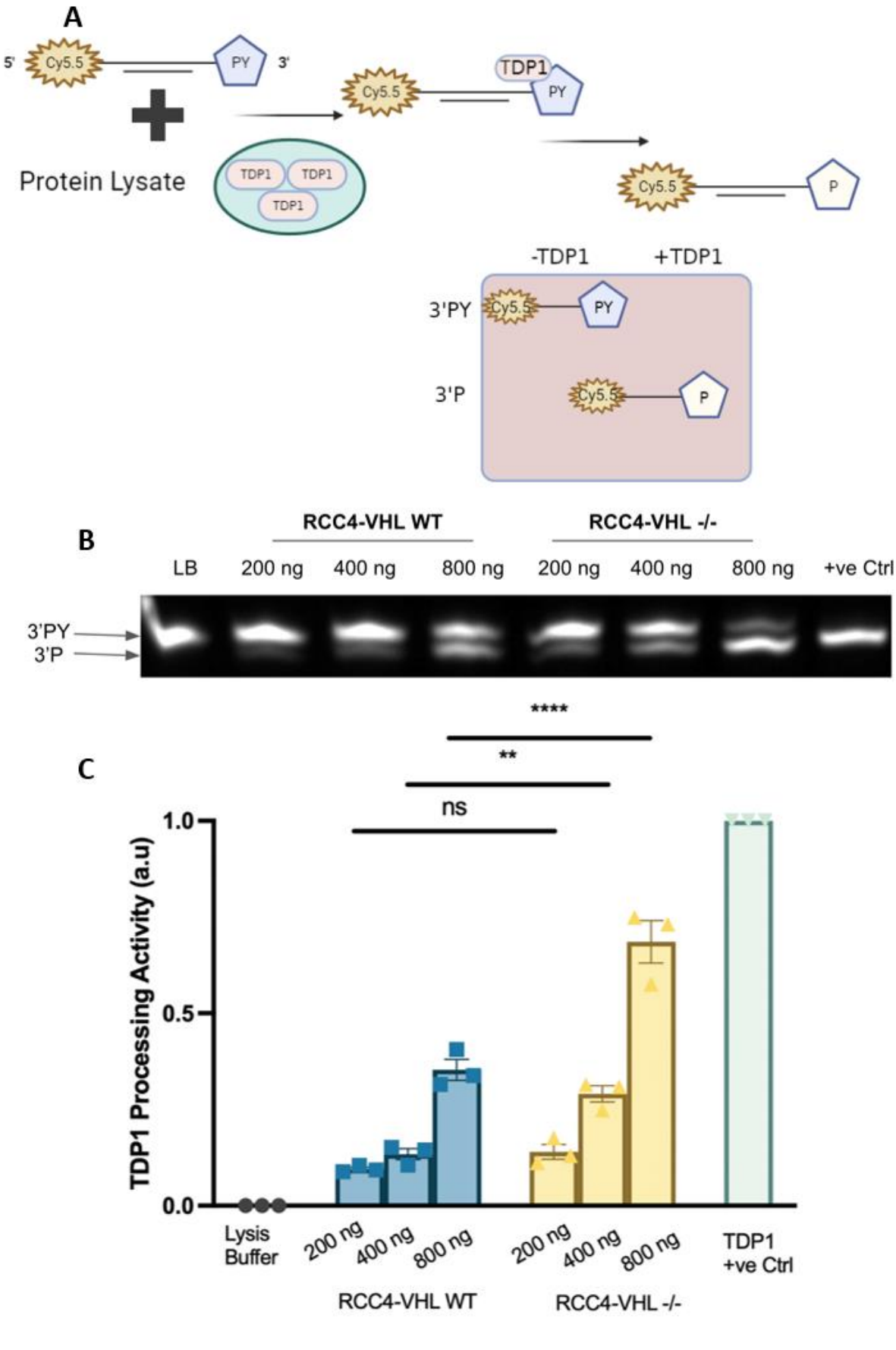
A
5'
Cy5.5
PY
3'
Protein Lysate
TDP1
TDP1
TDP1
Cy5.5
TDP1
PY
Cy5.5
P
-TDP1
+TDP1
3'PY
Cy5.5
PY
3'P
Cy5.5
P
B
RCC4-VHL WT
RCC4-VHL -/-
LB
200 ng
400 ng
800 ng
200 ng
400 ng
800 ng
+ve Ctrl
3'PY
3'P
****
**
ns
C
TDP1 Processing Activity (a.u)
1.0
0.5
0.0
Lysis Buffer
200 ng
400 ng
800 ng
200 ng
400 ng
800 ng
TDP1 +ve Ctrl
RCC4-VHL WT
RCC4-VHL -/-

Figure 3.7: TDP1 enzymatic activity is greater in RCC4-VHL -/- cells. A) Diagram explaining how the TDP1 activity assay works, whereby TDP1 causes a band shift on a urea gel by converting the 3' phosphotyrosyl group (PY) on an oligonucleotide to a phosphate group (P), which is detectable by Cy5.5 [adapted] (Zaksauskaite et al., 2021). **B)** Urea gel showing a greater shift in the 3' PY band to the 3' P in RCC4-VHL -/-, which corresponds to greater TDP1 activity. LB = Lysis Buffer. +ve Ctrl = purified TDP1 protein. **C)** Quantification of TDP1 activity assay. Two-way ANOVA with Šidák correction, ns=$p>0.05$, **$p<0.01$, ****$p<0.0001$, Mean ± SEM, n=3.

The effect of VHL on modulating HIF has been extensively described **(Section 1.2.2)**. Therefore, I hypothesised that the upregulation of HIF1α, HIF2α, or both, was responsible for the upregulation of TDP1. By looking at previously uploaded chromatin immunoprecipitation sequencing (ChIP-Seq) data (Smythies et al., 2019), I discovered that both HIF1α and HIF2α showed high interaction with TDP1 promoter regions **(Figure 3.8)**. Given the potential interaction between both HIFs and TDP1, this suggested that both HIFs may be modulating the activity of TDP1 in RCC4-VHL -/- cells.

To establish whether HIF expression can modulate TDP1 expression, I used siRNA targeting HIF1α/HIF2α **(Section 2.11)** and looked at what happened to TDP1 at the protein and gene expression levels. The siRNA effectively knocked down HIF1α/HIF2α gene and protein expression **(Figure 3.9 A/C)**. Interestingly, whilst HIF1α knockdown seemed to show no increase in TDP1 protein expression, HIF2α knockdown caused a trend towards downregulation in TDP1 protein expression and gene expression. Combining both HIF1α and HIF2α knockdown caused TDP1 protein expression to return close to baseline levels, suggesting that downregulating HIF1α may somehow be able to counteract the effect of HIF2α on TDP1 **(Figure 3.9 A-B)**. However, this effect was not seen in gene expression **(Figure 3.9D)**. In addition, I wanted to see whether the previously observed mild upregulation of pXRCC1 in RCC4-VHL -/- **(Figure 3.4)** was linked to HIF expression, so I probed for pXRCC1 on the same blots. However, I did not see any change in pXRCC1 expression, nor did I see a difference between RCC4-VHL WT and RCC4-VHL -/- **(Figure 3.9E)**, suggesting that any changes in pXRCC1 expression are likely to be minor and insignificant.

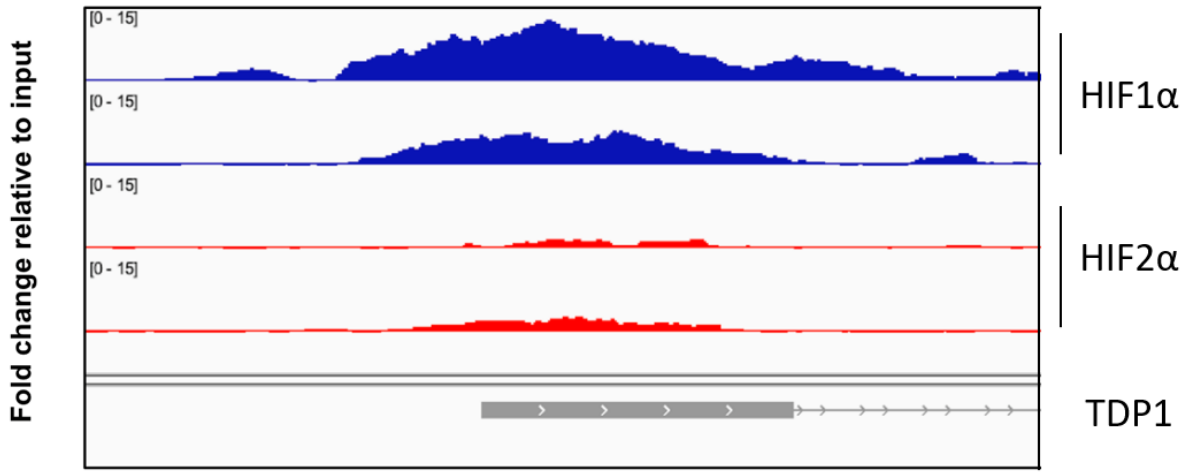

Figure 3.8: HIF1α and HIF2α show high interaction with TDP1 promoter region. Integrative Genome Viewer (IGV) snapshots of HIF1α and HIF2α ChIP-Seq signal over TDP1 promoter region. n=2. ChIP-Seq datasets uploaded by Smythies et al., (2019).

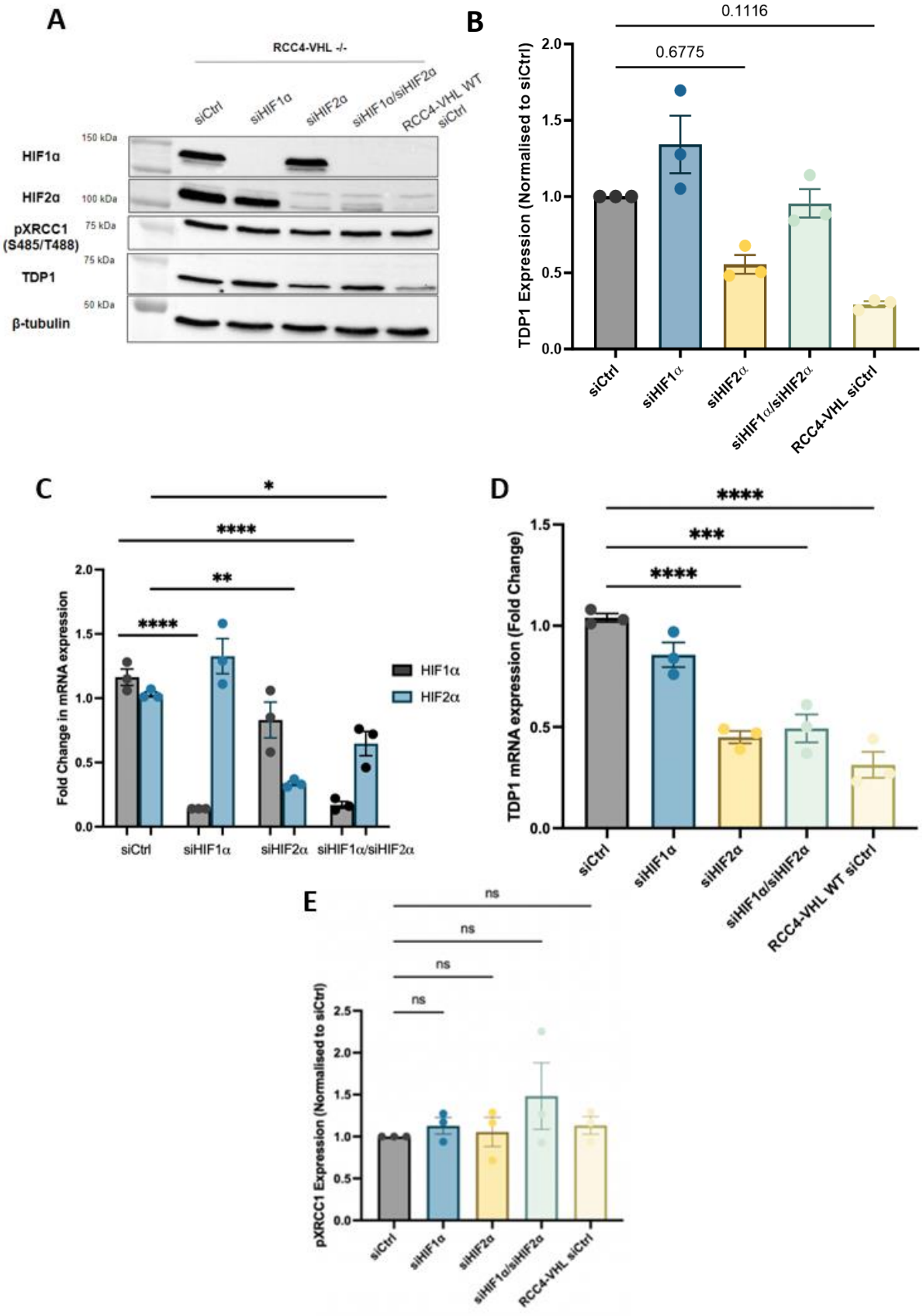
A
RCC4-VHL -/-
siCtrl
siHIF1α
siHIF2α
siHIF1α/siHIF2α
RCC4-VHL WT siCtrl
150 kDa
HIF1α
100 kDa
HIF2α
75 kDa
pXRCC1 (S485/T488)
75 kDa
TDP1
50 kDa
β-tubulin
B
0.1116
0.6775
TDP1 Expression (Normalised to siCtrl)
2.0
1.5
1.0
0.5
0.0
siCtrl
siHIF1α
siHIF2α
siHIF1α/siHIF2α
RCC4-VHL siCtrl
C
*
****
**
****
Fold Change in mRNA expression
2.0
1.5
1.0
0.5
0.0
HIF1α
HIF2α
siCtrl
siHIF1α
siHIF2α
siHIF1α/siHIF2α
D
****
***
****
TDP1 mRNA expression (Fold Change)
1.5
1.0
0.5
0.0
siCtrl
siHIF1α
siHIF2α
siHIF1α/siHIF2α
RCC4-VHL WT siCtrl
E
ns
ns
ns
ns
pXRCC1 Expression (Normalised to siCtrl)
2.5
2.0
1.5
1.0
0.5
0.0
siCtrl
siHIF1α
siHIF2α
siHIF1α/siHIF2α
RCC4-VHL siCtrl

Figure 3.9: TDP1 gene and protein expression can be reduced via HIF2α knockdown. A) Representative western blot showing protein expression of HIF1α, HIF2α, TDP1, and pXRCC1 after transfecting RCC4-VHL -/- cells with control siRNA (siCtrl), HIF1α siRNA (siHIF1α), and HIF2α siRNA (siHIF2α). TDP1 protein expression is downregulated after knocking down HIF2α. pXRCC1 expression does not change. RCC4-VHL WT was included as a control. β-tubulin was used as a loading control. **B)** Quantification of western blot showing a trend of TDP1 protein expression downregulation after siHIF2α. Kruskal-Wallis with Dunn's correction, ns=p>0.05, Mean ± SEM, n=3. **C)** RT-qPCR on RCC4-VHL -/- cells after transfecting with siCtrl, siHIF1α, and siHIF2α, showing successful knockdown of target genes. *PPIA* was used as a housekeeping gene. One-way ANOVA with Dunnet correction, *p<0.05, **p<0.01, ****p<0.0001, Mean ± SEM, n=3. **D)** RT-qPCR showing that *TDP1* gene expression is downregulated after siHIF2α. *PPIA* was used as a housekeeping gene. One-way ANOVA with Dunnet correction, ***p<0.001, ****p<0.0001, Mean ± SEM, n=3. **E)** Quantification of pXRCC1 expression on western blot showing no measurable difference in pXRCC1 expression following HIFα knockdowns. Kruskal-Wallis with Dunn's correction. ns=p>0.05, Mean ± SEM, n=3.

I wanted to see whether growing RCC4-VHL WT cells in a hypoxic incubator would cause TDP1 protein expression to increase alongside increased expression of HIF1α/HIF2α. I seeded the cells in a 6-well plate and left them to adhere overnight, before placing them in a 1% oxygen incubator for 8 hours, harvesting cells at 2-hour intervals. HIF levels increased the longer the cells were left in hypoxia, but this did not correlate with increased TDP1 expression **(Figure 3.10)**. An interesting observation was that TDP1 protein expression seemed to increase and then decrease over time, although as this was just one repeat the results may not be consistent if they were to be repeated. This experiment suggested that modulating HIF levels on their own via siRNA may not be sufficient to accurately establish the role of hypoxia in chemoresistance as I was not targeting other pathways that be impacted by hypoxia. Targeting HIFs using siRNA does not achieve the TDP1 oscillation that I saw when growing cells in the hypoxic incubator. However, as the concentration of oxygen used (1%) in the hypoxic incubator may not be an accurate model of tumour hypoxia as hypoxic cores can reach concentrations as low as 0.1%, which have been shown to trigger different pathways (Hu et al., 2003; McKeown, 2014; Hompland et al., 2018). The HIF-independent functions of VHL may also be behaving differently when the cells are grown in a hypoxic incubator compared to when cells are grown in a 20% oxygen incubator.

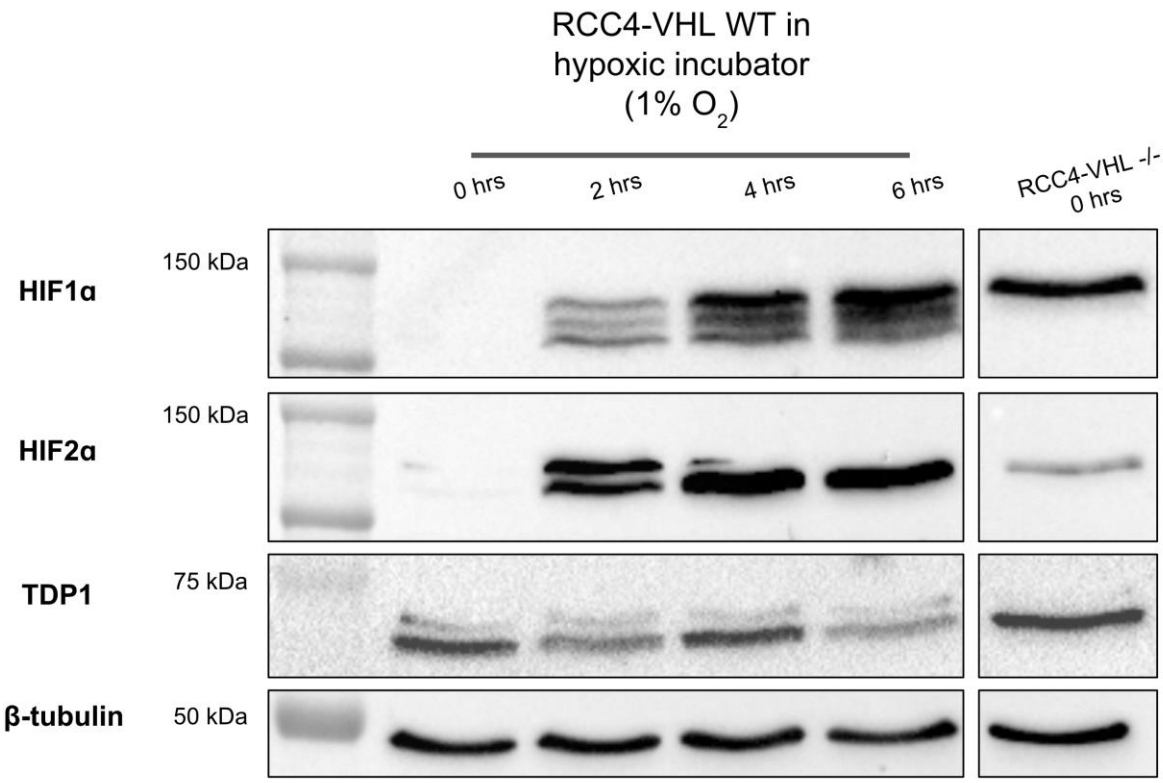

Figure 3.10: TDP1 protein expression is not upregulated in RCC4-VHL WT cells grown in hypoxia. Western blot for RCC4-VHL WT cells grown in a 1% oxygen incubator for different time periods, showing that growing cells in a 1% oxygen incubator was not sufficient to upregulate TDP1 protein levels, despite the upregulation in HIF1α and HIF2α levels. RCC4-VHL -/- cells were included to compare HIF1α, HIF2α, and TDP1 expression. HIF2α expression of RCC4-VHL WT cells was greater than that of the pseudohypoxic RCC4-VHL -/- cells. HIF1α appears to have three distinct bands between two- and six-hours hypoxic exposure, with a shift being observed from the bottom band to the bottom band. The top band of HIF1α is the phosphorylated form, whilst the bottom band is the unphosphorylated form. The middle band may be HIF1α phosphorylated on a different site. Phosphorylated HIF1α has higher transcription activity than unphosphorylated HIF1α (Bullen et al., 2016). β-tubulin was used as a loading control.

Lastly, I used the HIF2α-specific inhibitor PT2385 in RCC4-VHL -/- to see if pharmacologically targeting HIF2α only could cause a downregulation in TDP1 expression. PT2385 prevents the dimerisation of HIF2α with HIF1β, thereby preventing the upregulation of HIF2α-specific target genes, such as *VEGFA* (Wallace et al., 2016). I decided to look at the gene expression of *VEGFA* via RT-qPCR following PT2385 treatment to determine whether PT2385 worked as expected. This showed a strong downregulation of *VEGFA* following PT2385 treatment, indicating that PT2385 was functioning, as the HIF2α pathway had been downregulated **(Figure 3.11A)**, although I was only able to plot two data points as the mRNA extraction for the third repeat was not performed correctly. *TDP1* gene expression did not seem to change much after PT2385 treatment, only showing a minor downregulation. Interestingly, TDP1 protein expression seemed to increase, rather than decrease, after PT2385 treatment, although the increase was not statistically significant **(Figure 3.11 B-C)**. This ran counter to what I had observed when knocking down HIF2α expression using siRNA, suggesting a clear difference when using pharmacological inhibition or genetic interference. Alternatively, TDP1 expression may have mildly increased as an early response to HIF2α-mediated downregulation of other DNA repair proteins.

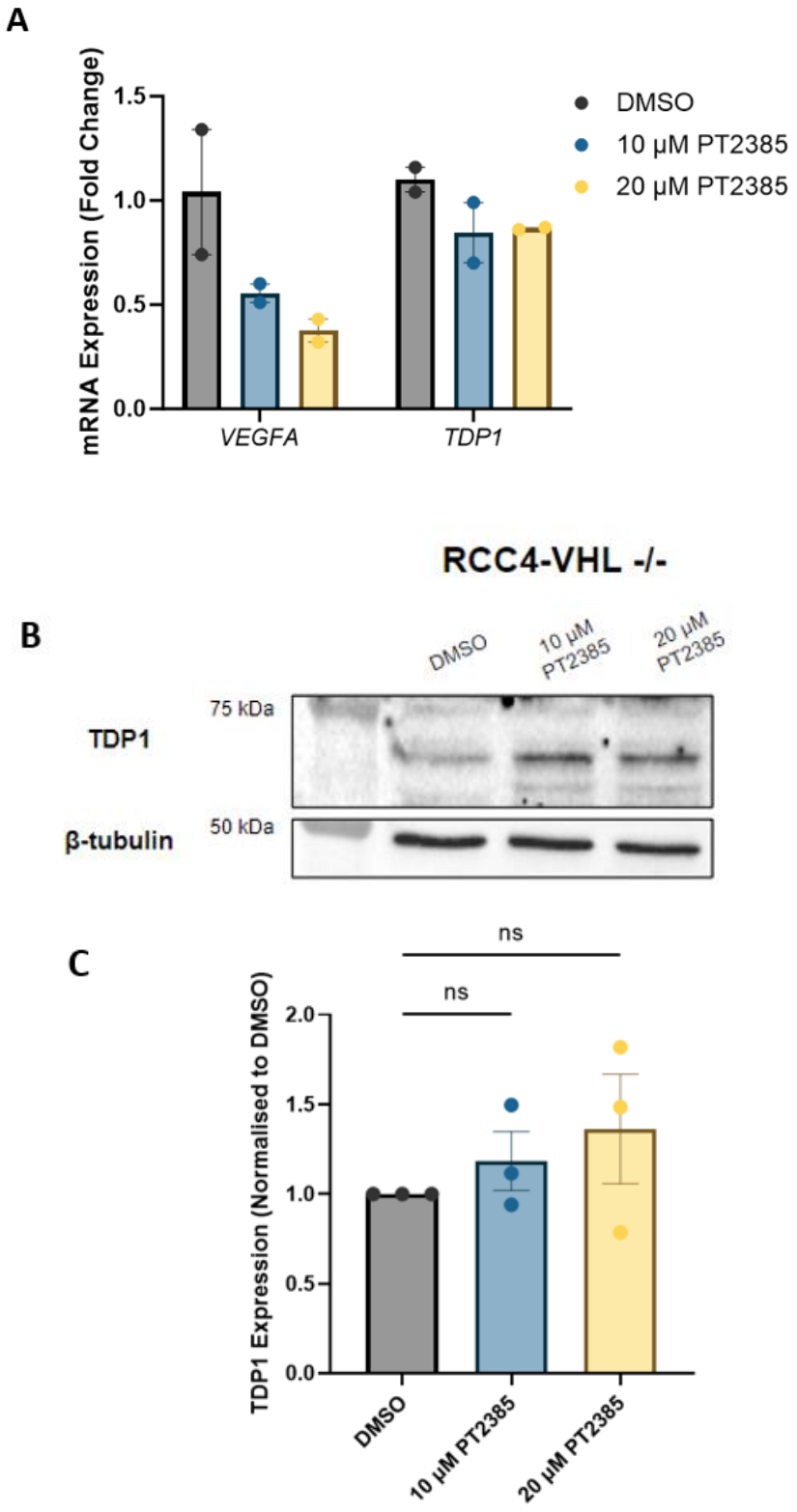
A
mRNA Expression (Fold Change)
1.5
1.0
0.5
0.0
VEGFA
TDP1
DMSO
10 μM PT2385
20 μM PT2385
RCC4-VHL -/-
B
DMSO
10 μM PT2385
20 μM PT2385
75 kDa
TDP1
50 kDa
β-tubulin
C
ns
ns
TDP1 Expression (Normalised to DMSO)
2.0
1.5
1.0
0.5
0.0
DMSO
10 μM PT2385
20 μM PT2385

Figure 3.11: PT2385 treatment in RCC4-VHL -/- cells does not cause reduced TDP1 expression. A) RT-qPCR on RCC4-VHL -/- cells after treating them with DMSO, 10 μM PT2385, or 20 μM PT2385 for 24 hours. *VEGFA* (HIF2α target gene) mRNA expression was downregulated upon PT2385 treatment, indicating that the chemical is working. *TDP1* gene expression did not change dramatically. *PPIA* was used as a housekeeping gene. Mean ± SEM, n=2. **B)** Representative western blot showing an upregulation in TDP1 protein expression in RCC4-VHL -/- cells after treating them with DMSO, 10 μM PT2385, or 20 μM PT2385 for 24 hours. β-tubulin was used as a loading control. **C)** Quantification of previous western blot showing that the upregulation of TDP1 protein expression is not statistically significant. Kruskal-Wallis with Dunn's correction, ns=p>0.05, Mean ± SEM, n=3.

3.4.4. RCC4-VHL -/- cells have a higher pNuMA/NuMA ratio compared to RCC4-VHL WT cells, in a HIF-independent manner

Ray et al., (2022) recently described a protein involved in enriching TDP1 and XRCC1 at DNA SSBs, called NuMA. Following oxidative stress, NuMA interaction with TDP1 and XRCC1 is enriched at chromatin regions, increasing TDP1 and XRCC1 transcription and their expression. Therefore, NuMA is important for repairing SSBs due to the recruitment of TDP1-repair machinery. When I had previously looked at NuMA expression, I found no significant difference between RCC4-VHL WT and RCC4-VHL -/- **(Figure 3.4A)**.

As I had previously found upregulation of TDP1 in RCC4-VHL -/- cells, I decided to revisit NuMA expression in RCC4. In response to DNA damage, NuMA is phosphorylated at S395, possibly to regulate DNA repair protein enrichment at damaged chromatin (Moreno et al., 2019). Even though NuMA expression was not different between RCC4 cells, I could see a clear difference in the levels of NuMA phosphorylation at S395 **(Figure 3.12 A-B)**. When quantifying NuMA phosphorylation, I decided to standardise pNuMA expression by comparing it to the expression of NuMA to counter any variations that may be seen in NuMA.

As it had previously been shown that ATM/ATR is involved in phosphorylating NuMA at S395 (Matsuoka et al., 2007), I decided to treat RCC4 cells with an ATM inhibitor (KU-5593) or ATR inhibitor (VE-821) to see if inhibiting the ATM/ATR pathway could reduce the expression levels of pNuMA (S395). Interestingly, it was found that despite ATM inhibition reducing pNuMA expression, ATR inhibition increased pNuMA expression **(Figure 3.12C)**.

One potential reason for upregulation of pNuMA in RCC4-VHL -/- is the enhanced expression of ATM, causing greater phosphorylation of NuMA. However, ATM expression was not found to be significantly different between the RCC4 cells **(Figure 3.12B)**. I hypothesised that the upregulation of pNuMA was due to the upregulation of either HIF1α or HIF2α in RCC4-VHL -/- cells. Therefore, I knocked down the expression of either HIF1α or HIF2α in the RCC4-VHL -/- cells to see if pNuMA or NuMA expression would decrease upon modulating HIFα. As pNuMA is not highly expressed under baseline conditions, I exaggerated pNuMA expression by treating the cells with 10 µM CPT for 1 hour and compared pNuMA

expression of the CPT-treated cells, whilst NuMA expression was compared for both DMSO-treated and CPT-treated cells. Modulating HIFα levels via siRNA had no measurable impact on either NuMA or pNuMA expression **(Figure 3.13)**, suggesting that pNuMA is upregulated in RCC4-VHL -/- cells via HIF-independent mechanisms.

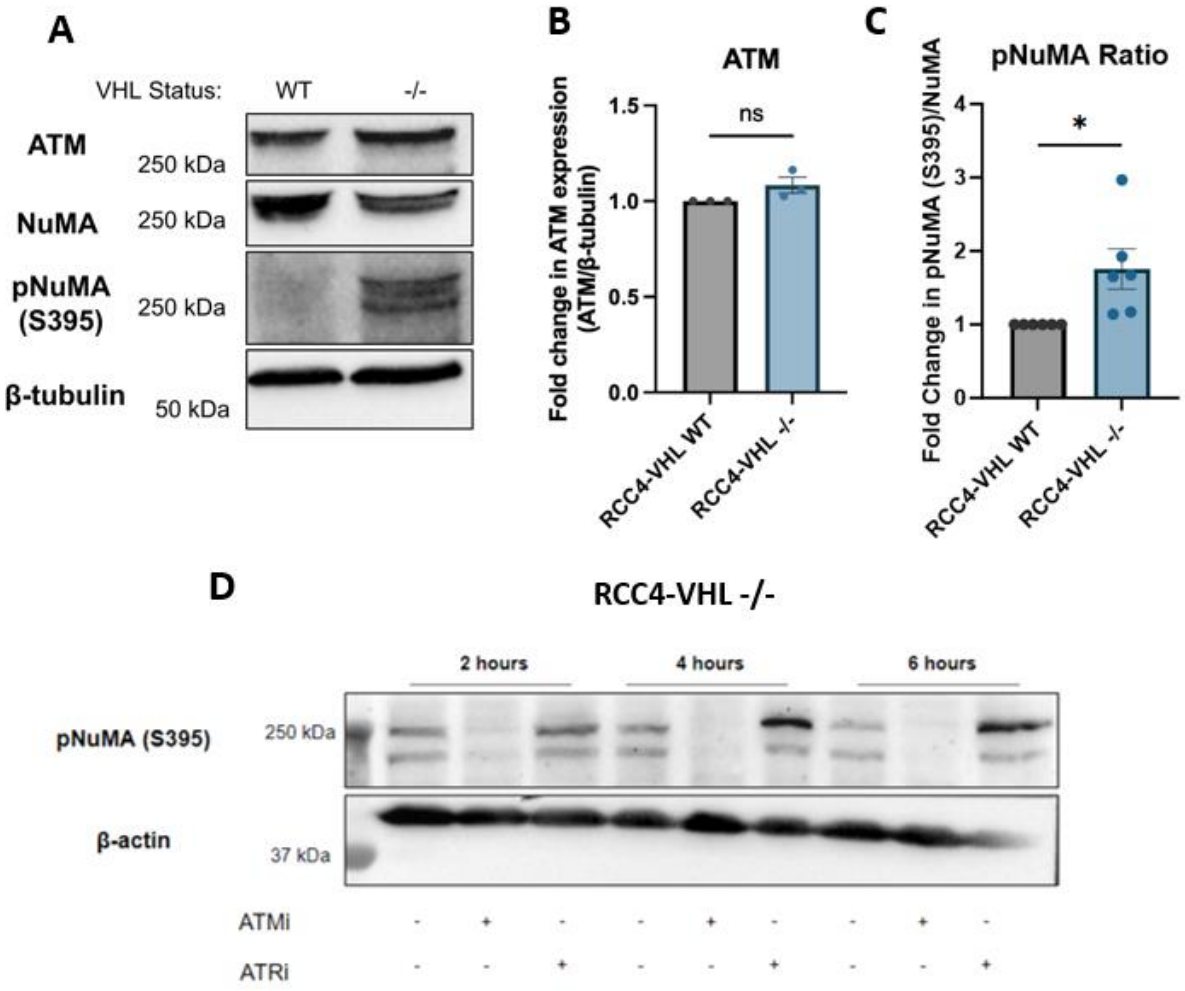

Figure 3.12: Phosphorylation of NuMA at S395 (pNuMA) is upregulated in VHL -/- cells. A) Western blot showing upregulation of pNuMA in RCC4-VHL -/- cells, and no difference in ATM and NuMA expression. β-tubulin was used as a loading control. **B-C)** Quantification of previous western blot. Wilcoxon signed-rank test, ns=p>0.05, *p<0.05, Mean ± SEM, n=3 (ATM), n=6 (pNuMA). **D)** Western blot showing that the phosphorylation of pNuMA is mediated by ATM and ATR at S395. ATM inhibition causes a downregulation of pNuMA (S395). ATR inhibition causes an upregulation of pNuMA (S395). RCC4-VHL -/- were treated with DMSO (Control), 10 µM KU-5593 (ATMi), or 10 µM VE-821 (ATRi). β-actin was used as a loading control.

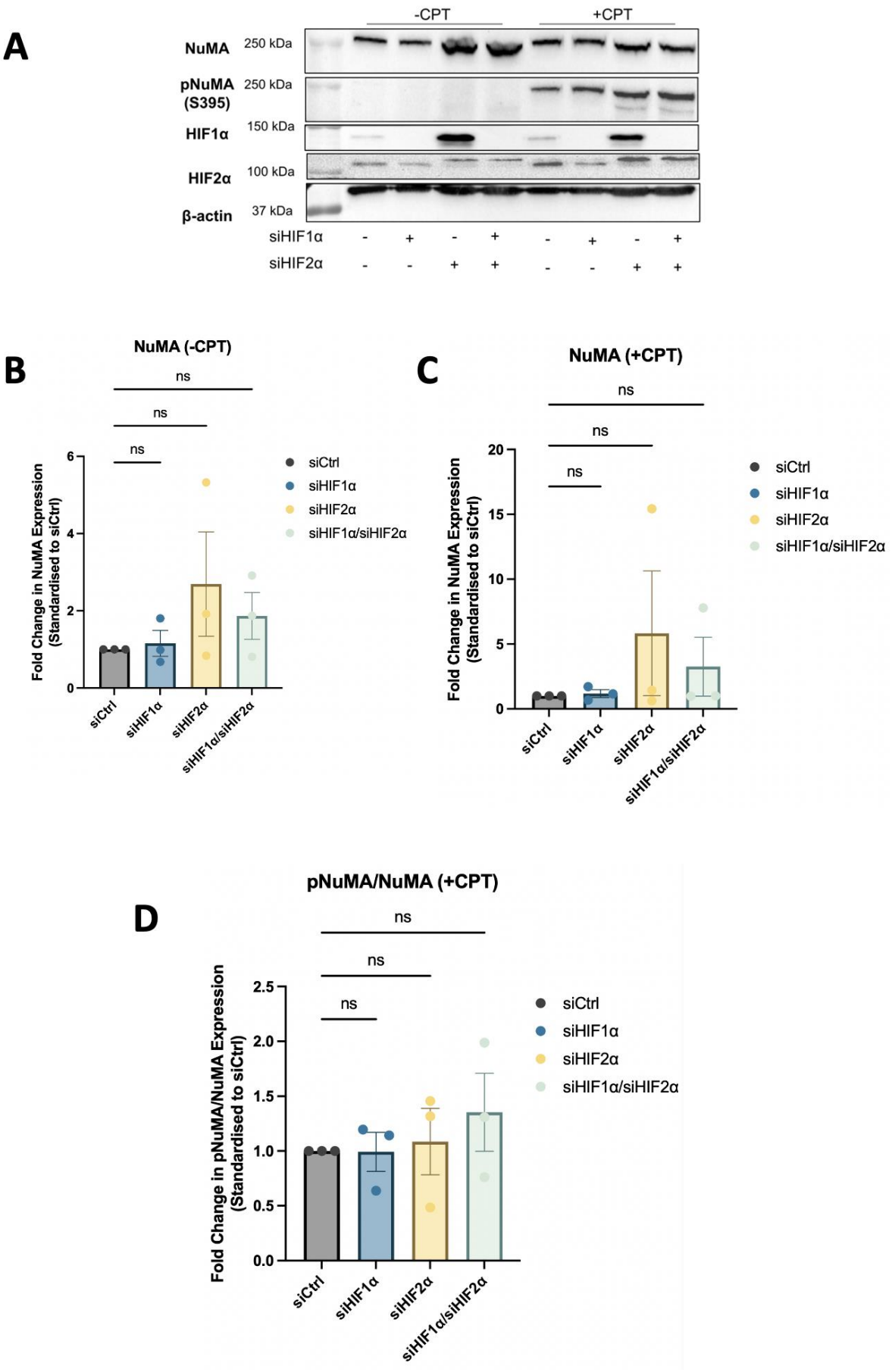
A
-CPT
+CPT
NuMA
250 kDa
pNuMA (S395)
250 kDa
HIF1α
150 kDa
HIF2α
100 kDa
β-actin
37 kDa
siHIF1α
siHIF2α
B
NuMA (-CPT)
ns
Fold Change in NuMA Expression (Standardised to siCtrl)
siCtrl
siHIF1α
siHIF2α
siHIF1α/siHIF2α
C
NuMA (+CPT)
D
pNuMA/NuMA (+CPT)
Fold Change in pNuMA/NuMA Expression (Standardised to siCtrl)

Figure 3.13: NuMA and pNuMA expression in RCC4-VHL -/- cells is independent of HIF expression. A) Representative western blot showing RCC4-VHL -/- cells treated with control siRNA (siCtrl), HIF1α siRNA (siHIF1α), and HIF2α siRNA (siHIF2α). pNuMA and NuMA expression does not change when knocking down HIF1α or HIF2α. pNuMA expression was accentuated by treating cells with 10 μM CPT for 1 hour. β-tubulin was used as a loading control. **B-D)** Quantifications of western blots showing no change in pNuMA or NuMA expression after siRNA treatments. Kruskal-Wallis test with Dunn's correction, ns=p>0.05, Mean ± SEM, n=3.

3.5. Discussion

3.5.1. RCC4-VHL -/- cells have enhanced chemoresistance, but not radioresistance

Enhanced chemoresistance and radioresistance in ccRCC patients has been commonly reported (Goyal et al., 2013). Investigating the molecular mechanisms underpinning this resistance is crucial to developing personalised therapy plans for patients that can resensitise them to standard chemotherapeutics and radiotherapeutics. The RCC4-VHL -/- and RCC4-VHL WT cell lines provided me with a good opportunity to model ccRCC therapy resistance by having one cell line mimic ccRCC patients (VHL -/-) and another cell line mimicking non-cancerous samples (VHL WT). The identity of these cell lines was confirmed via a western blot showing that VHL is only present in RCC4-VHL WT. The absence of VHL in RCC4-VHL -/- was correlated with a high expression of the two main HIF proteins, HIF1α and HIF2α. Furthermore, the HIF-activated gene *PHD3* was shown to be highly upregulated in RCC4-VHL -/-, demonstrating that this cell line had a constitutively upregulated HIF pathway **(Figure 3.1)**.

The observation that RCC4-VHL -/- cells are more resistant to CPT and Olaparib treatment is in line with clinical observations, but runs counter to previous literature (Scanlon and Glazer, 2015; Scanlon et al., 2018). These papers found a downregulation of DNA repair genes, such as *BRCA1*, under hypoxia were responsible for the increased sensitivity to chemotherapeutics. However, I found that RCC4-VHL -/- cells were more resistant to both CPT and Olaparib **(Figure 3.2)**. I demonstrated this through several ways. Firstly, a greater fraction of RCC4-VHL -/- cells treated with either CPT or Olaparib were able to survive and become viable colonies compared to RCC4-VHL WT cells **(Figure 3.2A)**. Secondly, RCC4-VHL -/- cells treated with CPT remained more metabolically viable than RCC4-VHL WT cells as measured by the CellTiter-Blue assay, although the difference between the two cell lines was not extreme **(Figure 3.2C)**. Clonogenic analysis and CellTiter-Blue assay are both good for measuring cell fate over a long period of time post-treatment. Therefore, I examined the immediate cellular response to a drug treatment, which is why I utilised the comet assay to look at the extent of DNA breaks. As CPT had been used extensively in the lab for other alkaline comet assays, I was familiar with the concentrations and timescales needed to get quantifiable comet tails. Treating RCC4-VHL WT cells with CPT caused clear comets to form,

indicating large amounts of SSB and DSB formation. However, I did not observe many comet tails when treating RCC4-VHL -/- with CPT, suggesting minimal sensitivity **(Figure 3.2 D-E)**. Overall, I was able to demonstrate that RCC4-VHL -/- cells are more resistant to DNA damaging agents compared to RCC4-VHL, and that they can maintain that resistance through the cellular proliferation stages.

It is unclear why my results differed so much with Scanlon et al., (2018), despite utilising the same cell lines and methods to measure DNA damage sensitivity. The difference in gene expression for *BRCA1* and *MRE11* could be explained by the different primers in RT-qPCR. There may be alternative isoforms of BRCA1 and MRE11 that are upregulated or downregulated under hypoxia, which would be reflected if selecting primers that target different isoforms.

I moved on to looking at the effect of irradiation on the RCC4 cells, with the expectation that RCC4-VHL -/- would show greater resistance than RCC4-VHL WT. I decided to treat the cells with various doses of IR and then allow the cells to form countable colonies. However, I unexpectedly did not observe any major differences in IR sensitivity between RCC4-VHL WT and RCC4-VHL -/- cells **(Figure 3.3)**. Radioresistance has not been looked at extensively in ccRCC cell lines, so it is difficult to make an accurate comparison with previous literature. Increased resistance to IR in hypoxic cells has been previously demonstrated (Frankenberg-Schwager et al., 1991; Olive and Banáth, 2004). Conversely, Scanlon et al., (2018) irradiated the RCC4 cell lines and compared their capacity to grow colonies, and interestingly found that the RCC4-VHL WT cells were more resistant to radiation. However, the findings in this paper often contradict our previous clonogenic analysis experiments. Bhatt et al., (2008) did find enhanced resistance in the 786-O cell line, although they measured cell death using an MTS-based assay, rather than clonogenic analysis, and also measured cell death via trypan blue exclusion. Also, as the 786-O cell line differs from RCC4, mainly due to the absence of HIF1α expression in 786-O, this may suggest that RCC4 cells intrinsically respond differently to radiation compared to 786-O. This could mean that the absence of HIF1α in 786-O cells is responsible for the enhanced radioresistance, which may explain why RCC4 cells are not radioresistant due to the presence of HIF1α. I would like to use the 786-O cells and apply the same IR doses as I did with RCC4 and see if they show resistance compared to their VHL-

supplied complement cell line, as well as observing whether they show chemoresistance, similar to the RCC4-VHL -/- cells. This would establish whether the presence of HIF1α in RCC4-VHL -/- is affecting chemoresistance and radioresistance.

3.5.2. DNA repair genes are upregulated in RCC4-VHL -/- cells

TDP1 and XRCC1 are part of a larger complex involved in DNA SSBR (Plo et al., 2003). The high expression of DNA repair genes has been associated with enhanced resistance to chemotherapeutics (Li et al., 2021). Although the upregulation of pXRCC1 was mild **(Figure 3.4)**, the increase in TDP1 expression was very strong at the protein (~5-fold change), gene (~3-fold change), and activity level **(Figure 3.6)**. This upregulation may play a part in the enhanced chemoresistance of RCC4-VHL -/- cells as greater expression of endogenous TDP1 could be priming the cells to repair DNA breaks at a more effective rate, similar to what has been reported elsewhere (Liu et al., 2007). During a later experiment, whereby I knocked down HIFα expression in RCC4-VHL -/- and used RCC4-VHL WT as a control cell line, I did not observe any difference in pXRCC1 expression **(Figure 3.9E)**. Therefore, pXRCC1 is likely not involved in enhancing VHL/HIF-mediated genoprotection and the previously observed mild upregulation was likely not physiologically relevant.

I also probed for the protein expression of both TOP1 and PARP1 as they are involved in the same repair pathway but could not find any significant difference. The gene expression of *BRCA1* was significantly upregulated in RCC4-VHL -/-, with minor upregulation in *MRE11* **(Figure 3.5)**. This suggested that the HR pathway might be enhanced, causing increased repair of DNA DSBs. This is in contrast to Scanlon et al., (2018) who showed downregulation of *BRCA1.* I did not see an increase in *PNK* gene expression.

Furthermore, I also probed for NuMA due to its role in recruiting TDP1 to sites of oxidative damage, but also found no measurable difference **(Figure 3.4)**. However, when looking at pNuMA I found a strong upregulation in RCC4-VHL -/- **(Figure 3.12 A-B).** The role of NuMA phosphorylation at S395 is not very well understood, except that phosphorylation occurs in response to DNA damage (Matsuoka et al., 2007). This suggests that RCC4-VHL -/- have a higher baseline of DNA damage compared to RCC4-VHL WT, perhaps due to downregulation or mutations in DNA repair genes. This higher level of baseline damage may have enhanced

the recruitment of TDP1, thereby priming cells to repair DNA damage caused by exogenous factors. We know that NuMA is involved in recruiting DNA repair factors to sites of DNA damage (Ray et al., 2022), although NuMA expression does not differ between both RCC4 cell lines. However, pNuMA could be involved in enhancing TDP1 and XRCC1 recruitment, or by enhancing the function of NuMA. This may explain the reduced comet tail formations in RCC4-VHL -/- cells **(Figure 3.2 D-E)**.

I was able to show that NuMA phosphorylation can be downregulated by inhibiting ATM; however, it was interesting to see that inhibiting ATR caused the opposing effect whereby pNuMA expression increased **(Figure 3.12C)**. It had been previously reported that ATM/ATR were both involved in NuMA phosphorylation (Stokes et al., 2007), so this was an unexpected result. One potential explanation is ATR inhibition causing increased DNA breaks, thereby activating ATM-dependent NuMA phosphorylation. This could be tested by inhibiting ATM alongside ATR inhibition. If pNuMA does not increase in ATM/ATR inhibited cells, this would suggest that the increase in pNuMA following ATR inhibition is due to ATM-dependent NuMA phosphorylation.

The molecular mechanisms underlying pNuMA upregulation in RCC4-VHL -/- cells remains unclear, as modulating HIF1α or HIF2α expression had no measurable impact on either pNuMA or NuMA expression **(Figure 3.13)**. Therefore, it is likely that pNuMA is upregulated due to mechanisms independent of HIF.

3.5.3. TDP1 is a direct or indirect target of HIF2α

Although there was not a lot of literature available surrounding the potential role of TDP1 in hypoxia-relevant cancers, there were a few findings that suggested TDP1 was a potential gene upregulated under hypoxic conditions. Cimmino et al., (2019) found that in a neuroblastoma cell line under hypoxia, *TDP1* expression increased in a HIF1α-independent manner, as well as observing hypermethylation at TDP1 CpG sites. Even though DNA methylation is often associated with repressed gene transcription (Klose and Bird, 2006), the genes of interest identified by Cimmino et al., (2019) did not always follow this trend. Therefore, the impact of TDP1 hypermethylation could be unrelated to gene expression.

Upon investigating previously uploaded ChIP-Seq datasets (Smythies et al., 2019), I found that HIF1α and HIF2α both seemed to bind to the promoter region of TDP1 **(Figure 3.8)**, suggesting that TDP1 could potentially be a target of HIFs. There had been no previous literature indicating a link between HIF2α and TDP1; therefore, it was interesting to observe that upon HIF2α knockdown via siRNA, TDP1 protein expression and gene expression was downregulated **(Figure 3.9)**. HIF1α knockdown did not appear to have an effect on TDP1 expression, which would match Cimmino et al., (2019).

As I had up until now been targeting only HIF1α/HIF2α specifically, I was interested to see whether my findings could be repeated in a general hypoxic setting, thus mimicking conditions observed in cancerous phenotypes. Therefore, I grew RCC4-VHL WT cells in a hypoxic incubator (1% O_2) for various time periods and probed for TDP1 protein expression. Despite seeing a strong upregulation of HIF2α, I did not see a meaningful difference in TDP1 expression **(Figure 3.10)**. However, hypoxia in cancer cells can often reach 0.1% O_2, which can trigger different pathways compared to 1% O_2 (Ramachandran et al., 2021). Furthermore, I incubated RCC4 cells in hypoxic conditions for a maximum of 8 hours, which is substantially shorter than cancer cells are often subjected to (Emami Nejad et al., 2021). Although HIF1α reaches maximal expression around 8 hours in most cells, HIF2α requires a substantially longer hypoxic exposure at approximately 24 hours (Bartoszewski et al., 2019), although this has been shown to be reversed in other cell lines with HIF2α reaching maximal expression before HIF1α (Imeri et al., 2019). Therefore, my experiment may not have provided a meaningful comparison as HIF and its downstream target genes are not fully activated. Establishing the precise times at which HIF1α/HIF2α reach maximal expression accompanied by activation of known downstream target genes in RCC4 cells will allow for a more accurate understanding of the relationship between HIF and TDP1 during hypoxic exposure. Interestingly, the upregulation of HIF2α in RCC4-VHL WT cells exceeded that of RCC4-VHL -/- cells, whilst HIF1α upregulation did not reach the same levels as RCC4-VHL -/- cells. The balance between HIF1α and HIF2α expression may be important in modulating TDP1 expression.

Since I observed that only HIF2α seemed to be modulating TDP1 expression, I decided to investigate HIF2α further. HIF2α has been described as responsible for promoting an

aggressive phenotype in ccRCC patients, whilst HIF1α is often described as a tumour suppressor (Keith et al., 2012; Hoefflin et al., 2020; Shi et al., 2021). PT2385 has been successfully used to inhibit tumour progression by specifically inhibiting the binding of HIF2α with HIF1β (Wallace et al., 2016). Therefore, I wanted to see whether treating RCC4-VHL -/- cells with PT2385 would show similar results as my HIF2α knockdowns. However, PT2385 did not appear to have a clear impact on TDP1 gene or protein expression, with a decrease and increase observed, respectively **(Figure 3.11)**. The conflicting results of PT2385 could be explained by enhanced stabilisation of TDP1 protein as a compensatory mechanism following HIF2α-mediated downregulation of other DNA repair proteins. Alternatively, HIF2α inhibition has been identified as a contributor to induced oxidative stress during intermittent hypoxia (Nanduri et al., 2009). Therefore, TDP1 may be stabilised to repair SSBs induced by oxidative stress (El-Khamisy et al., 2005).

3.6. Summary

RCC4-VHL -/- cells, which have a constitutively active HIF pathway, are more resistant to chemotherapeutics compared to RCC4-VHL WT cells. This matches what has been identified in ccRCC patients with *VHL* mutations. The DNA repair factors TDP1, BRCA1, and pNuMA were found to be upregulated in RCC4-VHL -/- ; the upregulation of TDP1 can be countered by knocking down HIF2α expression with siRNA. The upregulation of the DNA repair factors may be responsible for the enhanced chemoresistance.

The loss of functional VHL in RCC4-VHL -/- causes constitutive upregulation of HIF2α, causing increased expression of TDP1. pNuMA expression increases in a HIF-independent manner, which relies on ATM expression. Therefore, TDP1 recruitment to sites of SSBs are increased, enhancing DNA capability to repair itself after being damaged. This hypothetical model is visualised in **Figure 3.14**. The next steps are to determine whether HIF2α is acting directly or indirectly on TDP1, and whether modulating the expression of HIF2α or TDP1 is sufficient to resensitise cells to chemotherapeutics.

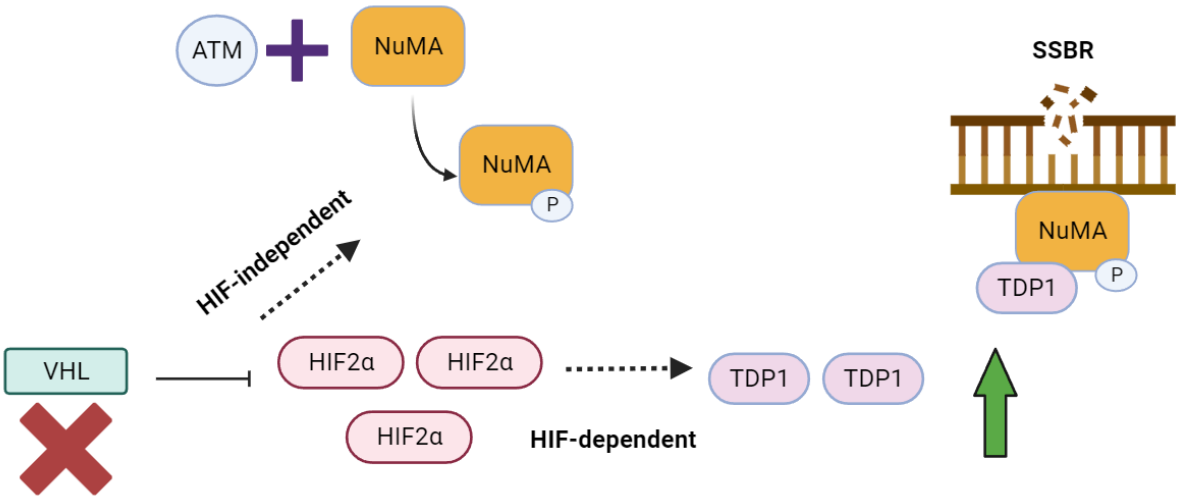

Figure 3.14: Model demonstrating the potential mechanisms by which *VHL* inactivation causes increased DNA break repair. Upon *VHL* inactivation, HIF2α expression is constitutively upregulated, triggering increased recruitment of TDP1 to sites of DNA damage through two methods: 1) Increasing the transcription and translation of TDP1. 2) Increasing the formation of phosphorylated NuMA (pNuMA), which recruits TDP1 to sites of DNA damage, leading to single-strand break repair (SSBR). The phosphorylation of NuMA occurs in a HIF-independent and ATM-dependent manner.

Chapter 4 Genetic modulation of HIFα or TDP1 in RCC4-VHL -/-

4.1. Introduction

RCC4-VHL -/- cells have an enhanced resistance to chemotherapeutics compared to RCC4-VHL WT cells**.** *VHL* inactivation in RCC4-VHL -/- caused upregulation of HIF1α and HIF2α, as well as a strong upregulation of DNA repair protein TDP1, which appeared to be modulated by HIF2α. Therefore, I was interested to see if HIF1α, HIF2α, and TDP1 contributed to enhanced chemoresistance mechanisms.

Targeting HIF2α is a relatively new strategy that has been introduced into clinical practice via the HIF2α inhibitor Belzutifan, with much of the focus centring on HIF2α's role in promoting angiogenesis (Bensalah et al., 2022). HIF2α inhibition in ccRCC patients may also have the impact of enhancing sensitivity to chemotherapeutics as DNA repair mechanisms in cancer cells become perturbed. Knocking down gene expression of *HIF1α, HIF2α*, and *TDP1* in cell lines expressing or lacking functional VHL will provide a greater understanding into the contribution of each of the respective genes and their downstream targets in chemoresistance.

4.2. Hypothesis

Knocking down TDP1 expression directly via siRNA, or indirectly by knocking down HIF2α, will cause increased sensitivity to DNA damaging agents such as CPT, Olaparib, and cisplatin. I have previously shown increased resistance to CPT and Olaparib in RCC4-VHL -/- cells, whilst high HIF expression has been demonstrated to provide a protective effect to cisplatin treatment (Guo et al., 2018). TDP1 is a key protein involved in DNA repair, so its downregulation will cause cells to be less effective at repairing DNA after breaks occur. HIF1α knock down will have no impact on chemoresistance as it does not appear to target TDP1. Furthermore, due to the differences in acute vs chronic hypoxia, HIF2α knockdown via CRISPR-Cas9 will cause a more dramatic increase in chemosensitivity.

4.3. Aims

1. Knock down HIF1α/HIF2α or TDP1 expression in RCC4 cells.
2. Establish the impact of HIF1α/HIF2α and TDP1 knockdowns on chemosensitivity.
3. Obtain a stable RCC4 cell line containing HIF1α/HIF2α knockdown via CRISPR-Cas9.
4. Identify impact of long-term HIFα knockdown via CRISPR-Cas9 on chemosensitivity.

4.4. Results

4.4.1. HIF1α/HIF2α knockdown via siRNA does not cause increased sensitivity to CPT in RCC4-VHL -/-

Knocking down gene expression using siRNA causes short-term downregulation of the gene mRNA of interest (Mocellin and Provenzano, 2004). By causing a reduction in HIFα expression, I wanted to establish if elevated levels of HIF1α or HIF2α were responsible for enhanced chemoresistance in RCC4-VHL -/- cells. Gene knockdown via siRNA targeted HIF1α, HIF2α, or a combination of both HIF1α and HIF2α in RCC4-VHL -/- cells.

Figure 4.1A shows that the HIFα expression in siRNA-treated RCC4-VHL -/- cells reached similar levels to RCC4-VHL WT cells, along with a reduction in TDP1 protein expression in siHIF2α-treated cells, which had been previously established **(Section 3.4.3)**. There was no measurable impact on colony formation propensity when reducing HIFα expression, as identified by clonogenic analysis **(Figure 4.1B)**. Furthermore, HIFα knockdown did not cause cells to take increased amounts of DNA damage in a comet assay as the quantity of comet tails did not increase in CPT-treated RCC4-VHL -/- following HIF1α or HIF2α depletion **(Figure 4.1 C-D)**. These results differed to the expected result of HIF2α knockdown causing greater chemosensitivity, as downregulating HIF2α caused a reduction in TDP1 expression.

These results suggested that HIFα is not involved in the enhanced chemoresistance observed in RCC4-VHL -/- cells. Alternatively, the short-term knockdown in HIFα expression initiated by siRNA may not provide an accurate comparison to RCC4-VHL WT cells, which have had HIFα expression inhibited for a longer period, causing downstream target genes of HIFα to be more transcriptionally repressed. Therefore, I wanted to create a stable knockdown of HIFα in RCC4 cells to establish whether the long-term modulation of HIFα is required to observe a difference in chemoresistance.

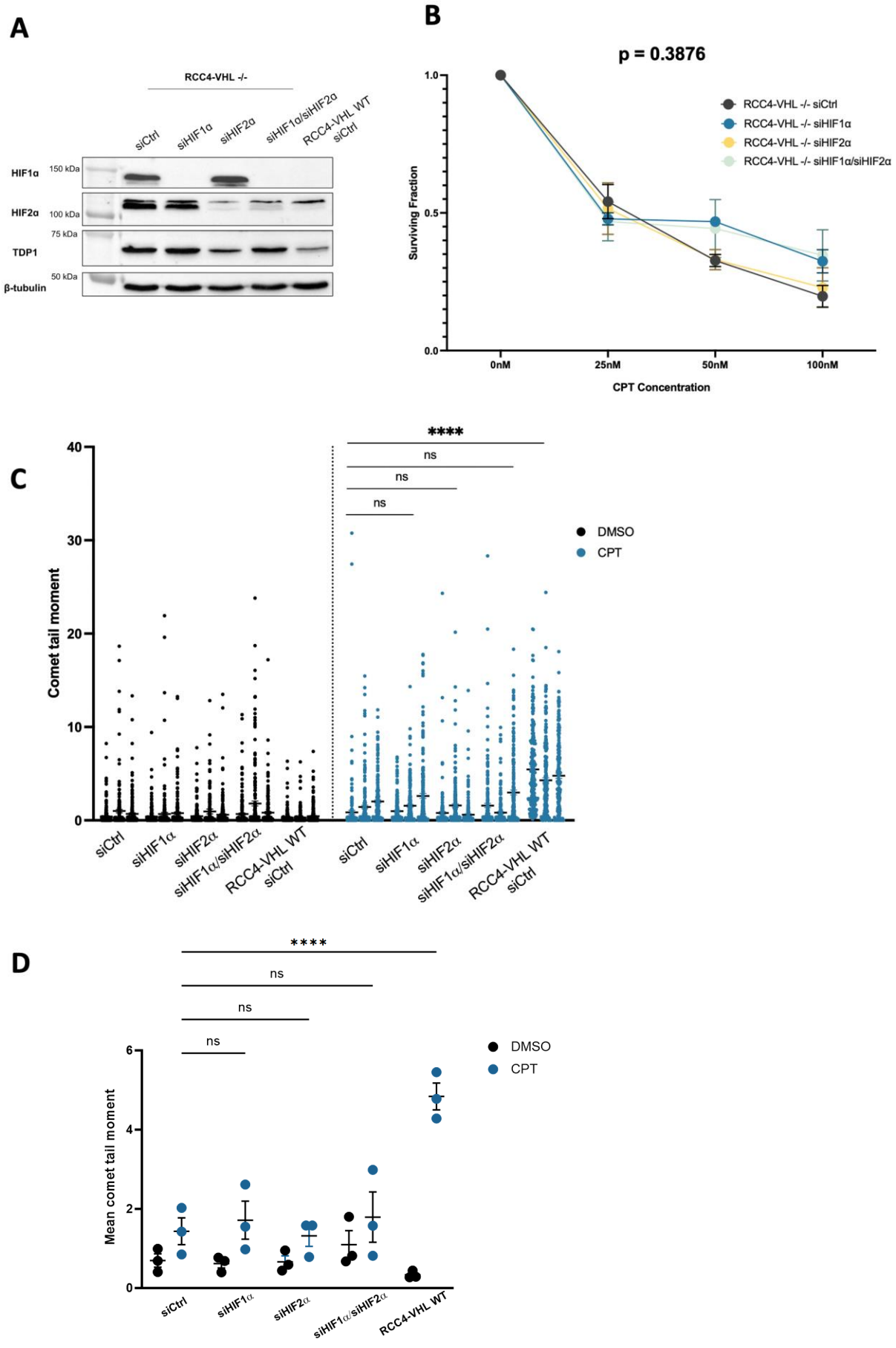
A
RCC4-VHL -/-
siCtrl
siHIF1α
siHIF2α
siHIF1α/siHIF2α
RCC4-VHL WT siCtrl
HIF1α
150 kDa
HIF2α
100 kDa
75 kDa
TDP1
50 kDa
β-tubulin
B
p = 0.3876
Surviving Fraction
1.0
0.5
0.0
0nM
25nM
50nM
100nM
CPT Concentration
RCC4-VHL -/- siCtrl
RCC4-VHL -/- siHIF1α
RCC4-VHL -/- siHIF2α
RCC4-VHL -/- siHIF1α/siHIF2α
C
Comet tail moment
40
30
20
10
0
****
ns
ns
ns
DMSO
CPT
siCtrl
siHIF1α
siHIF2α
siHIF1α/siHIF2α
RCC4-VHL WT siCtrl
D
Mean comet tail moment
6
4
2
0
****
ns
ns
ns
DMSO
CPT
siCtrl
siHIF1α
siHIF2α
siHIF1α/siHIF2α
RCC4-VHL WT

Figure 4.1: siHIF1α and siHIF2α have no measurable effect on sensitivity to CPT. A) Representative western blot showing HIF1α and HIF2α knockdown in RCC4-VHL -/- cells. RCC4-VHL WT included for comparison. β-tubulin was used as a loading control. **B)** Clonogenic analysis comparing CPT resistance between RCC4-VHL -/- cells transfected with control siRNA (siCtrl), HIF1α siRNA (siHIF1α), HIF2α siRNA (siHIF2α), or a combination of both siHIF1α and siHIF2α. CPT treatment was at the indicated concentrations for 1 hour. Two-way ANOVA with Tukey correction, Mean ± SEM, n=3. **C-D)** Comet assay comparing CPT resistance between RCC4-VHL -/- cells transfected with siCtrl, siHIF1α, siHIF2α, or a combination of both siHIF1α and siHIF2α. RCC4-VHL WT transfected with siCtrl was also included for comparison. CPT treatment was 40 μM for 30 mins. **C)** Raw values for comet tail moments. **D)** Mean come tail moment for all three biological repeats. Two-way ANOVA with Tukey correction, ns=p>0.05, ****p<0.0001, Mean ± SEM, n=3.

4.4.2. Creation of stable HIF1α/HIF2α knockdown lines in RCC4 using CRISPR-Cas9

To create a stable cell line in RCC4 with HIFα depletion, I followed the protocol established by Ann Ran et al., (2013) and summarised in **Section 2.12**. I initially started by identifying suitable gRNA sequences that had previously been shown to cause knockdowns in CRISPR plasmids (Sanjana et al., 2014). The HIF1α gRNA sequence was in exon 4, whilst the HIF2α gRNA sequence was in exon 2 **(Figure 4.2A)**. I started by using pSpCas9(BB)-2A-Puro plasmid to ligate my gRNAs, then once these plasmids were sequence-verified for correct insertion **(Figure 4.2B)**, I transfected the gRNA-containing plasmids into both RCC4 cell lines, as previously described. After puromycin selection and diluting transfected cells to single-cell populations, the only surviving clones were RCC4-VHL WT clones transfected with either HIF1α gRNA or HIF2α gRNA. As HIFα is expressed at low levels in RCC4-VHL WT, I pre-treated these cells with the HIF activator Roxadustat (ROX, 20 μM for 4 hours) or with DMSO as a control, then looked to see if HIF expression was upregulated in the clones. **Figure 4.2C** showed that ROX treatment was still able to upregulate HIF1α and HIF2α protein expression in the clones. Therefore, these transfections failed to target HIFα expression.

I moved towards trying pSpCas9(BB)-2A-GFP plasmid to ligate the gRNAs and repeated the transfections, as this would allow direct GFP-based selection of successfully transfected cells. After FACS sorting single-cells that were GFP positive, the only clones that survived were RCC4-VHL -/- cells transfected with HIF2α gRNA. I harvested these cells and analysed HIF2α expression on a western blot. Both clones showed a knockdown in HIF2α protein expression, indicating that the transfection was successful. Clone (B) showed a higher HIF1α expression, suggesting genetic compensation, whilst clone (A) did not. In addition, TDP1 expression was downregulated in Clone A, potentially due to the HIF2α knockdown. **(Figure 4.2D)**. Therefore, I expanded clone (A) RCC4-VHL -/- gHIF2α (RCC4-VHL -/-; HIF2α -/-) for further experiments.

A

HIF1α exon 4

5'TTTGAACTAACTGGACACAGTGTGTTTGATTTTACTCATCCATGT
GACCATGAGGAAATGAGAGAAATGCTTACACACAGAAATG 3'

HIF2α exon 2

5'GAGTAGCTCGGAGAGGAGGAAGGAGAAGTCCCGGGATGCT
GCGCGGTGCCGGCGGAGCAAGGAGACGGAGGTGTTCTATGAG
CTGGCCCATGAGCTGCCTCTGCCCCACAGTGTGAGCTCCCATCT
GGACAAGGCCTCCATCATGCGACTGGCAATCAGCTTCCTGCGAA
CACACAAGCTCCTCTCCTCAG3'

B

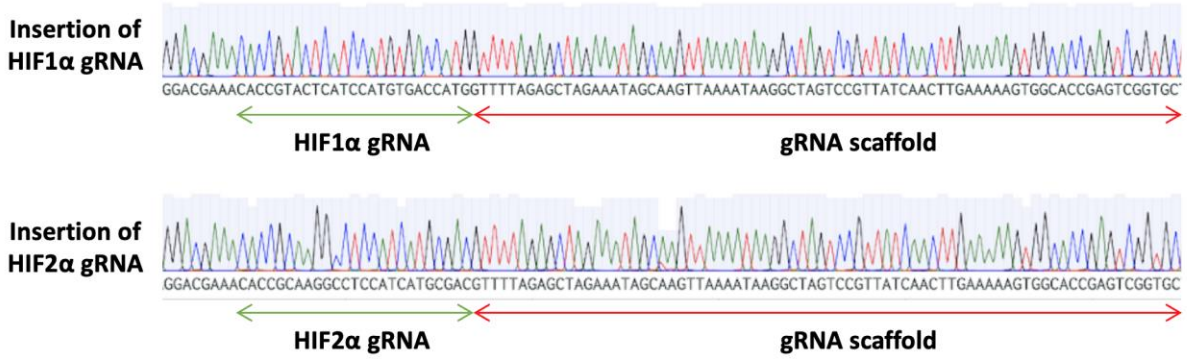

C

pSpCas9(BB)-2A-Puro Test

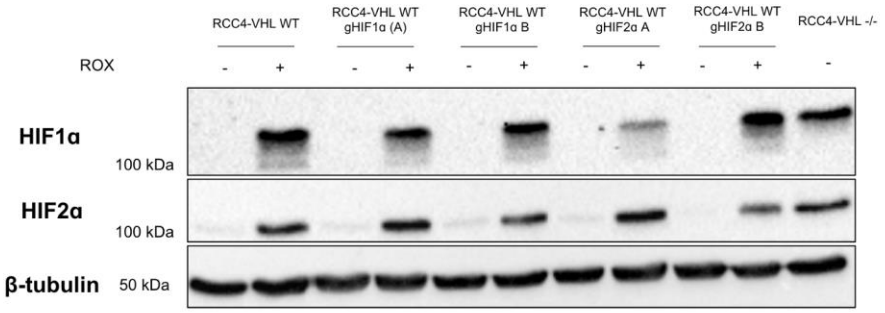

D

pSpCas9(BB)-2A-GFP Test

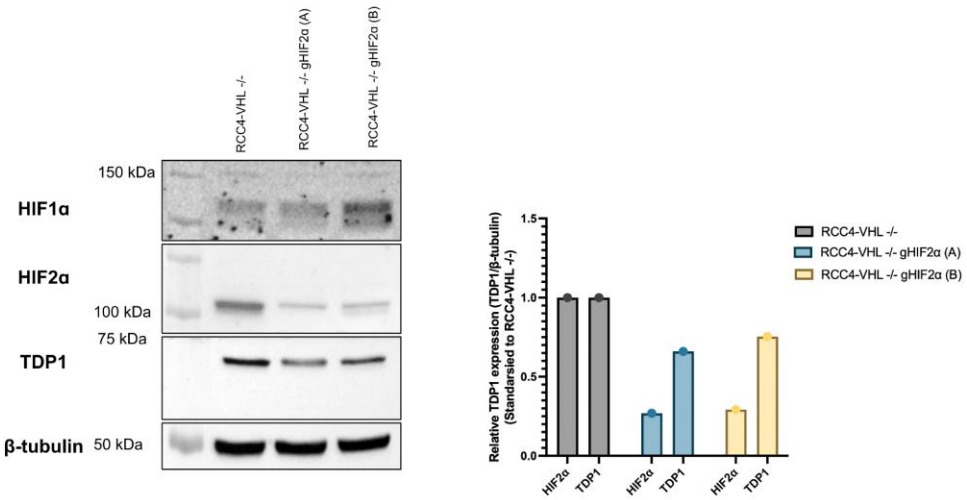

Figure 4.2: Generation of HIFα knockdown in RCC4 using CRISPR-Cas9. A) Target sequences within exon 4 (*HIF1α*) and exon 2 (*HIF2α*), with gRNA sequences highlighted in yellow. Sequences obtained using Ensembl (Version 110, Cunningham et al., (2022)). **B)** Sequence traces showing correct insertion of gRNA sequences into CRISPR plasmid. gRNA sequence labelled in green. gRNA scaffold labelled in red. Sequences were analysed using Benchling.com (2022). **C)** First attempt via western blot at validating HIFα knockdown using the puromycin-resistant plasmid pSpCas9(BB)-2A-Puro. Only clones containing RCC4-VHL WT cells transfected with either HIF1α or HIF2a survived, so cells were pre-treated with HIF activator ROX (20 µM for 4 hours) to upregulate HIF levels. RCC4-VHL WT and RCC4-VHL -/- included as controls. No knockdown was observed in any clones. β-tubulin was used as a loading control. **D)** Second attempt at validating HIFα knockdown but using the GFP-containing plasmid pSpCas9(BB)-2A-GFP. Only clones containing RCC4-VHL -/- cells transfected with HIF2α contained were GFP positive following FACS sorting. HIF2α knockdown was observed in both clones, as well as a reduction in TDP1 expression. β-tubulin was used as a loading control.

4.4.3. Long-term HIF2α knockdown via CRISPR-Cas9 does not cause a measurable increase in sensitivity to DNA damaging agents in RCC4-VHL -/-

Since there was no effect seen in response to CPT treatment after siRNA-mediated HIFα knockdown, I hypothesised that this may be due to the short-term nature of siRNA-mediated knockdowns, whereby the mRNA expression is only downregulated for a short period of time (Mocellin and Provenzano, 2004). The differences between acute hypoxia and chronic hypoxia have been discussed previously, with several areas remaining unsolved. Patients with ccRCC have a constitutive upregulation of HIFα, which mimics the increased expression of HIFα observed in RCC4-VHL -/- cells. Therefore, directing RCC4-VHL -/- to behave more similarly to RCC4-VHL WT on a molecular basis may require a more constant downregulation of HIFα.

Since HIF2α is responsible for the previously reported role in TDP1 upregulation **(Section 3.4.3)**, I aimed to establish whether TDP1 protein expression was downregulated in RCC4-VHL -/- ; HIF2α -/- . Interestingly, an early passage of RCC4-VHL -/- ; HIF2α -/- had downregulated TDP1 expression, but later passages showed TDP1 expression returning to previous levels **(Figure 4.3)**.

RCC4-VHL -/- demonstrated increased resistance to both CPT and Olaparib, which could not be reversed by knocking down HIF2α expression via siRNA **(Figure 3.2**/**Figure 4.1)**. Therefore, I repeated the clonogenic analysis experiment with RCC4-VHL -/- ; HIF2α -/- but did not find a significant difference when HIF2α was knocked down via CRISPR-Cas9 **(Figure 4.4 A-B).** To confirm that there was no measurable difference in chemoresistance, I also performed clonogenic analysis after treating cells with cisplatin, as cancer cell lines have enhanced resistance to cisplatin due to hypoxic signalling (Guo et al., 2018). However, no measurable difference was observed in resistance to cisplatin treatment **(Figure 4.4C)**.

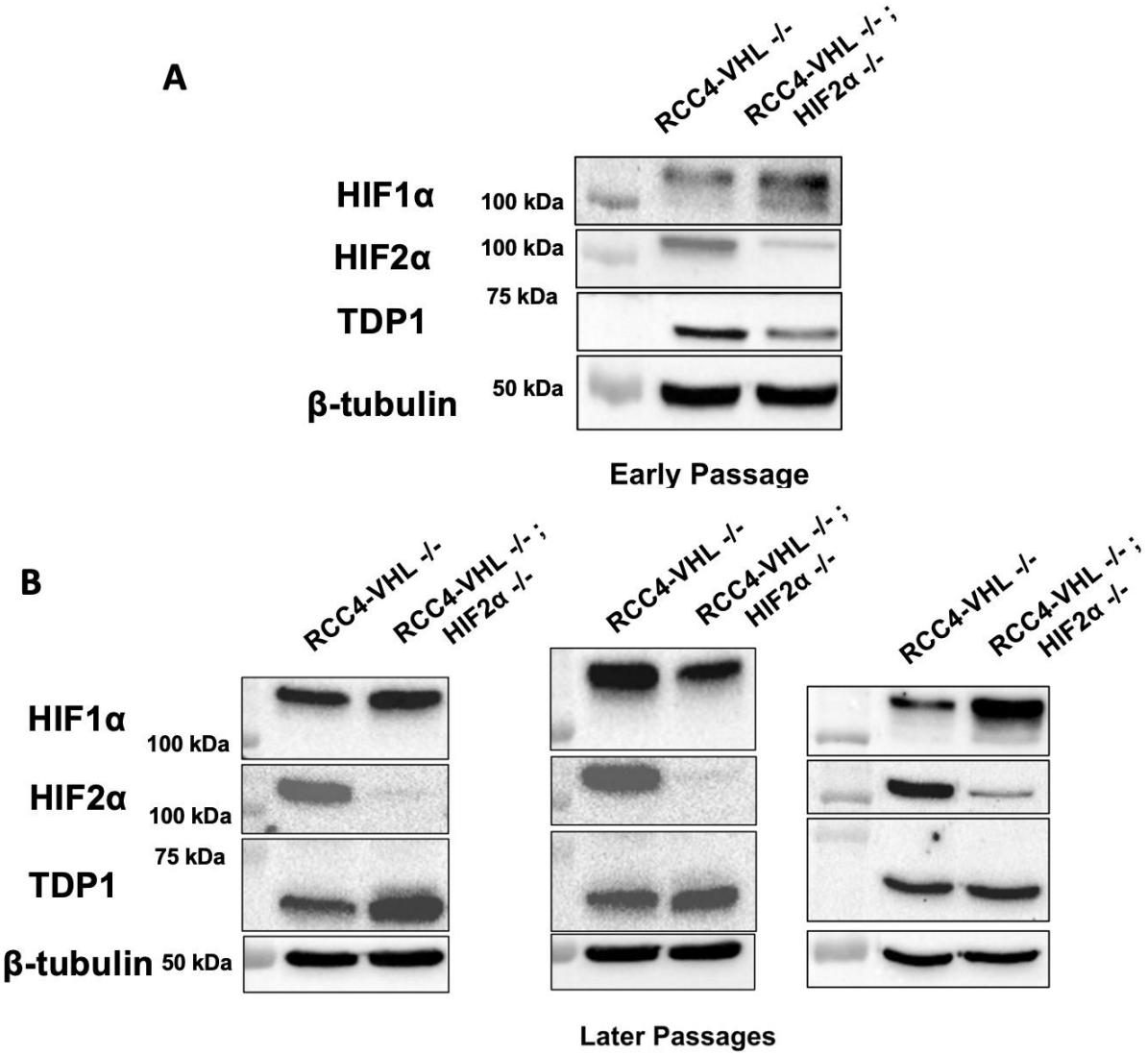
A
RCC4-VHL -/-
RCC4-VHL -/- ; HIF2α -/-
HIF1α
100 kDa
HIF2α
100 kDa
TDP1
75 kDa
β-tubulin
50 kDa
Early Passage
B
RCC4-VHL -/-
RCC4-VHL -/- ; HIF2α -/-
HIF1α
100 kDa
HIF2α
100 kDa
TDP1
75 kDa
β-tubulin
50 kDa
Later Passages

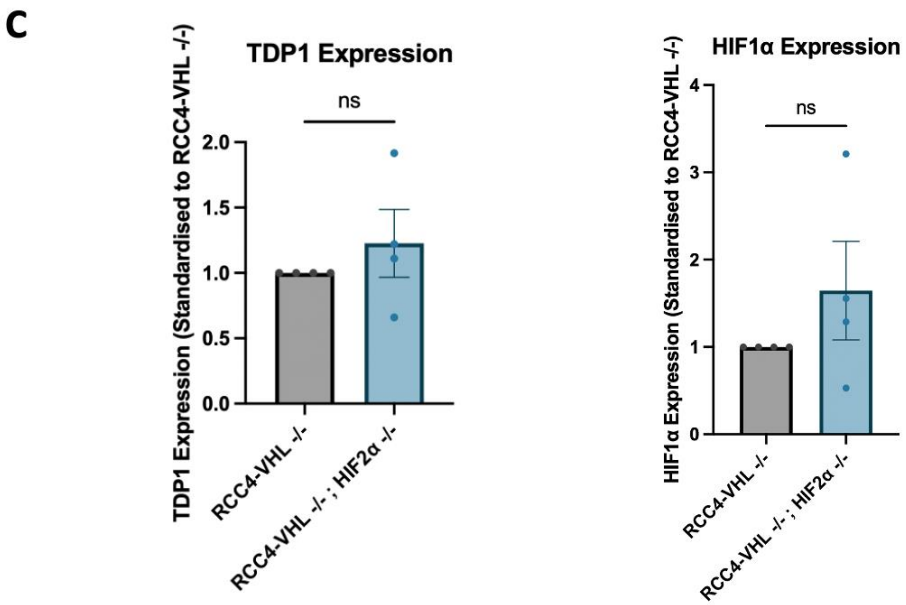
C
TDP1 Expression
ns
TDP1 Expression (Standardised to RCC4-VHL -/-)
2.0
1.5
1.0
0.5
0.0
RCC4-VHL -/-
RCC4-VHL -/- ; HIF2α -/-
HIF1α Expression
ns
HIF1α Expression (Standardised to RCC4-VHL -/-)
4
3
2
1
0
RCC4-VHL -/-
RCC4-VHL -/- ; HIF2α -/-

Figure 4.3: HIF2α knockdown via CRISPR-Cas9 in RCC4-VHL -/- has no measurable impact on TDP1 or HIF1α protein expression. A) Western blot from an early passage showing downregulation of HIF2α and TDP1. **B**) Western blots from later passages showing TDP1 protein expression is no longer downregulated and had varied HIF1α expression. β-tubulin was used as a loading control in all blots. **C)** Quantification of western blots for both TDP1 and HIF1α expression. Wilcoxon signed-rank test, Mean ± SEM, n=4, ns=p>0.05.

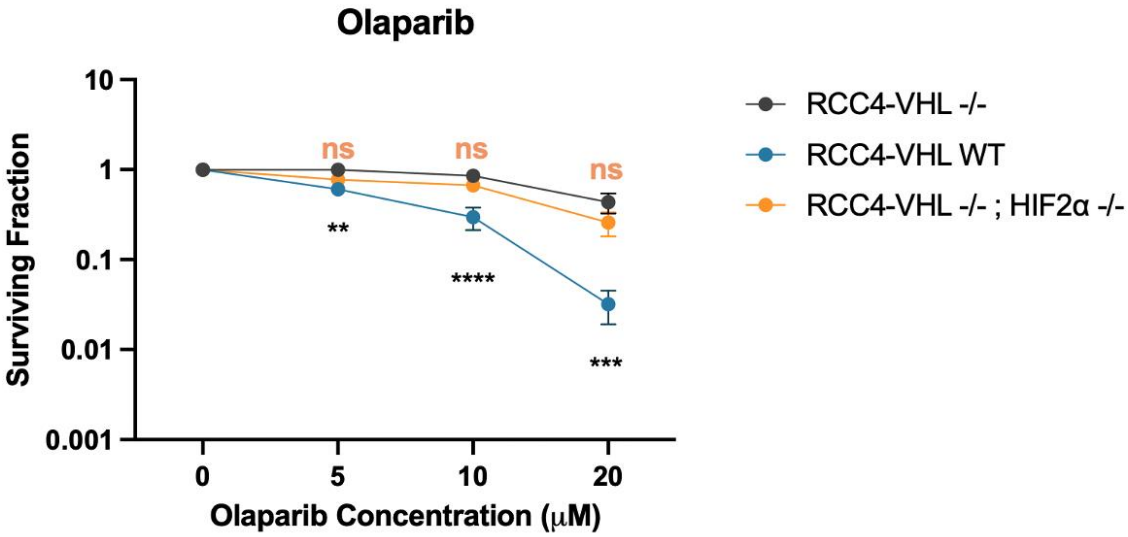
Olaparib
Surviving Fraction
10
1
0.1
0.01
0.001
ns
ns
ns
**
****
***
0
5
10
20
Olaparib Concentration (μM)
RCC4-VHL -/-
RCC4-VHL WT
RCC4-VHL -/- ; HIF2α -/-

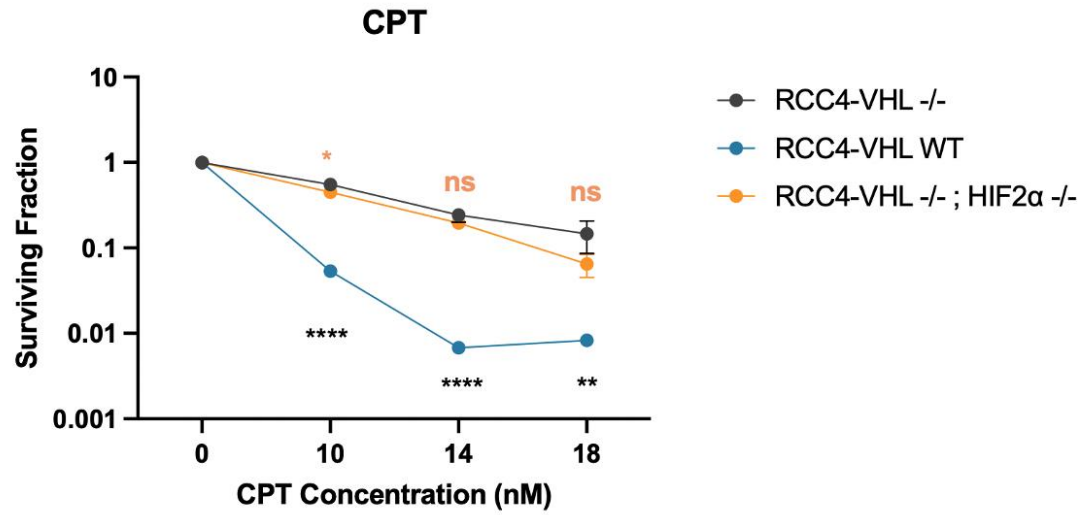
CPT
Surviving Fraction
10
1
0.1
0.01
0.001
*
ns
ns
****
****
**
0
10
14
18
CPT Concentration (nM)
RCC4-VHL -/-
RCC4-VHL WT
RCC4-VHL -/- ; HIF2α -/-

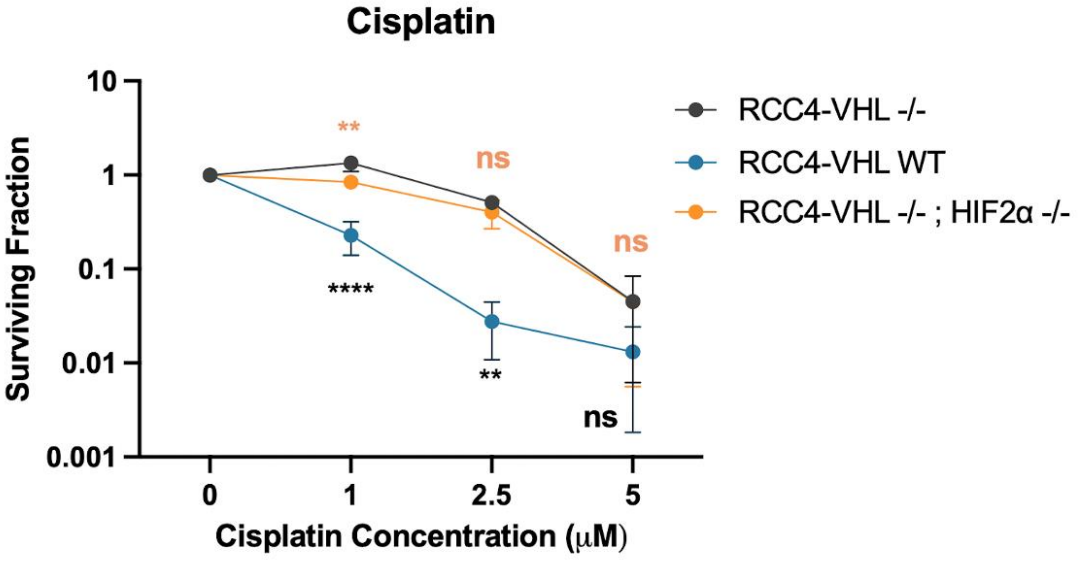
Cisplatin
Surviving Fraction
10
1
0.1
0.01
0.001
**
ns
ns
****
**
ns
0
1
2.5
5
Cisplatin Concentration (μM)
RCC4-VHL -/-
RCC4-VHL WT
RCC4-VHL -/- ; HIF2α -/-

Figure 4.4: HIF2α knockdown in RCC4-VHL -/- cells via CRISPR-Cas9 has no measurable impact on chemoresistance. Clonogenic analysis comparing drug resistance using **(A)** Olaparib, **(B)** CPT, and **(C)** cisplatin, between RCC4-VHL WT, RCC4-VHL -/-, and RCC4-VHL -/- ; HIF2α -/- cells. Two-way ANOVA with Dunnet correction, ns=p>0.05, *p<0.05, **p<0.01, ***p<0.001, ****p<0.0001, Mean ± SEM, n=3.

4.4.4. TDP1 knockdown does not cause a measurable increase in sensitivity to CPT in RCC4 cells

Although targeting TDP1 indirectly via HIF2α knockdown via siRNA/CRISPR did not have any impact on chemosensitivity, this may have been due to other targets of HIF2α being impacted by its knockdown alongside TDP1. I wanted to only target TDP1 to assess the overall impact on chemosensitivity, without interfering with the VHL/HIF pathway. As I have discussed previously, enhanced TDP1 expression has been connected to increased chemoresistance in other cancers (Plo et al., 2003; Liu et al., 2007). TDP1 deficiency has previously been shown to cause a reduction in colony formation propensity in various cell lines after treating with DNA damaging agents, including CPT (Huang et al., 2013; Alagoz et al., 2014; Chiang et al., 2017; Ray et al., 2022; Zhang et al., 2022). Therefore, I expected that reducing TDP1 expression via siRNA would cause increased sensitivity to CPT in both RCC4-VHL WT and RCC4-VHL -/- cells.

I knocked down TDP1 expression in the RCC4 cells via siRNA, then seeded the cells overnight either in a 24-well plate, which were harvested to confirm TDP1 knockdown, or seeded at low density for clonogenic analysis in 10 cm plates. As siRNA-mediated knockdowns are transient (Mocellin and Provenzano, 2004), I resorted to using acute CPT treatments, rather than chronic, ensuring that CPT treatment only took place when TDP1 was depleted. TDP1 depletion did not cause increased sensitivity to CPT in either RCC4-VHL WT or RCC4-VHL -/- when looking at colony formation propensity **(Figure 4.5)**. The absence of increased sensitivity in RCC4-VHL -/- could be due to alternative repair pathways enhanced by upregulated HIFs. However, the absence of enhanced chemosensitivity in TDP1-depleted RCC4-VHL WT cells was surprising due to the established role of TDP1 in DNA repair (El-Khamisy and Caldecott, 2006; Alagoz et al., 2014).

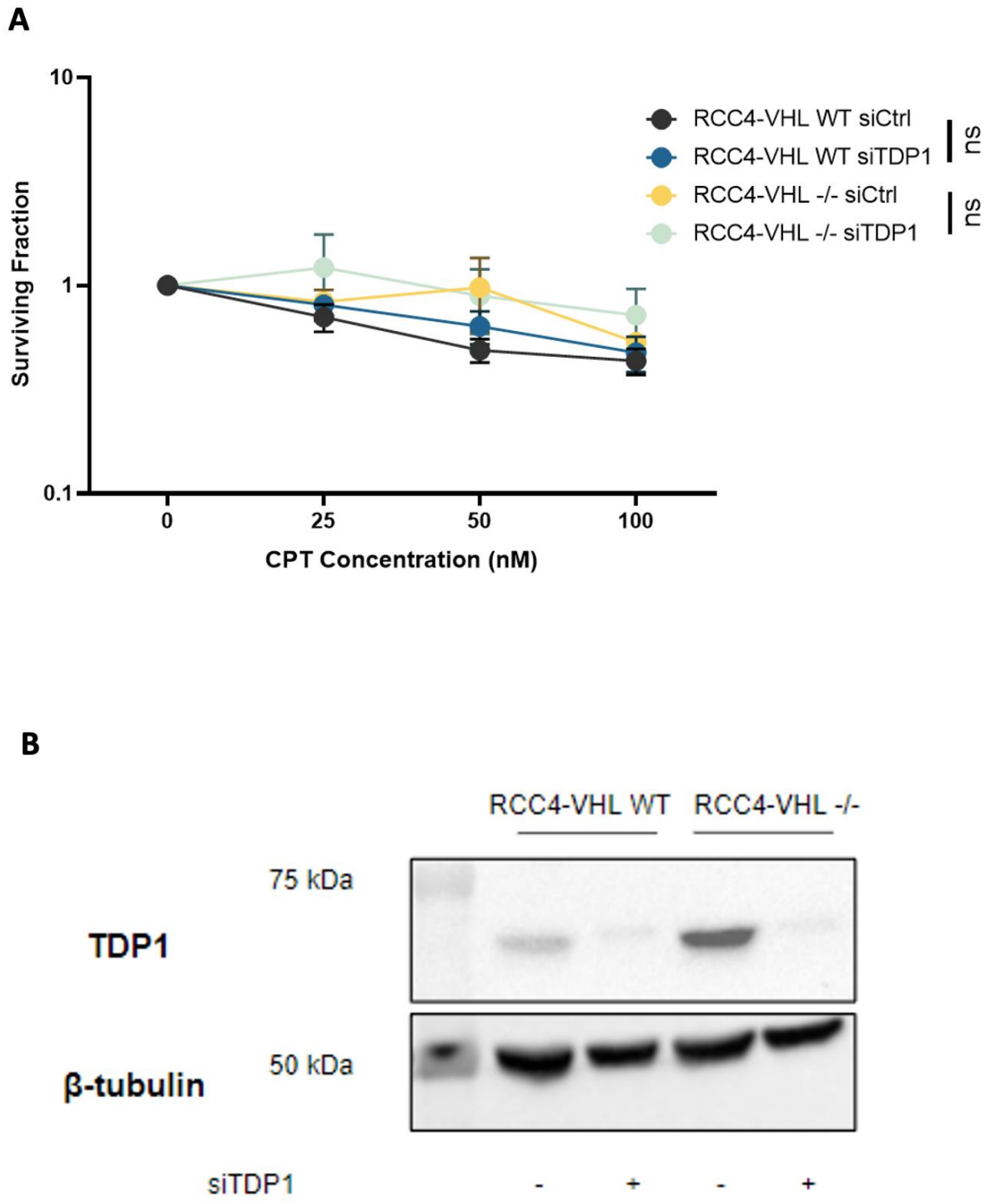

Figure 4.5: Knocking down TDP1 expression does not increase CPT sensitivity in RCC4 cells. **A)** Clonogenic analysis comparing CPT resistance between RCC4-VHL WT and RCC4-VHL -/- cells transfected with control siRNA (siCtrl) or TDP1 siRNA (siTDP1). CPT treatment was for 1 hour at the specified concentrations. Two-way ANOVA with Tukey correction. ns=p>0.05, Mean ± SEM, n=3. **B)** Representative western blot showing TDP1 knockdown in RCC4-VHL WT and RCC4-VHL -/- cells. β-tubulin was used as a loading control.

Zhang et al., (2022) showed that TDP1 depletion caused enhanced formation of phosphorylated checkpoint kinase 1 (pChk1) at S345 after CPT treatment, as well as enhanced formation of gamma H2A histone family member X (γH2AX). During the early response phase following DNA DSB formation, γH2AX is involved in chromatin remodelling increasing DNA accessibility to DDR proteins (Kinner et al., 2008). In addition, γH2AX stalls the cell cycle allowing DNA to repair, and facilitates the anchoring of broken DNA ends to promote rejoining (Celeste et al., 2002; Bassing and Alt, 2004). Therefore, γH2AX is considered to be a reliable marker of DNA DSB formation. Chk1 is phosphorylated via ATR in response to SSBs, activating cell cycle checkpoints that delay cell cycle progression, allowing DNA to repair (Dai and Grant, 2010). An enhanced ATR/Chk1 pathway has previously been implicated in protecting cells from chemotherapeutics, as DNA breaks induced by DNA damaging agents have more time to repair (Bartucci et al., 2012). Therefore, I was interested to see if the molecular pathways involved in DNA repair differed before and after depleting TDP1, which could explain why a downregulation of TDP1 did not cause enhanced sensitivity to CPT.

Similar to the previous experiment, I knocked down TDP1 expression in RCC4 cells and then seeded them in a 24-well plate, leaving them to adhere overnight. Cells were treated with either DMSO or 10 μM CPT for 1 hour, then cells were harvested for western blot. The background expression levels (DMSO-treated cells) of pChk1 did not differ between RCC4-VHL WT and RCC4-VHL -/-, with or without TDP1, although there was a trend towards upregulated pChk1 in RCC4-VHL -/- cells **(Figure 4.6B)**, indicating that the ATR/Chk1 pathway is likely behaving similarly in both cell lines. In addition, background expression levels of γH2AX were trended towards upregulation in RCC4-VHL -/- **(Figure 4.6C)**, suggesting that these cells were experiencing greater DSBs compared to RCC4-VHL WT. After treating cells with CPT, pChk1 and γH2AX expression would be expected to be greater in TDP1-depleted cells, compared to siCtrl cells (Zhang et al., 2022). Although an increase in pChk1 and γH2AX was observed following CPT treatment, this was not exaggerated by depleting TDP1 in either RCC4-VHL WT and RCC4-VHL -/- ; the opposite was actually observed for pChk1 expression. RCC4-VHL WT cells transfected with siCtrl and treated with CPT had a non-significant increase in pChk1 expression compared to the corresponding cells with TDP1 depletion. A similar trend was observed in RCC4-VHL -/- **(Figure 4.6D)**. γH2AX expression did increase

following CPT treatment, but TDP1 depletion did not have a significant impact on γH2AX expression in either RCC4-VHL WT or RCC4-VHL -/- **(Figure 4.6E)**.

pNuMA is an interacting protein of TDP1 (Ray et al., 2022), so its expression may be affected by TDP1 depletion. Therefore, pNuMA was also probed, initially to determine if pNuMA expression would also differ between RCC4-VHL WT and RCC4-VHL -/- following CPT treatment, as I had previously shown this to occur in the absence of exogenous DNA damage **(Figure 3.12)**. In addition, I discovered that pNuMA expression was significantly downregulated upon TDP1 depletion in RCC4-VHL -/- **(Figure 4.6F)**.

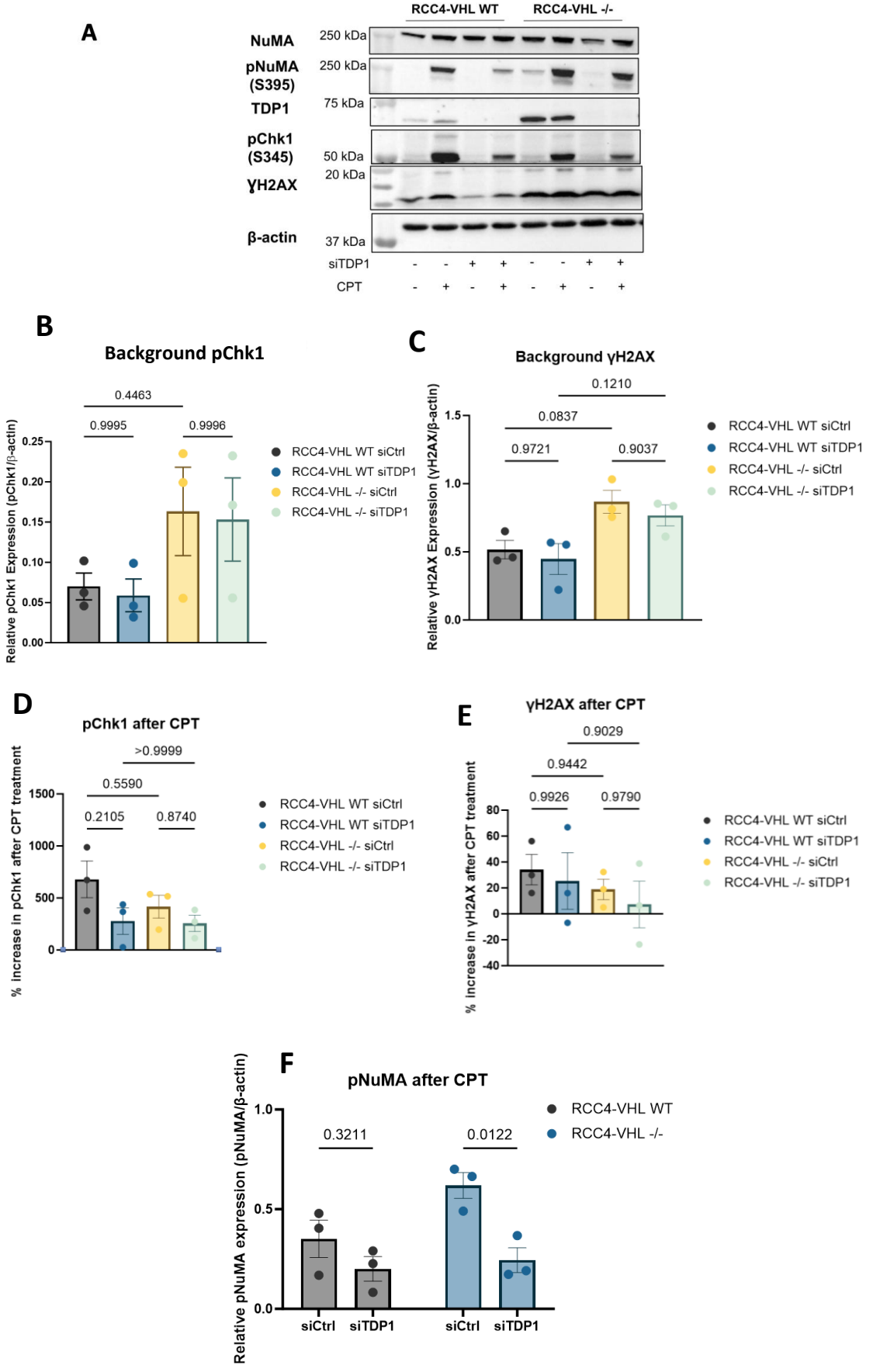
A
RCC4-VHL WT
RCC4-VHL -/-
NuMA
250 kDa
pNuMA (S395)
250 kDa
TDP1
75 kDa
pChk1 (S345)
50 kDa
γH2AX
20 kDa
β-actin
37 kDa
siTDP1
CPT
B
Background pChk1
Relative pChk1 Expression (pChk1/β-actin)
0.4463
0.9995
0.9996
RCC4-VHL WT siCtrl
RCC4-VHL WT siTDP1
RCC4-VHL -/- siCtrl
RCC4-VHL -/- siTDP1
C
Background γH2AX
Relative γH2AX Expression (γH2AX/β-actin)
0.1210
0.0837
0.9721
0.9037
D
pChk1 after CPT
% Increase in pChk1 after CPT treatment
>0.9999
0.5590
0.2105
0.8740
E
γH2AX after CPT
% Increase in γH2AX after CPT treatment
0.9029
0.9442
0.9926
0.9790
F
pNuMA after CPT
Relative pNuMA expression (pNuMA/β-actin)
0.3211
0.0122
RCC4-VHL WT
RCC4-VHL -/-
siCtrl
siTDP1

Figure 4.6: TDP1 knockdown does not cause increased expression of pChk1 or γH2AX after CPT treatment. A) Representative western blot showing successful knockdown of TDP1 in RCC4 cells after TDP1 siRNA (siTDP1). Control siRNA was used as a control (siCtrl). CPT treatment (10 μM for 1 hour) caused upregulation of pChk1 and mild upregulation of γH2AX in RCC4-VHL WT cells. pNuMA upregulation after CPT treatment was decreased in siTDP1 samples. β-actin was used as a loading control. **B-C)** Quantification of western blots showing background expression levels of pChk1 and γH2AX. pChk1 expression was not significantly different in any samples. γH2AX expression trended towards upregulation in RCC4-VHL -/- cells. One-way ANOVA with Šidák correction, p value < 0.05 considered significant, Mean ± SEM, n=3. **D-E)** Quantification of western blots showing fold changes in pChk1 and γH2AX following CPT treatment. TDP1 depletion via siTDP1 did not cause increased expression of either pChk1 or γH2AX. There was a trend whereby pChk1 expression in TDP1-depleted cells is reduced after CPT treatment, compared to siCtrl-transfected cells. One-way ANOVA with Šidák correction, p value < 0.05 considered significant, Mean ± SEM, n=3. **F)** Quantification of western blots showing pNuMA upregulation after CPT treatment significantly decreased after knocking down TDP1 expression via siRNA in RCC4-VHL -/- cells. Two-way ANOVA with Šidák correction, p value < 0.05 considered significant, Mean ± SEM, n=3.

The unexpected pattern of pChk1 expression decreasing after TDP1 depletion, whilst γH2AX expression did not change could have been due to the intrinsic properties of the RCC4 cells. I explored this possibility by repeating the previous experiment using a different cell line that had been well characterised and did not originate from a cancer patient. The MRC5 cell line originated from 14-week-old foetal lung tissue (Jacobs et al., 1970) and has previously been shown to be more sensitive to DNA damaging agents following TDP1 depletion (Alagoz et al., 2014; Ray et al., 2022). Depletion of TDP1 in MRC5 did not cause a significant increase in pChk1 or γH2AX expression following CPT treatment **(Figure 4.7)**. Therefore, this was different to the pattern observed in RCC4 cells, whereby TDP1 depletion caused a reduction in pChk1 following CPT treatment **(Figure 4.6)**.

As an alternative and potentially more sensitive technique to determine if TDP1-depleted RCC4 cells are accumulating more DNA breaks following CPT treatment, I decided to probe γH2AX via immunofluorescence as it would allow for foci detection in individual cells, rather than analysing total protein amount (Kinner et al., 2008). Another DNA repair protein of interest I wanted to observe was 53BP1, which is involved in NHEJ to repair DSBs (Lei et al., 2022). I performed immunofluorescence **(Section 2.13)** on RCC4 cells with or without TDP1 depletion via siRNA, followed by treating with 10 µM CPT for 1 hour. γH2AX foci formation increased following CPT treatment, but similar to previous experiments, this was not exaggerated after TDP1 depletion **(Figure 4.8E)**. 53BP1 foci formation did not significantly increase following CPT treatment in siCtrl cells. However, TDP1-depleted RCC4-VHL WT cells showed a significant increase in 53BP1 foci formation following CPT treatment, suggesting that the NHEJ pathway becomes activated to repair DSBs. Meanwhile, 53P1 foci formation did not significantly increase in TDP1-depleted RCC4-VHL -/- cells following CPT treatment (**Figure 4.8F)**. This suggested that an alternative pathway is involved in repairing DSBs in RCC4-VHL -/-.

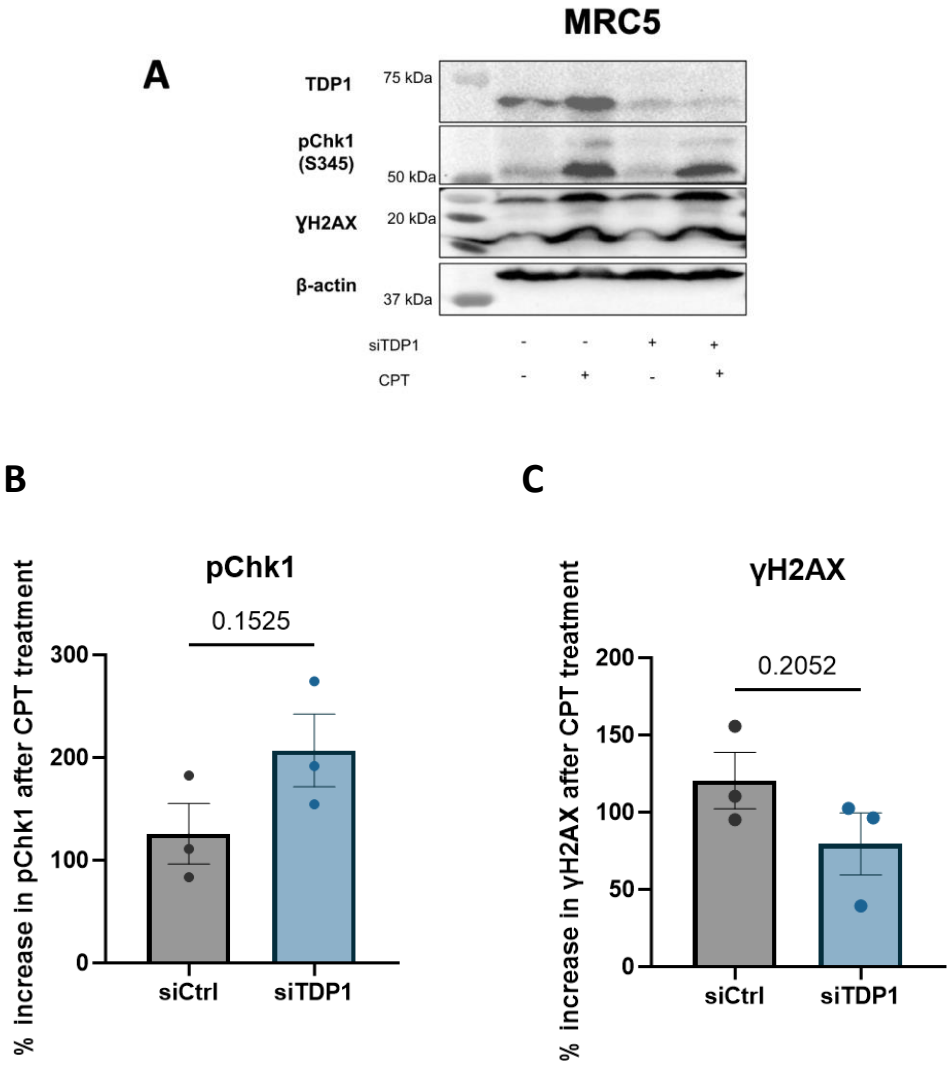

Figure 4.7: TDP1 knockdown in MRC5 cells does not cause increased sensitivity to CPT. A) Representative western blot showing successful knockdown of TDP1 in MRC5 cells after TDP1 siRNA (siTDP1). Control siRNA was used as a control (siCtrl). CPT treatment (10 µM for 1 hour) caused upregulation of pChk1 and γH2AX. β-actin was used as a loading control. **B-C)** Quantification of western blots showing that pChk1 and γH2AX expression in CPT-treated cells was not enhanced by TDP1 knockdown. Unpaired Student's t-test, p value < 0.05 considered significant. Mean ± SEM, n=3.

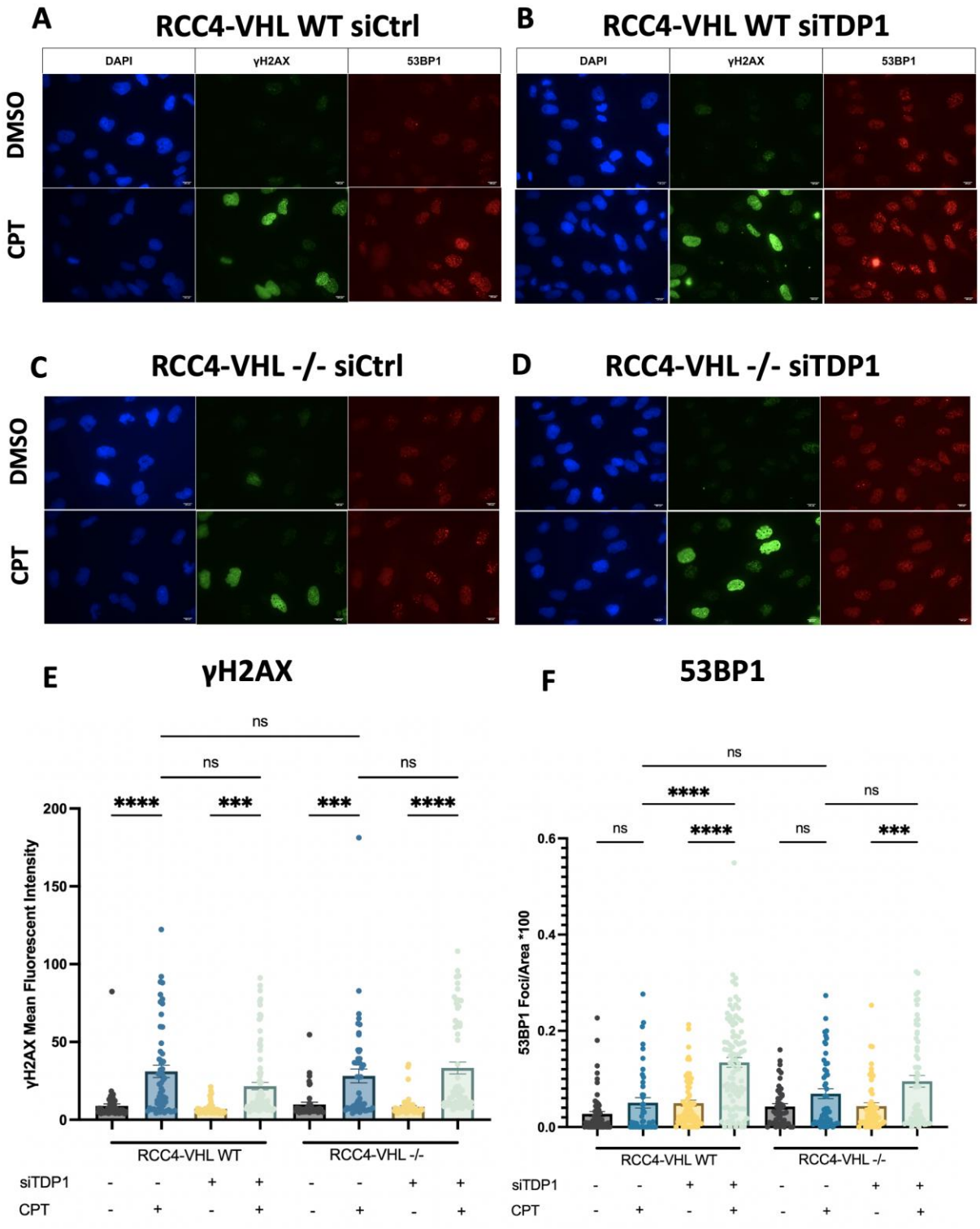
A
RCC4-VHL WT siCtrl
B
RCC4-VHL WT siTDP1
DAPI
γH2AX
53BP1
DMSO
CPT
C
RCC4-VHL -/- siCtrl
D
RCC4-VHL -/- siTDP1
E
γH2AX
F
53BP1
γH2AX Mean Fluorescent Intensity
53BP1 Foci/Area *100
ns
****
***
RCC4-VHL WT
RCC4-VHL -/-
siTDP1
CPT

Figure 4.8: TDP1 depletion followed by CPT treatment does not cause increased γH2AX foci formation but does cause increased 53BP1 foci formation only in RCC4-VHL WT cells. RCC4 cells were treated with either control siRNA (siCtrl) or TDP1 siRNA (siTDP1). **A-B)** Representative images for RCC4-VHL WT showing γH2AX foci and 53BP1 foci in DMSO treated cells (control) or CPT treatment (10 µM for 1 hour). **C-D)** Representative images for RCC4-VHL -/- γH2AX foci forming and 53BP1 foci in DMSO treated cells (control) or CPT treatment. Scale bars = 100 µm. γH2AX foci formation increased significantly following CPT treatment in both cell lines, but there was no measurable difference after TDP1 depletion. 53BP1 foci formation increase was not significant following CPT treatment but increased significantly in TDP1-depleted RCC4-VHL following CPT treatment. One-way ANOVA with Šidák correction, ns=p>0.05, ***p<0.001, ****p<0.0001, Mean ± SEM, Biological replicate = 1, Technical repeat = 45-92 cells.

The loss of TDP1 has been previously reported in some models to not cause increased sensitivity to CPT due to the recruitment of other DNA repair proteins that can compensate for the loss of TDP1. One such protein is tyrosyl-DNA phosphodiesterase 2 (TDP2), which has been shown to be capable of repairing TOP1-mediated breaks in the absence of TDP1 (Zeng et al., 2012; Shimizu et al., 2023). However, I did not observe an upregulation of TDP2 following TDP1 depletion **(Figure 4.9A)**. Zaksauskaite et al., (2021) identified *apex2* and *ercc4* as upregulated genes in *tdp1* -/- zebrafish embryos in response to CPT treatment. Meanwhile, the endonuclease MUS81 has been shown to be involved in TDP1-independent mechanisms of DNA repair (Zhang et al., 2022; Marini et al., 2023), whilst the association of XRCC1 with TDP1 is well-established (Plo et al., 2003). I harvested mRNA from RCC4-VHL -/- transfected with siTDP1, then treated with CPT, and analysed the mRNA expression for *APEX2, ERCC4, MUS81,* and *XRCC1* via RT-qPCR to see if any of the target genes were compensating for TDP1 depletion. All target genes showed a non-significant downregulation in mRNA expression following CPT treatment in both the siCtrl and TDP1-depleted cells. This was not obvious in *XRCC1* and *APEX2* due to the large variation across repeats. In TDP1-depleted cells, there was a non-significant downregulation following CPT treatment for *ERCC4* (p=0.0655) and *MUS81* (p=0.1108) **(Figure 4.9 B-F)**.

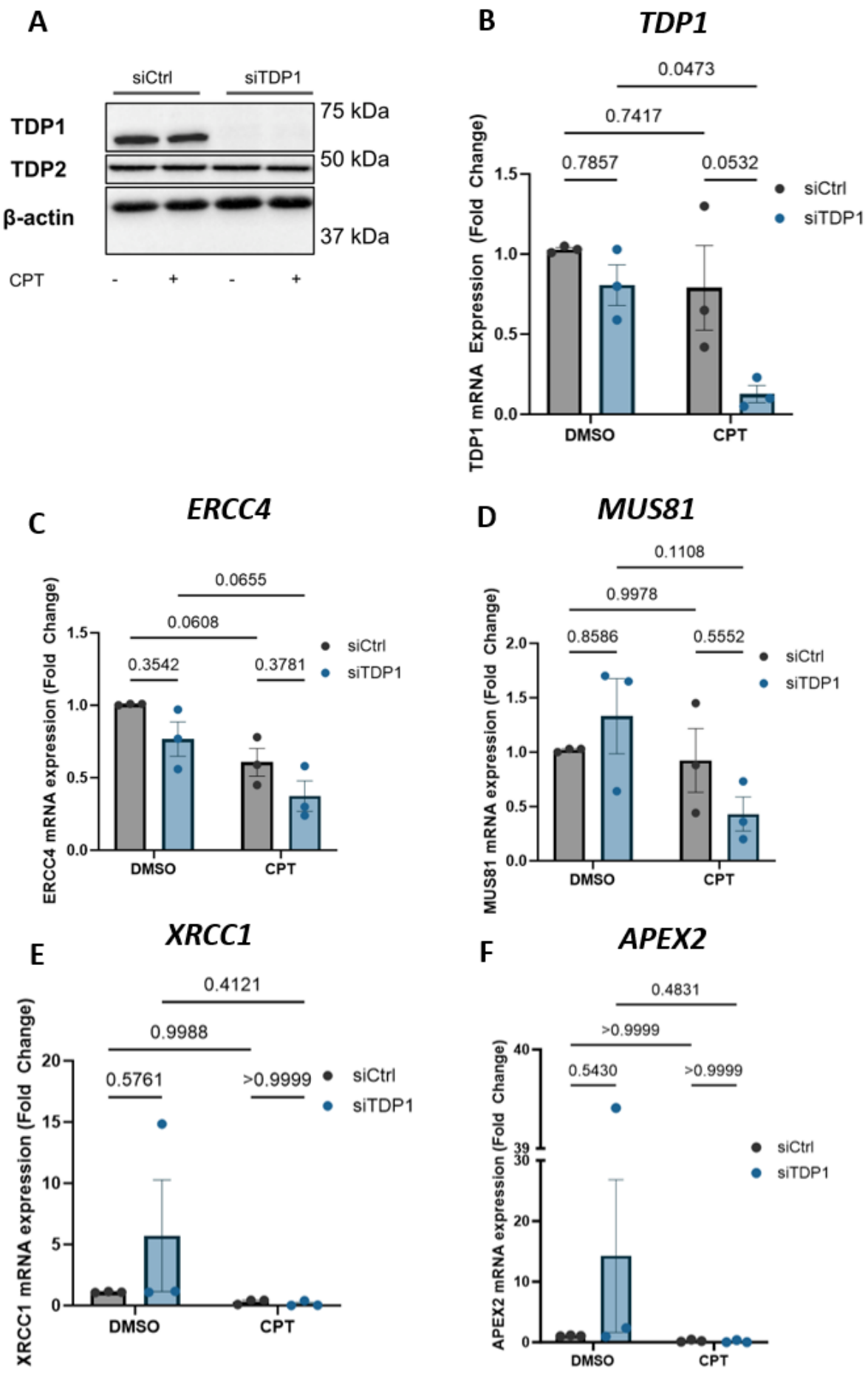
A
siCtrl
siTDP1
TDP1
TDP2
β-actin
75 kDa
50 kDa
37 kDa
CPT
- + - +
B
TDP1
0.0473
0.7417
0.7857
0.0532
TDP1 mRNA Expression (Fold Change)
siCtrl
siTDP1
DMSO
CPT
C
ERCC4
0.0655
0.0608
0.3542
0.3781
ERCC4 mRNA expression (Fold Change)
siCtrl
siTDP1
DMSO
CPT
D
MUS81
0.1108
0.9978
0.8586
0.5552
MUS81 mRNA expression (Fold Change)
siCtrl
siTDP1
DMSO
CPT
E
XRCC1
0.4121
0.9988
0.5761
>0.9999
XRCC1 mRNA expression (Fold Change)
siCtrl
siTDP1
DMSO
CPT
F
APEX2
0.4831
>0.9999
0.5430
>0.9999
APEX2 mRNA expression (Fold Change)
siCtrl
siTDP1
DMSO
CPT

Figure 4.9: Absence of clear compensatory mechanisms following *TDP1* knockdown in RCC4-VHL -/-. A) Representative western blot showing TDP1 knockdown in RCC4-VHL -/- following siTDP1. TDP2 expression did not differ between siCtrl and siTDP1 following CPT treatment. **B-F)** RT-qPCR showing TDP1 expression or potential *TDP1* compensatory factors *ERCC4*, *MUS81*, *XRCC1*, and *APEX 2* following control siRNA (siCtrl) or TDP1 siRNA (siTDP1), and CPT treatment (10 µM for 1 hour) or DMSO as a control. *TDP1* expression was close to significantly downregulated only when cells were treated with CPT ($p = 0.0532$), whilst there was significantly less *TDP1* when comparing DMSO vs CPT in siTDP1 cells. *ERCC4* expression decreased following CPT treatment in both siCtrl and siTDP1, whilst *MUS81* expression decreased in siTDP1 only following CPT treatment. There was no notable trend in either *XRCC1* or *APEX2*, as the variation in data was too extreme. Two-way ANOVA with Šidák correction. p value < 0.05 considered significant. Mean ± SEM, n=3.

4.5. Discussion

4.5.1. HIFα knockdowns do not reduce chemoresistance

Modulating either HIF1α or HIF2α via siRNA did not cause a measurable difference in chemoresistance following CPT treatment, measured by clonogenic analysis and comet assay **(Figure 4.1)**. ccRCC patients have regions of chronic tissue hypoxia, whilst siRNA-mediated downregulation of HIFα in cell lines occurs on a more acute scale. HIF1α expression appears to stabilise during acute hypoxia then gradually decreases, whereas HIF2α expression stabilises during chronic hypoxia (Saxena and Jolly, 2019). This suggests that downstream HIFα pathways differ whether cells have been exposed to acute or chronic hypoxia. It has been previously shown in a breast cancer cell line (MCF7) that different genes are upregulated or downregulated depending on whether cells have been exposed to acute hypoxia or chronic hypoxia. In addition, several genes were shown to be alternatively spliced depending on the extent of hypoxia (Han et al., 2017). Moreover, the PAS-B domain of HIF1α can repress the expression of *NBS1*, an important protein of the MRN complex involved in repairing DNA DSBs. However, the PAS-B domain of HIF2α is phosphorylated at Thr-324, preventing NBS1 repression (D'Amours and Jackson, 2002; To et al., 2006). It is possible that DNA repair genes in ccRCC cell lines are alternatively spliced when exposed to acute or chronic hypoxia, causing differential responses to DNA damaging agents.

CRISPR-Cas9-mediated gene downregulation can provide a stable cell line that could potentially overcome the limitations associated with siRNA knockdowns. Long-term knockdown via CRISPR-Cas9 could more accurately model the pathways downstream of HIFα, allowing for greater clinical relevance. In addition, as HIFα is constitutively upregulated in RCC4-VHL -/-, a constitutive downregulation would be required for an accurate comparison. I had aimed to create a stable cell line for each possible gene combination (*VHL*/*HIF1α*/*HIF2α*) to analyse the contributions of each gene to chemoresistance. However, the initial problem I faced was that I did not observe a knockdown following transfection with pSpCas9(BB)-2A-Puro (**Figure 4.2C)**. This could have been due to the single gRNA not being sufficient to cause mRNA degradation, or due to low transfection efficiency. I decided to use pSpCas9(BB)-2A-GFP, as FACS sorting GFP positive cells would provide a clearer answer as to how many cells were being transfected. There

were very few positively transfected cells following FACS sorting, and the only clones that proliferated enough for serial dilution were two clones from the same transfection: RCC4-VHL -/- ; gHIF2α. Both clones had a notable reduction in HIF2α protein expression, as well as a reduction in TDP1 expression **(Figure 4.2D)**, mimicking previous data that showed HIF2α downregulation in RCC4-VHL -/- via siRNA caused TDP1 downregulation **(Figure 3.9)**. As HIF1α expression was upregulated in clone (B) **(Figure 4.2D)**, potentially due to genetic compensation, I decided to expand clone (A) for further experiments.

I wanted to see if the TDP1 downregulation I initially observed in RCC4-VHL ; HIF2α was reproducible, so I harvested samples from later passages and analysed TDP1 protein expression. Interestingly, TDP1 appeared to return back to normal levels and was no longer downregulated **(Figure 4.3 B-C).** This could be due to genetic compensation (El-Brolosy et al., 2019; Salanga and Salanga, 2021), whereby an unknown protein could potentially assume the role of HIF2α, thus restoring TDP1 expression. In addition, the transfected cells may have undergone karyotypic changes providing a selective growth advantage that reversed the initially observed increase in TDP1 expression. This phenomenon is known as culture adaptation (Weissbein et al., 2019).

Despite TDP1 expression returning to baseline levels, I decided to continue with the planned experiment of comparing the chemosensitivity of RCC4-VHL -/- ; HIF2α -/- with the original RCC4 lines. I did this via clonogenic analysis using CPT, Olaparib, and cisplatin. Whilst RCC4-VHL -/- continued to show increased resistance compared to RCC4-VHL WT, the resistance of RCC4-VHL ; HIF2α -/- was comparable to RCC4-VHL -/- **(Figure 4.4)**. Therefore, I concluded that HIF2α downregulation via CRISPR-Cas9 had no measurable impact on chemoresistance.

4.5.2. TDP1 knockdown does not reduce chemoresistance

Due to the complications associated with analysing chemoresistance in HIF2α-depleted cells, I wanted to establish whether TDP1 depletion could restore chemosensitivity. Increased expression of TDP1 has been established in RCC4-VHL -/-, and high expression of TDP1 has been previously associated with chemoresistance in other disease models. TDP1 depletion in RCC4-VHL WT or RCC4-VHL -/- did not increase sensitivity to CPT when analysing colony formation in clonogenic analysis **(Figure 4.5)**. This was a surprising result as

TDP1 depletion appeared to be a reliable method to increase sensitivity to DNA damaging agents. TDP1 depletion not impacting RCC4-VHL -/- could be explained by the inherently high levels of chemoresistance present in these cells; however, RCC4-VHL WT do not demonstrate the same characteristics. Therefore, I aimed to investigate whether the RCC4 cell line had an inherently abnormal response to TDP1 depletion, whereby they are able to counteract this depletion by influencing another pathway. Alternatively, clonogenic analysis may not be the most sensitive method to detect chemosensitivity as the cells are allowed to grow in drug-free media for a long period of time, and clonogenic analysis only determines the colony-formation propensity of a cell, rather than how healthy a population of cells are.

I decided to look at pChk1 and γH2AX levels in RCC4 to establish if DNA repair pathways were impacted by TDP1 depletion (Zhang et al., 2022). γH2AX is also a reliable marker of DNA DSBs that can provide an alternative readout of DNA damage (Mah et al., 2010). In addition, the phosphorylated form of TDP1-interacting protein NuMA, which I had previously shown to be upregulated in RCC4-VHL -/- **(Figure 3.12)**, was probed to see if its expression was also impacted. The baseline expression levels of pChk1 were slightly higher in RCC4-VHL -/- compared to RCC4-VHL WT, although not to a significant extent **(Figure 4.6B)**, suggesting potential enhancement of DDR. Similarly, baseline γH2AX was non-significantly higher in RCC4-VHL -/-, suggesting that there are greater DSBs forming **(Figure 4.6C**)**.** However, as I have previously shown that RCC4-VHL -/- accumulate less DNA breaks than RCC4-VHL WT in a comet assay **(Figure 3.2D)**, this suggests that more DNA breaks are being detected in RCC4-VHL -/-, but they are able to repair themselves more efficiently than RCC4-VHL WT. TDP1 depletion did not impact background levels of pChk1 or γH2AX **(Figure 4.6 B-C)**. Following TDP1 depletion in RCC4-VHL WT, CPT treatment did not cause a significant increase in pChk1 and trended towards decreased expression compared to siCtrl-treated cells. TDP1 depletion did not cause any difference to pChk1 expression in RCC4-VHL -/- following CPT treatment **(Figure 4.6D)**. In addition, whilst γH2AX expression increased following CPT treatment in RCC4-VHL WT, TDP1 depletion did not exaggerate this increase. A similar trend was observed in RCC4-VHL -/-. **(Figure 4.6E**)**.** This suggests an inherent property within RCC4 cells, whereby TDP1 depletion does not cause increased DNA breaks due to a compensatory mechanism diverting DNA repair away from the pChk1 pathway. Alternatively, TDP1 depletion may be causing increased expression of another DNA repair

protein that can compensate for the loss of TDP1, and repair DNA breaks to a greater extent that the TDP1 pathway. Further solidifying the suggestion that DNA repair in RCC4 following TDP1 depletion commences via an alternative pathway, pNuMA expression in RCC4 cells lacking TDP1 is significantly downregulated **(Figure 4.6F**)**.** pNuMA recruits various DNA repair proteins, including TDP1, to DNA break sites for DNA repair. A reduction in pNuMA, while DNA damage levels remain stable, suggests that this pathway is downregulated and no longer required to maintain genomic stability. Alternatively, this could be indicative of pNuMA not being required to be upregulated as much as before due to TDP1 not being recruited to sites of DNA damage.

To determine if this was a cell line specific phenomenon, I repeated the experiment in the MRC5 cell line. CPT treatment caused an increase in pChk1 expression, which was further exaggerated upon TDP1 depletion, although not to a significant extent **(Figure 4.7B).** This pattern differed from RCC4 and suggested that RCC4 cells had a unique response to TDP1 depletion. γH2AX expression increased in CPT treatment, but was not significantly impacted by TDP1 depletion **(Figure 4.7C).** As the increase in γH2AX following CPT treatment in both RCC4 and MRC5 was relatively minor, it may have been difficult to observe clearer differences following TDP1 depletion. Therefore, it would potentially be beneficial to repeat this experiment with a higher concentration of CPT.

Immunofluorescence can provide a more sensitive readout of γH2AX formation, so I once more depleted TDP1 in RCC4 cells, treated with CPT, then quantified γH2AX foci formation, as well as 53BP1, which is involved in NHEJ. 53BP1 was chosen as a potential DNA repair protein upregulated after TDP1 depletion that could explain why TDP1 depletion does not cause increased formation of pChk1 or γH2AX. Similar to western blot, TDP1 depletion did not cause increased formation of γH2AX foci following CPT treatment **(Figure 4.8E).** 53BP1 foci formation following CPT treatment showed minor upregulation in RCC4-VHL WT and RCC4-VHL -/-. However, TDP1 depletion caused a significant increase in 53BP1 foci following CPT treatment, suggesting that activation of the NHEJ pathway was compensating for the loss of TDP1. This pattern was not observed in RCC4-VHL -/- **(Figure 4.8F)**, indicating that an alternative repair mechanism was involved. It is important to note that this experiment was repeated only once due to time constraints. Therefore, the conclusions drawn from this

experiment are based solely on technical repeats, so it is extremely important to repeat this experiment and take the average across three biological replicates before making any final conclusions.

4.5.3. No clear compensatory factors for *TDP1* depletion identified

RCC4-VHL -/- appears to be utilising unknown DNA repair mechanisms following TDP1 depletion. A potential protein that could be compensating for TDP1 depletion is the closely related TDP2, which has been shown to repair TOP1-induced DNA damage in the absence of TDP1 (Zeng et al., 2012). However, TDP2 protein expression did not change following TDP1 depletion **(Figure 4.9A)**. Several alternative DNA repair genes were identified: *ERCC4, MUS81, XRCC1,* and *APEX2*. Due to time and money constraints, I decided to look at the gene expression of these targets following TDP1 depletion and CPT treatment via RT-qPCR. Interestingly, *TDP1* expression was not downregulated in siTDP1 cells until CPT treatment occurred **(Figure 4.9B)**. This is despite protein expression being downregulated. A potential explanation for this may be due to the experimental set up. The cells were transfected with siCtrl or siTDP1 for 48 hours, then siRNA-containing media was removed, allowing the cells to be harvested and seeded for DMSO/CPT treatment the following day. Therefore, there was a 24-hour period whereby siRNA was not present in the media. Thus, mRNA expression may have started to recover towards baseline levels, while protein expression remained low. As TDP1 protein expression was still downregulated, this should still promote TDP1-independent repair mechanisms.

ERCC4 expression had a minor, non-specific downregulation in TDP1-depleted cells, which was exaggerated following CPT treatment, suggesting that *ERCC4* expression could be downregulated after TDP1 depletion **(Figure 4.9C)**. *MUS81* expression was non-significantly increased following TDP1 depletion, but CPT treatment caused minor downregulation **(Figure 4.9D)**. No conclusions could be drawn from *XRCC1* and *APEX2* expression as one repeat of the TDP1-depleted cells without CPT treatment had an unusually high increase in expression **(Figure 4.9E)**. There was nothing to suggest that this repeat was done incorrectly or was an outlier, so further repeats are required for *XRCC1* and *APEX2* before concluding any trends. In addition, I would use lower doses of CPT over longer periods of time, as opposed to a high dose over a short period, as transcriptional and translational changes in

TDP1 compensatory factors may require a longer time period to become quantifiable (Zaksauskaite et al., 2021).

Although I did not identify clear upregulation of any TDP1 compensatory factors, Zeng et al., (2012) identified that *Tdp1 -/-;Tdp2 -/-* murine models showed increased sensitivity to Top1 poisons, which can be partially reversed by overexpression of Tdp2. Therefore, follow up experiments in RCC4-VHL -/- should attempt to recreate this by creating a *TDP1 -/-;TDP2 -/-* knockout to see if this causes increased sensitivity to TOP1 poisons, followed by reintroduction of TDP2 to reverse the phenotype. Moreover, TDP2 expression may remain stable following *TDP1* depletion in RCC4-VHL -/-, but its enzymatic activity may increase as a result of posttranslational modifications. Therefore, lysates from RCC4-VHL -/- cells with and without TDP1/TDP2 depletion, and treated with CPT, or DMSO as a control, should be analysed on a TDP2 activity assay (Zaksauskaite et al., 2021) to see if TDP2 is able to resolve TOP1-CCs. TDP2 is the most well-characterised compensatory factor for *TDP1* depletion across multiple models (Zeng et al., 2012; Shimizu et al., 2023), so future work should focus on this area.

4.6. Summary

Reducing HIFα levels in RCC4-VHL -/-, either via siRNA or CRISPR-Cas9, did not cause reduced resistance to DNA damaging agents. This suggests that modulating HIFα alone is likely not sufficient to reestablish chemosensitivity and that HIF-independent targets of VHL need to be studied further, or gaining a better understanding of the lesser-known roles of HIF3α (Ravenna et al., 2016). Upregulated expression of TDP1 in RCC4-VHL -/- did not seem to be solely responsible for enhanced chemoresistance, as knocking down its expression did not restore chemosensitivity. Increased TDP1 expression could be a side effect of *VHL* inactivation that has no impact on chemoresistance, or other DNA repair proteins play a larger role than TDP1 in HIF-mediated chemoresistance. Both RCC4 cell lines could have a unique phenotype whereby alternative DNA repair mechanisms can take over from TDP1-mediated DNA repair, such as NHEJ in the case of RCC4-VHL WT, and this needs to be explored further. Overall, these experiments establish that chemoresistance in ccRCC is highly complex and potentially involves crosstalk across multiple pathways. A well-designed

experiment looking to counteract chemoresistance in ccRCC models will accurately identify how the pathways interact and target each one as a combinatorial effort, rather than focusing only on one pathway, as this does not mimic clinical observations.

Chapter 5 HIF activation and chemoresistance in zebrafish

5.1. Introduction

All cell lines have disadvantages associated with their use as disease models. Established cell lines derived years ago from patients undergo a continuous genomic evolution, causing them to lose resemblance to the primary tumour from which they were originally derived. These changes, which have been previously identified in well-known cell lines such as HeLa and MCF7, can include point mutations, copy number alterations, and chromosomal rearrangements (Burdall et al., 2003; Frattini et al., 2015; Ben-David et al., 2019). Genetic drift in established cell lines can cause certain mutated genes to increase in frequency, or it can lead to the loss of genetic variants. Therefore, genetic drift leads to the expansion of new subclones or the expansion of pre-existing subclones that were previously detected at low frequencies. Other factors that can influence subclone formation and expansion in cell lines includes changes to cell culture media, such as the use of antibiotics plus contamination from chemicals and other cell lines (Lucey et al., 2009; Weiskirchen et al., 2023). Furthermore, tumour cells naturally evolve as the tumour develops, potentially due to increased genomic instability being a common trait in many tumours (Jeggo et al., 2016). Genomic instability gives rise to new subclones, that no longer reflect the original tumour cell. However it has been shown that evolution in cell lines diverge from tumour evolution (Ben-David et al., 2017, 2018), so cell lines do not evolve in the same manner as the tumour of origin.

A key disadvantage of using cell lines as a cancer model is the absence of the tumour microenvironment (TME) surrounding the tumour cells. The TME consists of a heterogeneous grouping of cells, proteins, and soluble factors that can impact the tumour phenotype as well as communicating with distant cells in the body via secreted factors and extracellular vesicles (Peinado et al., 2017). Tumour cells do not act in a cell-autonomous fashion as the entire host organism plays a role in defining tumour cell behaviour, which in turn impacts how tumours respond to chemotherapy. Therefore, it is crucial to also use whole organisms to study the impact of potential therapeutics, due to the presence of the TME.

Zebrafish are an ideal organism to study cancer formation and drug resistance as the complexity of the TME is present. There is a high degree of TME conservation between humans and zebrafish, with many models having been created to study the contributions of each component of the TME to cancer formation and metastasis (Sturtzel et al., 2021; Weiss et al., 2022). In addition, the optical transparency of zebrafish embryos allows for high quality image analysis and identifying key signs of disease progression, such as cancer metastasis (Gupta and Massagué, 2006; Weiss et al., 2022).

Zebrafish *vhl* mutants develop key symptoms of VHL-associated diseases, such as constitutive upregulation of the HIF pathway, ectopic vessel formation, and kidney abnormalities (van Rooijen et al., 2011; Marchi, 2020). Human VHL function is divided between Vhl and Vll, with Hif-modulation appearing to be mostly controlled by Vhl, with minor contribution from Vll (Chen et al., 1995; Van Rooijen et al., 2009; Kim et al., 2020). *vhl* $^{-/-}$ *; vll* $^{-/-}$ embryos, which display a very strong upregulation of Hif pathway, have enhanced protection from genotoxic stress induced pharmacologically via CPT or via X-rays (Kim et al., 2020), mimicking phenotypes observed in ccRCC patients (Brugarolas, 2014).

5.2. Hypothesis

Pharmacological upregulation of Hifα via PHIs in WT zebrafish will protect them from CPT-induced genotoxic stress, as observed previously by Kim et al., (2020). This will be replicated in RCC4 cells, whereby pharmacologically targeting HIFα will modulate sensitivity to CPT treatment. In addition, *vhl* $^{-/-}$ *; vll* $^{-/-}$ embryos will have higher levels of Tdp1 due to constitutive upregulation of Hifα, thereby boosting chemoresistance.

5.3. Aims

1. Determine chemosensitivity in WT zebrafish embryos after pharmacological upregulation of Hifα.
2. Establish the impact of pharmacological modulation of HIFα on RCC4 cells' chemosensitivity.
3. Identify Tdp1 expression levels in zebrafish embryos with mutations in *vhl* and *vll.*

5.4. Results

5.4.1. Hif activation protects zebrafish from CPT treatment

Kim et al., (2020) demonstrated that pharmacological upregulation of Hifα in WT zebrafish embryos was sufficient to protect them from genotoxic stress induced by CPT. As I had been having issues modulating chemosensitivity in RCC4 cells, I wanted to see if targeting HIFα pharmacologically, rather than via siRNA/CRISPR-Cas9, would have an impact. I began by confirming that pharmacological upregulation of Hifα in WT zebrafish was sufficient to increase chemoresistance, as previously reported by Kim et al., (2020), who had used the Hif activator JNJ at 100 µM. As I had previously used ROX in RCC4 cells, I was also interested in using ROX. Unpublished data from the van Eeden lab suggested that 5 µM of ROX would be sufficient to cause increased Hif expression. To confirm this, I treated 3 dpf *vhl* ^{sibs} ; *vll* $^{-/-}$ embryos with ROX or DMSO for 42 hours. Sibs refers to a population of embryos containing one functioning allele of *vhl*, or two functioning alleles. As one functioning allele is sufficient for *vhl* to function properly (Hes et al., 2005), there is no phenotypic difference between the two populations. Higher levels of GFP expression in these embryos corresponds to increased expression of *hif* target Phd3, particularly in the liver (Santhakumar et al., 2012; Marchi et al., 2020). Accurately sorting GFP negative (*vhl* ^{sibs}) vs GFP positive (*vhl* $^{-/-}$) embryos from a *vhl* ^{sibs} ; *vll* $^{-/-}$ incross was only possible at 3 dpf (Marchi, 2020), so the embryos could not be treated any earlier. **Figure 5.1** confirms that ROX is sufficient to cause increased expression of *hif* target Phd3.

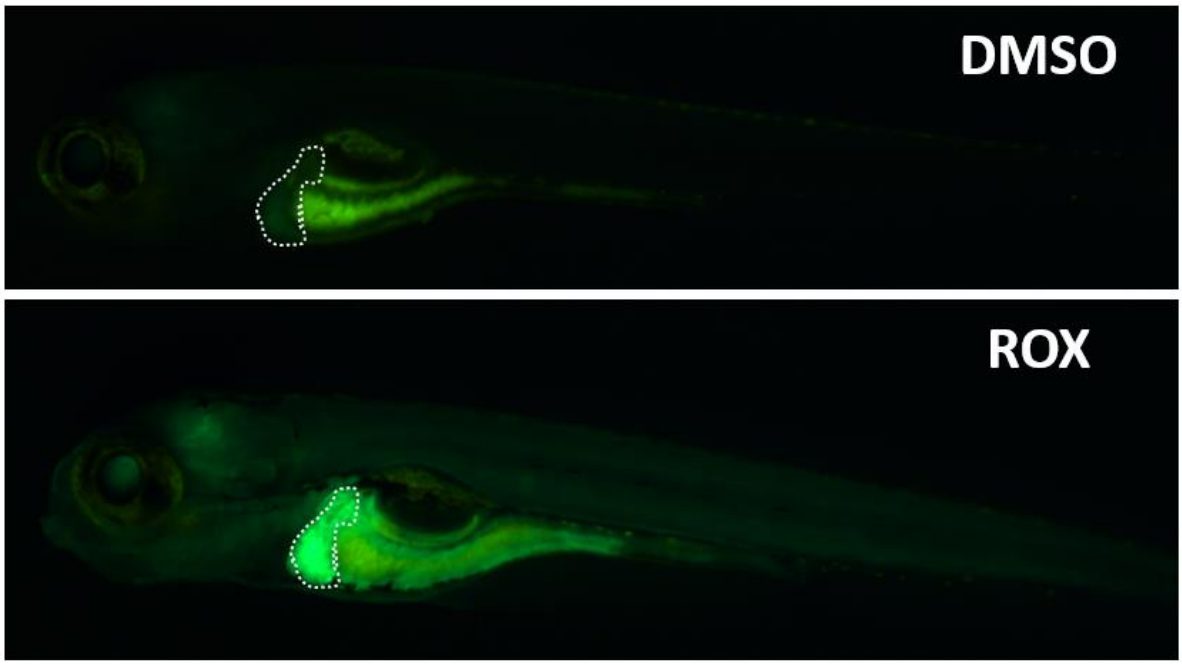

Figure 5.1: ROX treatment upregulates Hif expression in *vhl* ^{sibs};*vll* $^{-/-}$ zebrafish. Representative images of 5 dpf *vhl* sibs;*vll* -/- embryos after treating with Hif activator ROX or DMSO. ROX treatments occurred at 3 dpf for 42 hours. GFP expression corresponds to expression of *hif* target Phd3, as described in (Santhakumar et al., 2012). The region highlighted is the liver, where GFP expression increase is particularly prominent following ROX treatment. Images taken by my MSc student Ziyan Ma.

Once I had established the concentration of ROX to use, I dechorionated 1 dpf nacre embryos and pre-treated them for 8 hours with one of two Hif activators: ROX (5 µM) or JNJ (100 µM) in E3 media, as performed by (Kim et al., 2020). DMSO was used as a control. Following pre-treatment, embryos were treated overnight with 10 nM CPT or DMSO, alongside fresh Hif activator. At 2 dpf, drug-containing E3 media was replaced with fresh E3 media, then the embryos were imaged at 3 dpf. CPT treatment causes visible apoptosis in the zebrafish head, which is identifiable by dark colouration. In addition, eye size can be used as a measure of overall zebrafish health (Kim et al., 2020). Apoptosis in the head was measured by analysing 'mean grey value' on FIJI software, which was also used to measure eye size. Representative images can be found in **Figure 5.2 A-B**, whilst the regions of interest can be found in **Figure 5.2C**.

CPT treatment caused a reduction in mean grey value, correlating with increased apoptosis, which was expected. Pre-treating embryos with ROX followed by CPT did not rescue the phenotype; however, it was interesting to see that ROX treatment on its own had a higher mean grey value than DMSO treated embryos. JNJ pre-treatment alone showed no measurable difference to DMSO treated embryos, whilst JNJ combined with CPT caused the apoptotic phenotype to be rescued, suggesting that JNJ was protecting the embryos from CPT-induced genotoxic stress **(Figure 5.2D)**.

CPT-treated embryos had significantly smaller eye size compared to DMSO-treated embryos, confirming that CPT treatment causes the embryos to become unhealthy. However, a similar phenotype was also observed following ROX or JNJ treatment, albeit to a lesser extent. Combining ROX or JNJ with CPT treatment did not cause a rescue of eye size phenotype **(Figure 5.2E)**.

Although CPT treatment only caused a minor reduction in the overall survival of treated embryos, a combination of ROX and CPT caused a sharp decline in surviving embryos, suggesting that both drugs cause adverse effects when used together causing embryo death. This effect was not seen with JNJ/CPT **(Figure 5.2F)**. Overall, this suggests that ROX causes abnormal development in zebrafish embryos and that only JNJ should be used for

pharmacological upregulation of Hifα, which matches previously unpublished observations from the van Eeden lab.

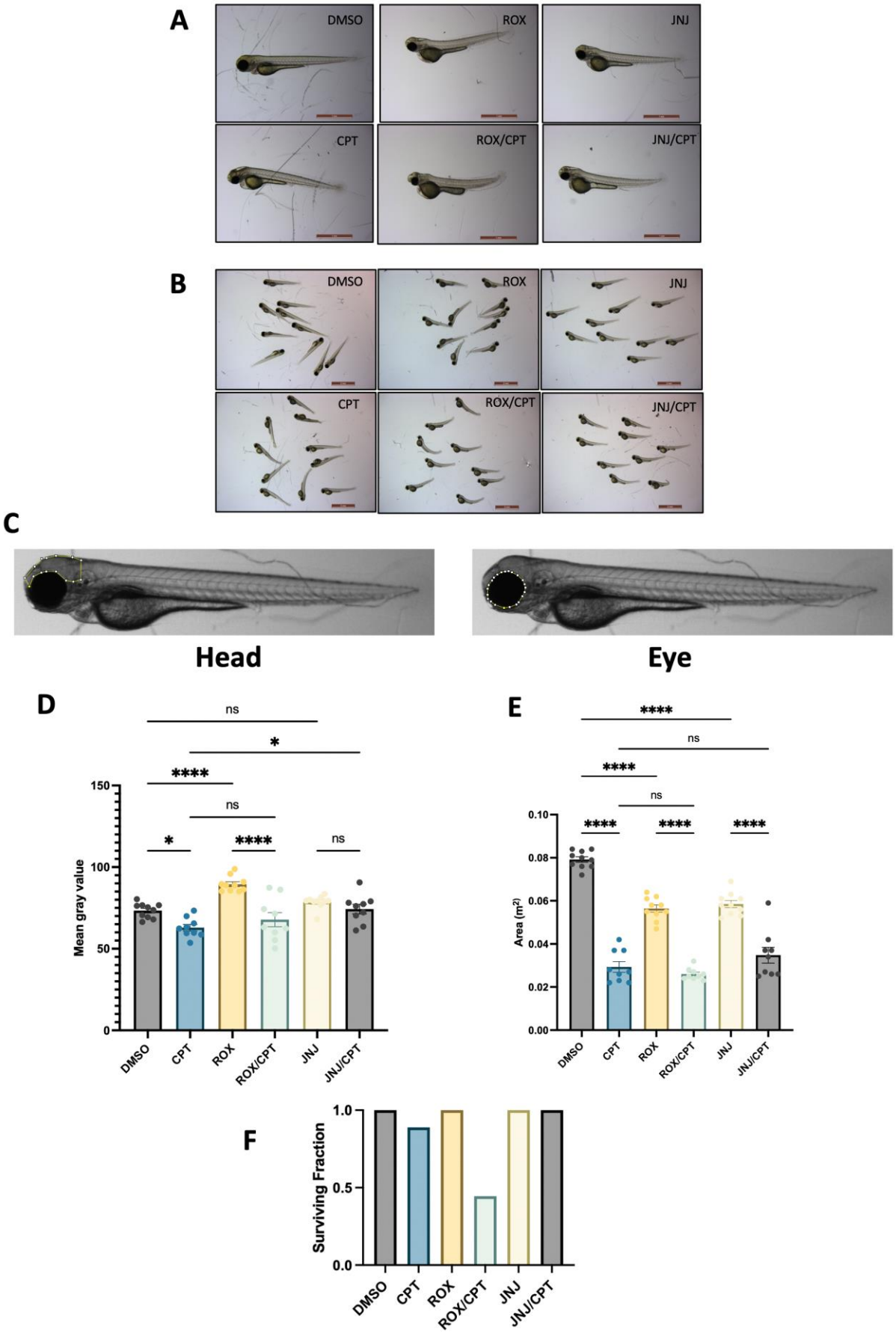
A
DMSO
ROX
JNJ
CPT
ROX/CPT
JNJ/CPT
B
DMSO
ROX
JNJ
CPT
ROX/CPT
JNJ/CPT
C
Head
Eye
D
Mean gray value
150
100
50
0
ns
*
****
ns
*
****
ns
DMSO
CPT
ROX
ROX/CPT
JNJ
JNJ/CPT
E
Area (m²)
0.10
0.08
0.06
0.04
0.02
0.00
****
ns
****
ns
****
****
****
DMSO
CPT
ROX
ROX/CPT
JNJ
JNJ/CPT
F
Surviving Fraction
1.0
0.5
0.0
DMSO
CPT
ROX
ROX/CPT
JNJ
JNJ/CPT

Figure 5.2: Hif activation via JNJ could protect zebrafish from CPT treatment, although Hif activation causes abnormal embryo development. A/B) Representative images of 3 dpf nacre embryos after treatment with Hif activators ROX or JNJ, CPT, or DMSO. Hif activator pre-treatments occurred at 1 dpf dechorionated embryos for 8 hours. CPT/DMSO treatment occurred overnight, alongside fresh Hif activator treatment, then embryos were left to grow in non-drug containing E3 media until 3 dpf. Scale bar is either (A) 1 mm or (B) 2 mm. **C)** Example image showing the region of interest (ROI) measured for each embryo in the head and eye. **D)** Quantification of head ROI in each drug treated embryo. Measurements are expressed as mean grey value, whereby 0=black and 255=white. The lower the value, the more apoptosis present in the ROI. CPT caused apoptosis in the embryo head, causing a reduction in mean grey value. JNJ rescued this phenotype. ROX appeared to increase mean grey value on its own. One-way ANOVA with Šidák correction, ns=p>0.05, *p<0.05, ****p<0.0001, Mean ± SEM, n numbers: DMSO (10), CPT (9), ROX (10), ROX/CPT (9), JNJ (10), JNJ/CPT (9). **(E)** Quantification of eye ROI in each drug-treated embryo. Larger eye size is indicative of healthy embryo. CPT caused a reduction in eye size, as did ROX and JNJ treatment to less of an extent. Combining ROX or JNJ with CPT did not rescue eye size phenotype. One-way ANOVA with Šidák correction, ns=p>0.05, ***p<0.001, ****p<0.0001, Mean ± SEM, n numbers: DMSO (10), CPT (9), ROX (10), ROX/CPT (9), JNJ (10), JNJ/CPT (9). **(F)** Surviving fraction of each population of drug-treated embryos. ROX/CPT treatment caused large number of embryos to not survive.

5.4.2. Pharmacological modulation of Hifα has no measurable impact on chemosensitivity in RCC4

As Hifα pharmacological upregulation in zebrafish embryos was shown to potentially have a protective effect, I wanted to repeat this in RCC4 cells. I used ROX as a HIF activator as ROX had been better characterised in clinical trials than JNJ and I had previously used ROX to upregulate HIFα when designing stable knockdowns of HIFα via CRISPR-Cas9 **(Figure 4.2C)**. In addition, I used the glucocorticoid receptor antagonist Mifepristone (RU486) as a potential HIF inhibitor. Marchi et al., (2020) had previously established a glucocorticoid-Hif interaction in zebrafish, whereby increased glucocorticoid activity stimulated an increase in Hif expression via a positive feedback loop. HIF inhibitors are not widely available and appear to be difficult to produce; therefore, I opted to try using RU486 as an indirect HIF inhibitor, which has also been shown to reduce the expression of HIF target VEGF and upregulate apoptotic pathways, causing increased sensitivity to chemotherapeutic agents in cancer cell lines (Llaguno-Munive et al., 2021). The glucocorticoid-HIF axis remains a complex pathway which has not been fully investigated as of yet, so the molecular mechanisms surrounding RU486-mediated downregulation of HIF should be studied further.

To assess chemosensitivity I did clonogenic analysis, whereby I pre-treated RCC4 VHL WT and RCC4-VHL -/- cells with either 20 μM ROX, or 20 μM RU486, followed by treating with 50 nM CPT or DMSO as a control for 1 hour. **Figure 5.3 A-B** shows ROX and RU486 working as intended to either upregulate or downregulate HIF1α/HIF2α protein expression levels after 4 hours. I did not see a significant difference in colony formation after pre-treating cells with either ROX or RU486, suggesting that pharmacological modulation of HIFα has no measurable impact on chemosensitivity **(Figure 5.3 C-D).**

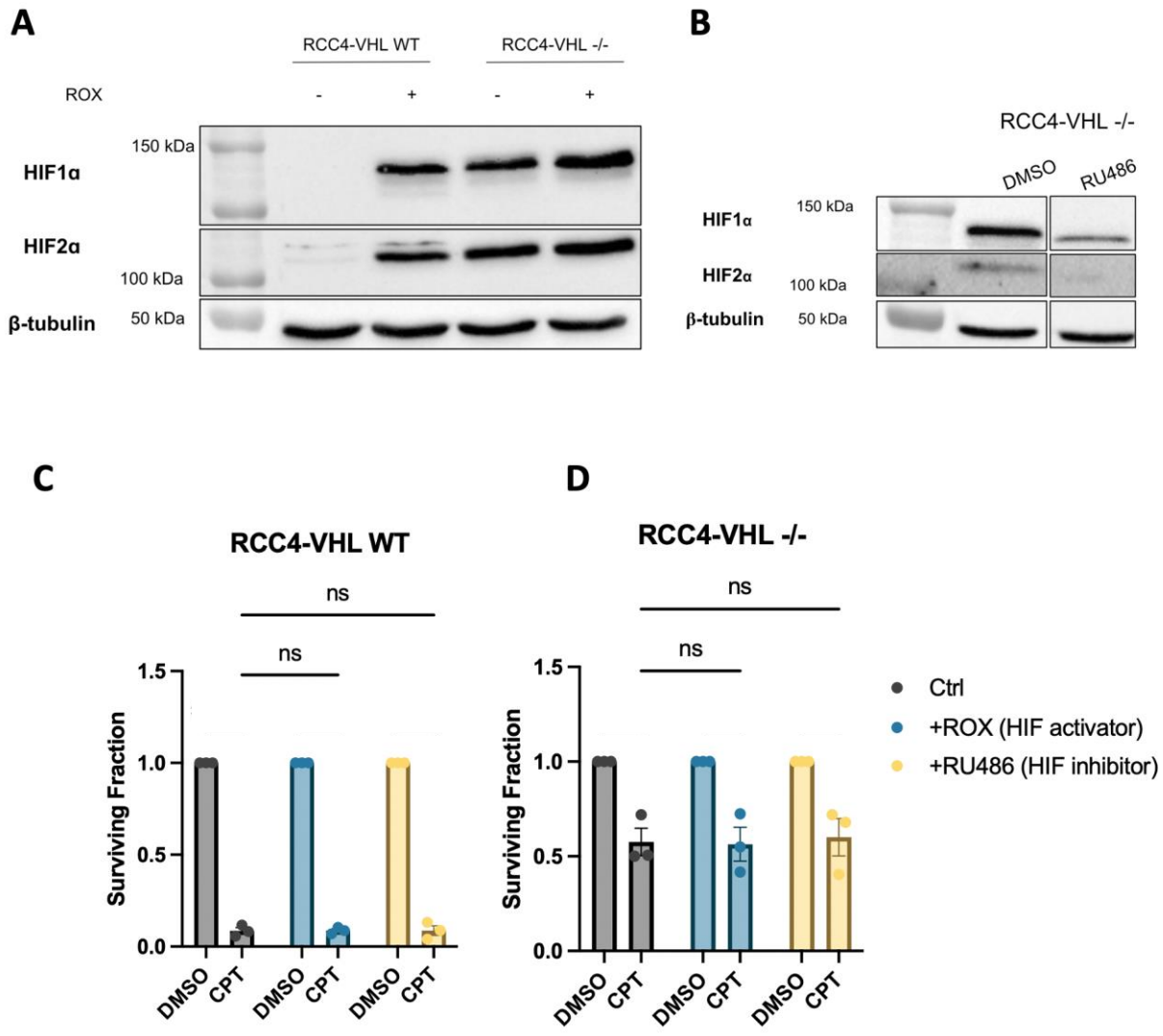

Figure 5.3: Modulating HIFα protein expression levels via chemicals has no measurable impact on chemosensitivity. **A)** Representative western blot showing ROX treatment (20 µM for 4 hours) was sufficient to cause an upregulation of HIF1α/HIF2α protein expression in RCC4-VHL WT and has no impact on RCC4-VHL -/-. β-tubulin was used as a loading control. **B)** Representative western blot showing RU486 treatment (20 µM for 4 hours) was sufficient to cause a downregulation of HIF1α/HIF2α protein expression in RCC4-VHL -/-. β-tubulin was used as a loading control. **C-D)** Clonogenic analysis comparing CPT resistance (50 nM for 1 hour) in **C)** RCC4-VHL WT and **D)** RCC4-VHL -/-. DMSO was used as a control. One-way ANOVA with Šidák correction, ns=p>0.05, Mean ± SEM, n=3.

5.4.3. Tdp1 expression and activity is not upregulated in zebrafish embryos deficient for *vhl* or *vll*

Despite *VHL* inactivation causing an upregulation of HIFα in both RCC4-VHL -/- cells and *vhl* $^{-/-}$ zebrafish embryos, both models behave differently following pharmacological modulation of HIFα. Hifα upregulation in zebrafish is sufficient to protect embryos from CPT-induced genotoxic stress as shown previously **(Figure 5.2)** and by Kim et al., (2020). However, this does not appear to be the case for RCC4 cells **(Figure 5.3)**. There are several fundamental differences between cell lines and zebrafish as a disease model, so it is important to understand the molecular differences between them. TDP1 expression and activity is upregulated in RCC4-VHL -/-, but the Tdp1 status of *vhl* $^{-/-}$ zebrafish embryos was unknown.

I started by looking at *tdp1* mRNA expression in four different genotypes: 1) *vhl* ^{sibs}, 2) *vhl* $^{-/-}$, 3) *vhl* ^{sibs};*vll* $^{-/-}$, and 4) *vhl* $^{-/-}$;vll $^{-/-}$. The embryos were raised by incrossing *vhl* $^{+/-}$, as well as incrossing *vhl* $^{+/-}$;v*ll* $^{-/-}$. The two incrosses were kept separate during GFP sorting, whereby high GFP expression from the *phd3*:GFP reporter correlated with *vhl* mutation as Hifα is no longer inhibited (Santhakumar et al., 2012) **(Figure 5.4A)**. mRNA was harvested from the embryos at 4 dpf, followed by RT-qPCR to analyse *tdp1* mRNA expression. As the role of human VHL is split between zebrafish Vhl and Vll, I expected that *vhl* $^{-/-}$;*vll* $^{-/-}$ embryos would have the highest *tdp1* mRNA expression. However, the opposite effect was seen as *tdp1* mRNA expression was lowest in *vhl* $^{-/-}$;*vll* $^{-/-}$ embryos **(Figure 5.4B)**. To confirm whether lower *tdp1* mRNA expression corresponded to reduced Tdp1 enzymatic activity, I performed a Tdp1 activity assay comparing Tdp1 activity of *vhl* ^{sibs};*vll* $^{-/-}$ and *vhl* $^{-/-}$;*vll* $^{-/-}$ embryos. Similar to RT-qPCR, there was a decrease in Tdp1 activity in *vhl* $^{-/-}$;*vll* $^{-/-}$, although this was not statistically significant **(Figure 5.4 C-D)**.

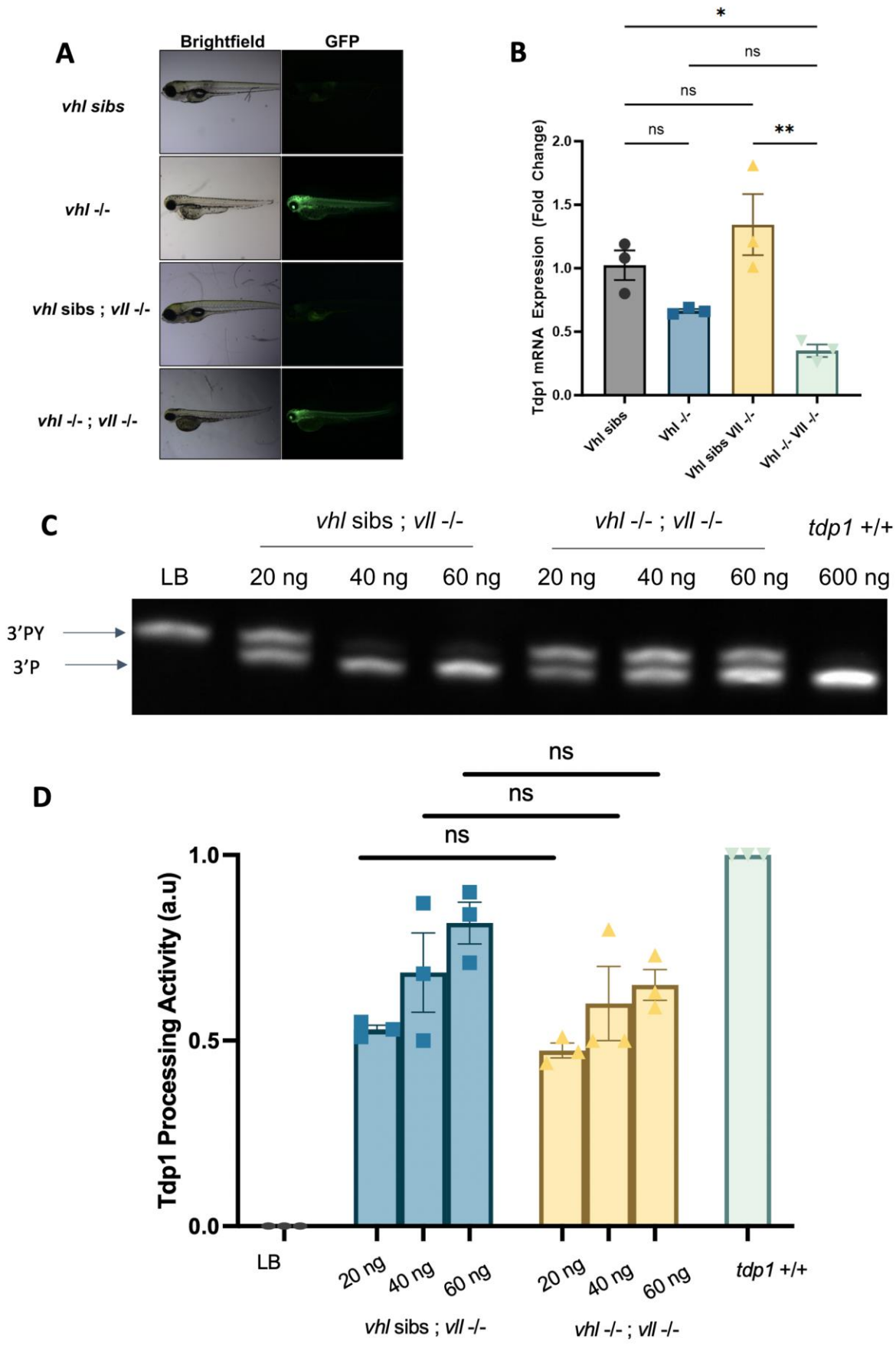
A
Brightfield
GFP
vhl sibs
vhl -/-
vhl sibs ; vll -/-
vhl -/- ; vll -/-
B
*
ns
ns
ns
**
Tdp1 mRNA Expression (Fold Change)
2.0
1.5
1.0
0.5
0.0
Vhl sibs
Vhl -/-
Vhl sibs Vll -/-
Vhl -/- Vll -/-
C
vhl sibs ; vll -/-
vhl -/- ; vll -/-
tdp1 +/+
LB
20 ng
40 ng
60 ng
20 ng
40 ng
60 ng
600 ng
3'PY
3'P
D
ns
ns
ns
Tdp1 Processing Activity (a.u)
1.0
0.5
0.0
LB
20 ng
40 ng
60 ng
20 ng
40 ng
60 ng
tdp1 +/+
vhl sibs ; vll -/-
vhl -/- ; vll -/-

Figure 5.4: Tdp1 expression and activity is downregulated in *vhl*$^{-/-}$ zebrafish. A) Representative images showing increased GFP expression when *vhl* was mutated in embryos, corresponding to increased Hifα expression. **B)** RT-qPCR in 4 dpf embryos showing downregulated *tdp1* expression when *vhl* is knocked out (*vhl* $^{-/-}$). *vll* $^{-/-}$ on its own does not influence *tdp1* expression, but *vhl* $^{-/-}$ *vll* $^{-/-}$ enhances *tdp1* downregulation. *rps29* was used as a housekeeping gene. LB = lysis buffer. *tdp1*$^{+/+}$ = lysate from zebrafish homozygous for WT *tdp1*. One-way ANOVA with Tukey correction, ns=p>0.05, *p<0.05, **p<0.01, Mean ± SEM, n=3. **C)** Urea gel shows no measurable difference in the shift from 3'PY to 3'P bands between the different genotypes at 5 dpf, suggesting no significant difference in Tdp1 activity. **D)** Quantification of Tdp1 activity assay. Two-way ANOVA with Šidák correction, Mean ± SEM, n=3, ns = p>0.05. Tdp1 activity assay and analysis performed by my MSc student Ziyan Ma.

5.5. Discussion

Targeting Hifα in zebrafish embryos via JNJ reduced the apoptotic phenotype induced by CPT treatment, although JNJ also caused the embryos to appear less healthy than DMSO-treated embryos, as indicated by eye size. ROX treated embryos showed a similar defect, whereby eye size was significantly smaller **(Figure 5.2 C-D)**. Combining ROX treatment with CPT caused a large fraction of embryos to die **(Figure 5.2 F)**, suggesting that ROX is not suitable to use in zebrafish embryos due to unknown molecular mechanisms. ROX is a reversible prolyl hydroxylase inhibitor, leading to the stabilisation of HIFs. It achieves this by mimicking the substrate 2-oxoglutarate, which is required for PHD enzyme function. It has been used in patients with anaemia and chronic kidney disease (CKD) as HIF stabilisation stimulates erythropoietin production (Jatho et al., 2022). **Figure 5.2 D-F** suggests that zebrafish embryos do not tolerate ROX very well, matching previous unpublished observations in the van Eeden lab. Yang et al., (2023) discovered that zebrafish embryos exposed to high concentrations of ROX caused abnormal embryonic development via shortened body length and liver defects. Zebrafish hepatotoxicity appeared to be induced by ROX downregulating Notch signalling, as well as upregulating oxidative stress, suggesting that ROX has off-target effects that are HIF-independent. Similar to ROX, JNJ mimics substrate 2-oxoglutarate, inhibiting PHD activity and stabilising HIFs (Barrett et al., 2011). There appears to be limited literature surrounding the use of JNJ in anaemic patients, so its efficacy and safety has not been properly assessed. Further studies are required to determine any off-target effects of JNJ.

A wide range of phenotypic abnormalities are observed in *vhl* $^{-/-}$ embryos aside from upregulation of *hif* target genes, such as increased cardiac output, increased circulation of red blood cells (polycythaemia), pericardial oedema, developmental retardation, and the embryos do not survive beyond 8-10 dpf (Van Rooijen et al., 2009; Kim et al., 2020; Marchi, 2020). Chemical activation of Hif signalling via Phd/Fih inhibitor dimethyloxalylglycine (DMOG) in WT embryos partially recapitulates *vhl* $^{-/-}$ phenotype as previously evidenced by upregulation of *hif* target genes and polycythaemia development (Van Rooijen et al., 2009). However, there were differences in where certain *hif* target genes were expressed when comparing DMOG treatment with *vhl* $^{-/-}$. DMOG treatment increased *vegfa* expression in

proximal renal tubule, which does not occur in *vhl* $^{-/-}$. In addition, *vhl* $^{-/-}$ embryos showed increased expression of *phd3* in the heart and *vegf* in the liver (Van Rooijen et al., 2009). A similar comparison of *hif* target gene expression and localisation has not been performed for ROX-treated and JNJ-treated embryos, which could be important to improve knowledge of the phenotypic differences between chemical Hif upregulation and *vhl* $^{-/-}$. A direct comparison is difficult as the time point at which a hypoxic stimulus is applied differs between chemical Hif upregulation and *vhl* $^{-/-}$, and the level of hypoxia induced by chemical Hif upregulation differs from *vhl* $^{-/-}$ (Van Rooijen et al., 2009). An in-depth analysis of the genetic and phenotypic effects of ROX/JNJ treatment in WT embryos is required to compare how effective these chemicals are at recapitulating the effects observed in *vhl* $^{-/-}$ embryos, as well as identifying drug concentrations that are not toxic to embryos.

Despite ROX and RU486 acting as expected to increase or decrease HIF1α/HIF2α protein expression **(Figure 5.3 A-B)**, I did not see any impact on sensitivity to CPT treatment **(Figure 5.3 C-D)**. Alongside its anti-glucocorticoid receptor activity, RU486 is also a prominent progesterone receptor inhibitor (Chabbert-Buffet et al., 2005). Therefore, there may be crosstalk between glucocorticoid and progesterone signalling nullifying any downstream effects of RU486-mediated HIF modulation. Accurately determining whether chemical downregulation of HIF is sufficient to resensitise RCC4 cells to CPT treatments requires a more specific HIF inhibitor to avoid off-target effects. ROX has not been approved by the FDA due to low efficacy in CKD patients with anaemia, and has also been associated with complicated side effects via unknown molecular mechanisms (Zhu et al., 2022; Gul et al., 2023; Haider et al., 2023). Therefore, whilst trials are still ongoing with ROX, new PHIs have been developed, such as Daprodustat, which has been approved by the FDA as the only available oral treatment for CKD patients managing anaemia (Haider et al., 2023). Due to the uncertainty surrounding ROX, the apparent differences between ROX and JNJ, as well as the emergence of new PHIs, future experiments should focus on characterising the on-target and off-target effects of various PHIs on ccRCC cell lines and zebrafish.

Unlike cell lines, zebrafish have a complex TME, providing a more accurate understanding into how diseases progress (Weiss et al., 2022). Cell lines lack the complexity observed in zebrafish, or indeed any other model organism, therefore, it was not surprising to see

differences in how the two models respond to certain chemical treatments and differences in genetic background. Answering the major challenges involved in treating ccRCC will require combining cell lines and model organism work.

5.6. Summary

Pharmacological modulation of HIFα was only able to reduce CPT-induced genotoxic stress in zebrafish. This was achieved using the JNJ compound, which caused the zebrafish to develop abnormally, although the side effects were less severe than that of ROX. Further research is required to investigate the differences between the various PHIs, as well as differences between zebrafish ccRCC models and cell lines, as Tdp1 expression was not upregulated in *vhl*$^{-/-}$ embryos, unlike RCC4-VHL -/- cells.

Chapter 6 Discussion

6.1. General overview

ccRCC is the most common form of RCC and is characterised by resistance to radiotherapy and chemotherapy (Gacche and Meshram, 2014; Li et al., 2017b; Makhov et al., 2018). Hereditary ccRCC is closely linked to VHL disease, whilst non-hereditary ccRCC often occurs due to inactivation of *VHL*, followed by inactivation of several genes surrounding *VHL* on chromosome 3p (Maher, 1996; Brugarolas, 2014). Hypoxic regions of tissue are common in many cancers, including ccRCC (Bertout et al., 2008). During hypoxia, HIFs accumulate and translocate to the nucleus, whereby they activate the transcription of HIF target genes allowing cells to survive under low oxygen levels, such as inducing a shift from aerobic to anaerobic metabolism and promoting angiogenesis (Semenza, 2007; Majmundar et al., 2010). VHL is an E3 ubiquitin ligase and forms part of a larger VHL/E3 ligase complex, which is responsible for binding to HIFs under normoxia and targeting them for proteasomal degradation, thereby ensuring that they do not accumulate (Haase, 2009). During hypoxia, the VHL complex is unable to bind to HIFs to prevent their accumulation, therefore HIFs only accumulate under hypoxia. However, in patients with *VHL* inactivation, there is a constitutive upregulation of HIFs as the VHL/E3 ligase complex is non-functional. Therefore, the downstream targets of HIFs are transcriptionally upregulated continuously, resulting in tumour formation (Krieg et al., 2000).

There have been several proposed mechanisms of ccRCC chemoresistance and radioresistance, such as modulation of apoptotic pathways (Acharya et al., 2022); however, there remains a gap in knowledge regarding DNA repair pathways implicated in ccRCC resistance to DNA damaging agents. Constitutive upregulation of HIFs has been linked to enhanced DNA repair in zebrafish ccRCC models (Kim et al., 2020), and has been proposed as the key transcription factor involved in mediating downstream targets that protect cells from genotoxic stress. Previous work regarding cellular response in hypoxic cells following genotoxic stress has been mixed, with some papers suggesting that hypoxia downregulates DNA repair genes, whilst other papers have suggested the opposite. There also remains questions regarding the contribution of HIFs to genoprotection, due to the various HIF-

independent factors involved in the hypoxic response, such as the HIF-independent roles of VHL (Metcalf et al., 2014) which remain not fully understood.

The aim of this thesis was to identify DNA repair proteins that had not previously been implicated in hypoxia-mediated genoprotection. I aimed to start by establishing the chemo- and radiosensitivity of a ccRCC cell line, RCC4-VHL -/-, in comparison with a VHL functional cell line, RCC4-VHL WT, to see if high levels of HIFs correlated with enhanced resistance to genotoxic agents. Depending on which agents RCC4-VHL WT were resistant or sensitive to, I would examine the expression of target DNA repair proteins that may be implicated in this response. If I were to find differing expression in DNA repair proteins between my two cell lines, I would then modulate the expression of the corresponding gene and see if there is a change in response to genotoxic stress. In addition, I also planned to modulate the expression of both HIF1α and HIF2α to see what contribution they both play towards any potential differences in DDR and expression of target genes. Lastly, I planned on establishing any key differences between ccRCC zebrafish models and cell lines due to their differing microenvironments and genomes.

6.2. Lessons from DDR in RCC4

In **Chapter 3**, I discussed the differences in DDR between RCC4-VHL -/- and RCC4-VHL WT following exposure to genotoxic stress. I demonstrated that RCC4-VHL -/- has constitutively higher protein expression of both HIF1α and HIF2α, coupled with higher expression of HIF target gene *PHD3* **(Figure 3.1)**. Therefore, I was able to confirm the identity of both RCC4 cell lines. There were two initial hypotheses I aimed to investigate:

1) RCC4-VHL -/- cells will be more resistant to genotoxic stress.
2) RCC4-VHL -/- cells will have increased expression of DNA repair proteins dependent on the type of resistance.

I identified greater resistance to DNA damaging agents CPT and Olaparib in RCC4-VHL -/- cells in clonogenic assays **(Figure 3.2 A-B)** .To confirm the enhanced chemoresistance in RCC4-VHL -/-, I applied a readout of mitochondrial metabolic viability (CellTiter-Blue assay)

as well as a direct readout of DNA breaks (comet assay). Due to time constraints, I decided on only using CPT for these experiments, as I was familiar with the CPT concentrations and incubation times required. I found similar results to clonogenic assays, whereby RCC4-VHL -/- cells were more metabolically viable and showed less accumulation of DNA breaks **(Figure 3.2 C-E)**. Overall, this suggested that RCC4-VHL -/- cells are more resistant to chemotherapeutic agents. ccRCC patients also present with increased resistance to IR; however, there was no statistically significant difference in colony formation following IR treatment in RCC4 cells **(Figure 3.3)**. Bhatt et al., (2008) demonstrated that HIF2α depletion in 786-O cells caused increased sensitivity to IR as measured by trypan blue exclusion. However, Scanlon et al., (2018) utilised a clonogenic assay to show increased IR sensitivity in RCC4-VHL -/-. Future experiments should focus on characterising differences in radiosensitivity and chemosensitivity between different ccRCC lines, such as RCC4 and 786-O, to establish how cell lines obtained from different genetic background respond to genotoxic stress. In addition, future experiments should apply consistent methods of measuring radioresistance and chemoresistance.

Resistance to CPT treatment had been previously associated with increased expression of TDP1 (Liu et al., 2007), which is an enzyme responsible for removing TOP1 from DNA, thus reversing TOP1-CC formation (Kawale and Povirk, 2018). Data from this thesis shows mild upregulation of *BRCA1* mRNA levels in RCC4-VHL -/- cells, as well as strong upregulation of TDP1 mRNA, protein, and enzymatic activity **(Figure 3.4, Figure 3.5, Figure 3.6)**. TDP1 had the clearest difference in expression between RCC4-VHL WT and RCC4-VHL -/-, so I initially focused on the potential protective role of TDP1 in RCC4-VHL -/-. The main molecular difference between RCC4-VHL WT and RCC4-VHL -/- is differing HIFα expression, so I hypothesised that HIFα subunits were responsible for upregulation of TDP1. There had been very limited data previously exploring TDP1 expression in hypoxic cells or in ccRCC models. A ChIP-Seq dataset published by Smythies et al., (2019) suggested that HIF1α/HIF2α interacted with TDP1 promoter regions **(Figure 3.8)**, suggesting that HIF1α/HIF2α could be having a modulatory role on TDP1. Following siRNA-mediated knockdown of HIFα, I observed a transcriptional and translational downregulation of TDP1 following HIF2α knockdown **(Figure 3.9)**, suggesting that TDP1 is a direct or indirect target of HIF2α.

NuMA has recently been characterised as a novel interacting protein of TDP1, pXRCC1, and PARP1 during SSBR (Ray et al., 2022). NuMA is phosphorylated in response to DNA damage, which has been suggested to regulate DNA repair protein enrichment at damaged chromatin (Moreno et al., 2019). Therefore, greater expression of pNuMA could correlate with enhanced recruitment of TDP1 to sites of DNA breaks. Although NuMA expression did not differ between RCC4-VHL WT and RCC4-VHL -/-, there was a significantly higher expression of pNuMA in RCC4-VHL -/- **(Figure 3.12 A/C)**. NuMA phosphorylation had been reported to be ATM-dependent, which I confirmed in RCC4-VHL -/- via ATM inhibition **(Figure 3.12D).** This data could suggest that RCC4-VHL -/- cells have an enhanced ability to repair both SSBs and DSBs via the increased transcription, translation, and recruitment of various DNA repair proteins across multiple pathways.

It remained unclear whether HIF2α was acting directly or indirectly on TDP1. Therefore, I hypothesised that pNuMA was acting as an intermediary between HIF2α and TDP1. However, siRNA-mediated downregulation of HIF2α did not cause a shift in pNuMA expression **(Figure 3.13)**, suggesting that HIF2α and pNuMA are not linked. This suggests that pNuMA is upregulated through HIF-independent mechanisms, one of which may be linked to the little-known HIF-independent roles of VHL.

Upregulation of both pNuMA and TDP1 could suggest that RCC4-VHL -/- accumulate greater DNA breaks; however, comet assays show less DNA break formation **(Figure 3.2 D-E)**. Therefore, RCC4-VHL -/- could have a greater degree of genomic instability, but a more efficient DDR. Thus, RCC4-VHL -/- may be chemoresistant due to constitutive upregulation of DDR components that are efficiently repairing DNA breaks induced by genomic instability and allows RCC4-VHL -/- to quickly repair DNA breaks induced by exogenous genotoxic stress. This could partially explain why ccRCC patients are resistant to chemotherapeutic agents.

6.3. Lessons from genetic modulation of HIFα and TDP1 in RCC4

In **Chapter 4**, I discussed the consequences of modulating HIFα or TDP1 expression in RCC4 cells. HIF2α had been previously identified as the main HIF factor influencing an aggressive

ccRCC phenotype (Kondo et al., 2003). In addition, I had identified that HIF2α was directly or indirectly causing increased expression of TDP1, a key DNA repair protein reversing TOP1-CC formation (Kawale and Povirk, 2018). Therefore, the hypothesis for this chapter was that downregulation of either HIF2α or TDP1 in RCC4-VHL -/- cells would cause increased sensitivity to CPT-induced DNA damage.

siRNA-mediated knockdown of HIF2α did not show any measurable impact following CPT treatment on colony formation propensity, or DNA break formation **(Figure 4.1)**. Although this was a surprising result, I hypothesised that siRNA-mediated knockdown was only causing an acute reduction in HIF2α expression. Several studies have suggested that downstream HIFα pathways behave differently depending on acute or chronic hypoxic exposure (Mihaylova et al., 2003; Bindra et al., 2005; Kang et al., 2008; Cam et al., 2010). Therefore, I hypothesised that a more long-term downregulation of HIF2α would be required to increase sensitivity to CPT. CRISPR-Cas9-mediated long-term downregulation of HIF2α produced a stable cell line RCC4-VHL -/- ; HIF2α -/-. This downregulation of HIF2α did not have a measurable impact on CPT sensitivity **(Figure 4.4)**. TDP1 expression was initially downregulated during an early passage of the stable cell line; however, after several more passages TDP1 expression was no longer downregulated. This could be an indication that culture adaptation (Weissbein et al., 2019) in RCC4-VHL -/- ; HIF2α -/- positively selected for cells with higher TDP1 expression due to a growth advantage. Alternatively, the downregulation of HIF2α may reduce the genomic instability commonly observed in ccRCC cell lines (Scanlon et al., 2018), thereby causing a reduction in background DNA damage and a reduction in TDP1 expression.

TDP1 depletion in either RCC4 cell line did not cause a measurable change in CPT sensitivity **(Figure 4.5)**, despite extensive literature suggesting that TDP1 depletion increases sensitivity to CPT treatment (Huang et al., 2013; Alagoz et al., 2014; Chiang et al., 2017; Ray et al., 2022; Zhang et al., 2022). TDP1-depleted RCC4-VHL WT cells showed a greater reduction in pChk1, which is induced in response to genotoxic stress (Dai and Grant, 2010), compared to TDP1-depleted RCC4-VHL -/- cells. In addition, RCC4-VHL -/- cells had a mild, non-significant increase in baseline levels of pChk1 and γH2AX, which are a common marker for DSBs via the HR pathway (Mah et al., 2010) **(Figure 4.6)**. Immunofluorescence showed greater 53BP1

foci formation in TDP1-depleted RCC4-VHL WT cells only **(Figure 4.8)**. 53BP1 are crucial for instigating NHEJ DSBR (Callen et al., 2013). Altogether, this suggests that DNA breaks induced by CPT in RCC4-VHL WT cells may be repaired by the error-prone NHEJ pathway, whilst DNA breaks induced by CPT in RCC4-VHL -/- cells may be repaired by the more accurate HR pathway. Alternatively, DNA breaks may be repaired by the Alt-EJ pathway, SSBR, or other TDP1-independent DNA repair pathways. I probed for DNA repair factors that had previously been reported as potentially compensating for TDP1 loss in other models (Zeng et al., 2012; Zaksauskaite et al., 2021; Shimizu et al., 2023); however, I did not find a significant upregulation in any candidate genes **(Figure 4.9)**.

6.4. Future work utilising RCC4

Several questions remain unanswered from this thesis, one of which is understanding the precise contributions of VHL, HIF1α, and HIF2α to genoprotection in RCC4. Stable cell lines should be created with every combination of VHL/HIF1α/HIF2α deletions, followed by RNA-sequencing analysis (Li and Li, 2018), to understand which DDR genes are modulated by VHL/HIF1α/HIF2α. Due to time constraints and issues with transfection efficiency, this was not feasible during my project. Establishing which genes are regulated by individual components of the VHL/HIF pathway will allow for more targeted therapy in patients with differing ccRCC molecular phenotypes and will allow for predicting response to chemotherapeutic agents. Deletions in VHL/HIF pathway components can be achieved by CRISPR-Cas9; however, as I have demonstrated this can lead to potential cell culture adaptation and off-target effects. An alternative strategy is to induce rapid protein deletion via auxin-inducible degron technology, which reportedly has less off-target effects due to its specificity compared to CRISPR-Cas9 (Kanemaki, 2013; Yesbolatova et al., 2020).

I have identified that the HR and NHEJ pathway response may differ between RCC4-VHL WT and RCC4-VHL -/- following CPT treatment; therefore, the protein expression of components in these pathways should be analysed to see if there are any differences that could explain why both cell lines have different responses to CPT. If RCC4-VHL WT cells prefer NHEJ, whilst RCC4-VHL -/- prefer HR, I would expect to see a greater mutation rate in RCC4-VHL WT cells following CPT treatment due to error-prone repair resulting from NHEJ. In addition, it would

be interesting to compare DDR component expression and response to chemotherapeutic agents across multiple ccRCC cell lines with different genetic backgrounds, such as 786-O cells which do not express HIF1α, and Caki-1, which does not harbour *VHL* inactivation (Brodaczewska et al., 2016).

Lastly, the contributions of HIF3α in DNA repair and ccRCC tumour progression have not been properly characterised, despite literature suggesting that HIF3α has many splice variants with different roles (Ravenna et al., 2016). The expression pattern of HIF3α is not well established; therefore, HIF3α expression should be analysed in RCC4-VHL -/- cells. If HIF3α is expressed in kidney cells, then it may have a contributing role in modulating DDR components.

6.5. Lessons from comparing zebrafish and cell lines as ccRCC models

In **Chapter 5**, I aimed to characterise the molecular differences in CPT sensitivity following pharmacological modulation of HIFα in both zebrafish and RCC4. Kim et al., (2020) identified that Hif upregulation in zebrafish was sufficient to cause increased resistance to CPT treatment. Data in this thesis confirmed the previous observations; however, I had concerns regarding the safety of the Hif-activators used in the study as shown by defects in zebrafish eye size **(Figure 5.2)**. Therefore, off-target effects of Hif-activation need to be investigated further before confirming that pharmacological Hif activation has a genoprotective effect in zebrafish. Some of the unintended targets of PHD inhibition via ROX/JNJ that need to be considered in future experiments are the known HIF-independent effects of PHD inhibition. Notably, p53 appear to be both a hydroxylation target of PHDs (Deschoemaeker et al., 2015; Rodriguez et al., 2018), as well as a hydroxylase-independent target of PHDs which aids in p53 protein stability (Xu et al., 2019). A wide range of other HIF-independent targets of PHDs has been discussed by Yu et al., (2021b). Therefore, there are clear differences between chemical PHD inhibition and *Vhl* -/- in both human cells and zebrafish embryos.

I did not see an impact on CPT sensitivity in RCC4 cells following pharmacological modulation of HIFα in RCC4 **(Figure 5.3)**, suggesting that this effect is zebrafish specific. *vhl*$^{-/-}$ *; vll*$^{-/-}$ had significant downregulation of *tdp1* expression **(Figure 5.4B)**, which is opposite to

what I had found in RCC4 cells, although Tdp1 activity assay showed only a minor, non-significant impact from *vhl* on Tdp1 enzymatic activity **(Figure 5.4 C-D)**. These results emphasise the importance of using a combination of human cell lines and whole organisms when modelling disease progression and response to chemotherapeutics. The TME in zebrafish may be contributing to the DDR, negating the need for elevated Tdp1 expression to repair DNA breaks.

6.6. Future work utilising zebrafish

Further experiments should continue characterising differences in DDR in VHL-deficient cell lines and Vhl-deficient zebrafish. Both models show increased resistance to chemotherapeutic agents; however, only zebrafish embryos were able to demonstrate increased resistance via external Hif modulators. Zebrafish have become an important resource to study DDR due to the TME presence and the ability to track response to genotoxic stress throughout their life course. In addition, there is a high degree of DDR gene homology between zebrafish and human genomes (Cayuela et al., 2019). Future work should focus on analysing the expression of DNA repair genes that could be implicated in Hif-mediated genoprotection that I have discovered, such as *tp53bp1 (53BP1* orthologue*), bard1* (*BRCA1*-associated *BARD1* orthologue), and *numa* (Howe et al., 2013; Yang et al., 2019; Thomas, 2022), as well as other HR/NHEJ components and Tdp1-independent mechanisms of Top1-CC removal.

An interesting future experiment would be to use the zebrafish xenograft model (Chen et al., 2021a) to increase understanding of the zebrafish TME contribution to DDR. Chemotherapeutic agents often require a high dose to observe a functional response in cancer patients, which can lead to harmful side effects targeting healthy tissue. However, pre-treatment with HIF activator, such as ROX or JNJ, could potentially protect healthy tissue from genotoxic stress while eliminating cells. This can be modelled in zebrafish by injecting cancer cells, followed by CPT treatment, with or without Hif activator pre-treatment. If Hif activation is shown to produce a protective effect following CPT treatment, ccRCC patients, and indeed patients with other chemoresistant cancers, could be treated with higher doses of chemotherapeutic agents.

6.7. Summary

I have characterised potentially novel mechanisms of enhanced DNA repair in *VHL*-mutant ccRCC cell line RCC4-VHL-/- through the upregulation of TDP1, pNuMA, and *BRCA1* mRNA expression. pNuMA promotes the translation and recruitment of DNA repair components, such as TDP1, to sites of SSBs. Therefore, upregulation of TDP1 and pNuMA suggests the presence of an enhanced SSBR pathway. Following exogenous genotoxic stress, such as CPT treatment, RCC4-VHL -/- appear to prefer the more accurate HR DSBR pathway, whilst RCC4-VHL WT prefer the error-prone NHEJ DSBR pathway. To confirm these findings, further work will need to be performed to identify the accuracy of DNA repair following CPT treatment in RCC4-VHL WT and RCC4-VHL -/-. If NHEJ pathway predominates in RCC4-VHL WT, then repaired DNA is likely to contain more mutations compared to HR-repaired cells in RCC4-VHL -/-. I have also shown that siRNA-mediated downregulation of HIF2α reduces the transcription and translation of TDP1, indicating that TDP1 is a direct or indirect target of HIF2α. This suggests that HIF2α is at least partially responsible for enhancing chemoresistance in CPT-treated RCC4-VHL -/- cells. However, siRNA or CRISPR-Cas9-mediated downregulation of HIF2α or TDP1 was not sufficient to increase sensitivity to CPT treatment, suggesting that multiple proteins are involved in promoting chemoresistance in RCC4-VHL -/-, such as HIF-independent mechanisms of VHL. Lastly, I demonstrated that Hif-activation in zebrafish embryos was sufficient to increase resistance to CPT treatment; however, *vhl*-deficient zebrafish embryos do not show enhanced Tdp1 expression or activity, suggesting that CPT resistance in zebrafish embryos could be Tdp1-independent.

In summary, I have shown that analysing HIF-mediated genoprotection in ccRCC patients is highly complex and requires the utilisation of multiple models to achieve an accurate representation of DNA repair mechanisms influenced by HIF. Further work should continue utilising RCC4 as a representative model of ccRCC patients, as well as zebrafish due to the presence of the TME. A summary of the results found in this thesis as well as potential models describing my data is found in **Figure 6.1.**

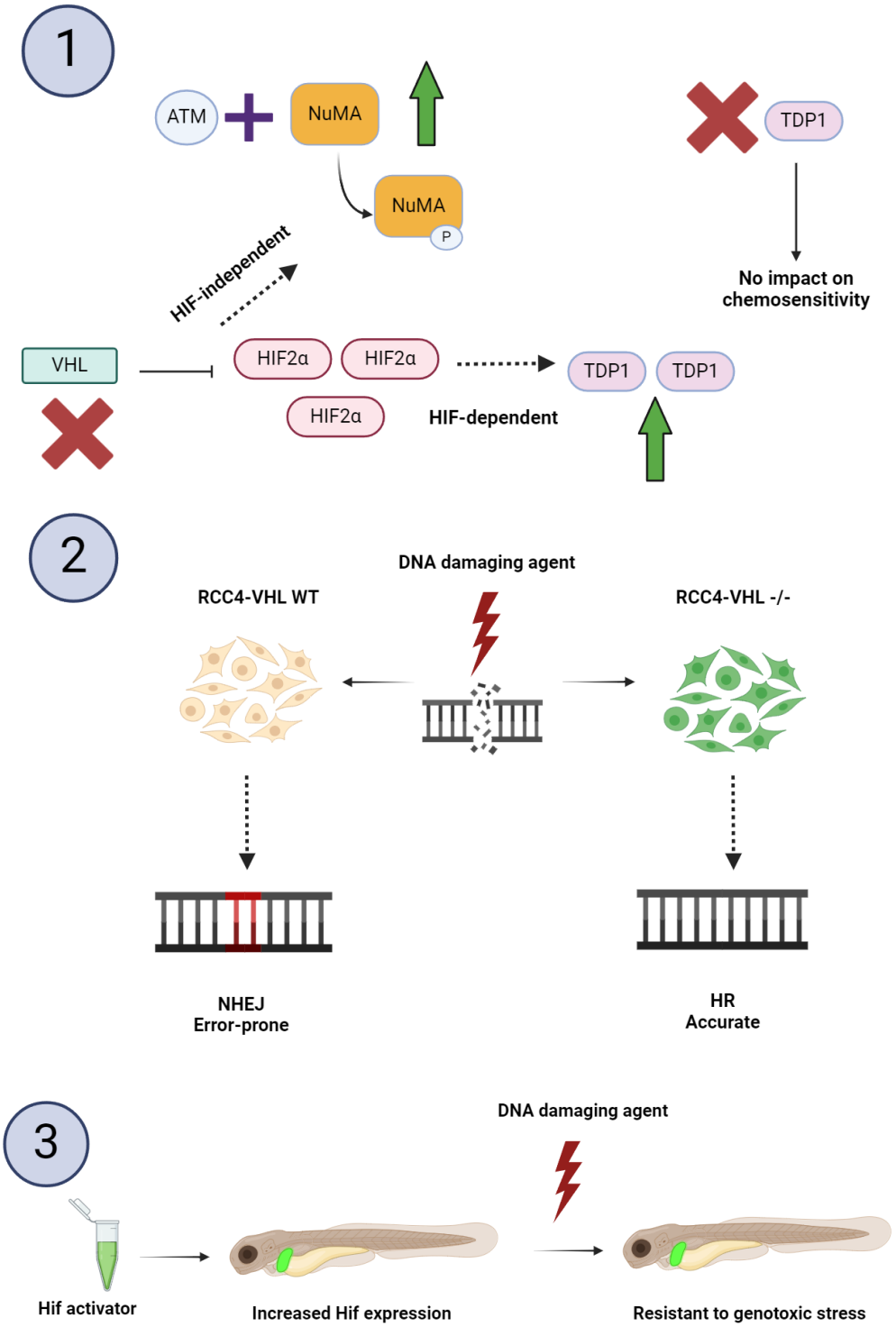

Figure 6.1: Lessons learned from this thesis and potential models. 1) *VHL* inactivation causes upregulation of TDP1 and phosphorylated NuMA (pNuMA), which are recruited to sites of DNA damage. TDP1 recruitment is HIF-dependent, whilst pNuMA expression is HIF-independent and ATM-dependent. TDP1 -/- has no impact on chemosensitivity in RCC4. **2)** DNA double-strand breaks following exogenous DNA damage appears to be preferentially repaired via error-prone non-homologous end-joining (NHEJ) in RCC4-VHL WT, and the more accurate homologous recombination (HR) in RCC4-VHL -/-. **3)** Increasing HIF expression via chemical Hif activators can protect zebrafish from genotoxic stress induced by DNA damaging agents.

References

Abbots R, Wilson III DM (2017) Coordination of DNA Single Strand Break Repair. Free Radic Biol Med 107:228–224 Available at: doi:10.1016/j.freeradbiomed.2016.11.039.

AbdulSalam SF, Thowfeik FS, Merino EJ (2016) Excessive reactive oxygen species and exotic DNA lesions as an exploitable liability. Biochemistry 55:5341–5352.

Acharya N, Singh KP, Kamaleshwar Singh CP (2022) Recent advances in the molecular basis of chemotherapy resistance and potential application of epigenetic therapeutics in chemorefractory renal cell carcinoma. WIREs Mech Dis 14:e1575 Available at: https://onlinelibrary.wiley.com/doi/full/10.1002/wsbm.1575 [Accessed August 24, 2023].

Ackerson SM, Romney C, Schuck PL, Stewart JA (2021) To Join or Not to Join: Decision Points Along the Pathway to Double-Strand Break Repair vs. Chromosome End Protection. Front Cell Dev Biol 9:1–19.

Aguilar-Quesada R, Muñoz-Gámez JA, Martín-Oliva D, Peralta A, Valenzuela MT, Matínez-Romero R, Quiles-Pérez R, Menissier-de Murcia J, de Murcia G, Ruiz de Almodóvar M, Javier FJ (2007) Interaction between ATM and PARP-1 in response to DNA damage and sensitization of ATM deficient cells through PARP inhibition. BMC Mol Biol 8:1–8.

Alagoz M, Wells OS, El-Khamisy SF (2014) TDP1 deficiency sensitizes human cells to base damage via distinct topoisomerase I and PARP mechanisms with potential applications for cancer therapy. Nucleic Acids Res 42:3089–3103.

Andersen S, Heine T, Sneve R, König I, Krokan HE, Epe B, Nilsen H (2005) Incorporation of dUMP into DNA is a major source of spontaneous DNA damage, while excision of uracil is not required for cytotoxicity of fluoropyrimidines in mouse embryonic fibroblasts. Carcinogenesis 26:547–555.

Andrés Juan C, Manuel Pérez de la Lastra J, Plou FJ, Pérez-Lebeña E, Reinbothe S (2021) Molecular Sciences The Chemistry of Reactive Oxygen Species (ROS) Revisited: Outlining Their Role in Biological Macromolecules (DNA, Lipids and Proteins) and Induced Pathologies. Int J Mol Sci 22:4642.

Appelhoffl RJ, Tian YM, Raval RR, Turley H, Harris AL, Pugh CW, Ratcliffe PJ, Gleadle JM (2004) Differential function of the prolyl hydroxylases PHD1, PHD2, and PHD3 in the regulation of hypoxia-inducible factor. J Biol Chem 279:38458–38465 Available at:

http://dx.doi.org/10.1074/jbc.M406026200.

Aquila L, Atanassov BS (2020) Regulation of Histone Ubiquitination in Response to DNA Double Strand Breaks. Cells 9.

Arany Z, Huang LE, Eckner R, Bhattacharya S, Jiang C, Goldberg MA, Bunn HF, Livingston DM (1996) An essential role for p300/CBP in the cellular response to hypoxia. Proc Natl Acad Sci U S A 93:12969–12973.

Arnaiz E, Miar A, Bridges E, Prasad N, Hatch SB, Ebner D, Lawrie CH, Harris AL (2021) Differential effects of HIF2α antagonist and HIF2α silencing in renal cancer and sensitivity to repurposed drugs. BMC Cancer 21:1–12 Available at: https://bmccancer.biomedcentral.com/articles/10.1186/s12885-021-08616-8 [Accessed March 14, 2022].

Augstein A, Poitz DM, Braun-Dullaeus RC, Strasser RH, Schmeisser A (2011) Cell-specific and hypoxia-dependent regulation of human HIF-3α: Inhibition of the expression of HIF target genes in vascular cells. Cell Mol Life Sci 68:2627–2642.

Bandarra D, Biddlestone J, Mudie S, Müller HAJ, Rocha S (2015) HIF-1α restricts NF-κB-dependent gene expression to control innate immunity signals. DMM Dis Model Mech 8:169–181.

Barrett TD et al. (2011) Pharmacological characterization of 1-(5-chloro-6-(trifluoromethoxy)-1H-benzoimidazol-2-yl)-1H-pyrazole-4-carboxylic acid (JNJ-42041935), a potent and selective hypoxia-inducible factor prolyl hydroxylase inhibitor. Mol Pharmacol 79:910–920 Available at: https://pubmed.ncbi.nlm.nih.gov/21372172/ [Accessed August 29, 2023].

Barthelmes HU, Habermeyer M, Christensen MO, Mielke C, Interthal H, Pouliot JJ, Boege F, Marko D (2004) TDP1 overexpression in human cells counteracts DNA damage mediated by topoisomerases I and II. J Biol Chem 279:55618–55625 Available at: http://dx.doi.org/10.1074/jbc.M405042200.

Bartoszewski R, Moszyńska A, Serocki M, Cabaj A, Polten A, Ochocka R, Dell'Italia L, Bartoszewska S, Króliczewski J, Dąbrowski M, Collawn JF (2019) Primary endothelial-specific regulation of hypoxiainducible factor (HIF)-1 and HIF-2 and their target gene expression profiles during hypoxia. FASEB J 33:7929–7941.

Bartucci M, Svensson S, Romania P, Dattilo R, Patrizii M, Signore M, Navarra S, Lotti F, Biffoni M, Pilozzi E, Duranti E, Martinelli S, Rinaldo C, Zeuner A, Maugeri-Saccà M, Eramo A, De

Maria R (2012) Therapeutic targeting of Chk1 in NSCLC stem cells during chemotherapy. Cell Death Differ 19:768–778.

Bassing CH, Alt FW (2004) H2AX may function as an anchor to hold broken chromosomal DNA ends in close proximity. Cell Cycle 3:147–148.

Ben-David U et al. (2018) Genetic and transcriptional evolution alters cancer cell line drug response. Nat 2018 5607718 560:325–330 Available at: https://www.nature.com/articles/s41586-018-0409-3 [Accessed August 30, 2023].

Ben-David U, Beroukhim R, Golub TR (2019) Genomic evolution of cancer models: perils and opportunities. Nat Rev Cancer 19:97–109 Available at: http://dx.doi.org/10.1038/s41568-018-0095-3.

Ben-David U, Ha G, Tseng YY, Greenwald NF, Oh C, Shih J, McFarland JM, Wong B, Boehm JS, Beroukhim R, Golub TR (2017) Patient-derived xenografts undergo mouse-specific tumor evolution. Nat Genet 2017 4911 49:1567–1575 Available at: https://www.nature.com/articles/ng.3967 [Accessed August 30, 2023].

Bencokova Z, Kaufmann MR, Pires IM, Lecane PS, Giaccia AJ, Hammond EM (2009) ATM Activation and Signaling under Hypoxic Conditions. Mol Cell Biol 29:526–537.

Bensalah K, Khene ZE, Massard C (2022) Belzutifan for Renal Cell Carcinoma in von Hippel–Lindau Disease. Eur Urol 81:545–546.

Bersten DC, Sullivan AE, Peet DJ, Whitelaw ML (2013) bHLH–PAS proteins in cancer. Nat Rev Cancer 2013 1312 13:827–841 Available at: https://www.nature.com/articles/nrc3621 [Accessed July 19, 2023].

Bertout JA, Majmundar AJ, Gordan JD, Lam JC, Ditsworth D, Keith B, Brown EJ, Nathanson KL, Simon MC (2009) HIF2α inhibition promotes p53 pathway activity, tumor cell death, and radiation responses. Proc Natl Acad Sci U S A 106:14391–14396 Available at: https://www.pnas.org/doi/abs/10.1073/pnas.0907357106 [Accessed August 3, 2023].

Bertout JA, Patel SA, Simon MC (2008) The impact of O2 availability on human cancer. Nat Rev Cancer 8:967 Available at: /pmc/articles/PMC3140692/ [Accessed July 17, 2023].

Bhatt RS, Landis DM, Zimmer M, Torregrossa J, Chen S, Sukhatme VP, Iliopoulos O, Balk S, Bubley GJ (2008) Hypoxia-inducible factor-2α: effect on radiation sensitivity and differential regulation by an mTOR inhibitor. BJU Int 102:358 Available at: /pmc/articles/PMC4112353/ [Accessed July 10, 2023].

Bhutta BS, Alghoula F, Berim I (2022) Hypoxia. StatPearls Available at:

https://www.ncbi.nlm.nih.gov/books/NBK482316/ [Accessed January 11, 2024].

Bian L, Meng Y, Zhang M, Li D (2019) MRE11-RAD50-NBS1 complex alterations and DNA damage response: Implications for cancer treatment. Mol Cancer.

Biddlestone J, Bandarra D, Rocha S (2015) The role of hypoxia in inflammatory disease (Review). Int J Mol Med 35:859–869 Available at: http://www.spandidos-publications.com/10.3892/ijmm.2015.2079/abstract [Accessed July 17, 2023].

Bindra RS, Gibson SL, Meng A, Westermark U, Jasin M, Pierce AJ, Bristow RG, Classon MK, Glazer PM (2005) Hypoxia-induced down-regulation of BRCA1 expression by E2Fs. Cancer Res.

Bindra RS, Glazer PM (2005) Genetic instability and the tumor microenvironment: Towards the concept of microenvironment-induced mutagenesis. Mutat Res - Fundam Mol Mech Mutagen 569:75–85 Available at: http://www.ncbi.nlm.nih.gov/pubmed/15603753 [Accessed April 28, 2020].

Boehler C, Gauthier LR, Mortusewicz O, Biard DS, Saliou JM, Bresson A, Sanglier-Cianferani S, Smith S, Schreiber V, Boussin F, Dantzer F (2011) Poly(ADP-ribose) polymerase 3 (PARP3), a newcomer in cellular response to DNA damage and mitotic progression. Proc Natl Acad Sci U S A 108:2783–2788 Available at: /pmc/articles/PMC3041075/ [Accessed September 4, 2023].

Boiteux S, Guillet M (2004) Abasic sites in DNA: Repair and biological consequences in Saccharomyces cerevisiae. DNA Repair (Amst) 3:1–12.

Borrego-Soto G, Ortiz-López R, Rojas-Martínez A (2015) Ionizing radiation-induced DNA injury and damage detection in patientswith breast cancer. Genet Mol Biol 38:420 Available at: /pmc/articles/PMC4763322/ [Accessed June 29, 2023].

Brem R, Hall J (2005) XRCC1 is required for DNA single-strand break repair in human cells. Nucleic Acids Res 33:2512–2520.

Brettel K, Byrdin M (2010) Reaction mechanisms of DNA photolyase. Curr Opin Struct Biol 20:693–701 Available at: http://dx.doi.org/10.1016/j.sbi.2010.07.003.

Brodaczewska KK, Szczylik C, Fiedorowicz M, Porta C, Czarnecka AM (2016) Choosing the right cell line for renal cell cancer research. Mol Cancer 15 Available at: /pmc/articles/PMC5168717/?report=abstract [Accessed July 20, 2020].

Brown E, Taylor CT (2018) Hypoxia-sensitive pathways in intestinal inflammation. J Physiol 596:2985–2989.

Brugarolas J (2014) Molecular genetics of clear-cell renal cell carcinoma. J Clin Oncol 32:1968–1976.

Bullen JW, Tchernyshyov I, Holewinski RJ, Devine L, Wu F, Venkatraman V, Kass DL, Cole RN, Van Eyk J, Semenza GL (2016) Protein kinase A-dependent phosphorylation stimulates the transcriptional activity of hypoxia-inducible factor. Sci Signal 9 Available at: https://www.science.org/doi/10.1126/scisignal.aaf0583 [Accessed July 25, 2023].

Burdall SE, Hanby AM, Lansdown MRJ, Speirs V (2003) Breast cancer cell lines: friend or foe? Breast Cancer Res 5:89 Available at: /pmc/articles/PMC154155/ [Accessed August 30, 2023].

Calabrese V, Mallette FA, Deschênes-Simard X, Ramanathan S, Gagnon J, Moores A, Ilangumaran S, Ferbeyre G (2009) SOCS1 Links Cytokine Signaling to p53 and Senescence. Mol Cell 36:754–767.

Callen E et al. (2013) 53BP1 mediates productive and mutagenic DNA repair through distinct phosphoprotein interactions. Cell 153:1266–1280.

Cam H, Easton JB, High A, Houghton PJ (2010) mTORC1 signaling under hypoxic conditions is controlled by atm-dependent phosphorylation of HIF-1α. Mol Cell 40:509–520 Available at: http://dx.doi.org/10.1016/j.molcel.2010.10.030.

Capitanio U, Bensalah K, Bex A, Boorjian SA, Bray F, Coleman J, Gore JL, Sun M, Wood C, Russo P (2019) Epidemiology of Renal Cell Carcinoma. Eur Urol 75:74–84.

Cappellini MD, Musallam KM, Taher AT (2009) Overview of Iron Chelation Therapy with Desferrioxamine and Deferiprone. https://doi.org/103109/03630260903346924 33 Available at: https://www.tandfonline.com/doi/abs/10.3109/03630260903346924 [Accessed September 1, 2023].

Carmeliet P, Dor Y, Herbert J-M, Fukumura D, Brusselmans K, Dewerchin M, Neeman M, Bono F, Abramovitch R, Maxwell P, Koch CJ, Ratcliffe P, Moons L, Jain RK, Collen D, Keshert E (1998) Role of HIF-1α in hypoxia- mediated apoptosis, cell proliferationand tumourangiogenesis. 394:485–490.

Carver LA, Hogenesch JB, Bradfield CA (1994) Tissue specific expression of the rat Ah-receptor and ARNT mRNAs. Nucleic Acids Res 22:3038–3044.

Cayuela ML, Claes KBM, Ferreira MG, Henriques CM, van Eeden F, Varga M, Vierstraete J, Mione MC (2019) The Zebrafish as an Emerging Model to Study DNA Damage in Aging, Cancer and Other Diseases. Front Cell Dev Biol.

Celeste A et al. (2002) Genomic instability in mice lacking histone H2AX. Science (80-) 296:922–927 Available at: https://www.science.org/doi/10.1126/science.1069398 [Accessed August 21, 2023].

Chabbert-Buffet N, Meduri G, Bouchard P, Spitz IM (2005) Selective progesterone receptor modulators and progesterone antagonists: Mechanisms of action and clinical applications. Hum Reprod Update 11:293–307.

Champoux JJ (2001) DNA Topoisomerases: Structure, Function, and Mechanism. Annu Rev Biochem 70:369–413.

Chan GL, Doetsch PW, Haseltine WA (1985) Cyclobutane Pyrimidine Dimers and (6-4) Photoproducts Block Polymerization by DNA Polymerase I†. Biochemistry 24:5723–5728.

Chan N, Ali M, McCallum GP, Kumareswaran R, Koritzinsky M, Wouters BG, Wells PG, Gallinger S, Bristow RG (2014) Hypoxia provokes base excision repair changes and a repair-deficient, mutator phenotype in colorectal cancer cells. Mol Cancer Res 12:1407–1415.

Chan N, Koritzinsky M, Zhao H, Bindra R, Glazer PM, Powell S, Belmaaza A, Wouters B, Bristow RG (2008) Chronic hypoxia decreases synthesis of homologous recombination proteins to offset chemoresistance and radioresistance. Cancer Res 68:605–614.

Chand MK, Carle V, Anuvind KG, Saikrishnan K (2020) DNA-mediated coupling of ATPase, translocase and nuclease activities of a Type ISP restriction-modification enzyme. Nucleic Acids Res 48:2594–2603.

Chang HHY, Pannunzio NR, Adachi N, Lieber MR (2017) Non-homologous DNA end joining and alternative pathways to double-strand break repair. Nat Rev Mol Cell Biol 18:495–506 Available at: http://dx.doi.org/10.1038/nrm.2017.48.

Chang P, Coughlin M, Mitchison TJ (2005) Tankyrase-1 polymerization of poly(ADP-ribose) is required for spindle structure and function. Nat Cell Biol 2005 711 7:1133–1139 Available at: https://www.nature.com/articles/ncb1322 [Accessed September 4, 2023].

Chatterjee N, Walker GC (2017) Mechanisms of DNA damage, repair, and mutagenesis. Environ Mol Mutagen.

Chen F et al. (1995) Germline mutations in the von Hippel–Lindau disease tumor suppressor gene: Correlations with phenotype. Hum Mutat.

Chen X, Li Y, Yao T, Jia R (2021a) Benefits of Zebrafish Xenograft Models in Cancer Research.

Front Cell Dev Biol 9:1–14.

Chen Y, Liang Y, Chen Y, Ouyang S, Liu K, Yin W (2021b) Identification of Prognostic Metabolism-Related Genes in Clear Cell Renal Cell Carcinoma. J Oncol 2021.

Chiang SC, Meagher M, Kassouf N, Hafezparast M, McKinnon PJ, Haywood R, El-Khamisy SF (2017) Mitochondrial protein-linked DNA breaks perturb mitochondrial gene transcription and trigger free radical–induced DNA damage. Sci Adv 3.

Chiche J, Rouleau M, Gounon P, Brahimi-Horn MC, Pouysségur J, Mazure NM (2010) Hypoxic enlarged mitochondria protect cancer cells from apoptotic stimuli. J Cell Physiol 222:648–657.

Chittezhath M, Dhillon MK, Lim JY, Laoui D, Shalova IN, Teo YL, Chen J, Kamaraj R, Raman L, Lum J, Thamboo TP, Chiong E, Zolezzi F, Yang H, VanGinderachter JA, Poidinger M, Wong ASC, Biswas SK (2014) Molecular Profiling Reveals a Tumor-Promoting Phenotype of Monocytes and Macrophages in Human Cancer Progression. Immunity 41:815–829 Available at: http://dx.doi.org/10.1016/j.immuni.2014.09.014.

Chiu YH, Hsu SH, Hsu HW, Huang KC, Liu W, Wu CY, Huang WP, Chen JYF, Chen BH, Chiu CC (2018) Human non-small cell lung cancer cells can be sensitized to camptothecin by modulating autophagy. Int J Oncol 53:1967–1979.

Chong ZX, Yeap SK, Ho WY (2021) Transfection types, methods and strategies: A technical review. PeerJ 9:1–37.

Chowdhuri SP, Das BB (2021) Top1-PARP1 association and beyond: from DNA topology to break repair. NAR Cancer 3 Available at: /pmc/articles/PMC8095074/ [Accessed June 30, 2023].

Chválová K, Brabec V, Kašpárková J (2007) Mechanism of the formation of DNA-protein cross-links by antitumor cisplatin. Nucleic Acids Res 35:1812–1821.

Cimmino F, Avitabile M, Lasorsa VA, Montella A, Pezone L, Cantalupo S, Visconte F, Corrias MV, Iolascon A, Capasso M (2019) HIF-1 transcription activity: HIF1A driven response in normoxia and in hypoxia. BMC Med Genet 20:1–15 Available at: https://bmcmedgenet.biomedcentral.com/articles/10.1186/s12881-019-0767-1 [Accessed July 11, 2023].

Comandone A, Vana F, Comandone T, Tucci M (2021) Antiangiogenic Therapy in Clear Cell Renal Carcinoma (CCRC): Pharmacological Basis and Clinical Results. Cancers 2021, Vol 13, Page 5896 13:5896 Available at: https://www.mdpi.com/2072-

6694/13/23/5896/htm [Accessed August 16, 2023].

Courtney KD, Infante JR, Lam ET, Figlin RA, Rini BI, Brugarolas J, Zojwalla NJ, Lowe AM, Wang K, Wallace EM, Josey JA, Choueiri TK (2018) Phase I dose-escalation trial of PT2385, a first-in-class hypoxia-inducible factor-2a antagonist in patients with previously treated advanced clear cell renal cell carcinoma. J Clin Oncol 36:867–874.

Cowman SJ, Koh MY (2022) Revisiting the HIF switch in the tumor and its immune microenvironment. Trends in Cancer 8:28–42.

Cummins EP, Taylor CT (2005) Hypoxia-responsive transcription factors. Pflugers Arch Eur J Physiol 450:363–371 Available at: https://link.springer.com/article/10.1007/s00424-005-1413-7 [Accessed July 17, 2023].

Cunningham F et al. (2022) Ensembl 2022. Nucleic Acids Res 50:D988–D995 Available at: https://dx.doi.org/10.1093/nar/gkab1049 [Accessed August 25, 2023].

D'Amours D, Jackson SP (2002) The Mre11 complex: At the crossroads of DNA repair and checkpoint signalling. Nat Rev Mol Cell Biol 3:317–327.

D'Ignazio L, Bandarra D, Rocha S (2016) NF-κB and HIF crosstalk in immune responses. FEBS J 283:413–424.

Dai Y, Grant S (2010) New insights into checkpoint kinase 1 in the DNA damage response signaling network. Clin Cancer Res 16:376–383 Available at: https://dx.doi.org/10.1158/1078-0432.CCR-09-1029 [Accessed August 21, 2023].

Das BB, Dexheimer TS, Maddali K, Pommier Y (2010) Role of tyrosyl-DNA phosphodiesterase (TDP1) in mitochondria. Proc Natl Acad Sci U S A 107:19790–19795 Available at: https://www.pnas.org/doi/abs/10.1073/pnas.1009814107 [Accessed September 4, 2023].

Davies DR, Interthal H, Champoux JJ, Hol WGJ (2002) The crystal structure of human tyrosyl-DNA phosphodiesterase, Tdp1. Structure 10:237–248.

de Heer EC, Jalving M, Harris AL (2020) HIFs, angiogenesis, and metabolism: elusive enemies in breast cancer. J Clin Invest 130:5074 Available at: /pmc/articles/PMC7524491/ [Accessed August 3, 2023].

De Meerleer G, Khoo V, Escudier B, Joniau S, Bossi A, Ost P, Briganti A, Fonteyne V, Van Vulpen M, Lumen N, Spahn M, Mareel M (2014) Radiotherapy for renal-cell carcinoma. Lancet Oncol 15:e170–e177 Available at: http://www.thelancet.com/article/S1470204513705692/fulltext [Accessed September

18, 2023].

Deschoemaeker S, Di Conza G, Lilla S, Martín-Pérez R, Mennerich D, Boon L, Hendrikx S, Maddocks OD, Marx C, Radhakrishnan P, Prenen H, Schneider M, Myllyharju J, Kietzmann T, Vousden KH, Zanivan S, Mazzone M (2015) PHD 1 regulates p53-mediated colorectal cancer chemoresistance . EMBO Mol Med 7:1350–1365.

Desouky O, Ding N, Zhou G (2015) Targeted and non-targeted effects of ionizing radiation. J Radiat Res Appl Sci 8:247–254.

Dexheimer T, Antony S, Marchand C, Pommier Y (2012) Tyrosyl-DNA Phosphodiesterase as a Target for Anticancer Therapy. Anticancer Agents Med Chem 8:381–389.

Diesing K, Ribback S, Winter S, Gellert M, Oster AM, Stühler V, Gläser E, Adler F, Hartwig C, Scharpf M, Bedke J, Burchardt M, Schwab M, Lillig CH, Kroeger N (2021) p53 is functionally inhibited in clear cell renal cell carcinoma (ccRCC): a mechanistic and correlative investigation into genetic and molecular characteristics. J Cancer Res Clin Oncol 147:3565–3576 Available at: https://doi.org/10.1007/s00432-021-03786-1.

Dizdaroglu M, Kirkali G, Jaruga P (2008) Formamidopyrimidines in DNA: Mechanisms of formation, repair, and biological effects. Free Radic Biol Med 45:1610–1621 Available at: http://dx.doi.org/10.1016/j.freeradbiomed.2008.07.004.

Doan H, Parsons A, Devkumar S, Selvarajah J, Miralles F, Carroll VA (2019) HIF-mediated Suppression of DEPTOR Confers Resistance to mTOR Kinase Inhibition in Renal Cancer. iScience 21:509 Available at: /pmc/articles/PMC6849413/ [Accessed January 6, 2022].

Douiev L, Miller C, Ruppo S, Benyamini H, Abu-Libdeh B, Saada A (2021) Upregulation of COX4-2 via HIF-1α in Mitochondrial COX4-1 Deficiency. Cells 2021, Vol 10, Page 452 10:452 Available at: https://www.mdpi.com/2073-4409/10/2/452/htm [Accessed July 20, 2023].

Drutel G, Kathmann M, Heron A, Schwartz JC, Arrang JM (1996) Cloning and selective expression in brain and kidney of ARNT2 homologous to the Ah receptor nuclear translocator (ARNT). Biochem Biophys Res Commun 225:333–339.

Du Q, Macara IG (2004) Mammalian Pins is a conformational switch that links NuMA to heterotrimeric G proteins. Cell 119:503–516.

Dudás J, Schartinger VH, Romani A, Schweigl G, Kordsmeyer K, Marta PI, Url C, Kral F, Riechelmann H (2014) Cell cycle association and hypoxia regulation of excision repair cross complementation group 1 protein (ERCC1) in tumor cells of head and neck

cancer. Tumor Biol 35:7807–7819.

Eckardt KU, Bernhardt WM, Weidemann A, Warnecke C, Rosenberger C, Wiesener MS, Willam C (2005) Role of hypoxia in the pathogenesis of renal disease. Kidney Int 68:46–51.

El-Brolosy MA, Kontarakis Z, Rossi A, Kuenne C, Günther S, Fukuda N, Kikhi K, Boezio GLM, Takacs CM, Lai SL, Fukuda R, Gerri C, Giraldez AJ, Stainier DYR (2019) Genetic compensation triggered by mutant mRNA degradation. Nature.

El-Khamisy SF (2023) Oxidative DNA damage and repair at non-coding regulatory regions. Trends Cell Biol 0 Available at: http://www.cell.com/article/S0962892423000454/fulltext [Accessed July 10, 2023].

El-Khamisy SF, Caldecott KW (2006) TDP1-dependent DNA single-strand break repair and neurodegeneration. Mutagenesis 21:219–224 Available at: https://academic.oup.com/mutage/article/21/4/219/1269822 [Accessed May 12, 2021].

El-Khamisy SF, Saifi GM, Weinfeld M, Johansson F, Helleday T, Lupski JR, Caldecott KW (2005) Defective DNA single-strand break repair in spinocerebellar ataxia with axonal neuropathy-1. Nature 434:108–113 Available at: www.nature.com/nature. [Accessed May 4, 2021].

Emami Nejad A, Najafgholian S, Rostami A, Sistani A, Shojaeifar S, Esparvarinha M, Nedaeinia R, Haghjooy Javanmard S, Taherian M, Ahmadlou M, Salehi R, Sadeghi B, Manian M (2021) The role of hypoxia in the tumor microenvironment and development of cancer stem cell: a novel approach to developing treatment. Cancer Cell Int 21:1–26 Available at: https://doi.org/10.1186/s12935-020-01719-5.

Erdel F, Schubert T, Marth C, Längst G, Rippe K (2010) Human ISWI chromatin-remodeling complexes sample nucleosomes via transient binding reactions and become immobilized at active sites. Proc Natl Acad Sci U S A 107:19873–19878.

Ericsson JLE, Seljelid R, Orrenius S (1966) Comparative light and electron microscopic observations of the cytoplasmic matrix in renal carcinomas. Virchows Arch Pathol Anat Physiol Klin Med 341:204–223 Available at: https://link.springer.com/article/10.1007/BF00961071 [Accessed August 5, 2023].

Escudier B, Porta C, Schmidinger M, Rioux-Leclercq N, Bex A, Khoo V, Grünwald V, Gillessen S, Horwich A (2019) Renal cell carcinoma: ESMO Clinical Practice Guidelines for

diagnosis, treatment and follow-up. Ann Oncol 30:706–720.

Fallah J et al. (2022) FDA Approval Summary: Belzutifan for von Hippel-Lindau Disease–Associated Tumors. Clin Cancer Res 28:4843–4848 Available at: https://dx.doi.org/10.1158/1078-0432.CCR-22-1054 [Accessed August 17, 2023].

Fallone F, Britton S, Nieto L, Salles B, Muller C (2013) ATR controls cellular adaptation to hypoxia through positive regulation of hypoxia-inducible factor 1 (HIF-1) expression. Oncogene 32:4387–4396.

Falnes P, Klungland A, Alseth I (2007) Repair of methyl lesions in DNA and RNA by oxidative demethylation. Neuroscience 145:1222–1232 Available at: http://dx.doi.org/10.1016/j.neuroscience.2006.11.018.

Feldman DR, Kondagunta GV, Schwartz L, Patil S, Ishill N, DeLuca J, Russo P, Motzer RJ (2008) Phase II trial of pegylated interferon-α2b in patients with advanced renal cell carcinoma. Clin Genitourin Cancer 6:25–30.

Fisher R, Pusztai L, Swanton C (2013) Cancer heterogeneity: implications for targeted therapeutics. Br J Cancer 2013 1083 108:479–485 Available at: https://www.nature.com/articles/bjc2012581 [Accessed August 16, 2023].

Fizazi K, Rolland F, Chevreau C, Droz JP, Mery-Mignard D, Culine S, Escudier B (2003) A phase II study of irinotecan in patients with advanced renal cell carcinoma. Cancer 98:61–65.

Flanigan RC, Mickisch G, Sylvester R, Tangen C, Van Poppel H, Crawford ED (2004) Cytoreductive Nephrectomy in Patients With Metastatic Renal Cancer: A Combined Analysis. J Urol 171:1071–1076.

Forman HJ, Maiorino M, Ursini F (2010) Signaling functions of reactive oxygen species. Biochemistry 49:835–842.

Forslund JME, Pfeiffer A, Stojkovič G, Wanrooij PH, Wanrooij S (2018) The presence of rNTPs decreases the speed of mitochondrial DNA replication. PLOS Genet 14:e1007315 Available at: https://journals.plos.org/plosgenetics/article?id=10.1371/journal.pgen.1007315 [Accessed September 6, 2023].

Fousteri M, Mullenders LHF (2008) Transcription-coupled nucleotide excision repair in mammalian cells: Molecular mechanisms and biological effects. Cell Res 18:73–84.

Frankenberg-Schwager M, Frankenberg D, Harbich R (1991) Different oxygen enhancement ratios for induced and unrejoined DNA double- strand breaks in eukaryotic cells. Radiat

Res 128:243–250.

Frattini A, Fabbri M, Valli R, De Paoli E, Montalbano G, Gribaldo L, Pasquali F, Maserati E (2015) High variability of genomic instability and gene expression profiling in different HeLa clones. Sci Rep 5:1–9 Available at: http://dx.doi.org/10.1038/srep15377.

Fukuda R, Zhang H, Kim J whan, Shimoda L, Dang C V., Semenza GLL (2007) HIF-1 Regulates Cytochrome Oxidase Subunits to Optimize Efficiency of Respiration in Hypoxic Cells. Cell 129:111–122 Available at: http://www.cell.com/article/S0092867407003078/fulltext [Accessed July 20, 2023].

Furman D et al. (2020) Chronic inflammation in the etiology of disease across the life span. Nat Med 25:1822–1832.

Gaber T, Dziurla R, Tripmacher R, Burmester GR, Buttgereit F (2005) Hypoxia inducible factor (HIF) in rheumatology: Low O2! See what HIF can do! Ann Rheum Dis 64:971–980.

Gacche RN, Meshram RJ (2014) Angiogenic factors as potential drug target: Efficacy and limitations of anti-angiogenic therapy. Biochim Biophys Acta - Rev Cancer 1846:161–179.

Gao W, Li W, Xiao T, Liu XS, Kaelin WG (2017) Inactivation of the PBRM1 tumor suppressor gene amplifies the HIF-response in VHL-/- clear cell renal carcinoma. Proc Natl Acad Sci U S A 114:1027–1032.

Gavini K, Parameshwaran K (2023) Western Blot. StatPearls Publishing. Available at: https://www.ncbi.nlm.nih.gov/books/NBK542290/.

Gibson BA, Kraus WL (2012) New insights into the molecular and cellular functions of poly(ADP-ribose) and PARPs. Nat Rev Mol Cell Biol 13:411–424.

Gibson SL, Bindra RS, Glazer PM (2005) Hypoxia-induced phosphorylation of Chk2 in an ataxia telangiectasia mutated-dependent manner. Cancer Res 65:10734–10741.

Gibson SL, Bindra RS, Glazer PM (2006) CHK2-Dependent Phosphorylation of BRCA1 in Hypoxia. https://doi.org/101667/RR06601 166:646–651 Available at: https://bioone.org/journals/radiation-research/volume-166/issue-4/RR0660.1/CHK2-Dependent-Phosphorylation-of-BRCA1-in-Hypoxia/10.1667/RR0660.1.full [Accessed September 10, 2023].

Giglia-Mari G, Zotter A, Vermeulen W (2011) DNA damage response. Cold Spring Harb Perspect Biol 3:1–19.

Goldberg MA, Dunning SP, Bunn HF (1988) Regulation of the erythropoietin gene: Evidence

that the oxygen sensor is a heme protein. Science (80-) 242:1412–1418.

Gore ME, Larkin JMG (2011) Challenges and opportunities for converting renal cell carcinoma into a chronic disease with targeted therapies. Br J Cancer 104:399–406 Available at: https://pubmed.ncbi.nlm.nih.gov/21285971/ [Accessed June 26, 2023].

Gottlin EB, Rudolph AE, Zhao Y, Matthews HR, Dixon JE (1998) Catalytic mechanism of the phospholipase D superfamily proceeds via a covalent phosphohistidine intermediate. Proc Natl Acad Sci U S A 95:9202–9207.

Goulooze SC, Cohen AF, Rissmann R (2016) Olaparib. Br J Clin Pharmacol 81:171 Available at: /pmc/articles/PMC4693566/ [Accessed June 29, 2023].

Goyal R, Gersbach E, Yang XJ, Rohan SM (2013) Differential diagnosis of renal tumors with clear cytoplasm: clinical relevance of renal tumor subclassification in the era of targeted therapies and personalized medicine. Arch Pathol Lab Med 137:467–480 Available at: https://pubmed.ncbi.nlm.nih.gov/23544936/ [Accessed July 6, 2023].

Greijer AE, Van Der Wall E (2004) The role of hypoxia inducible factor 1 (HIF-1) in hypoxia induced apoptosis. J Clin Pathol 57:1009–1014.

Gresch O, Altrogge L (2012) Transfection of difficult-to-transfect primary mammalian cells. Methods Mol Biol 801:65–74 Available at: https://link.springer.com/protocol/10.1007/978-1-61779-352-3_5 [Accessed September 1, 2023].

Gu X, Enane F, Tohme R, Schuerger C, Radivoyevitch T, Parker Y, Zuberi E, Przychodzen B, Jha BK, Lindner D, Rini B, Saunthararajah Y (2021) PBRM1 loss in kidney cancer unbalances the proximal tubule master transcription factor hub to repress proximal tubule differentiation. Cell Rep 36:109747.

Gul K, Zaman N, Azam SS (2023) Roxadustat and its failure: A comparative dynamic study. J Mol Graph Model 120:108422.

Guo Q, Lan F, Yan X, Xiao Z, Wu Y, Zhang Q (2018) Hypoxia exposure induced cisplatin resistance partially via activating p53 and hypoxia inducible factor-1α in non-small cell lung cancer A549 cells. Oncol Lett 16:801 Available at: /pmc/articles/PMC6019907/ [Accessed April 11, 2023].

Gupta GP, Massagué J (2006) Cancer Metastasis: Building a Framework. Cell 127:679–695 Available at: http://www.cell.com/article/S0092867406014140/fulltext [Accessed September 1, 2023].

Gurova K V., Hill JE, Razorenova O V., Chumakov PM, Gudkov A V. (2004) p53 Pathway in Renal Cell Carcinoma Is Repressed by a Dominant Mechanism. Cancer Res 64:1951–1958 Available at: https://aacrjournals.org/cancerres/article/64/6/1951/512366/p53-Pathway-in-Renal-Cell-Carcinoma-Is-Repressed [Accessed August 3, 2022].

Guschin DY, Waite AJ, Katibah GE, Miller JC, Holmes MC, Rebar EJ (2010) A rapid and general assay for monitoring endogenous gene modification. Methods Mol Biol 649:247–256 Available at: https://pubmed.ncbi.nlm.nih.gov/20680839/ [Accessed June 21, 2022].

Haase V (2009) The VHL Tumor Suppressor: Master Regulator of HIF. Curr Pharm Des 15:3895–3903.

Haider MU, Furqan M, Mehmood Q (2023) Daprodustat: A potential game-changer in renal anemia therapy - A perspective. Front Pharmacol 14:1–2.

Han J, Li J, Ho JC, Chia GS, Kato H, Jha S, Yang H, Poellinger L, Lee KL (2017) Hypoxia is a Key Driver of Alternative Splicing in Human Breast Cancer Cells. Sci Rep 7:1–17.

Harrison LB, Chadha M, Hill RJ, Hu K, Shasha D (2002) Impact of tumor hypoxia and anemia on radiation therapy outcomes. Oncologist 7:492–508 Available at: https://pubmed.ncbi.nlm.nih.gov/12490737/ [Accessed July 10, 2023].

Harten SK, Esteban MA, Shukla D, Ashcroft M, Maxwell PH (2011) Inactivation of the von Hippel-Lindau tumour suppressor gene induces Neuromedin U expression in renal cancer cells. Mol Cancer 10:89.

Hashimoto T, Shibasaki F (2015) Hypoxia-Inducible Factor as an Angiogenic Master Switch. Front Pediatr 3:143021.

Hegde ML, Izumi T, Mitra S (2012) Oxidized base damage and single-strand break repair in mammalian genomes: Role of disordered regions and posttranslational modifications in early enzymes. Prog Mol Biol Transl Sci 110:123–153.

Heiden MGV, Cantley LC, Thompson CB (2009) Understanding the Warburg Effect: The Metabolic Requirements of Cell Proliferation. Science (80-) 324:1029–1033 Available at: https://www.science.org/doi/10.1126/science.1160809 [Accessed July 20, 2023].

Heikkilä M, Pasanen A, Kivirikko KI, Myllyharju J (2011) Roles of the human hypoxia-inducible factor (HIF)-3α variants in the hypoxia response. Cell Mol Life Sci 68:3885–3901.

Henle ES, Linn S (1997) Formation, prevention, and repair of DNA damage by iron/hydrogen peroxide. J Biol Chem 272:19095–19098.

Hes FJ, Höppener JW, Luijt RB van der, Lips CJ (2005) Von Hippel-Lindau Disease. Hered Cancer Clin Pract 3:171 Available at: /pmc/articles/PMC2837060/ [Accessed August 30, 2023].

Hes FJ, van der Luijt RB, Janssen ALW, Zewald RA, De Jong GJ, Lenders JW, Links TP, Luyten GPM, Sijmons RH, Eussen HJ, Halley DJJ, Lips CJM, Pearson PL, van den Ouweland AMW, Majoor-Krakauer DF (2007) Frequency of Von Hippel-Lindau germline mutations in classic and non-classic Von Hippel-Lindau disease identified by DNA sequencing, Southern blot analysis and multiplex ligation-dependent probe amplification. Clin Genet 72:122–129.

Hirota K (2021) HIF-α Prolyl Hydroxylase Inhibitors and Their Implications for Biomedicine: A Comprehensive Review. Biomed 2021, Vol 9, Page 468 9:468 Available at: https://www.mdpi.com/2227-9059/9/5/468/htm [Accessed September 1, 2023].

Hoefflin R et al. (2020) HIF-1α and HIF-2α differently regulate tumour development and inflammation of clear cell renal cell carcinoma in mice. Nat Commun 2020 111 11:1–21 Available at: https://www.nature.com/articles/s41467-020-17873-3 [Accessed November 29, 2021].

Hoeijmakers JHJ (2009) DNA Damage, Aging, and Cancer. :1475–1485.

Holness MJ, Sugden MC (2003) Regulation of pyruvate dehydrogenase complex activity by reversible phosphorylation. Biochem Soc Trans 31:1143–1151 Available at: /biochemsoctrans/article/31/6/1143/64556/Regulation-of-pyruvate-dehydrogenase-complex [Accessed July 20, 2023].

Holt IJ (2009) Mitochondrial DNA replication and repair: all a flap. Trends Biochem Sci 34:358–365.

Hompland T, Fjeldbo CS, Lyng H (2018) Tumor Hypoxia as a Barrier in Cancer Therapy: Why Levels Matter. :1–22 Available at: https://doi.org/10.3390/cancers13030499.

Howe K et al. (2013) The zebrafish reference genome sequence and its relationship to the human genome. Nature.

Hsieh JJ, Purdue MP, Signoretti S, Swanton C, Albiges L, Schmidinger M, Heng DY, Larkin J, Ficarra V (2017) Renal cell carcinoma. Nat Rev Dis Prim 2017 31 3:1–19 Available at: https://www.nature.com/articles/nrdp20179 [Accessed August 14, 2023].

Hu C-J, Wang L-Y, Chodosh LA, Keith B, Simon MC (2003) Differential Roles of Hypoxia-Inducible Factor 1α (HIF-1α) and HIF-2α in Hypoxic Gene Regulation. Mol Cell Biol

23:9361 Available at: /pmc/articles/PMC309606/ [Accessed July 14, 2023].

Huang SYN, Murai J, Dalla Rosa I, Dexheimer TS, Naumova A, Gmeiner WH, Pommier Y (2013) TDP1 repairs nuclear and mitochondrial DNA damage induced by chain-terminating anticancer and antiviral nucleoside analogs. Nucleic Acids Res 41:7793–7803.

Iliopoulos O, Kibel A, Gray S, Kaelin, Jr. WG (1995) Tumour suppression by the human von Hippel-Lindau gene product. Nature 1:1–6.

Iliopoulos O, Levy AP, Jiang C, Kaelin WG, Goldberg MA (1996) Negative regulation of hypoxia-inducible genes by the von Hippel-Lindau protein. Proc Natl Acad Sci U S A.

Imeri F, Nolan KA, Bapst AM, Santambrogio S, Abreu-Rodríguez I, Spielmann P, Pfundstein S, Libertini S, Crowther L, Orlando IMC, Dahl SL, Keodara A, Kuo W, Kurtcuoglu V, Scholz CC, Qi W, Hummler E, Hoogewijs D, Wenger RH (2019) Generation of renal Epo-producing cell lines by conditional gene tagging reveals rapid HIF-2 driven Epo kinetics, cell autonomous feedback regulation, and a telocyte phenotype. Kidney Int 95:375–387.

Imseng S, Aylett CH, Maier T (2018) Architecture and activation of phosphatidylinositol 3-kinase related kinases. Curr Opin Struct Biol 49:177–189 Available at: https://doi.org/10.1016/j.sbi.2018.03.010.

Ince W, Eisen T (2022) Combination therapies in clinical trials for renal cell carcinoma: how could they impact future treatments? https://doi.org/101080/1354378420212014814 30:1221–1229 Available at: https://www.tandfonline.com/doi/abs/10.1080/13543784.2021.2014814 [Accessed September 16, 2023].

Ito A, Koshikawa N, Mochizuki S, Omura K, Takenaga K (2006) Hypoxia-inducible factor-1 mediates the expression of DNA polymerase ι in human tumor cells. Biochem Biophys Res Commun 351:306–311.

Iyer N V., Kotch LE, Agani F, Leung SW, Laughner E, Wenger RH, Gassmann M, Gearhart JD, Lawler AM, Yu AY, Semenza GL (1998) Cellular and developmental control of O2 homeostasis by hypoxia-inducible factor 1α. Genes Dev 12:149–162 Available at: http://genesdev.cshlp.org/content/12/2/149.full [Accessed July 18, 2023].

Jaakkola P, Mole DR, Tian YM, Wilson MI, Gielbert J, Gaskell SJ, Von Kriegsheim A, Hebestreit HF, Mukherji M, Schofield CJ, Maxwell PH, Pugh CW, Ratcliffe PJ (2001) Targeting of

HIF-α to the von Hippel-Lindau ubiquitylation complex by O 2 -regulated prolyl hydroxylation. Science (80-).

Jacobs JP, Jones CM, Baille JP (1970) Characteristics of a human diploid cell designated MRC-5. Nature 227:168–170.

Jakobsen AK, Lauridsen KL, Samuel EB, Proszek J, Knudsen BR, Hager H, Stougaard M (2015) Correlation between topoisomerase I and tyrosyl-DNA phosphodiesterase 1 activities in non-small cell lung cancer tissue. Exp Mol Pathol 99:56–64.

Jatho A, Zieseniss A, Brechtel-Curth K, Guo J, Böker KO, Salinas G, Wenger RH, Katschinski DM (2022) The HIFα-Stabilizing Drug Roxadustat Increases the Number of Renal Epo-Producing Sca-1+ Cells. Cells 11 Available at: /pmc/articles/PMC8869801/ [Accessed August 29, 2023].

Jeggo PA, Pearl LH, Carr AM (2016) DNA repair, genome stability and cancer: A historical perspective. Nat Rev Cancer 16:35–42.

Jiang Y, Li W, Yan Y, Yao X, Gu W, Zhang H (2020) LINC01094 triggers radio-resistance in clear cell renal cell carcinoma via miR-577/CHEK2/FOXM1 axis. Cancer Cell Int 20:1–10 Available at: https://cancerci.biomedcentral.com/articles/10.1186/s12935-020-01306-8 [Accessed July 10, 2023].

Jiang Y, Zhang W, Kondo K, Clco JM, St. Martin TB, Dufault MR, Madden SL, Kaelin JWG, Nacht M (2003) Gene Expression Profiling in a Renal Cell Carcinoma Cell Line: Dissecting VHL and Hypoxia-Dependent Pathways | Molecular Cancer Research | American Association for Cancer Research. Mol Cancer Res 1:453–462 Available at: https://aacrjournals.org/mcr/article/1/6/453/232288/Gene-Expression-Profiling-in-a-Renal-Cell [Accessed September 1, 2023].

Kais Z, Rondinelli B, Holmes A, O'Leary C, Kozono D, D'Andrea AD, Ceccaldi R (2016) FANCD2 maintains fork stability in BRCA1/2-deficient tumors and promotes alternative end-joining DNA repair. Cell Rep 15:2488 Available at: /pmc/articles/PMC4939765/ [Accessed July 14, 2023].

Kanemaki MT (2013) Frontiers of protein expression control with conditional degrons. Pflugers Arch Eur J Physiol 465:419–425.

Kang MJ, Jung SM, Kim MJ, Bae JH, Kim HB, Kim JY, Park SJ, Song HS, Kim DW, Kang CD, Kim SH (2008) DNA-dependent protein kinase is involved in heat shock protein-mediated accumulation of hypoxia-inducible factor-1α in hypoxic preconditioned HepG2 cells.

FEBS J 275:5969–5981.

Kawale AS, Povirk LF (2018) Tyrosyl-DNA phosphodiesterases: Rescuing the genome from the risks of relaxation. Nucleic Acids Res 46:520–537.

Keith B, Johnson RS, Simon MC (2012) HIF1α and HIF2α: sibling rivalry in hypoxic tumor growth and progression. Nat Rev Cancer 12:9 Available at: /pmc/articles/PMC3401912/ [Accessed August 1, 2022].

Khomenko TM, Zakharenko AL, Chepanova AA, Ilina ES, Zakharova OD, Kaledin VI, Nikolin VP, Popova NA, Korchagina D V., Reynisson J, Chand R, Ayine-tora DM, Patel J, Leung IKH, Volcho KP, Salakhutdinov NF, Lavrik OI (2020) Promising new inhibitors of tyrosyl-DNA phosphodiesterase I (Tdp 1) combining 4- arylcoumarin and monoterpenoid moieties as components of complex antitumor therapy. Int J Mol Sci 21.

Kim HR, Santhakumar K, Markham E, Baldera D, Greenald D, Bryant HE, El-Khamisy SF, van Eeden FJ (2020) Investigation of the role of VHL-HIF signaling in DNA repair and apoptosis in zebrafish. Oncotarget 11:1109–1130.

Kim JY, Ahn HJ, Ryu JH, Suk K, Park JH (2004) BH3-only Protein Noxa Is a Mediator of Hypoxic Cell Death Induced by Hypoxia-inducible Factor 1α. J Exp Med 199:113–123.

Kimmel CB, Ballard WW, Kimmel SR, Ullmann B, Schilling TF (1995) Stages of embryonic development of the zebrafish. Dev Dyn.

Kinner A, Wu W, Staudt C, Iliakis G (2008) Gamma-H2AX in recognition and signaling of DNA double-strand breaks in the context of chromatin. Nucleic Acids Res 36:5678–5694.

Kirste S, Rühle A, Zschiedrich S, Schultze-Seemann W, Jilg CA, Neumann-Haefelin E, Lo SS, Grosu AL, Kim E (2022) Stereotactic Body Radiotherapy for Renal Cell Carcinoma in Patients with Von Hippel–Lindau Disease—Results of a Prospective Trial. Cancers (Basel) 14.

Kiyomitsu T, Boerner S (2021) The Nuclear Mitotic Apparatus (NuMA) Protein: A Key Player for Nuclear Formation, Spindle Assembly, and Spindle Positioning. Front Cell Dev Biol 9:1–12.

Klose RJ, Bird AP (2006) Genomic DNA methylation: the mark and its mediators. Trends Biochem Sci 31:89–97 Available at: https://pubmed.ncbi.nlm.nih.gov/16403636/ [Accessed July 11, 2023].

Knudson AG (1971) Mutation and Cancer: Statistical Study of Retinoblastoma. Proc Natl Acad Sci 68:820–823 Available at:

https://www.pnas.org/doi/abs/10.1073/pnas.68.4.820 [Accessed August 5, 2023].

Koehler AN (2010) A complex task? Direct modulation of transcription factors with small molecules. Curr Opin Chem Biol 14:331–340.

Kondo K, Kim WY, Lechpammer M, Kaelin WG (2003) Inhibition of HIF2α Is Sufficient to Suppress pVHL-Defective Tumor Growth. PLOS Biol 1:e83 Available at: https://journals.plos.org/plosbiology/article?id=10.1371/journal.pbio.0000083 [Accessed August 17, 2023].

Kornepati AVR, Vadlamudi RK, Curiel TJ (2022) Programmed death ligand 1 signals in cancer cells. Nat Rev Cancer 2022 223 22:174–189 Available at: https://www.nature.com/articles/s41568-021-00431-4 [Accessed August 16, 2023].

Krieg M, Haas R, Brauch H, Acker T, Flamme I, Plate KH (2000) Up-regulation of hypoxia-inducible factors HIF-1α and HIF-2α under normoxic conditions in renal carcinoma cells by von Hippel-Lindau tumor suppressor gene loss of function. Oncogene 2000 1948 19:5435–5443 Available at: https://www.nature.com/articles/1203938 [Accessed January 12, 2022].

Krokan HE, Bjoras M (2013) Chapter 06: Base Excision Repair. Cold Spring Harb Perspect Biol 5:a012583 Available at: http://www.ncbi.nlm.nih.gov/pubmed/23545420%0Ahttp://www.pubmedcentral.nih.gov/articlerender.fcgi?artid=PMC3683898%0Apapers://a0f45058-72ca-4dc9-be03-e459899c7713/Paper/p615.

Kumar D, Abdulovic AL, Viberg J, Nilsson AK, Kunkel TA, Chabes A (2011) Mechanisms of mutagenesis in vivo due to imbalanced dNTP pools. Nucleic Acids Res 39:1360–1371.

Kunkel TA (2004) DNA Replication Fidelity. J Biol Chem 279:16895–16898.

Lei T, Du S, Peng Z, Chen L (2022) Multifaceted regulation and functions of 53BP1 in NHEJ-mediated DSB repair (Review). Int J Mol Med 50 Available at: /pmc/articles/PMC9162042/ [Accessed August 23, 2023].

Lelièvre SA, Weaver VM, Nickerson JA, Larabell CA, Bhaumik A, Petersen OW, Bissell MJ (1998) Tissue phenotype depends on reciprocal interactions between the extracellular matrix and the structural organization of the nucleus. Proc Natl Acad Sci U S A 95:14711–14716.

Li B, Gao YJ, Wu XY, Cui J, Long Y, Xu JL, Ding DG (2017a) Tumor-initiating cells contribute to radiation resistance in primary human renal clear cell carcinomas by activating the dna

damage checkpoint response. Oncol Lett 14:3261–3267.

Li B, Gao YJ, Wu XY, Cui J, Long Y, Xu JL, Ding DG (2017b) Tumor-initiating cells contribute to radiation resistance in primary human renal clear cell carcinomas by activating the dna damage checkpoint response. Oncol Lett 14:3261–3267.

Li LY, Guan Y Di, Chen XS, Yang JM, Cheng Y (2021) DNA Repair Pathways in Cancer Therapy and Resistance. Front Pharmacol 11:1–13.

Li WV, Li JJ (2018) Modeling and analysis of RNA-seq data: a review from a statistical perspective. Quant Biol 6:195–209.

Lieber MR (2011) The mechanism of DSB repair by the NHEJ. Annu Rev Biochem 79:181–211.

Lindahl T (1993) Instability and decay of the primary structure of DNA. Nature 362:709–715.

Lister JA, Robertson CP, Lepage T, Johnson SL, Raible DW (1999) nacre encodes a zebrafish microphthalmia-related protein that regulates neural-crest-derived pigment cell fate. Development 126:3757–3767 Available at: https://dx.doi.org/10.1242/dev.126.17.3757 [Accessed August 8, 2023].

Liu C, Vyas A, Kassab MA, Singh AK, Yu X (2017) The role of poly ADP-ribosylation in the first wave of DNA damage response. Nucleic Acids Res 45:8129–8141.

Liu C, Zhou S, Begum S, Sidransky D, Westra WH, Brock M, Califano JA (2007) Increased expression and activity of repair genes TDP1 and XPF in non-small cell lung cancer. Lung Cancer 55:303–311.

Liu LF, Desai SD, Li TK, Mao Y, Sun M, Sim SP (2000) Mechanism of Action of Camptothecin. Ann N Y Acad Sci 922:1–10 Available at: https://onlinelibrary.wiley.com/doi/full/10.1111/j.1749-6632.2000.tb07020.x [Accessed June 28, 2023].

Liu XH, Yu EZ, Li YY, Kagan E (2006) HIF-1α has an anti-apoptotic effect in human airway epithelium that is mediated via Mcl-1 gene expression. J Cell Biochem 97:755–765.

Liu Y, Bernauer AM, Yingling CM, Belinsky SA (2012) HIF1α regulated expression of XPA contributes to cisplatin resistance in lung cancer. Carcinogenesis 33:1187–1192.

Liu Y, Zhang Z, Liu R, Wei W, Zhang Z, Mai L, Guo S, Han H, Zhou F, He L, Dong P (2021) Stereotactic body radiotherapy in combination with non-frontline PD-1 inhibitors and targeted agents in metastatic renal cell carcinoma. Radiat Oncol 16:4–11 Available at: https://doi.org/10.1186/s13014-021-01937-9.

Livak KJ, Schmittgen TD (2001) Analysis of Relative Gene Expression Data Using Real-Time Quantitative PCR and the 2−ΔΔCT Method. Methods 25:402–408.

Llaguno-Munive M, Vazquez-Lopez MI, Jurado R, Garcia-Lopez P (2021) Mifepristone Repurposing in Treatment of High-Grade Gliomas. Front Oncol 11:1–8.

Locatelli F, Fishbane S, Block GA, MacDougall IC (2017) Targeting Hypoxia-Inducible Factors for the Treatment of Anemia in Chronic Kidney Disease Patients. Am J Nephrol 45:187–199 Available at: https://dx.doi.org/10.1159/000455166 [Accessed September 1, 2023].

Loeb LA, Loeb KR, Anderson JP (2003) Multiple mutations and cancer. Proc Natl Acad Sci U S A 100:776–781.

Lorson MA, Horvitz HR, Van Den Heuvel S (2000) LIN-5 is a novel component of the spindle apparatus required for chromosome segregation and cleavage plane specification in Caenorhabditis elegans. J Cell Biol 148:73–86.

Lu SC (2000) S-Adenosylmethionine. Int J Biochem Cell Biol 32:391–395.

Lucey BP, Nelson-Rees WA, Hutchins GM (2009) Henrietta Lacks, HeLa Cells, and Cell Culture Contamination. Arch Pathol Lab Med 133:1463–1467 Available at: https://dx.doi.org/10.5858/133.9.1463 [Accessed August 30, 2023].

Ludérus ME, Blaauwen JL den, Smit OJ de, Compton DA, Driel R van (1994) Binding of matrix attachment regions to lamin polymers involves single-stranded regions and the minor groove. Mol Cell Biol 14:6297 Available at: /pmc/articles/PMC359156/?report=abstract [Accessed September 4, 2023].

Ma B, Stepanov I, Hecht SS (2019) Recent studies on DNA adducts resulting from human exposure to tobacco smoke. Toxics 7.

Ma J, Wang MD (2016) DNA supercoiling during transcription. Biophys Rev 8:75–87 Available at: http://dx.doi.org/10.1007/s12551-016-0215-9.

Madan E, Gogna R, Pati U (2012) p53 Ser15 phosphorylation disrupts the p53–RPA70 complex and induces RPA70-mediated DNA repair in hypoxia. Biochem J 443:811–820 Available at: /biochemj/article/443/3/811/80766/p53-Ser15-phosphorylation-disrupts-the-p53-RPA70 [Accessed September 10, 2023].

Mah LJ, El-Osta A, Karagiannis TC (2010) γh2AX: A sensitive molecular marker of DNA damage and repair. Leukemia 24:679–686.

Maher ER (1996) Inherited renal cell carcinoma. Br J Urol 78:542–545.

Maher ER, Kaelin WG (1997) von Hippel-Lindau Disease. Medicine (Baltimore) 76:381–391.

Maher ER, Yates JRW, Harries R, Benjamin C, Harris R, Moore AT, Ferguson-Smith MA (1990) Clinical features and natural history of von hippel-lindau disease. Qjm 77:1151–1163.

Majmundar AJ, Wong WJ, Simon MC (2010) Hypoxia inducible factors and the response to hypoxic stress. Mol Cell 40:294 Available at: /pmc/articles/PMC3143508/ [Accessed July 17, 2023].

Makhov P, Joshi S, Ghatalia P, Kutikov A, Uzzo RG, Kolenko VM (2018) Resistance to Systemic Therapies in Clear Cell Renal Cell Carcinoma: Mechanisms and Management Strategies. Mol Cancer Ther 17:1355–1364 Available at: https://dx.doi.org/10.1158/1535-7163.MCT-17-1299 [Accessed September 13, 2023].

Maltepe E, Keith B, Arsham AM, Brorson JR, Simon MC (2000) The role of ARNT2 in tumor angiogenesis and the neural response to hypoxia. Biochem Biophys Res Commun 273:231–238.

Mansoury M, Hamed M, Karmustaji R, Al Hannan F, Safrany ST (2021) The edge effect: A global problem. The trouble with culturing cells in 96-well plates. Biochem Biophys Reports 26:100987.

Marchi D (2020) Bidirectional crosstalk between Hypoxia-Inducible Factor and glucocorticoid signalling in zebrafish larvae. Phd thesis Univ Sheff Available at: https://etheses.whiterose.ac.uk/28224/.

Marchi D, Santhakumar K, Markham E, Li N, Storbeck KH, Krone N, Cunliffe VT, Van Eeden FJM (2020) Bidirectional crosstalk between hypoxia-inducible factor and glucocorticoid signalling in zebrafish larvae. PLoS Genet 16.

Marini V, Nikulenkov F, Samadder P, Juul S, Knudsen BR, Krejci L (2023) MUS81 cleaves TOP1-derived lesions and other DNA–protein cross-links. BMC Biol 21:1–16.

Martinvalet D, Walch M (2022) The Role of Reactive Oxygen Species in Protective Immunity. Front Immunol 12:10–13.

Matsuoka S, Ballif BA, Smogorzewska A, McDonald ER, Hurov KE, Luo J, Bakalarski CE, Zhao Z, Solimini N, Lerenthal Y, Shiloh Y, Gygi SP, Elledge SJ (2007) ATM and ATR substrate analysis reveals extensive protein networks responsive to DNA damage. Science (80-) 316:1160–1166 Available at: https://www.science.org/doi/10.1126/science.1140321 [Accessed July 10, 2023].

Matthiesen S, Jahnke R, Knittler MR (2021) A Straightforward Hypoxic Cell Culture Method

Suitable for Standard Incubators. Methods Protoc 4 Available at: /pmc/articles/PMC8167595/ [Accessed September 1, 2023].

Maxwell PH, Wlesener MS, Chang GW, Clifford SC, Vaux EC, Cockman ME, Wykoff CC, Pugh CW, Maher ER, Ratcliffe PJ (1999) The tumour suppressor protein VHL targets hypoxia-inducible factors for oxygen-dependent proteolysis. Nature.

Maynard MA, Qi H, Chung J, Lee EHL, Kondo Y, Hara S, Conaway RC, Conaway JW, Ohh M (2003) Multiple splice variants of the human HIF-3α locus are targets of the von Hippel-Lindau E3 ubiquitin ligase complex. J Biol Chem 278:11032–11040 Available at: http://dx.doi.org/10.1074/jbc.M208681200.

Mazumder S, Higgins PJ, Samarakoon R (2023) Downstream Targets of VHL/HIF-α Signaling in Renal Clear Cell Carcinoma Progression: Mechanisms and Therapeutic Relevance. Cancers 2023, Vol 15, Page 1316 15:1316 Available at: https://www.mdpi.com/2072-6694/15/4/1316/htm [Accessed April 12, 2023].

McHugh ML (2011) Multiple comparison analysis testing in ANOVA. Biochem Medica 21:203–209 Available at: https://www.biochemia-medica.com/en/journal/21/10.11613/BM.2011.029 [Accessed February 22, 2024].

McKeown SR (2014) Defining normoxia, physoxia and hypoxia in tumours—implications for treatment response. Br J Radiol 87 Available at: /pmc/articles/PMC4064601/ [Accessed July 14, 2023].

Mehibel M, Xu Y, Li CG, Moon EJ, Thakkar KN, Diep AN, Kim RK, Bloomstein JD, Xiao Y, Bacal J, Saldivar JC, Le QT, Cimprich KA, Rankin EB, Giaccia AJ (2021) Eliminating hypoxic tumor cells improves response to PARP inhibitors in homologous recombination–deficient cancer models. J Clin Invest 131.

Meisenberg C, Ward SE, Schmid P, El-Khamisy SF (2014) TDP1/TOP1 Ratio as a Promising Indicator for the Response of Small Cell Lung Cancer to Topotecan. J Cancer Sci Ther 6:258 Available at: /pmc/articles/PMC4163653/ [Accessed October 26, 2021].

Merdes A, Ramyar K, Vechio JD, Cleveland DW (1996) A complex of NuMA and cytoplasmic dynein is essential for mitotic spindle assembly. Cell 87:447–458 Available at: http://www.cell.com/article/S0092867400813653/fulltext [Accessed September 4, 2023].

Merla G, Micale L, Muscarella LA, Marzulli M, Augello B, Tritto P, D'Agruma L, Zelante L, Palumbo G (2009) VHL Frameshift Mutation as Target of Nonsense-Mediated mRNA

Decay in Drosophila melanogaster and Human HEK293 Cell Line. J Biomed Biotechnol 2009 Available at: /pmc/articles/PMC2817372/ [Accessed August 15, 2023].

Metcalf JL, Bradshaw PS, Komosa M, Greer SN, Stephen Meyn M, Ohh M (2014) K63-Ubiquitylation of VHL by SOCS1 mediates DNA double-strand break repair. Oncogene.

Miao D et al. (2018) Genomic correlates of response to immune checkpoint therapies in clear cell renal cell carcinoma. Science (80-) 359:801–806.

Michaelis J, Grabbert M, Sigle A, Yilmaz M, Schlager D, Gratzke C, Miernik A, Schoeb DS (2022) Tyrosine Kinase Inhibitors in the Treatment of Metastasised Renal Cell Carcinoma—Future or the Past? Cancers (Basel) 14 Available at: /pmc/articles/PMC9367545/ [Accessed August 16, 2023].

Mihaylova VT, Bindra RS, Yuan J, Campisi D, Narayanan L, Jensen R, Giordano F, Johnson RS, Rockwell S, Glazer PM (2003) Decreased Expression of the DNA Mismatch Repair Gene Mlh1 under Hypoxic Stress in Mammalian Cells . Mol Cell Biol 23:3265–3273.

Minamishima YA, Moslehi J, Padera RF, Bronson RT, Liao R, William G. Kaelin J (2009) A Feedback Loop Involving the Phd3 Prolyl Hydroxylase Tunes the Mammalian Hypoxic Response In Vivo. Mol Cell Biol 29:5729 Available at: /pmc/articles/PMC2772748/ [Accessed March 8, 2023].

Mittal MK, Sureka B (2016) Solid renal masses in adults. Indian J Radiol Imaging 26:429 Available at: /pmc/articles/PMC5201069/ [Accessed August 14, 2023].

Mocellin S, Provenzano M (2004) RNA interference: Learning gene knock-down from cell physiology. J Transl Med 2:1–6.

Mohamed MO, Al-Rubaye S, Reilly IW, McGoldrick S (2015) Renal cell carcinoma presenting as an upper gastrointestinal bleeding. Case Reports 2015:bcr2015211553 Available at: https://casereports.bmj.com/content/2015/bcr-2015-211553 [Accessed August 14, 2023].

Moreno NS, Liu J, Haas KM, Parker LL, Chakraborty C, Kron SJ, Hodges K, Miller LD, Langefeld C, Robinson PJ, Leliévre SA, Vidi PA (2019) The nuclear structural protein NuMA is a negative regulator of 53BP1 in DNA double-strand break repair. Nucleic Acids Res 47:2703–2715 Available at: https://dx.doi.org/10.1093/nar/gkz138 [Accessed July 10, 2023].

Msaouel P, Thall PF, Yuan Y, Chen I, Tannir NM (2018) A phase I/II study of sitravatinib (MGCD-516) plus nivolumab in patients (pts) with metastatic clear-cell renal cell

carcinoma (ccRCC) that progressed on prior VEGF-targeted therapy. https://doi.org/101200/JCO2018366_supplTPS708 36:TPS708–TPS708 Available at: https://ascopubs.org/doi/10.1200/JCO.2018.36.6_suppl.TPS708 [Accessed January 17, 2024].

Müller M, Mentel M, van Hellemond JJ, Henze K, Woehle C, Gould SB, Yu R-Y, van der Giezen M, Tielens AGM, Martin WF (2012) Biochemistry and Evolution of Anaerobic Energy Metabolism in Eukaryotes. Microbiol Mol Biol Rev 76:444–495 Available at: https://journals.asm.org/doi/10.1128/mmbr.05024-11 [Accessed July 20, 2023].

Munkuev AA, Mozhaitsev ES, Chepanova AA, Suslov E V., Korchagina D V., Zakharova OD, Ilina ES, Dyrkheeva NS, Zakharenko AL, Reynisson J, Volcho KP, Salakhutdinov NF, Lavrik OI (2021) Novel tdp1 inhibitors based on adamantane connected with monoterpene moieties via heterocyclic fragments. Molecules 26:1–23.

Muñoz-Sánchez J, Chánez-Cárdenas ME (2019) The use of cobalt chloride as a chemical hypoxia model. J Appl Toxicol 39:556–570.

Murphy MP (2009) How mitochondria produce reactive oxygen species. Biochem J 417:1–13.

Nagao M, Ebert BL, Ratcliffe PJ, Pugh CW (1996) Drosophila melanogaster SL2 cells contain a hypoxically inducible DNA binding complex which recognises mammalian HIF-1 binding sites. FEBS Lett.

Nanduri J, Wang N, Yuan G, Khan SA, Souvannakitti D, Peng Y (2009) Intermittent hypoxia degrades HIF-2α via calpains resulting in oxidative stress: Implications for recurrent apnea-induced morbidities. PNAS 106:1199–1204.

Nickerson ML et al. (2008) Improved Identification of von Hippel-Lindau Gene Alterations in Clear Cell Renal Tumors. Clin Cancer Res 14:4726 Available at: /pmc/articles/PMC2629664/ [Accessed August 15, 2023].

Nivens MC, Felder T, Galloway AH, Pena MMO, Pouliot JJ, Spencer HT (2004) Engineered resistance to camptothecin and antifolates by retroviral coexpression of tyrosyl DNA phosphodiesterase-I and thymidylate synthase. Cancer Chemother Pharmacol 53:107–115.

Okamoto A, Sumi C, Tanaka H, Kusunoki M, Iwai T, Nishi K, Matsuo Y, Harada H, Takenaga K, Bono H, Hirota K (2017) HIF-1-mediated suppression of mitochondria electron transport chain function confers resistance to lidocaine-induced cell death. Sci Rep 7

Available at: /pmc/articles/PMC5476559/ [Accessed February 3, 2022].

Olive PL, Banáth JP (2004) Phosphorylation of histone H2AX as a measure of radiosensitivity. Int J Radiat Oncol Biol Phys 58:331–335 Available at: https://pubmed.ncbi.nlm.nih.gov/14751500/ [Accessed July 11, 2023].

Oudard S, Elaidi RT (2012) Sequential therapy with targeted agents in patients with advanced renal cell carcinoma: Optimizing patient benefit. Cancer Treat Rev 38:981–987.

Ozaki T, Nakagawara A (2011) Role of p53 in cell death and human cancers. Cancers (Basel) 3:994–1013.

Pal SK, Figlin RA (2010) Treatment options in metastatic renal cell carcinoma: Focus on mTOR inhibitors. Clin Med Insights Oncol 4:43–53 Available at: https://journals.sagepub.com/doi/10.4137/CMO.S1590 [Accessed August 16, 2023].

Palapattu GS, Kristo B, Rajfer J (2002) Paraneoplastic Syndromes in Urologic Malignancy: The Many Faces of Renal Cell Carcinoma. Rev Urol 4:163 Available at: /pmc/articles/PMC1475999/ [Accessed August 14, 2023].

Palazzo L, Mikoč A, Ahel I (2017) ADP-ribosylation: new facets of an ancient modification. FEBS J 284:2932–2946.

Pećina-Šlaus N, Kafka A, Salamon I, Bukovac A (2020) Mismatch Repair Pathway, Genome Stability and Cancer. Front Mol Biosci 7:1–12.

Pegg AE (2011) Multifaceted Roles of Alkyltransferase and Related Proteins In DNA Repair, DNA Damage, Resistance to Chemotherapy and Research Tools. Chem Res Toxicol 24:618–639 Available at: doi:10.1021/tx200031q.

Peinado H, Zhang H, Matei IR, Costa-Silva B, Hoshino A, Rodrigues G, Psaila B, Kaplan RN, Bromberg JF, Kang Y, Bissell MJ, Cox TR, Giaccia AJ, Erler JT, Hiratsuka S, Ghajar CM, Lyden D (2017) Pre-metastatic niches: organ-specific homes for metastases. Nat Rev Cancer 2017 175 17:302–317 Available at: https://www.nature.com/articles/nrc.2017.6 [Accessed August 30, 2023].

Perkins ND, Gilmore TD (2006) Good cop, bad cop: The different faces of NF-κB. Cell Death Differ 13:759–772.

Perrotta S et al. (2020) Effects of Germline VHL Deficiency on Growth, Metabolism, and Mitochondria. N Engl J Med 382:835–844.

Pfeifer GP (2020) Mechanisms of UV-induced mutations and skin cancer. Genome Instab Dis

1:99–113.

Plo I, Liao ZY, Barceló JM, Kohlhagen G, Caldecott KW, Weinfeld M, Pommier Y (2003) Association of XRCC1 and tyrosyl DNA phosphodiesterase (Tdp1) for the repair of topoisomerase I-mediated DNA lesions. DNA Repair (Amst) 2:1087–1100.

Poklar N, Pilch DS, Lippard SJ, Redding EA, Dunham SU, Breslauer KJ (1996) Influence of cisplatin intrastrand crosslinking on the conformation, thermal stability, and energetics of a 20-mer DNA duplex. Proc Natl Acad Sci U S A 93:7606–7611.

Pommier Y, Huang S yin N, Gao R, Das BB, Murai J, Marchand C (2014) Tyrosyl-DNA-phosphodiesterases (TDP1 and TDP2). DNA Repair (Amst) 19:114–129.

Pommier Y, Sun Y, Huang SYN, Nitiss JL (2016) Roles of eukaryotic topoisomerases in transcription, replication and genomic stability. Nat Rev Mol Cell Biol 2016 1711 17:703–721 Available at: https://www.nature.com/articles/nrm.2016.111 [Accessed September 5, 2023].

Pyrhönen S, Salminen E, Ruutu M, Lehtonen T, Nurmi M, Tammela T, Juusela H, Rintala E, Hietanen P, Kellokumpu-Lehtinen PL (1999) Prospective randomized trial of interferon alfa-2a plus vinblastine versus vinblastine alone in patients with advanced renal cell cancer. J Clin Oncol 17:2859–2867.

Qin W Sen, Wu J, Chen Y, Cui FC, Zhang FM, Lyu GT, Zhang HM (2017) The short isoform of nuclear mitotic apparatus protein 1 functions as a putative tumor suppressor. Chin Med J (Engl) 130:1824–1830.

Qiu B, Ackerman D, Sanchez DJ, Li B, Ochocki JD, Grazioli A, Bobrovnikova-Marjon E, Alan Diehl J, Keith B, Celeste Simon M (2015) HIF-2α dependent lipid storage promotes endoplasmic reticulum homeostasis in clear cell renal cell carcinoma. Cancer Discov 5:652 Available at: /pmc/articles/PMC4456212/ [Accessed August 3, 2023].

Ramachandran S, Ma T, Griffin J, Ng N, Foskolou IP, Hwang M-S, Victori P, Cheng W-C, Buffa FM, Leszczynska KB, El-Khamisy SF, Gromak N, Hammond EM (2021) Hypoxia-induced SETX links replication stress with the unfolded protein response. Nat Commun 12 Available at: https://pubmed.ncbi.nlm.nih.gov/34140498/ [Accessed August 23, 2021].

Ran FA, Hsu PD, Wright J, Agarwala V, Scott DA, Zhang F (2013) Genome engineering using the CRISPR-Cas9 system. Nat Protoc 2013 811 8:2281–2308 Available at: https://www.nature.com/articles/nprot.2013.143 [Accessed June 21, 2022].

Ranganathan P (2021) An Introduction to Statistics: Choosing the Correct Statistical Test.

Indian J Crit Care Med 25:S184 Available at: /pmc/articles/PMC8327789/ [Accessed February 22, 2024].

Rankin EB, Rha J, Selak MA, Unger TL, Keith B, Liu Q, Haase VH (2009) Hypoxia-Inducible Factor 2 Regulates Hepatic Lipid Metabolism. Mol Cell Biol 29:4527 Available at: /pmc/articles/PMC2725738/ [Accessed July 21, 2023].

Raval RR, Weng Lau K, Tran MGB, Sowter HM, Mandriota SJ, Li J-L, Pugh CW, Maxwell PH, Harris AL, Ratcliffe PL (2005) Contrasting Properties of Hypoxia-Inducible Factor 1 (HIF-1) and HIF-2 in von Hippel-Lindau-Associated Renal Cell Carcinoma. Mol Cell Biol 25:5675–5686.

Ravenna L, Cardillo I, Curzio G, Baldi A, Mattioni M, Vincenzi B, Russo, Matteo Antonio, Soddu S, Verdina A (2014) Mesothelioma and Hypoxia: Modulation of the Inflammation-Related Phenotype and Identification of Prognostic Markers. J Cancer Sci Ther 06:378–387.

Ravenna L, Salvatori L, Russo MA (2016) HIF3α: The little we know. FEBS J.

Ray Chaudhuri A, Nussenzweig A (2017) The multifaceted roles of PARP1 in DNA repair and chromatin remodelling. Nat Rev Mol Cell Biol 18:610–621.

Ray S, Abugable AA, Parker J, Liversidge K, Palminha NM, Liao C, Acosta-Martin AE, Souza CDS, Jurga M, Sudbery I, El-Khamisy SF (2022) A mechanism for oxidative damage repair at gene regulatory elements. Nat 2022 6097929 609:1038–1047 Available at: https://www.nature.com/articles/s41586-022-05217-8 [Accessed February 27, 2023].

Ren Y, Hao P, Dutta B, Cheow ESH, Sim KH, Gan CS, Lim SK, Sze SK (2013) Hypoxia modulates A431 cellular pathways association to tumor radioresistance and enhanced migration revealed by comprehensive proteomic and functional studies. Mol Cell Proteomics 12:485–498.

Rey S, Semenza GL (2010) Hypoxia-inducible factor-1-dependent mechanisms of vascularization and vascular remodelling. Cardiovasc Res 86:236 Available at: /pmc/articles/PMC2856192/ [Accessed July 18, 2023].

Rezvani HR, Mahfouf W, Ali N, Chemin C, Ged C, Kim AL, de Verneuil H, Taïeb A, Bickers DR, Mazurier F ric (2009) Hypoxia-inducible factor-1α regulates the expression of nucleotide excision repair proteins in keratinocytes. Nucleic Acids Res 38:797–809.

Richter M, Piwocka O, Musielak M, Piotrowski I, Suchorska WM, Trzeciak T (2021) From Donor to the Lab: A Fascinating Journey of Primary Cell Lines. Front Cell Dev Biol 9

Available at: /pmc/articles/PMC8356673/ [Accessed September 1, 2023].

Rini BI (2010) New strategies in kidney cancer: therapeutic advances through understanding the molecular basis of response and resistance. Clin Cancer Res 16:1348–1354 Available at: https://pubmed.ncbi.nlm.nih.gov/20179240/ [Accessed June 26, 2023].

Riss TL, Moravec RA, Niles AL, Duellman S, Benink HA, Worzella TJ, Minor L (2004) Cell Viability Assays. Assay Guid Man:1–25 Available at: http://www.ncbi.nlm.nih.gov/pubmed/23805433.

Rodríguez-Jiménez FJ, Moreno-Manzano V, Lucas-Dominguez R, Sánchez-Puelles J-M (2008) Hypoxia Causes Downregulation of Mismatch Repair System and Genomic Instability in Stem Cells. Stem Cells 26:2052–2062.

Rodriguez J, Herrero A, Li S, Rauch N, Quintanilla A, Wynne K, Krstic A, Acosta JC, Taylor C, Schlisio S, von Kriegsheim A (2018) PHD3 Regulates p53 Protein Stability by Hydroxylating Proline 359. Cell Rep 24:1316–1329 Available at: https://doi.org/10.1016/j.celrep.2018.06.108.

Roques C, Coulombe Y, Delannoy M, Vignard J, Grossi S, Brodeur I, Rodrigue A, Gautier J, Stasiak AZ, Stasiak A, Constantinou A, Masson JY (2009) MRE11–RAD50–NBS1 is a critical regulator of FANCD2 stability and function during DNA double-strand break repair. EMBO J 28:2400–2413 Available at: https://onlinelibrary.wiley.com/doi/full/10.1038/emboj.2009.193 [Accessed July 14, 2023].

Rossi E, Bersanelli M, Gelibter AJ, Borsellino N, Caserta C, Doni L, Maruzzo M, Mosca A, Pisano C, Verzoni E, Zucali PA (2021) Combination Therapy in Renal Cell Carcinoma: the Best Choice for Every Patient? Curr Oncol Rep 23 Available at: https://doi.org/10.1007/s11912-021-01140-9.

Roth JR (1974) Frameshift mutations. Annu Rev Genet 8:319–346.

Roy I, Nadar P, Khurana S (2021) Neutral Comet Assay to Detect and Quantitate DNA Double-Strand Breaksin Hematopoietic Stem Cells. Bio-protocol 11 Available at: https://pubmed.ncbi.nlm.nih.gov/34541048/ [Accessed June 29, 2023].

Russell RC, Sufan RI, Zhou B, Heir P, Bunda S, Sybingco SS, Greer SN, Roche O, Heathcote SA, Chow VWK, Boba LM, Richmond TD, Hickey MM, Barber DL, Cheresh DA, Simon MC, Irwin MS, Kim WY, Ohh M (2011) Loss of JAK2 regulation via a heterodimeric VHL-SOCS1 E3 ubiquitin ligase underlies Chuvash polycythemia. Nat Med 17:845–853.

Ryan HE, Lo J, Johnson RS (1998) HIF-1 alpha is required for solid tumor formation and embryonic vascularization. EMBO J 17:3005 Available at: /pmc/articles/PMC1170640/?report=abstract [Accessed July 18, 2023].

Rytkönen KT, Akbarzadeh A, Miandare HK, Kamei H, Duan C, Leder EH, Williams TA, Nikinmaa M (2013) Subfunctionalization of cyprinid hypoxia-inducible factors for roles in development and oxygen sensing. Evolution (N Y).

Ryu JH, Chae CS, Kwak JS, Oh H, Shin Y, Huh YH, Lee CG, Park YW, Chun CH, Kim YM, Im SH, Chun JS (2014) Hypoxia-Inducible Factor-2α Is an Essential Catabolic Regulator of Inflammatory Rheumatoid Arthritis. PLoS Biol 12:1–16.

Salanga CM, Salanga MC (2021) Genotype to Phenotype: CRISPR Gene Editing Reveals Genetic Compensation as a Mechanism for Phenotypic Disjunction of Morphants and Mutants. Int J Mol Sci 22 Available at: /pmc/articles/PMC8036752/ [Accessed August 23, 2023].

Sale JE (2013) Translesion DNA synthesis and mutagenesis in prokaryotes. Cold Spring Harb Perspect Biol 5.

Sallmyr A, Tomkinson AE (2018) Repair of DNA double-strand breaks by mammalian alternative end-joining pathways. J Biol Chem 293:10536–10549 Available at: http://dx.doi.org/10.1074/jbc.TM117.000375.

Sanjana NE, Shalem O, Zhang F (2014) Improved vectors and genome-wide libraries for CRISPR screening. Nat Methods 11:783 Available at: /pmc/articles/PMC4486245/ [Accessed June 21, 2022].

Santhakumar K, Judson EC, Elks PM, McKee S, Elworthy S, Van Rooijen E, Walmsley SS, Renshaw SA, Cross SS, Van Eeden FJM (2012) A zebrafish model to study and therapeutically manipulate hypoxia signaling in tumorigenesis. Cancer Res.

Sasabe E, Tatemoto Y, Li D, Yamamoto T, Osaki T (2005) Mechanism of HIF-1α-dependent suppression of hypoxia-induced apoptosis in squamous cell carcinoma cells. Cancer Sci 96:394–402.

Sato Y et al. (2013) Integrated molecular analysis of clear-cell renal cell carcinoma. Nat Genet 2013 458 45:860–867 Available at: https://www.nature.com/articles/ng.2699 [Accessed August 15, 2023].

Saxena K, Jolly MK (2019) Acute vs. Chronic vs. Cyclic Hypoxia: Their Differential Dynamics, Molecular Mechanisms, and Effects on Tumor Progression. Biomol 2019, Vol 9, Page

339 9:339 Available at: https://www.mdpi.com/2218-273X/9/8/339/htm [Accessed August 2, 2023].

Scanlon SE, Glazer PM (2014) Hypoxic stress facilitates acute activation and chronic downregulation of Fanconi anemia proteins. Mol Cancer Res.

Scanlon SE, Glazer PM (2015) Multifaceted control of DNA repair pathways by the hypoxic tumor microenvironment. DNA Repair (Amst) 32:180–189.

Scanlon SE, Hegan DC, Sulkowski PL, Glazer PM (2018) Suppression of homology-dependent DNA double-strand break repair induces PARP inhibitor sensitivity in VHL-deficient human renal cell carcinoma. Oncotarget.

Schärer OD (2013) Nucleotide Excision Repair in Eukaryotes. Encycl Biol Chem Second Ed:341–344.

Scherer G, Urban M, Hagedorn HW, Serafin R, Feng S, Kapur S, Muhammad R, Jin Y, Sarkar M, Roethig HJ (2010) Determination of methyl-, 2-hydroxyethyl- and 2-cyanoethylmercapturic acids as biomarkers of exposure to alkylating agents in cigarette smoke. J Chromatogr B Anal Technol Biomed Life Sci 878:2520–2528.

Schoket B (1999) DNA damage in humans exposed to environmental and dietary polycyclic aromatic hydrocarbons. Mutat Res - Fundam Mol Mech Mutagen 424:143–153.

Schvartzman JB, Martínez-Robles ML, Herná ndez P, Krimer DB (2013) The benefit of DNA supercoiling during replication. Biochem Soc Trans 41:646–651.

Scortegagna M, Ding K, Oktay Y, Gaur A, Thurmond F, Yan LJ, Marck BT, Matsumoto AM, Shelton JM, Richardson JA, Bennet MJ, Garcia JA (2003) Multiple organ pathology, metabolic abnormalities and impaired homeostasis of reactive oxygen species in Epas1-/- mice. Nat Genet 35:331–340.

Scully R, Panday A, Elango R, Willis NA (2019) DNA double-strand break repair-pathway choice in somatic mammalian cells. Nat Rev Mol Cell Biol 20:698–714 Available at: http://dx.doi.org/10.1038/s41580-019-0152-0.

Semenza GL (2007) Life with Oxygen. Science (80-) 318:62–64 Available at: https://www.science.org/doi/10.1126/science.1147949 [Accessed July 20, 2023].

Semenza GL, Jiang BH, Leung SW, Passantino R, Concordat JP, Maire P, Giallongo A (1996) Hypoxia response elements in the aldolase A, enolase 1, and lactate dehydrogenase a gene promoters contain essential binding sites for hypoxia-inducible factor 1. J Biol Chem 271:32529–32537 Available at: http://dx.doi.org/10.1074/jbc.271.51.32529.

Sendoel A, Hengartner MO (2023) Apoptotic Cell Death Under Hypoxia. 95:168–176.

Shah NR, Declouette B, Ansari-Gilani K, Alhomoud MS, Hoimes C, Ramaiya NH, Güler E (2021) High-dose interleukin-2 therapy related adverse events and implications on imaging From the Departments of Radiology (N. Diagn Interv Radiol 27:684–689.

Shapiro DD, Virumbrales-Muñoz M, Beebe DJ, Abel EJ (2022) Models of Renal Cell Carcinoma Used to Investigate Molecular Mechanisms and Develop New Therapeutics. Front Oncol 12:1–13.

Sharma V, Collins LB, Chen T, Herr N, Takeda S, Sun W, Swenberg JA, Nakamura J (2016) Oxidative stress at low levels can induce clustered DNA lesions leading to NHEJ mediated mutations. Oncotarget 7:25377–25390.

Shi J, Xiong Z, Wang K, Yuan C, Huang Y, Xiao W, Meng X, Chen Z, Lv Q, Miao D, Liang H, Xu T, Xie K, Yang H, Zhang X (2021) HIF2α promotes tumour growth in clear cell renal cell carcinoma by increasing the expression of NUDT1 to reduce oxidative stress. Clin Transl Med 11:e592 Available at: https://onlinelibrary.wiley.com/doi/full/10.1002/ctm2.592 [Accessed November 9, 2021].

Shimba S, Ishii N, Ohta Y, Ohno T, Watabe Y, Hayashi M, Wada T, Aoyagi T, Tezuka M (2005) Brain and muscle Arnt-like protein-1 (BMAL1), a component of the molecular clock, regulates adipogenesis. Proc Natl Acad Sci U S A 102:12071–12076.

Shimizu N, Hamada Y, Morozumi R, Yamamoto J, Iwai S, Sugiyama K ichi, Ide H, Tsuda M (2023) Repair of topoisomerase 1–induced DNA damage by tyrosyl-DNA phosphodiesterase 2 (TDP2) is dependent on its magnesium binding. J Biol Chem 299:104988 Available at: https://doi.org/10.1016/j.jbc.2023.104988.

Shrivastav M, De Haro LP, Nickoloff JA (2008) Regulation of DNA double-strand break repair pathway choice. Cell Res 18:134–147.

Siddens LK, Bunde KL, Harper TA, McQuistan TJ, Löhr C V., Bramer LM, Waters KM, Tilton SC, Krueger SK, Williams DE, Baird WM (2015) Cytochrome P450 1b1 in polycyclic aromatic hydrocarbon (PAH)-induced skin carcinogenesis: Tumorigenicity of individual PAHs and coal-tar extract, DNA adduction and expression of select genes in the Cyp1b1 knockout mouse. Toxicol Appl Pharmacol 287:149–160.

Silk AD, Holland AJ, Cleveland DW (2009) Requirements for NuMA in maintenance and establishment of mammalian spindle poles. J Cell Biol 184:677–690 Available at: www.jcb.org/cgi/doi/10.1083/jcb.200810091 [Accessed September 4, 2023].

Sim GC, Radvanyi L (2014) The IL-2 cytokine family in cancer immunotherapy. Cytokine Growth Factor Rev 25:377–390.

Simon MC, Keith B (2008) The role of oxygen availability in embryonic development and stem cell function. Nat Rev Mol Cell Biol 2008 94 9:285–296 Available at: https://www.nature.com/articles/nrm2354 [Accessed July 18, 2023].

Smythies JA, Sun M, Masson N, Salama R, Simpson PD, Murray E, Neumann V, Cockman ME, Choudhry H, Ratcliffe PJ, Mole DR (2019) Inherent DNA-binding specificities of the HIF-1α and HIF2-α transcription factors in chromatin. EMBO Rep 20 Available at: https://onlinelibrary.wiley.com/doi/abs/10.15252/embr.201846401 [Accessed April 21, 2020].

Souma T, Nezu M, Nakano D, Yamazaki S, Hirano I, Sekine H, Dan T, Takeda K, Fong GH, Nishiyama A, Ito S, Miyata T, Yamamoto M, Suzuki N (2016) Erythropoietin synthesis in renal myofibroblasts is restored by activation of hypoxia signaling. J Am Soc Nephrol 27:428–438 Available at: /pmc/articles/PMC4731118/ [Accessed August 14, 2023].

Soussi T, Dehouche K, Beroud C (2000) Analysis of p53 gene mutations in human cancer: The link between epidemiology and carcinogenesis. Medecine/Sciences 16:1387–1396.

Sriraman A, Debnath TK, Xhemalce B, Miller KM (2020) Making it or breaking it: DNA methylation and genome integrity Anusha. Essays Biochem 64:687–703.

Stebbins CE, Kaelin WG, Pavletich NP (1999) Structure of the VHL-ElonginC-ElonginB Complex: Implications for VHL Tumor Suppressor Function. Science (80-) 284:455–461 Available at: https://www.science.org/doi/10.1126/science.284.5413.455 [Accessed August 15, 2023].

Stokes MP, Rush J, MacNeill J, Jian MR, Sprott K, Nardone J, Yang V, Beausoleil SA, Gygi SP, Livingstone M, Zhang H, Polakiewicz RD, Comb MJ (2007) Profiling of UV-induced ATM/ATR signaling pathways. Proc Natl Acad Sci U S A 104:19855–19860.

Stransky LA, Vigeant SM, Huang B, West D, Denize T, Walton E, Signoretti S, Kaelin WG (2022) Sensitivity of VHL mutant kidney cancers to HIF2 inhibitors does not require an intact p53 pathway. Proc Natl Acad Sci U S A 119.

Sturtzel C, Hocking J, Kirchberger S, Distel M (2021) Studying the Tumor Microenvironment in Zebrafish. Adv Exp Med Biol 1329:69–92 Available at: https://link.springer.com/chapter/10.1007/978-3-030-73119-9_4 [Accessed August 31, 2023].

Tanaka T, Wiesener M, Bernhardt W, Eckardt KU, Warnecke C (2009) The human HIF (hypoxia-inducible factor)-3alpha gene is a HIF-1 target gene and may modulate hypoxic gene induction. Biochem J 424:143–151 Available at: https://pubmed.ncbi.nlm.nih.gov/19694616/ [Accessed September 12, 2023].

Taylor C, Craven RA, Harnden P, Selby PJ, Banks RE (2012) Determination of the consequences of VHL mutations on VHL transcripts in renal cell carcinoma. Int J Oncol 41:1229–1240.

Thomas R (2022) Characterisation of DNA Repair Deficient Zebrafish for the Investigation of Neurological Disease. Phd thesis Univ Sheff.

Thompson M (2009) Polybromo-1: the chromatin targeting subunit of the PBAF complex. Biochimie 91:309–319.

Thompson PS, Cortez D (2020) New insights into abasic site repair and tolerance. DNA Repair (Amst) 90:102866.

To KKW, Sedelnikova OA, Samons M, Bonner WM, Huang LE (2006) The phosphorylation status of PAS-B distinguishes HIF-1α from HIF-2α in NBS1 repression. EMBO J 25:4784–4794 Available at: https://onlinelibrary.wiley.com/doi/full/10.1038/sj.emboj.7601369 [Accessed August 23, 2023].

Totsuka Y, Kobayashi M, Matsuo H, Imai K, Ito Z, Yamanaka H (1989) SIDE EFFECTS OF INTERFERON-α (INF-α) THERAPY FOR RENAL CELL CARCINOMA. KITAKANTO Med J 39:81–84.

Vacaru AM, Unlu G, Spitzner M, Mione M, Knapik EW, Sadler KC (2014) In vivo cell biology in zebrafish - providing insights into vertebrate development and disease. J Cell Sci.

van Rooijen E, Santhakumar K, Logister I, Voest E, Schulte-Merker S, Giles R, van Eeden F (2011) A Zebrafish Model for VHL and Hypoxia Signaling. Methods Cell Biol 105:163–190.

Van Rooijen E, Voest EE, Logister I, Korving J, Schwerte T, Schulte-Merker S, Giles RH, Van Eeden FJ (2009) Zebrafish mutants in the von Hippel-Lindau tumor suppressor display a hypoxic response and recapitulate key aspects of Chuvash polycythemia. Blood.

Viault F (1890) Sur l'augmentation considerable du nombre des globules rouges dans sang chez les habitants des haut plateauz de l'Amerique de Sud. Comp rend Acad d sc 111:917–918 Available at: https://cir.nii.ac.jp/crid/1572543025880402432.bib?lang=en [Accessed July 18, 2023].

Vidi PA, Liu J, Salles D, Jayaraman S, Dorfman G, Gray M, Abad P, Moghe P V., Irudayaraj JM, Wiesmüller L, Lelièvre SA (2014) NuMA promotes homologous recombination repair by regulating the accumulation of the ISWI ATPase SNF2h at DNA breaks. Nucleic Acids Res 42:6365 Available at: /pmc/articles/PMC4041463/ [Accessed September 4, 2023].

Vignard J, Mirey G, Salles B (2013) Ionizing-radiation induced DNA double-strand breaks: A direct and indirect lighting up. Radiother Oncol 108:362–369.

Viguera E, Canceill D, Ehrlich SD (2001) Replication slippage involves DNA polymerase pausing and dissociation. EMBO J 20:2587–2595.

Wagh V, Joshi P, Jariyal H, Chauhan N (2020) ATM and ATR checkpoint kinase pathways: A concise review. Adv Hum Biol 10:51.

Wallace EM et al. (2016) A Small-Molecule Antagonist of HIF2α Is Efficacious in Preclinical Models of Renal Cell Carcinoma. Cancer Res 76:5491–5500 Available at: https://cancerres.aacrjournals.org/content/76/18/5491 [Accessed January 24, 2022].

Wang GL, Semenza GL (1993a) Characterization of hypoxia-inducible factor 1 and regulation of DNA binding activity by hypoxia. J Biol Chem.

Wang GL, Semenza GL (1993b) General involvement of hypoxia-inducible factor 1 in transcriptional response to hypoxia. Proc Natl Acad Sci U S A.

Wang LC, Gautier J (2010) The Fanconi anemia pathway and ICL repair: implications for cancer therapy. Crit Rev Biochem Microbiol 45:424–439 Available at: doi:10.3109/10409238.2010.502166.

Wang Y, Branicky R, Noë A, Hekimi S (2018) Superoxide dismutases: Dual roles in controlling ROS damage and regulating ROS signaling. J Cell Biol 217:1915–1928.

Webb JD, Coleman ML, Pugh CW (2009) Hypoxia, hypoxia-inducible factors (HIF), HIF hydroxylases and oxygen sensing. Cell Mol Life Sci 66:3539–3554 Available at: https://link.springer.com/article/10.1007/s00018-009-0147-7 [Accessed July 17, 2023].

Weiskirchen S, Schröder SK, Buhl EM, Weiskirchen R (2023) A Beginner's Guide to Cell Culture: Practical Advice for Preventing Needless Problems. Cells 2023, Vol 12, Page 682 12:682 Available at: https://www.mdpi.com/2073-4409/12/5/682/htm [Accessed August 30, 2023].

Weiss JM, Lumaquin-Yin D, Montal E, Suresh S, Leonhardt CS, White RM (2022) Shifting the focus of zebrafish toward a model of the tumor microenvironment. Elife 11.

Weissbein U, Peretz M, Plotnik O, Yanuka O, Sagi I, Golan-Lev T, Benvenisty N (2019)

Genome-wide Screen for Culture Adaptation and Tumorigenicity-Related Genes in Human Pluripotent Stem Cells. iScience 11:398–408.

Wheaton WW, Chandel NS (2011) Hypoxia. 2. Hypoxia regulates cellular metabolism. Am J Physiol - Cell Physiol 300:385–393 Available at: https://journals.physiology.org/doi/10.1152/ajpcell.00485.2010 [Accessed July 19, 2023].

Williams HL, Gottesman ME, Gautier J (2013) The differences between ICL repair during and outside of S- Phase. Trends Biochem Sci 38:386–393 Available at: doi:10.1016/j.tibs.2013.05.004.

Winter C, Kerros ME, Weinbauer MG (2012) Effects of sodium azide on the abundance of prokaryotes and viruses in marine samples. PLoS One 7:5–8.

Wu J, Xu Z, He D, Lu G (2014) Identification and characterization of novel NuMA isoforms. Biochem Biophys Res Commun 454:387–392.

Xu Y, Gao Q, Xue Y, Li X, Xu L, Li C, Qin Y, Fang J (2019) Prolyl hydroxylase 3 stabilizes the p53 tumor suppressor by inhibiting the p53-MDM2 interaction in a hydroxylase-independent manner. J Biol Chem 294:9949–9958 Available at: http://dx.doi.org/10.1074/jbc.RA118.007181.

Yang CH, Lambie EJ, Snyder M (1992) NuMA: An unusually long coiled-coil related protein in the mammalian nucleus. J Cell Biol 116:1303–1317.

Yang D, Xiao J, Wan M, Liu J, Huang L, Li X, Zhang L, Liu F, Liang D, Zheng Y, Xie B, Liao X, Xiong G, Lu H, Cao Z, Zhang S (2023) Roxadustat induces hepatotoxicity in zebrafish embryos via inhibiting Notch signaling. J Appl Toxicol 43:1073–1082.

Yang S, Lian G (2020) ROS and diseases: role in metabolism and energy supply. Mol Cell Biochem 467:1–12.

Yang X, Li X, Gu Q, Li Q, Cui Z (2019) Nucleoporin 62-Like Protein Is Required for the Development of Pharyngeal Arches through Regulation of Wnt/β-Catenin Signaling and Apoptotic Homeostasis in Zebrafish. Cells 8.

Yesbolatova A, Saito Y, Kitamoto N, Makino-Itou H, Ajima R, Nakano R, Nakaoka H, Fukui K, Gamo K, Tominari Y, Takeuchi H, Saga Y, Hayashi K ichiro, Kanemaki MT (2020) The auxin-inducible degron 2 technology provides sharp degradation control in yeast, mammalian cells, and mice. Nat Commun 11 Available at: http://dx.doi.org/10.1038/s41467-020-19532-z.

Yonekura SI, Nakamura N, Yonei S, Zhang-Akiyama QM (2009) Generation, biological consequences and repair mechanisms of cytosine deamination in DNA. J Radiat Res 50:19–26.

Yu EM, Linville L, Rosenthal M, Aragon-Ching JB (2021a) A contemporary review of immune checkpoint inhibitors in advanced clear cell renal cell carcinoma. Vaccines 9:1–13.

Yu M, Lun J, Zhang H, Zhu L, Zhang G, Fang J (2021b) The non-canonical functions of HIF prolyl hydroxylases and their dual roles in cancer. Int J Biochem Cell Biol 135:105982.

Yuan J, Narayanan L, Rockwell S, Glazer PM (2000) Diminished DNA repair and elevated mutagenesis in mammalian cells exposed to hypoxia and low pH. Cancer Res 60:4372–4376.

Yuen JSP, Cockman ME, Sullivan M, Protheroe A, Turner GDH, Roberts IS, Pugh CW, Werner H, Macaulay VM (2007) The VHL tumor suppressor inhibits expression of the IGF1R and its loss induces IGF1R upregulation in human clear cell renal carcinoma. Oncogene.

Yurkow EJ, Laskin JD (1991) Mechanism of action of psoralens: isobologram analysis reveals that ultraviolet light potentiation of psoralen action is not additive but synergistic. Cancer Chemother Pharmacol 27:315–319.

Zaksauskaite R, Thomas RC, Van Eeden F, El-Khamisy SF (2021) Tdp1 protects from topoisomerase 1-mediated chromosomal breaks in adult zebrafish but is dispensable during larval development. Sci Adv 7:eabc4165 Available at: http://wormweb.org/exonintron [Accessed May 17, 2021].

Zeng Z, Sharma A, Ju L, Murai J, Umans L, Vermeire L, Pommier Y, Takeda S, Huylebroeck D, Caldecott KW, El-Khamisy SF (2012) TDP2 promotes repair of topoisomerase I-mediated DNA damage in the absence of TDP1. Nucleic Acids Res 40:8371–8380.

Zhang H, Xiong Y, Su D, Wang C, Srivastava M, Tang M, Feng X, Huang M, Chen Z, Chen J (2022) TDP1-independent pathways in the process and repair of TOP1-induced DNA damage. Nat Commun 13.

Zhao J et al. (2022) Integrated multi-omics analyses reveal that BCAM is associated with epigenetic modification and tumor microenvironment subtypes of clear cell renal cell carcinoma. Clin Epigenetics 14 Available at: /pmc/articles/PMC9361577/ [Accessed August 17, 2023].

Zhu X, Jiang L, Wei X, Long M, Du Y (2022) Roxadustat: Not just for anemia. Front Pharmacol 13:971795.

Appendix

Fluorescent intensity macro (γH2AX)

```
1. //macro to extract foci from nuclei

2. //check to see if any ROIs in manager list. If so delete them
3. anyROIs = roiManager("count");

4. if (anyROIs > 0) {
5. roiManager("Deselect");
6. roiManager(Delete");

7. }

8. //prompt user to open the dapi channel image
9. filepath = File.openDialog("Select dapi channel image");
10. open(filepath);
11. rename("dapi");

12. //prompt user to open the h2ax channel image
13. filepath = File.openDialog("Select h2ax channel image");
14. open(filepath);
15. rename("h2ax");

16. //merge channels
17. run("Merge Channels...", "c2=[h2ax] c3=[dapi] create");

18. //analyse fluorescent intensity
19. selectWindow("Composite");
20. run("Split Channels");
21. selectWindow("C2-Composite");
```

```
22. run("Convert to Mask");
23. run("Fill Holes");
24. run("Analyze Particles...", "size=1000-20000 show=Outlines exclude include add
    in_situ");
25. run("Set Measurements...", "area mean integrated limit redirect=None decimal=3");
26. selectWindow("C1-Composite");
27. roiManager("Measure");

28. //close all image files on screen
29. close("*");

30.//Mean values = fluorescent intensity
```

Foci counter macro (53BP1)

```
1. //macro to extract foci from nuclei

2. //check to see if any ROIs in manager list. If so delete them
3. anyROIs = roiManager("count");

4. if (anyROIs > 0) {
5. roiManager("Deselect");
6. roiManager("Delete");

7. }

8. //prompt user to open the dapi channel image
9. filepath = File.openDialog("Select dapi channel image");
10. open(filepath);



11. //set threshold for dapi and create mask
12. setAutoThreshold("Default dark");
13. run("Convert to Mask");
14. run("Create Mask");
15. run("Fill Holes");

16. //create outline map of nuclei
17. run("Set Measurements...", "area integrated limit redirect=None decimal=3");
18. run("Analyze Particles...", "size=1000-20000 show=Outlines exclude include add");

19. //prompt user to open the h2ax channel image
20. filepath = File.openDialog("Select h2ax channel image");
21. open(filepath);
```

```
22. //find maxima
23. run("Find Maxima...", "prominence=30 exclude output=[Single Points]");
24. rename("Maxima");

25. //redirect maxima
26. selectWindow("mask");
27. run("Set Measurements...", "area integrated limit redirect=[Maxima] decimal=3");
28. selectWindow("Maxima");
29. roiManager("Show None");
30. roiManager("Show All");
31. roiManager("Measure");

32. //close all image files on screen
33. close("*");

34.//Number of foci per cell = integrated density / 255
```